US Army Corps of Engineers

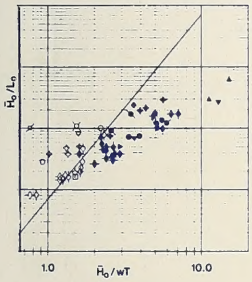


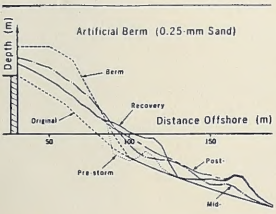


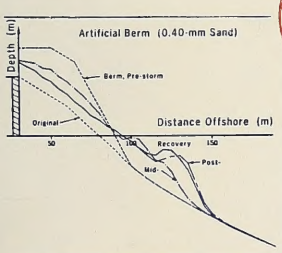




TECHNICAL REPORT CERC-89-9

# SBEACH: NUMERICAL MODEL FOR SIMULATING STORM-INDUCED BEACH CHANGE

## Report 1
## EMPIRICAL FOUNDATION AND MODEL DEVELOPMENT

by

Magnus Larson

Department of Water Resources Engineering
Institute of Science and Technology
University of Lund
Box 118, Lund, Sweden S-221 00

and

Nicholas C. Kraus

DEPARTMENT OF THE ARMY
Coastal Engineering Research Center
Waterways Experiment Station, Corps of Engineers
PO Box 631, Vicksburg, Mississippi 39181-0631



July 1989
Report 1 of a Series



Prepared for DEPARTMENT OF THE ARMY
US Army Corps of Engineers
Washington, DC 20314-1000
Under Surf Zone Sediment Transport Processes
Work Unit 34321

Destroy this report when no longer needed. Do not return it to the originator.

The findings in this report are not to be construed as an official Department of the Army position unless so designated by other authorized documents.

This program is furnished by the Government and is accepted and used by the recipient with the express understanding that the United States Government makes no warranties, expressed or implied, concerning the accuracy, completeness, reliability, usability, or suitability for any particular purpose of the information and data contained in this program or furnished in connection therewith, and the United States shall be under no liability whatsoever to any person by reason of any use made thereof. The program belongs to the Government. Therefore, the recipient further agrees not to assert any proprietary rights therein or to represent this program to anyone as other than a Government program.

The contents of this report are not to be used for advertising, publication, or promotional purposes. Citation of trade names does not constitute an official endorsement or approval of the use of such commercial products.

Unclassified

SECURITY CLASSIFICATION OF THIS PAGE

## REPORT DOCUMENTATION PAGE

*Form Approved OMB No. 0704-0188*

| | |
|---|---|
| 1a. REPORT SECURITY CLASSIFICATION<br>Unclassified | 1b. RESTRICTIVE MARKINGS |
| 2a. SECURITY CLASSIFICATION AUTHORITY | 3. DISTRIBUTION/AVAILABILITY OF REPORT<br>Approved for public release; distribution unlimited. |
| 2b. DECLASSIFICATION/DOWNGRADING SCHEDULE | |
| 4. PERFORMING ORGANIZATION REPORT NUMBER(S)<br>Technical Report CERC-89-9 | 5. MONITORING ORGANIZATION REPORT NUMBER(S) |
| 6a. NAME OF PERFORMING ORGANIZATION<br>USAEWES, Coastal Engineering Research Center<br>6b. OFFICE SYMBOL *(If applicable)* | 7a. NAME OF MONITORING ORGANIZATION |
| 6c. ADDRESS *(City, State, and ZIP Code)*<br>3909 Halls Ferry Road<br>Vicksburg, MS 39180-6199 | 7b. ADDRESS *(City, State, and ZIP Code)* |
| 8a. NAME OF FUNDING/SPONSORING ORGANIZATION<br>US Army Corps of Engineers<br>8b. OFFICE SYMBOL *(If applicable)* | 9. PROCUREMENT INSTRUMENT IDENTIFICATION NUMBER |
| 8c. ADDRESS *(City, State, and ZIP Code)*<br>Washington, DC 20314-1000 | 10. SOURCE OF FUNDING NUMBERS<br>PROGRAM ELEMENT NO. / PROJECT NO. / TASK NO. / WORK UNIT ACCESSION NO. 34321 |

11. TITLE *(Include Security Classification)*
SBEACH: Numerical Model for Simulating Storm-Induced Beach Change; Report 1: Empirical Foundation and Model Development

12. PERSONAL AUTHOR(S)
Larson, Magnus; Kraus, Nicholas C.

| 13a. TYPE OF REPORT | 13b. TIME COVERED | 14. DATE OF REPORT *(Year, Month, Day)* | 15. PAGE COUNT |
|---|---|---|---|
| Report 1 of a series | FROM Aug 86 TO Mar 89 | July 1989 | 267 |

16. SUPPLEMENTARY NOTATION
Available from National Technical Information Service, 5285 Port Royal Road, Springfield, VA 22161.

| 17. COSATI CODES | | | 18. SUBJECT TERMS *(Continue on reverse if necessary and identify by block number)* | | |
|---|---|---|---|---|---|
| FIELD | GROUP | SUB-GROUP | Accretion | Cross-shore sand transport | Longshore bars |
| | | | Beach erosion | Dune erosion | Numerical models |
| | | | Berms | Erosion | Storm erosion |

19. ABSTRACT *(Continue on reverse if necessary and identify by block number)*

A two-dimensional numerical model is presented for calculating dune and beach erosion produced by storm waves and water levels. The model is empirically based and was first developed from a large data set of net cross-shore sand transport rates and geomorphic change observed in large wave tanks, then verified using high-quality field data. The model is aimed to reproduce macroscale features of the beach profile, with focus on the formation and movement of longshore bars. The ultimate goal of the modeling effort is prediction of storm-induced beach erosion and post-storm recovery. Bars are simulated satisfactorily, but berm processes are less well reproduced, due in part to a lack of data for defining accretionary wave and profile processes. A new criterion is developed for predicting erosion and accretion, and the model uses this criterion to calculate net sand transport rates in four regions of the nearshore extending from deep water to the limit of wave runup. Wave height and setup across the profile are calculated to obtain the net cross-shore sand

(Continued)

| 20. DISTRIBUTION/AVAILABILITY OF ABSTRACT | 21. ABSTRACT SECURITY CLASSIFICATION |
|---|---|
| ☒ UNCLASSIFIED/UNLIMITED ☐ SAME AS RPT. ☐ DTIC USERS | Unclassified |
| 22a. NAME OF RESPONSIBLE INDIVIDUAL | 22b TELEPHONE *(Include Area Code)* / 22c. OFFICE SYMBOL |

DD Form 1473, JUN 86 *Previous editions are obsolete.*

SECURITY CLASSIFICATION OF THIS PAGE
Unclassified

19. ABSTRACT (Continued).

transport rate. The model is driven by engineering data, with main inputs of time series of wave height and period in deep water, time series of water level, median beach grain size, and initial profile shape. Comprehensive sensitivity testing is performed, and example applications are made to evaluate the response of the profile to the presence of a vertical seawall and the behavior of different beach fill cross sections in adjustment to normal and storm wave action.

## PREFACE

This study was conducted at the Coastal Engineering Research Center (CERC), US Army Engineer Waterways Experiment Station (WES), and the Department of Water Resources Engineering (DWRE), Institute of Science and Technology, University of Lund (UL), Lund, Sweden. The work described herein was authorized as a part of the Civil Works Research and Development Program by the US Army Corps of Engineers (USACE) and was performed under the Surf Zone Sediment Transport Processes Work Unit 34321 which is in the Shore Protection and Restoration Program, CERC. Messrs. John H. Lockhart, Jr., James E. Crews, Charles W. Hummer, and John G. Housley are USACE Technical Monitors. Dr. Charles L. Vincent is Program Manager for the Shore Protection and Restoration Program at CERC.

This study was performed and the report prepared over the period 1 August 1986 through 30 March 1989 by Dr. Magnus Larson, Assistant Professor, DWRE, and Dr. Nicholas C. Kraus, Senior Scientist, Research Division (CR), CERC. The content of this report is substantially the same as the thesis submitted to UL by Dr. Larson in partial fulfillment of the requirements for a Ph.D. degree in civil engineering. Dr. Kraus was a thesis committee member. The report updates and extends some material in the thesis.

Work at UL was performed under the general supervision of Dr. Gunnar Lindh, Head, DWRE, and was partially funded by Work Unit 34321 through the US Army Research, Development, and Standardization Group, UK, under contract No. DAJA-86-C-0046. Dr. Larson was in residence at CERC over the period 15 July 1986 through 30 August 1987. Work performed at CERC was under general administrative supervision of Dr. James R. Houston, Chief, CERC; Mr. Charles C. Calhoun, Jr., Assistant Chief, CERC; and Mr. H. Lee Butler, Chief, CR, CERC.

Dr. Kraus was the Principal Investigator of Work Unit 34321 during the technical phase of the study. Ms. Kathryn J. Gingerich, Coastal Processes Branch (CR-P), CERC, was Principal Investigator during the publication phase of the report and provided review and technical editing. Ms. Carolyn J. Dickson (CR-P) assisted in formatting and preparation of the final manuscript. Mr. Bruce A. Ebersole was Chief, CR-P. This report was edited by Ms. Shirley

A. J. Hanshaw, Information Products Division, Information Technology Laboratory, WES.

COL Dwayne G. Lee, CE, was Commander and Director of WES during the research and report preparation phases of this study. COL Larry B. Fulton was Commander and Director upon publication. Dr. Robert W. Whalin was Technical Director.

CONTENTS

LIST OF TABLES

LIST OF FIGURES

SBEACH: NUMERICAL MODEL FOR SIMULATING STORM-INDUCED BEACH CHANGE

EMPIRICAL FOUNDATION AND MODEL DEVELOPMENT

# PART I: INTRODUCTION

## Problem Statement and Objectives

1. The study of beach profile change in the broad sense encompasses nearshore processes that shape the beach on all spatial and temporal scales. Beach profile change is a phenomenon of fundamental interest and, as such, has been studied by geologists, oceanographers, and coastal engineers.

2. In coastal engineering, quantitative understanding of beach profile change is pursued mainly to allow prediction of beach evolution in the vicinity of planned or existing engineering projects. Two types of coastal engineering problems of particular importance for which predictive tools are needed are beach and dune erosion that occurs under storm waves and high water levels and adjustment of beach fill to long-term wave action. The time scale associated with storm-induced beach erosion is on the order of 1 to 3 days and depends on the level and duration of the storm surge as well as the wave characteristics, whereas the time scale of beach fill adjustment is several weeks to several months and depends on season of placement, fill material, and wave climate at the coast.

3. It is often convenient to separate nearshore sediment movement into two components, longshore sediment transport and cross-shore sediment transport, although this separation is not always valid in a strict sense because it is implicitly based on the assumption of plane and parallel profile contours. Longshore sediment transport figures prominently in situations involving loss of sediment supply, such as damming of rivers, and in impoundment at structures such as groins and jetties. In these cases longshore transport is the major process governing nearshore topography change and cannot be neglected.

4. For beaches located away from structures, inlets, and river mouths, it may be appropriate to neglect longshore transport as a first approximation, i.e., assume the gradient of the longshore transport rate is negligibly small

at the site. In this case, cross-shore transport will determine the change in beach profile contours. This assumption will be made in this investigation: longshore sediment transport is neglected and profile change produced solely by cross-shore sediment transport is considered.

5. The ultimate goal of this investigation is development of a numerical model to predict beach profile change produced by wave action. Numerous such models have been reported in the literature; however, apart from the present work only one highly schematized numerical model has been considered sufficiently accurate to be of engineering use. Most efforts appear to have failed because the level of detail attempted was beyond the state of knowledge of the physical processes involved. At present, knowledge is very limited on the collective motion of sediment particles in spatially varying flows of oscillatory currents, wave-induced mean current, and turbulence fields of breaking waves. Numerous other complicating factors, such as the complex fluid motion over an irregular bottom and absence of rigorous descriptions of broken waves and sediment-sediment interaction, also make the problem of computing sediment transport and resultant beach profile change essentially impossible if a first-principles approach at the microscale is taken.

6. On the other hand, despite the incredibly complex and diverse processes and factors involved, beach profile change, if viewed on the macroscale (spatial scale on the order of meters, and temporal scale on the order of hours), is remarkably smooth and simple. Certain prominent features, such as bars, troughs, and berms go through cycles of formation, growth, movement, and erasure with a morphodynamic pattern that has been reasonably well described by a number of qualitative conceptual models. The question can then be asked whether it is possible to develop a quantitative (numerical) model of beach profile change based on empirically determined global relations for the wave-induced net cross-shore sediment (sand) transport rate that can be inferred from the smooth and regular change observed to occur during beach profile evolution. Development of such a model is the subject of this investigation. Consideration is limited to sediment in the sand range of grain size (particle diameters in the range of 0.062 - 2.00 mm).

## Procedure Used

7. The principal physical mechanisms which determine beach profile change must be quantitatively described to model the profile response numerically. For this purpose it is necessary to study profile evolution under varying waves, sand characteristics, and profile shape. However, to establish cause and effect relationships between the governing factors and the profile response, it must be possible to clearly delineate these relationships. Laboratory facilities provide an environment where such investigations may be carried out efficiently, while allowing for data sampling at almost any spatial or temporal scale. The difficulty of transforming observations made under scale distortion is eliminated if experiments are performed at the scale of the prototype, i.e., at a sufficiently large scale as to satisfactorily represent the interaction between fluid forces and sand grains that produces significant sand transport in the field.

8. Use of field profile data as a basis for developing a numerical model is extremely difficult due to the complexity and randomness of naturally occurring conditions and cost of data collection. Ultimately a numerical model must be verified against field data, but, in the process of model development, laboratory data can provide considerably more insight into the relative influence of the factors producing the profile change. Study of these individual factors implicitly assumes the validity of the superposition principle for application of the model to the general case. For example, examination of the effect of water level variation on profile evolution under fixed incident waves isolates the influence of this factor and allows understanding of the related physical processes involved. A combination of such observations constitutes the foundation for a numerical model which is used in a predictive mode for varying water level and wave conditions, even though these factors have been evaluated separately. Consequently, careful data analysis is the basis for many assumptions and empirical relationships employed in the numerical model developed here and the first logical step toward understanding beach profile change by this procedure.

9. From an engineering point of view it is of considerable importance to quantify the various properties related to beach profile change. This

regards both geometric parameters such as bar volume and depth-to-bar crest, as well as more complex quantities such as the net cross-shore sand transport rate. Any structure or activity extending into the nearshore region is influenced by and exerts influence on the evolution of the beach profile, thus requiring quantitative estimates of profile change under various environmental and design conditions. A thorough analysis of various geometric characteristics of the profile and their dependence on the wave and sand properties is in this respect valuable. Through this analysis the important processes shaping the beach and generating various topographic features may be clarified, forming the conceptual framework for a numerical model.

10. A fundamental assumption of this study is that beach profile change is mainly governed by breaking of short-period waves (periods in the approximate range of 3-20 sec). No attempt has been made to include the effect of long-period waves, such as partially standing waves or infragravity waves, in the driving force of profile evolution, because no adequate data on profile change are available that permit firm conclusions to be made. Recent field investigations have indicated that, in some cases, infragravity or long-period wave energy can be more energetic near the shoreline than that of the existing short-period waves. This dominance of the wave energy spectrum in very shallow water by long-period waves is expected to play an important role in beach profile processes on the beach face and, possibly, the inner surf zone. However, no relationship between beach profile change and infragravity waves exists at present due to lack of data. When such data become available, superposition should allow calculation of profile change under both short- and long-period waves.

11. The main purpose of the data analysis is not to derive widely applicable relationships for geometric properties of the profile, but to identify the important factors governing profile change. These factors will be integral parts in the conceptual foundation underlying the numerical model development. In some cases, however, empirical relationships derived from the data are used directly in the model if general conclusions about the behavior of the quantity can be made.

## Basic Terminology

12. Nomenclature associated with the beach profile and nearshore region which is used throughout the report is presented in this section. Terms defined in the Shore Protection Manual (SPM 1984) have been adopted to a large extent. However, for some quantities, slightly different descriptions are employed that are better suited for nearshore processes as related to beach profile change. Figures 1a and 1b are definition sketches pertaining to beach profile morphology and nearshore wave dynamics, respectively. The portion of the beach profile of interest spans across the shore from the dunes to the seaward limit of the nearshore zone.

### Profile morphology

13. As waves approach the beach from deep water, they enter the nearshore zone. The seaward boundary of the nearshore zone is dynamic and for our purpose is considered to be the depth at which incident waves begin to shoal. The shoreward boundary of wave action is also dynamic and is at the limit of wave runup located at the intersection between the maximum water level and the beach profile. A gently sloping bottom will cause a gradual shoaling of the waves, leading to an increase in wave height and finally to breaking at a point where the wave height is about equal to the water depth. The region seaward of wave breaking is denoted as the offshore; the inshore encompasses the surf zone, i.e., that portion of the profile exposed to breaking and broken waves. The broken waves both propagate and dissipate with large energy through turbulence, initiating and maintaining sand movement. At the beach face, the remaining wave energy is expended by a runup bore as the water rushes up the profile.

14. The flat area shoreward of the beach face is called the backshore and is only wetted during severe (storm) wave conditions or when the water level is unusually high. On the backshore, one or several berms may exist; these are accretionary features formed of material which has been deposited by wave runup. The term "accretionary" refers to features generated by sand transport directed onshore. A step often develops immediately seaward of a

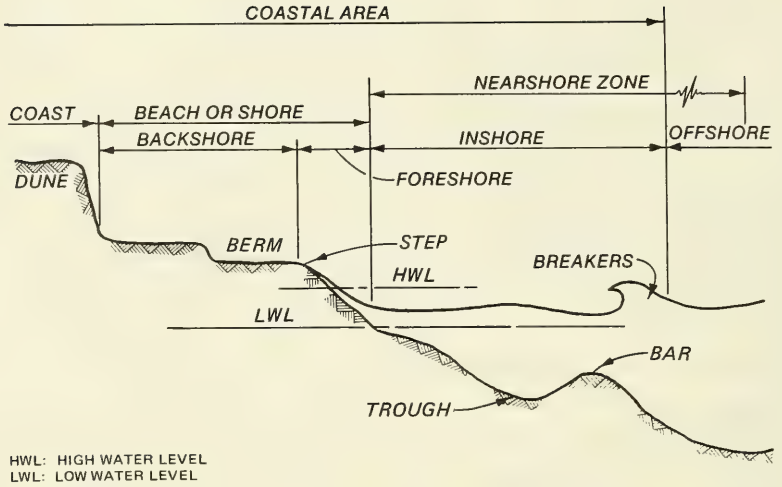


a. Morphology

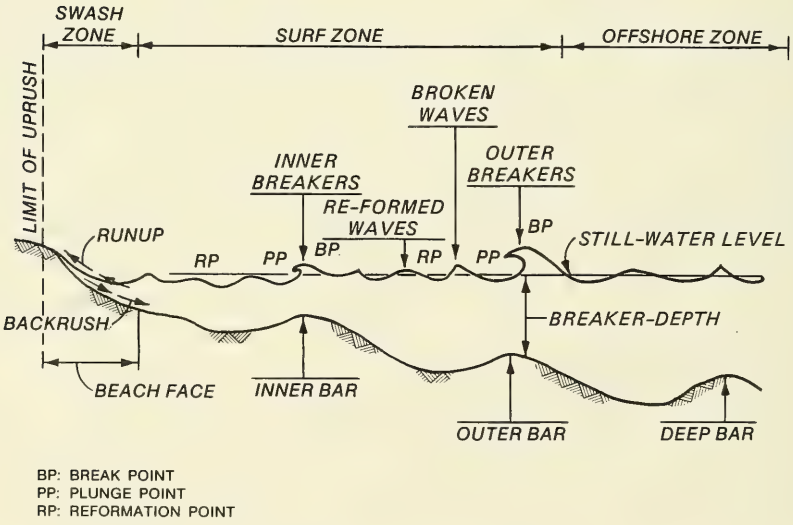


b. Nearshore wave dynamics

Figure 1. Definition sketch of the beach profile (after SPM (1984))

berm, and the slope of the step depends on the properties of the runup bore and the sand grains. Under storm wave action a scarp may also form; here, the term "step" will sometimes be used to denote both a scarp and a step. On many beaches a line of dunes is present shoreward of the backshore. Dunes consist of large ridges of unconsolidated sand that has been transported by wind from the backshore.

15. A bar is a depositional feature formed by sand transported from neighboring areas. Several bars may appear along a beach profile, often having a distinct trough on the shoreward side. Bars are highly dynamic features that respond to the existing wave climate by changing form and translating across-shore, but at the same time bars influence the waves incident upon them. If a bar was created during an episode of high waves, it may be located at such great depth that very little or almost no sand transport activity takes place until another period of high waves occurs. Some transport from the bar caused by shoaling waves may take place, but the time scale of this process is considerably longer than if the bar is located close to the surf zone and the breaking or broken waves.

Nearshore waves

16. The above-discussed terminology is related mainly to the various regions and features of the beach profile. Nearshore waves are also described by a specialized terminology (Figure 1b). Again, some definitions are not unique and describe quantities that change in space and time. The region between the break point and the limit of the backrush, where mainly broken waves exist, is called the surf zone. The swash zone extends approximately from the limit of the backrush to the maximum point of uprush, coinciding with the region of the beach face. As waves break and propagate toward shore, reformation may occur depending on the profile shape; that is, the translatory broken wave form reverts to an oscillatory wave. This oscillatory wave will break again as it reaches sufficiently shallow water, transforming into a broken wave with considerable energy dissipation. A region where broken waves have reformed to oscillatory waves is called a reformation zone, and the point where this occurs is the wave reformation point. Depending on the regularity of the incident waves and shape of the beach profile, wave breaking and reformation may occur several times.

17. The break point is located where the maximum particle velocity of the wave exceeds the wave celerity and the front face of the wave becomes vertical. As a wave breaks, the crest falls over into the base of the wave accompanied by large amount of energy dissipation. If the breaking waves are of the plunging type, the point of impingement is easily recognized and denoted as the plunge point. For spilling breakers, however, the plunge point concept is not commonly used, but such a point could be defined using the location of maximum energy dissipation. This definition is in accordance with the conditions prevailing at the plunge point for a plunging breaker.

18. A beach profile exposed to constant wave and water level conditions over a sufficiently long time interval, as can be done in the laboratory, will attain a fairly stable shape known as the equilibrium profile. On a beach in nature, where complex wave and water level variations exist, an equilibrium profile may never develop or, if so, only for a short time before the waves or water level again change. However, the equilibrium concept remains useful since it provides information on the amount of sand that has to be redistributed within the profile to attain the natural shape for a specific set of wave conditions. The equilibrium profile is in general considered to be a function of sand and wave characteristics.

## Organization of This Report

19. Part I is an introduction and gives a statement of the problem and objectives of the investigation. Part II reviews the literature of beach profile change, covering laboratory, field, and theoretical studies, and ends with a synthesis of results considered to be of particular relevance to the present investigation. Since the approach taken relies extensively on measurements, the data sets used are discussed in detail in Part III.

20. The main portion of the original work in this investigation was performed in a logical progression of three substudies. The first substudy, presented in Part IV, quantifies the morphology of the beach profile and the dynamics of its change under wave action. Based on these results, general features of cross-shore transport and empirically-based transport rate formulas needed for the development of the predictive numerical model are

derived in Part V. The profile change numerical model and the required wave model are described in Part VI. Part VII presents the results of extensive testing of the model, including sensitivity analyses, application to describe profile change in the field, and examples of its use to predict the adjustment of beach fill to storm wave action, together with the subsequent recovery process.

21. Part VIII gives conclusions and summarizes results. A summary of statistical procedures and terminology used is given in Appendix A, and mathematical notation is listed in Appendix B. The second report in the SBEACH series (Larson, Kraus, and Byrnes in prep) presents a detailed discussion of the numerical solution procedure used in both the wave and profile change models. It also gives additional examples of field verification and refinements in model usage.

## PART II: LITERATURE REVIEW

22. From the earliest investigations of beach morphology, the study of profile change has focused to a large extent upon the properties of bars. A wide range of morphologic features has been classified as bar formations by various authors, and different terminology has been used to denote the same feature. The literature on beach profile change is vast, and this chapter is intended to give a chronological survey of results relevant to the present work.

### Chronological Survey of Literature

23. Many of the first contributions to the study of bars were made by German researchers around the beginning of this century. Lehmann (1884) noted the role of breaking waves in suspending sand and found that profile change could occur very rapidly with respect to offshore bar movement. Otto (1911) and Hartnack (1924) measured geometric properties of bars in the Baltic Sea, such as depth-to-bar crest, distance from shoreline to bar crest, and bar slopes. Hartnack (1924) pointed out the importance of breaking waves in the process of bar formation and noted that the distance between bar crests increased with distance from shore for multiple bars, with the depth-to-bar crest increasing correspondingly.

24. Systematic laboratory modeling of beach profile evolution appears to have been first performed by Meyer (1936) who mainly investigated scaling effects in movable bed experiments. He also derived an empirical relationship between beach slope and wave steepness. Waters (1939) performed pioneering work on the characteristic response of the beach profile to wave action and classified profiles as ordinary or storm type. He concluded that wave steepness can be used to determine the type of beach profile that developed under a set of specific wave conditions. The process of sediment sorting along the profile was demonstrated in the experiments in which the coarser material remained near the plunge point and finer material moved offshore.

25. Bagnold (1940) studied beach profile evolution in small-scale laboratory experiments using rather coarse material (0.5-7.0 mm), resulting in

accretionary profiles with berm buildup. He found that the foreshore slope was independent of the wave height and mainly a function of grain size. However, the equilibrium height of the berm was linearly related to wave height. The effect of a seawall on the beach profile was investigated by allowing waves to reach the end of the tank. By varying the water level, a tide was simulated; in other experiments, a varying wave height was employed.

26. Evans (1940) studied bars and troughs (named balls and lows by Evans) along the eastern shore of Lake Michigan and concluded these features to be the result of plunging breakers. He regarded the bar and trough to form a unit, with the trough always located shoreward of the bar. If the profile slope was mild so that several break points appeared, a series of bars and troughs would develop. Also, a change in wave conditions could result in a change in bar shape and migration of the bar seaward or shoreward. A decreasing water level would cause the innermost bar to migrate onshore and take the form of a subaqueous dune, whereas an increase in water level would allow a new bar system to develop inshore. The most seaward bars would then become inactive.

27. In support of amphibious landing operations during World War II, Keulegan (1945) experimentally obtained simple relations for predicting the depth-to-bar crest and the trough depth. He found the ratio between trough and crest depths to be approximately constant and independent of wave steepness. Important contributions to the basic understanding of the physics of beach profile change were also made through further laboratory experiments by Keulegan (1948). The objective of the study was to determine the shape and characteristics of bars and the process through which they were molded by the incident waves. He recognized the surf zone as being the most active area of beach profile change and the breaking waves as the cause of bar formation. The location of the maximum sand transport rate, measured by traps, was found to be close to the break point, and the transport rate showed a good correlation with the wave height envelope. Keulegan (1948) noted three distinct regions along the profile where the transport properties were different from a morphologic perspective. A gentler initial beach slope implied a longer time before the equilibrium profile was attained for fixed wave conditions. For a constant wave steepness, an increase in wave height moved the bar seaward,

whereas for a constant wave height, an increase in wave steepness (decrease in wave period) moved the bar shoreward. He noted that bars developed in the laboratory experiments were shorter and more peaked than bars in the field and attributed this difference to variability in the wave climate on natural beaches.

28. King and Williams (1949), in work also connected with the war effort, distinguished between bars generated on nontidal beaches and bars occurring on beaches with a marked tidal variation (called ridge and runnel systems by them). They assumed that nonbreaking waves moved sand shoreward and broken waves moved sand seaward. Field observations from the Mediterranean confirmed the main ideas of this conceptualization. In laboratory experiments the cross-shore transport rate was measured with traps, showing a maximum transport rate located around the break point. Furthermore, the term "breakpoint bar" was introduced, whereas berm formations were denoted as "swash bars." The slope of the berm was related to the wavelength, where a longer wave period produced a more gentle slope. King and Williams hypothesized that ridge and runnel systems were not created by breaking waves but were a result of swash processes.

29. Johnson (1949) gave an often cited review of scale effects in movable bed modeling and referenced the criterion for distinguishing ordinary and storm profiles discovered by Waters (1939).

30. Shepard (1950) made profile surveys along the pier at Scripps Institution of Oceanography, La Jolla, California, in 1937 and 1938, and discussed the origin of troughs. He suggested that the combination of plunging breakers and longshore currents was the primary cause. He also showed that the trough and crest depths depended on breaker height. Large bars formed somewhat seaward of the plunge point of the larger breakers, and the ratios for the trough-to-crest depth were smaller than those found by Keulegan (1948) in laboratory experiments. Shepard (1950) also observed the time scale of beach profile response to the incident wave climate and concluded that the profile change was better related to the existing wave height than to the greatest wave height from the preceding 5 days.

31. Bascom (1951) studied the slope of the foreshore along the Pacific coast and attempted to relate it to grain size. A larger grain size implied a

steeper foreshore slope. He also determined a trend in variation in grain size across the profile that is much cited in the literature. A bimodal distribution was found with peaks at the summer berm and at the step of the foreshore. The largest particles were found on the beach face close to the limit of the backrush, and the grain size decreased in the seaward direction.

32. Scott (1954) modified the wave steepness criterion of Waters (1939) for distinguishing between ordinary (summer) and storm profiles, based on his laboratory experiments. He also found that the rate of profile change was greater if the initial profile was farther from equilibrium shape, and he recognized the importance of wave-induced turbulence for promoting bar formation. Some analysis of sediment stratification and packing along the profile was carried out.

33. Rector (1954) investigated the shape of the equilibrium beach profile in a laboratory study. Equations were developed for profile shapes in two sections separated at the base of the foreshore. Coefficients in the equilibrium profile equation were a function of deepwater wave steepness and grain size normalized by the deepwater wavelength. An empirical relationship was derived for determining the maximum depth of profile adjustment as a function of the two parameters. These parameters were also used to predict net sand transport direction.

34. Watts (1954) and Watts and Dearduff (1954) studied the effect on the beach profile of varying wave period and water level, respectively. A varying wave period reduced the bar and trough system as compared to waves of constant period but only slightly affected beach slope in the foreshore and offshore. The influence of the water level variation for the range tested (at most 20 percent variation in water level with respect to the tank depth in the horizontal portion) was small, producing essentially the same foreshore and offshore slopes. However, the active profile translated landward for the tidal variation, allowing the waves to attack at a higher level and thus activating a larger portion of the profile.

35. Bruun (1954) developed a predictive equation for the equilibrium beach profile by studying beaches along the Danish North Sea coast and the California coast. The equilibrium shape (depth) followed a power curve with distance offshore, with the power evaluated as 2/3.

36. Ippen and Eagleson (1955) experimentally and theoretically investigated sorting of sediments by wave shoaling on a plane beach. The movement of single spherical particles was investigated and a "null point" was found on the beach where the particle was stable for the specific grain size.

37. Saville (1957) was the first to employ a large wave tank capable of reproducing near-prototype wave and beach conditions, and he studied equilibrium beach profiles and model scale effects. Waves with very low steepness were found to produce storm profiles, contrary to results from small-scale experiments (Waters 1939, Scott 1954). Comparisons were made between the large wave tank studies and small-scale experiments, but no reliable relationship between prototype and model was obtained. The data set from this experiment is used extensively in the present work.

38. Caldwell (1959) presented a summary of the effects of storm (northeaster) and hurricane wave attack on natural beach profiles for a number of storm events.

39. McKee and Sterrett (1961) investigated cross-stratification patterns in bars by spreading layers of magnetite over the sand.

40. Kemp (1961) introduced the concept of "phase difference," referring to the relation between time of uprush and wave period. He assumed the transition from a step (ordinary) to a bar (storm) profile to be a function of the phase difference and to occur roughly if the time of uprush was equal to the wave period.

41. Bruun (1962) applied his empirical equation (Bruun 1954) for an equilibrium beach profile to estimate the amount of erosion occurring along the Florida coast as a result of long-term sea level rise.

42. Bagnold (1963, 1966) developed formulas for calculating sediment transport rates, including cross-shore transport, based on a wave energy approach, and distinguishing between bed load and suspended load. This work has been refined and widely applied by others (e.g., Bailard and Inman 1981, Bailard 1982, Stive 1987). Bed-load transport occurs through the contact between individual grains, whereas in suspended load transport the grains are supported by the diffusion of upward eddy momentum. A superimposed steady current moves the grains along the bed. Inman and Bagnold (1963) derived an expression for the local equilibrium slope of a beach based on wave energy

considerations. The equilibrium slope was a function of the angle of repose and the ratio between energy losses at the bed during offshore- and onshore-directed flow.

43. Eagleson, Glenne, and Dracup (1963) studied equilibrium profiles in the region seaward of the influence of breaking waves. They pointed out the importance of bed load for determining equilibrium conditions and used equations for particle stability to establish a classification of beach profile shapes.

44. Iwagaki and Noda (1963) derived a graphically presented criterion for predicting the appearance of bars based on two nondimensional parameters, deepwater wave steepness, and ratio between deepwater wave height and median grain size. The change in character of breaking waves due to profile evolution in time was discussed. The potential importance of suspended load was recognized and represented through the grain size, this quantity emerging as a significant factor in beach profile change.

45. Zenkovich (1967) presented a summary of a number of theories suggested by various authors for the formation of bars.

46. Wells (1967) proposed an expression for the location of a nodal line of the net cross-shore sand transport based on the horizontal velocity skewness being zero, neglecting gravity, and derived for the offshore, outside the limit of breaking waves. Seaward of the nodal line material could erode and shoreward-moving sand could accumulate, depending on the sign of the velocity skewness.

47. Berg and Duane (1968) studied the behavior of beach fills during field conditions and suggested the use of coarse, well-sorted sediment for the borrow material to achieve a more stable fill. The mean diameter of the grains in the profile roughly decreased with depth, with the coarsest material appearing at the waterline (Bascom 1951, Scott 1954).

48. Mothersill (1970) found evidence through grain size analysis that longshore bars are formed by plunging waves and a seaward-directed undertow (Dally 1987). Sediment samples taken in troughs were coarser, having the properties of winnowed residue, whereas samples taken from bars were finer grained, having the characteristics of sediments that had been winnowed out and then redeposited.

49. Sonu (1969) distinguished six major types of profiles and described beach change in terms of transitions between these types.

50. Edelman (1969, 1973) studied dune erosion and developed a quantitative predictive procedure by assuming that all sand eroded from the dune was deposited within the breaker zone. On the basis of a number of simplifying assumptions, such as the shape of the after-storm profile being known together with the highest storm surge level, dune recession as produced by a storm could be estimated.

51. Sonu (1970) discussed beach change caused by the 1969 hurricane Camille, documenting the rapid profile recovery that took place during the end of the storm itself and shortly afterward (see also, Kriebel 1987).

52. Nayak (1970, 1971) performed small-scale laboratory experiments to investigate the shape of equilibrium beach profiles and their reflection characteristics. He developed a criterion for the generation of longshore bars that is similar to that of Iwagaki and Noda (1963) but included the specific gravity of the material. The slope at the still-water level for the equilibrium profile was controlled more by specific gravity than by grain size. Furthermore, the slope decreased as the wave steepness at the beach toe or the dimensionless fall speed (wave height divided by fall speed and period) increased. The dimensionless fall speed was also found to be a significant parameter for determining the reflection coefficient of the beach.

53. Allen (1970) quantified the process of avalanching on dune slopes for determining the steepest stable slope a profile can attain. He introduced the concepts of angle of initial yield and residual angle after shearing to denote the slopes immediately before and after the occurrence of avalanching.

54. Dyhr-Nielsen and Sorensen (1971) proposed that longshore bars were formed from breaking waves which generated secondary currents directed toward the breaker line. On a tidal beach with a continuously moving break point, a distinct bar would not form unless severe wave conditions prevailed.

55. Saylor and Hands (1971) studied characteristics of longshore bars in the Great Lakes. The distance between bars increased at greater than linear rate with distance from the shoreline, whereas the depth to crest increased linearly. A rise in water level produced onshore movement of the bars (cf. Evans 1940).

56. Davis and Fox (1972) and Fox and Davis (1973) developed a conceptual model of beach change by relating changes to barometric pressure. They reproduced complex nearshore features by schematizing the beach shape and using empirical relationships formed with geometric parameters describing the profile. Davis et al. (1972) compared development of ridge and runnel systems (King and Williams 1949) in Lake Michigan and off the coast of northern Massachusetts where large tidal variations prevailed. The tides only affected the rate at which onshore migration of ridges occurred and not the sediment sequence that accumulated as ridges.

57. Dean (1973) assumed suspended load to be the dominant mode of transport in most surf zones and derived on physical grounds the dimensionless fall speed as governing parameter. Sand grains suspended by the breaking waves would be transported onshore or offshore depending on the relation between the fall speed of the grains and the wave period. A criterion for predicting the cross-shore transport direction based on the nondimensional quantities of deepwater wave steepness and fall speed divided by wave period and acceleration of gravity (fall speed parameter) was proposed. The criterion of transport direction was also used for predicting profile response (normal or storm profile).

58. Carter, Liu, and Mei (1973) suggested that longshore bars could be generated by standing waves and associated reversal of the mass transport in the boundary layer, causing sand to accumulate at either nodes or antinodes of the wave. In order for flow reversal to occur, significant reflection had to be present. Lau and Travis (1973), and Short (1975a, b) discussed the same mechanism for longshore bar formation.

59. Hayden et al. (1975) analyzed beach profiles from the United States Atlantic and gulf coasts to quantify profile shapes. Eigenvector analysis was used as a powerful tool to obtain characteristic shapes in time and space. The first three eigenvectors explained a major part of the variance and were given the physical interpretation of being related to bar and trough morphology. The number of bars present on a profile showed no dependence on profile slope, but an inverse relationship between slopes in the inshore and offshore was noted.

60. Winant, Inman, and Nordstrom (1975) also used eigenvector analysis to determine characteristic beach shapes and related the first eigenvector to mean beach profile, the second to the bar/berm morphology, and the third to the terrace feature. The data set consisted of 2 years of profile surveys at Torrey Pines, California, performed at monthly intervals.

61. Davidson-Arnott (1975) and Greenwood and Davidson-Arnott (1975) performed field studies of a bar system in Kouchibouguac Bay, Canada, and identified conditions for bar development; namely, gentle offshore slope, small tidal range, availability of material, and absence of long-period swell. They distinguished between the inner and outer bar system and described in detail the characteristics of these features. The break point of the waves was located on the seaward side of the bar in most cases and not on the crest. Greenwood and Davidson-Arnott (1972) did textural analysis of sand from the same area, revealing distinct zones with different statistical properties of the grain size distribution across the profile (Mothersill 1970).

62. Exon (1975) investigated bar fields in the western Baltic Sea which were extremely regular due to evenly distributed wave energy alongshore. He noted that the presence of engineering structures reduced the size of the bar field.

63. Kamphuis and Bridgeman (1975) performed wave tank experiments to evaluate the performance of artificial beach nourishment. They concluded that the inshore equilibrium profile was independent of the initial slope and a function only of beach material and wave climate. However, the time elapsed before equilibrium was attained, as well as the bar height, depended upon the initial slope.

64. Sunamura and Horikawa (1975) classified beach profile shapes into three categories distinguished by the parameters of wave steepness, beach slope, and grain size divided by wavelength. The criterion was applied to both laboratory and field data, only requiring a different value of an empirical coefficient to obtain division between the shapes. The same parameters were used by Sunamura (1975) in a study of stable berm formations. He also found that berm height (datum not given) was approximately equal to breaking wave height.

65. Swart (1975, 1977) studied cross-shore transport properties and characteristic shapes of beach profiles. A cross-shore sediment transport equation was proposed where the rate was proportional to a geometrically-defined deviation from the equilibrium profile shape. A numerical model was developed based on the derived empirical relationships and applied to a beach fill case.

66. Wang, Dalrymple, and Shiau (1975) developed a computer-intensive three-dimensional numerical model of beach change assuming that cross-shore transport occurred largely in suspension. The transport rate was related to the energy dissipation across shore.

67. Van Hijum (1975, 1977) and Van Hijum and Pilarczyk (1982) investigated equilibrium beach profiles of gravel beaches in laboratory tests and derived empirical relationships for geometric properties of profiles. The net cross-shore sand transport rate was calculated from the mass conservation equation, and a criterion for the formation of bar/step profiles was proposed for incident waves approaching at an angle to the shoreline.

68. Hands (1976) observed in field studies at Lake Michigan that plunging breakers were not essential for bar formation. He also noted a slower response of the foreshore to a rising lake level than for the longshore bars. A number of geometric bar properties were characterized in time and space for the field data.

69. Dean (1976) discussed equilibrium profiles in the context of energy dissipation from wave breaking. Various causes of beach profile erosion were identified and analyzed from the point of view of the equilibrium concept. Dean (1977) analyzed beach profiles from the United States Atlantic and gulf coasts and arrived at a 2/3 power law as the optimal function to describe the profile shape, as previously suggested by Bruun (1954). Dean (1977) proposed a physically-based explanation for the power shape assuming that the profile was in equilibrium if the energy dissipation per unit water volume from wave breaking was uniform across shore. Dean (1977b) developed a schematized model of beach recession produced by storm activity based on the equilibrium profile shape (Edelman 1969, 1973).

70. Owens (1977) studied beach and nearshore morphology in the Gulf of St. Lawrence, Canada, describing the cycles of erosion and accretion resulting from storms and post-storm recovery.

71. Chiu (1977) mapped the effect of the 1975 Hurricane Eloise on the beach profiles along the Gulf of Mexico (Sonu 1970). Profiles with a gentle slope and a wide beach experienced less erosion compared with steep slopes, whereas profiles in the vicinity of structures experienced greater amounts of erosion.

72. Dalrymple and Thompson (1977) related foreshore slope to the dimensionless fall speed using laboratory data and presented an extensive summary of scaling laws for movable-bed modeling.

73. Felder (1978) and Felder and Fisher (1980) divided the beach profile into various regions with specific transport relationships and developed a numerical model to simulate bar response to wave action. In the surf zone, the transport rate depended on the velocity of a solitary wave.

74. Aubrey (1978) and Aubrey, Inman, and Winant (1980) used the technique of eigenvector analysis (Hayden et al. 1975) in beach profile characterization to predict beach profile change. Both profile evolution on a daily and weekly basis were predicted from incident wave conditions where the weekly mean wave energy was found to be the best predictor for weekly changes. Aubrey (1979) used measurements of beach profiles in southern California spanning 5 years to investigate temporal properties of profile change. He discovered two pivotal (fixed) points, one located at 2 to 3-m depth and one at 6-m depth. Sediment exchange across the former point was estimated at 85 $m^3/m$ and across the latter at 15 $m^3/m$ per year.

75. Hunter, Clifton, and Phillips (1979) studied nearshore bars on the Oregon coast which attached to the shoreline and migrated alongshore. A seaward net flow (undertow) along the bottom was occasionally observed shoreward of the bar during field investigations (Mothersill 1970).

76. Greenwood and Mittler (1979) found support in the studies of sedimentary structures of the bar system being in dynamic equilibrium from sediment movement in two opposite directions. An asymmetric wave field moved the sand landward and rip currents moved the material seaward.

77. Greenwood and Davidson-Arnott (1979) presented a classification of wave-formed bars and a review of proposed mechanisms for bar formation (Zenkovich 1967).

78. Hallermeier (1979, 1984) studied the limit depth for intense bed agitation and derived an expression for this depth based on linear wave shoaling. He also proposed an equation for the yearly limit depth for significant profile change involving wave conditions which exceeded 12 hours per year (see also Birkemeier 1985b).

79. Hattori and Kawamata (1979) investigated the behavior of beach profiles in front of a seawall by means of laboratory experiments. Their conclusion was that material eroded during a storm returned to the seawall during low wave conditions to form a new beach (cf. reviews of Kraus 1987, 1988).

80. Chappell and Eliot (1979) performed statistical analyses of morphological patterns from data obtained along the southern coast of Australia. Seven inshore states were identified which could be related to the current, the antecedent wave climate, and the general morphology (Sonu 1969).

81. Nilsson (1979) assumed bars to be formed by partially reflected Stokes wave groups and developed a numerical model based on this mechanism. Sediment transport rates were calculated from the bottom stress distribution, and an offshore directed mean current was superimposed on the velocity field generated by the standing waves.

82. Short (1979) conducted field studies along the southeast Australian coast which formed the basis for proposing a conceptual three-dimensional beach-stage model. The model comprised ten different stages ranging from pure erosive to pure accretive conditions. Transitions between stages were related to the breaking wave height and breaker power. Wright et al. (1979) discussed the characteristics of reflective and dissipative beaches as elucidated from Australian field data. The surf scaling parameter (Guza and Bowen 1977) was considered an important quantity for determining the degree of reflectivity of a specific profile. Long-period waves (infragravity waves, edge waves) were believed to play a major role in the creation of three-dimensional beach morphology.

83. Bowen (1980) investigated bar formation by standing waves and presented analytical solutions for standing waves on plane sloping beaches. He also derived equilibrium slopes for beach profiles based on Bagnold's (1963) transport equations and assuming simple flow variations.

84. Dally (1980) and Dally and Dean (1984) developed a numerical model of profile change based on the assumption that suspended transport is dominant in the surf zone. The broken wave height distribution across-shore determined by the numerical model supplied the driving mechanism for profile change. An exponential-shaped profile was assumed for the sediment concentration through the water column.

85. Davidson-Arnott and Pember (1980) compared bar systems at two locations in southern Georgian Bay, the Great Lakes, and found them to be very similar despite large differences in fetch length. The similarity was attributed to the same type of breaking conditions prevailing, with spilling breakers occurring at multiple break points giving rise to multiple bar formations (Hands 1976).

86. Hashimoto and Uda (1980) related beach profile eigenvectors for a specific beach to shoreline position. Once the shoreline movement could be predicted, the eigenvectors were given from empirical equations and the three-dimensional response obtained.

87. Shibayama and Horikawa (1980a, 1980b) proposed sediment transport equations for bed load and suspended load based on the Shields parameter (Madsen and Grant 1977). A numerical beach profile model was applied using these equations which worked well in the offshore region but failed to describe profile change in the surf zone.

88. Davidson-Arnott (1981) developed a numerical model to simulate multiple longshore bar formation. The model was based on the mechanism proposed by Greenwood and Mittler (1979) for bar genesis, and the model qualitatively produced offshore bar movement; but no comparison with measurements was made.

89. Bailard and Inman (1981) and Bailard (1982) used Bagnold's (1963) sediment transport relationships to develop a model for transport over a plane sloping beach. They determined the influence in the model of the longshore current on the equilibrium profile slope. The beach profile was flattened in

the area of the maximum longshore current and the slope increased with sand fall velocity and wave period.

90. Hughes and Chiu (1981) studied dune recession by means of small-scale movable-bed model experiments. The amount of dune erosion was found by shifting the barred profile horizontally until eroded volume agreed with deposited volume (Vellinga 1983). Geometric properties of the equilibrium bar profile were expressed in terms of dimensionless fall speed.

91. Sawaragi and Deguchi (1981) studied cross-shore transport and beach profile change in a small wave tank and distinguished three transport rate distributions. They developed an expression for the time variation of the maximum transport rate and discussed the relation between bed and suspended load.

92. Gourlay (1981) emphasized the significance of the dimensionless fall speed (Gourlay 1968) in describing equilibrium profile shape, relative surf zone width, and relative uprush time.

93. Hattori and Kawamata (1981) developed a criterion for predicting the direction of cross-shore sediment transport similar to Dean (1973), but including beach slope. The criterion was derived from the balance between gravitational and turbulent forces keeping the grains in suspension.

94. Watanabe, Riho, and Horikawa (1981) calculated net cross-shore transport rates from the mass conservation equation (van Hijum 1975, 1977) and measured profiles in the laboratory, arriving at a transport relationship of the Madsen and Grant (1977) type. They introduced a critical Shields stress below which no transport occurred and assumed a linear dependence of the transport rate on the Shields parameter.

95. Moore (1982) developed a numerical model to predict beach profile change produced by breaking waves. He assumed the transport rate to be proportional to the energy dissipation from breaking waves per unit water volume above an equilibrium value (Dean 1977). An equation was given which related this equilibrium energy dissipation to grain size. The beach profile calculated with the model approached an equilibrium shape in accordance with the observations of Bruun (1954) if exposed to the same wave conditions for a sufficiently long time.

96. Kriebel (1982, 1986) and Kriebel and Dean (1984, 1985a) developed a numerical model to predict beach and dune erosion using the same transport relationship as Moore (1982). The amount of erosion was determined primarily by water-level variation, and breaking wave height entered only to determine the width of the surf zone. The model was verified both against large wave tank data (Saville 1957) and data from natural beaches taken before and after Hurricane Eloise (Chiu 1977). The model was applied to predict erosion rates at Ocean City, Maryland, caused by storm activity and sea level rise (Kriebel and Dean 1985b).

97. Holman and Bowen (1982) derived idealized three-dimensional morphologic patterns resulting from interactions between edge waves and reflected waves, assuming that drift velocities associated with these waves caused bar formation.

98. Watanabe (1982, 1985) introduced a cross-shore transport rate which was a function of the Shields parameter to the 3/2 power in a three-dimensional model of beach change. The model simulated the effects of both waves and nearshore currents on the beach profile. The transport direction was obtained from an empirical criterion (Sunamura and Horikawa 1975).

99. Vellinga (1982, 1986) presented results from large wave tank studies of dune erosion and discussed scaling laws for movable-bed experiments (Hughes and Chiu 1981). The dimensionless fall speed proved to provide a reasonable scaling parameter in movable-bed studies. He also emphasized the dependence of the sediment concentration on wave breaking.

100. Dolan (1983) and Dolan and Dean (1984) investigated the origin of the longshore bar system in Chesapeake Bay and concluded that multiple breaking was the most likely cause (Hands 1976). Other possible mechanisms discussed were standing waves, edge waves, secondary waves, and tidal currents, but none of these could satisfactorily explain the formations.

101. Kajima et al. (1983a, b) discussed beach profile evolution using data obtained in a large wave tank with waves of prototype size. Beach profile shapes and distributions of the net cross-shore transport rates were classified according to the criterion developed by Sunamura and Horikawa (1975). A model of beach profile change was proposed based on a schematized

transport rate distribution which decayed exponentially with time. The data set given by Kajima et al. (1983b) is used in the present work.

102. Sasaki (1983) developed a conceptual three-dimensional beach stage model based on extensive field measurement from two beaches in Japan (see also Sonu 1969, Short 1979). Transition between the different stages was determined as a function of the average deepwater wave steepness and the average breaker height divided by the median grain size. A larger breaker height and deepwater wave steepness caused greater shoreline recession during storms, whereas a coarser grain size gave reduced shoreline retreat.

103. Sunamura (1983) developed a simple numerical model of shoreline change caused by short-term cross-shore events and described both erosional and accretional phases of a field beach. Exponential response functions were used to calculate the magnitude of shoreline change, and direction was given by the criterion proposed by Sunamura and Horikawa (1975).

104. Vellinga (1983, 1986) presented an empirically based mathematical model for calculating dune erosion during high surge-short duration storm events. The amount of dune recession was determined from the significant wave height, storm surge level, and beach profile shape during storm conditions. Van de Graaff (1983) discussed a probabilistic approach for estimating dune erosion. Distribution functions for a number of important parameters regarding dune erosion were suggested such as maximum storm surge level, significant wave height, median grain size, and profile shape. Visser (1983) applied a probability-based design scheme to the dunes in the Delta area of The Netherlands (Verhagen 1985).

105. Seelig (1983) analyzed large wave tank data from Saville (1957) and developed a simple prediction method to estimate beach volume change above the still-water level.

106. Balsillie (1984) related longshore bar formation to breaking waves from field data and developed a numerical model to predict profile recession produced by storm and hurricane activity.

107. Davidson-Arnott and Randall (1984) performed field measurements of the spatial and temporal characteristics of the surface elevation and cross-shore current spectra on a barred profile at St. Georgian Bay, Lake Ontario.

The greatest portion of the energy was found in the frequencies of the incident short-period waves.

108. Sunamura (1984a) derived a formula to determine the cross-shore transport rate in the swash zone taken as an average over 1 hour. The transport rate was related to the near-bottom orbital velocity, and the transport equation predicted the net direction of sand movement.

109. Takeda (1984) studied the behavior of beaches during accretionary conditions. Based on field investigations from Naka Beach, Japan, he derived predictive relationships for determining if onshore movement of bars occurs, average speed of onshore bar migration, and berm height. He pointed out the rapid formation of berms in the field where the buildup may be completed in one or two days (cf. Kriebel, Dally, and Dean 1986).

110. Greenwood and Mittler (1984) inferred the volume flux of sediment over a bar by means of rods driven into the bed on which a freely moving fitting was mounted to indicate changes in bed elevation. Their study indicated an energetics approach in accordance with Bagnold (1963) to be reasonable for predicting equilibrium slopes seaward of the break point.

111. Sunamura (1984b) obtained empirical expressions for the beach face slope involving the breaking wave height, wave period, and grain size. Equations were developed and applied for laboratory and field conditions.

112. Shibayama (1984) investigated the role of vortices in sediment transport and derived transport formulas for bed and suspended load based on Shields parameter. The generation of vortices was not confined to plunging breakers but could occur under spilling breakers as well.

113. Sunamura and Takeda (1984) quantified onshore migration of bars from a 2-year series of profile data from a beach in Japan. They derived a criterion to determine the occurrence of onshore bar movement and an equation to estimate the migration speed (Takeda 1984). Onshore transport typically took place in the form of bed load carried shoreward in a hydraulic bore.

114. Wright and Short (1984) used the dimensionless fall speed, based on the breaking wave height, in a classification process of three-dimensional beach stages.

115. Mei (1985) mathematically analyzed resonant reflection from nearshore bars that can enhance the possibility for standing waves to generate bars.

116. Shimizu et al. (1985) analyzed data obtained with a large wave tank to investigate the characteristics of the cross-shore transport rate. Transport rate distributions were classified in three categories, and the criterion of Sunamura and Horikawa (1975) was used to delineate between different types. The transport rate distribution was modeled by superimposing three separate curves representing the transport rate on the foreshore, in the surf zone, and in the offshore zone (cf. Kajima et al. 1983a).

117. Aubrey and Ross (1985) used eigenvector and rotary component analysis to identify different stages in the beach profile and the corresponding frequency of change. A frequency of one year related to exchange of sediment between bar and berm was the dominant mode found in the analysis.

118. Deguchi and Sawaragi (1985) measured the sediment concentration at different locations across the beach profile in a wave tank. Both the bed load and suspended load were determined, and sediment concentration decayed exponentially with distance above the bed (Kraus and Dean 1987).

119. Mason et al. (1985) summarized a field experiment conducted at Duck, North Carolina, where a nearshore bar system was closely monitored during a storm. Bar dynamics showed a clear dependence on wave height, the bar becoming better developed and migrating offshore as the wave height increased. Birkemeier (1985a) analyzed the time scale of beach profile change from a data set comprising 3-1/2 years of profile surveying at Duck, North Carolina. Large bar movement occurred with little change in the depth to crest. If low-wave conditions prevailed for a considerable time, a barless profile developed.

120. Jaffe, Sternberg, and Sallenger (1985) measured suspended sediment concentration in a field surf zone with an optical back-scattering device. The concentration decreased with elevation above the bed, and an increase in concentration was found over the nearshore bar.

121. Birkemeier (1985b) modified parameter values in an equation proposed by Hallermeier (1979) to describe the seaward limit of profile change at Duck, North Carolina.

122. Gourlay (1985) identified four different kinds of profile response related to dominant breaker type. The dimensionless fall speed (sediment mobility parameter) was decisive for describing both profile response and profile geometry (Hughes and Chiu 1981). The effect of beach permeability was discussed with respect to wave setup and berm height.

123. Sallenger, Holman, and Birkemeier (1985) observed the rapid response of a natural beach profile at Duck, North Carolina, to changing wave conditions. Both offshore and onshore bar movement occurred at much higher speeds than expected, and the ratio between trough and crest depth was approximately constant during offshore bar movement but varied during onshore movement. Since bars appeared to be located well within the surf zone, they concluded that wave breaking was not directly responsible for bar movement.

124. In a numerical model developed by Stive and Battjes (1985), offshore sand transport was assumed to occur through the undertow and as bed load only. They verified the model against laboratory measurements of profile evolution produced by random waves. Stive (1987) extended the model to include effects of asymmetry in the velocity field from the waves in accordance with the transport relations of Bailard (1982).

125. Verhagen (1985) developed a probabilistic technique for estimating the risk of breakthrough of dunes during storm surge and wave action. A main part of this technique was the use of a model to calculate expected dune erosion during a storm (Vellinga 1983) modified by statistical distributions of the factors influencing dune erosion (van de Graaff 1983, Visser 1983).

126. Wood and Weishar (1985) made profile surveys at monthly intervals on the east shore of (tideless) Lake Michigan. They found a strong temporal correlation between berm undulation and the annual lake-level variation.

127. Kriebel, Dally, and Dean (1986) studied beach recovery after storm events both during laboratory and field conditions, noting the rapid process of berm formation. They could not find evidence for breakpoint bars moving onshore and welding onto the beach face during the recovery process; instead, the berm was built from material originating farther inshore. Beach recovery following the 1985 Hurricane Elena was also discussed by Kriebel (1987), who concluded that the presence of a seawall did not significantly affect the process of beach recovery at the site.

128. Wright et al. (1986) concluded from field measurements that bar-trough morphology was favored by moderate breaker heights combined with small tidal ranges. Short-period waves were the main cause of sediment suspension in the surf zone, although long period waves were believed to be important in the overall net drift pattern.

129. Rushu and Liang (1986) proposed a criterion for distinguishing between beach erosion and accretion involving a number of dimensionless quantities. A new parameter consisting of the bottom friction coefficient, critical velocity for incipient motion of the grains, and the fall speed of the grains was introduced.

130. Thomas and Baba (1986) studied berm development produced by onshore migration of bars for a field beach at Valiathura, at the southwest coast of India, and related the conditions for onshore movement to wave steepness.

131. Dette (1986), Uliczka and Dette (1987), and Dette and Uliczka (1987a, b) investigated beach profile evolution generated in a large wave tank under prototype-scale conditions. The tests were carried out with both monochromatic and irregular waves for a dunelike foreshore with and without a significant surf zone. For one case starting from a beach without "foreshore," monochromatic waves produced a bar, whereas irregular waves of significant height and peak spectral period of the monochromatic waves did not. The incident wave energy was different between the cases, however. Sediment concentration and cross-shore velocity were measured through the water column at selected points across the profile.

132. Wright et al. (1987) investigated the influence of tidal variations and wave groupiness on profile configuration. Higher values of the wave groupiness factor tended to correlate with beach states of more dissipative character.

133. Howd and Birkemeier (1987) presented 4 years of profile data obtained at four different shore normal survey lines at Duck, North Carolina. Corresponding wave and water level data were also published, making this data set one of the most complete descriptions available of beach profile response to wave action in the field.

134. Seymour (1987) summarized results from the Nearshore Sediment Transport Study (NSTS) 6-year program in which nearshore sediment transport conditions were investigated. He pointed out the importance of bar formation for protecting the foreshore against wave action and the resulting rapid offshore movement of the bar on a beach exposed to storm waves.

135. Takeda and Sunamura (1987) found from field studies in Japan the great influence of bar formation on the subaerial response of beaches with fine sand.

136. Dally (1987) tested the possibility of generating bars by long period waves (surf beat) in a small wave tank, but he found little evidence for this mechanism. Instead, breaking waves in combination with undertow proved to be the cause of bar formation in the studied cases, whether spilling or plunging breakers prevailed.

137. Hallermeier (1987) stressed the importance of large wave tank experiments for providing valuable information of the beach response to storm conditions. He compared results from a large wave tank experiment (Case 401 in Kraus and Larson 1988a) with a natural erosion episode at Bethany Beach, Delaware, and found similar erosive geometry.

138. Sunamura and Maruyama (1987) estimated migration speeds for seaward moving bars as given by large wave tank experiments using monochromatic waves. The bars were generated by breaking waves and located somewhat shoreward of the break point (Greenwood and Davidson-Arnott 1975). They emphasized that spilling breakers could also form bars, although the approach to equilibrium was much slower than for bars formed by plunging breakers.

139. Kobayashi (1987) presented analytical solutions to idealized cases of dune erosion simplifying the governing equations to result in the heat diffusion equation (cf. Edelman 1969, 1973).

140. Hughes and Cowell (1987) studied the behavior of reflective beaches in southern Australia, in particular, changes in the foreshore step. The height of the beach step was correlated to the breaking wave height and the grain size where a larger wave height and a coarser grain size both produced a higher step.

141. Kriebel, Dally, and Dean (1987) performed laboratory experiments using a small wave tank and beach shapes designed with the dimensionless fall

speed as the scaling parameter. They found marked differences in profile response depending on the initial shape being planar or equilibrium profile type (Bruun 1954, Dean 1977). An initially plane beach produced a more pronounced bar and steeper offshore slopes. The fall speed parameter (Dean 1973) and the deepwater wave steepness were used to distinguish erosional and accretionary profiles using large wave tank data.

142. Mimura, Otsuka, and Watanabe (1987) performed a laboratory experiment with a small wave tank to investigate the effect of irregular waves on the beach profile. They addressed the question of which representative wave height to use for describing profile response. The mean wave height represented macroscopic beach changes such as bar and berm development most satisfactorily, whereas microscopic phenomena such as threshold of transport and ripple formation were better described by use of significant wave height.

143. Nishimura and Sunamura (1987) applied a numerical model to simulate a number of test cases from the large wave tank experiments by Kajima et al. (1983a). The cross-shore transport rate expression employed the Ursell number and a mobility parameter proposed by Hallermeier (1982). The numerical model had the capability of generating bars but failed to predict bar location.

144. Boczar-Karakiewicz and Davidson-Arnott (1987) proposed the non-linear interaction between shallow-water waves as a possible cause of bar formation. A mathematical model was developed to predict the generation of bars, and model results were compared with field data.

145. Kraus and Larson (1988a) described the large wave tank experiments on beach profile change performed by Saville (1957) and a similar experiment performed by the US Army Corps of Engineers, giving a listing of all the data.

146. Nairn (1988) developed a cross-shore sediment transport model involving random wave transformation. Two different methods of wave height transformation were investigated, namely using the root mean square wave height as a representative measure in the wave height calculations and the complete transfer of the probability density function based on the response of individual wave components.

147. Möller and Swart (1988) collected data on beach profile change on a natural beach at Oranjemund on the South West African coast during a severe

storm event. Artificial beach nourishment was carried out during the storm to prevent beach recession, and the event involved some of the highest loss rates recorded.

148. Seymour and Castel (1988) evaluated a number of cross-shore models (the concept of a model taken in a very general sense), focusing on their possibility of predicting transport direction. Of the models studied, the one proposed by Hattori and Kawamata (1981) proved to have the highest predictive capability when applying it to three different field sites. Most models were not considered successful at predicting transport direction.

149. Fenaish, Overton, and Fisher (1988) and Overton and Fisher (1988) studied dune erosion induced by swash action and developed a numerical model based on laboratory and field measurements. The amount of dune erosion during an event was linearly related to the summation of the impact force from the individual swashes.

150. Sunamura (in press) gave a comprehensive summary of beach profile morphology presenting quantitative relationships for many of the geometric parameters of the beach profile. Laboratory data were mainly used to derive the predictive equations. Furthermore, a descriptive model of three-dimensional beach change was proposed consisting of eight topographic stages delineated by a dimensionless quantity (breaking wave height squared to the product of gravitational acceleration, median grain size, and wave period squared).

## Synthesis of Previous Work

151. This section summarizes findings from previous work of particular relevance to this study. The role of breaking waves in bar formation was pointed out in pioneering field studies by Lehmann (1884), Hartnack (1924), Evans (1940), King and Williams (1949), and Shepard (1950). Numerous early laboratory investigations also showed that breaking waves were a main cause of bar genesis, e.g., Waters (1939), Keulegan (1948), Rector (1954), and Saville (1957). Wave breaking generates turbulent motion and provides the necessary mechanism for suspending and keeping sediment in suspension, thus mobilizing the grains for transport by mean currents. The importance of transport as

suspended load in the surf zone was emphasized by Dean (1973) and verified through measurements under prototype-scale laboratory conditions by Dette (1986) and under field conditions by Kraus and Dean (1987) among others.

152. Although profile change is highly stochastic on a microscale involving turbulence, movement of individual and collective grains, and various types of organized flows, if viewed on a macroscale, changes in the profile are surprisingly regular and consistent with respect to large features such as bars and berms. Several landmark studies, such as Keulegan (1945), Shepard (1950), Hands (1976), and Sunamura (in press) have characterized the geometry of morphologic features of beach profiles in the field. The possibility of successfully describing morphologic features under complex wave and water level conditions, as indicated by the above studies, formed much of the early foundation of the present study in the development of a numerical model of beach profile change.

153. It was shown by Sonu (1969), Short (1979), Sasaki (1983), Wright and Short (1984), and Sunamura (in press) that even very complex three-dimensional beach changes may be described by a small number of schematized beach states characterized by different values of one or two nondimensional parameters. Consequently, if the main processes of beach profile change are identified, response of the profile to wave and water level variations may be predicted based on semi-empirical relationships developed from relevant data.

154. Several criteria for delineating bar and berm profile response expressed in terms of wave and sediment properties have been proposed. The first criterion involved only wave steepness (Waters 1939, Scott 1954), whereas later-developed criteria included nondimensional quantities characterizing the beach sediment (Kemp 1961; Iwagaki and Noda 1963; Nayak 1970; Dean 1973; Sunamura and Horikawa 1975; Rushu and Liang 1986; Kriebel, Dally, and Dean 1987). The formation of bar and berm profiles is closely related to the direction of cross-shore transport. Criteria similar to those used to distinguish between bar and berm formation have been applied to determine transport direction (Rector 1954, Hattori and Kawamata 1979).

155. The existence of an equilibrium profile, a profile of constant shape which is approached if exposed to fixed wave and water level conditions, was proven to be a valid concept under laboratory conditions by Waters (1939),

Rector (1954), and Swart (1977). Bruun (1954) proposed a power law to relate water depth to distance offshore, which was given support by Dean (1977) on theoretical grounds. The empirical shape parameter in this simple power equation was related to grain size by Moore (1982).

156. Characteristics of cross-shore sand transport were studied first by Keulegan (1948) and King and Williams (1949) through trap measurements in laboratory wave tanks. By integrating the mass conservation equation between consecutive profiles in time, the net cross-shore transport rate distribution can be obtained, as discussed by van Hijum (1975, 1977); Watanabe, Riho, and Horikawa (1981); Kajima et al. (1983a, b); and Shimizu et al. (1985). Classification of the cross-shore transport rate distributions has been performed by Sawaragi and Deguchi (1981), Kajima et al. (1983a), and Shimizu et al. (1985).

157. Various formulas for predicting the cross-shore sand transport rate have been expressed in terms of local fluid velocity (Bagnold 1963, 1966; Bailard and Inman 1981); local shear stress (Madsen and Grant 1977, Shibayama and Horikawa 1980a, Watanabe 1982); and local energy dissipation per unit volume (Moore 1982, Kriebel 1982, Kriebel and Dean 1985a). A cross-shore transport equation based on energy dissipation per unit volume under breaking and broken waves was successfully applied in engineering numerical models for predicting beach profile change (Moore 1982, Kriebel 1982, Kriebel and Dean 1985a).

158. Several numerical models for predicting beach profile change have been developed, although few have been used for engineering predictions. Many of the earlier models included mechanisms for bar generation that did not explicitly assume breaking waves as the primary factor (Felder 1978, Nilsson 1979). Numerical models of profile change based on breaking waves as the cause of bar formation were developed by Dally (1980), Dally and Dean (1984), Moore (1982), Kriebel (1982), and Kriebel and Dean (1985a). At present, the most successful and widely used numerical model is that developed by Kriebel (1982) and Kriebel and Dean (1985a), and it has been applied to a number of sites along the U.S. coast (Kriebel and Dean 1985b, Kraus et al. 1988). However, this model does not incorporate bar formation and movement, nor does it simulate beach accretion.

159. In the present work, an empirically-based model of beach profile change is developed with the express aim of replicating the dynamics of macroscale features of bars and berms by using standard data available in most engineering applications.

## PART III: DATA EMPLOYED IN THIS STUDY

### Data Acquisition Approaches

160. Three approaches can be used to obtain data for studying beach profile change and the underlying physical processes; laboratory experiments using small wave tanks, field measurements, and experiments employing large wave tanks. For reference, a small wave tank is considered to generate wave heights on the order of 0.1 m, whereas wave heights on the order of 1 m can be generated in large wave tanks.

#### Small-scale laboratory approach

161. Numerous laboratory studies of beach profile change have been performed with small wave tanks (for example, Waters 1939, Bagnold 1940, Keulegan 1945, 1948, Nayak 1970, Rector 1954, Scott 1954, Watts 1954, Watts and Dearduff 1954, McKee and Sterrett 1961, Iwagaki and Noda 1963, Sunamura 1975, Sunamura and Horikawa 1975, Hughes and Chiu 1981, van Hijum and Pilarczyk 1982, Shibayama 1984). Such experiments have proven valuable for identifying potential parameters controlling beach change and qualitatively describing profile features. However, as demonstrated in a landmark paper by Saville (1957), in which profile change generated in small and large wave tanks was compared, a large scale effect is introduced through the magnitude of the wave height. Other independent variables may also produce a scaling distortion, and generally applicable scaling laws for interpreting results of small-scale movable bed models of beach change have yet to be determined (Hughes 1983, 1984, Sayao 1984, Vellinga 1984). Thus, data sets from laboratory experiments performed with small-scale facilities are of limited value for establishing quantitative understanding of profile change in nature.

#### Field approach

162. Field data sets useful for quantitative study of beach profile change are extremely rare because of the required high resolution in time and space of morphology and associated wave climate and water level. Because of the great spatial and temporal variability of waves and the three-dimensional character of nearshore bathymetry in the field, it is difficult to extract conclusive cause and effect relationships between waves and profile change

resulting solely from the wave-induced, cross-shore component of sediment transport. Recently, Birkemeier (1985a), Sallenger, Holman, and Birkemeier (1985), and Howd and Birkemeier (1987) have reported results from repetitive concurrent field measurements of the beach profile, waves, and water level. However, horizontal spacing between measurements along the profile was typically tens of meters, and the time interval between surveys was on the order of a half day to a week, during which wave conditions and water level varied substantially. Hands (1976) quantified several geometric properties of a longshore bar system in Lake Michigan but could not make direct correlations with the waves and water level due to a lack of measurements. Wright, Short, and Green (1985) made daily observations over 6-1/2 years of Narrabeen Beach, Australia, and related gross change in nearshore morphology to a single parameter, the dimensionless fall speed, discussed further below.

163. Several descriptive models of beach profile change have been developed based on field observations and measurements, but these are primarily statistical or conceptual and are not capable of quantitative prediction (e.g., Evans 1940; King and Williams 1949; Shepard 1950; Bascom 1951; Sonu 1969; Davis and Fox 1972; Davidson-Arnott 1975; Aubrey, Inman, and Nordstrom 1977; Owens 1977; Short 1979; Sasaki 1983; Takeda 1984; Wright and Short 1984; Wright, Short, and Green 1985; Wright et al. 1986; Sunamura in press).

Prototype-scale laboratory approach

164. The third approach available for quantitative investigation of beach profile change is use of large wave tanks (LWT). Such facilities enable controlled reproduction of near-prototype conditions of beach slope, wave height and period, turbulence induced by wave breaking, and resultant sediment transport and beach change. The problem of scaling is eliminated, and the required high resolution measurement of the profile can also be attained. Disadvantages associated with wave tanks include contamination by reflection from the beach and wave generator and formation of wave harmonics (Buhr Hansen and Svendsen 1975). Experience suggests that these factors are negligibly small under reasonable experiment design.

165. Experiments using LWTs have been performed with monochromatic waves (Saville 1957; Caldwell 1959; Kajima et al. 1983a, b; Dette and Uliczka 1987a; Kraus and Larson 1988a) and irregular waves with random heights and

periods (Vellinga 1986, Dette and Uliczka 1987b, Uliczka and Dette 1987). Irregular waves will most closely reproduce naturally occurring profile change. Mimura, Otsuka, and Watanabe (1987) compared beach change produced in a small laboratory wave tank by irregular waves and corresponding representative monochromatic waves. They found that macroscale patterns of profile change, such as bar and berm development, were similar if representative monochromatic waves were chosen as the mean wave height and period of the irregular wave train. On the other hand, microscale features, such as initiation of sand motion and ripple size, were best described by the significant wave height. Properties compared included profile morphology, cross-shore sand transport rate, and critical depth for sediment motion.

166. Irregular waves introduce additional independent parameters associated with the wave spectrum, whereas in monochromatic wave tests the effects produced by the basic parameters of wave height and period can be isolated and systematically investigated. Hughes and Chiu (1981) discuss theoretical and practical problems associated with use of irregular waves in movable bed modeling. At this first stage of quantification of prototype beach change, it is probably most fruitful to examine the response of the profile to elemental, monochromatic waves.

167. Recently, two independent data sets on beach profile change have become available from experiments performed using LWTs and monochromatic waves (Kajima et al. 1983a, 1983b, Kraus and Larson 1988a). These experiments involved combinations of waves, water levels, beach slopes, and sands of the scale that exist in the field, but with the advantages of true two-dimensionality, control of the external (wave) force, and an optimized measurement schedule. These data sets formed the core data for this study and are described next.

## Laboratory and Field Data Sets

### Laboratory data

168. Two data sets on beach profile change generated in experiment programs using LWTs were employed. These independent data sets allowed systematic examination of profile evolution through time for a wide range of

realistic incident wave heights and periods, water levels, initial beach slopes, and sand grain sizes. The LWT facilities generated monochromatic waves, so that phenomena associated with random waves as occur in nature, such as wave grouping and long period wave motion, were absent. This simplification is viewed as an asset in the present study, allowing focus on transport produced solely by short-period incident waves without ambiguities.

169. One data set was obtained in experiments performed by the US Army Corps of Engineers (CE) in the years 1956-1957 and 1962 (Saville 1957, Caldwell 1959, Kraus and Larson 1988a) at Dalecarlia Reservation, Washington, DC. The second data set pertains to experiments performed at the Central Research Institute of Electric Power Industry (CRIEPI) in Chiba, Japan (Kajima et al. 1983a, b).

CE experiments

170. The CE experiments were performed using American customary units. Conversion is made here to metric units to achieve generality, but customary units are retained for equipment specifications. The concrete tank used was 193.5 m long, 4.6 m wide, and 6.1 m deep (635 x 15 x 20 ft). The standard operating depth of the tank was 4.6 m (15 ft), which required a water volume of approximately 3,800 $m^3$. A mobile instrument carriage mounted on rails on top of the tank carried equipment and personnel for making measurements. A picture of the CE tank is displayed in Figure 2, in which the wave generator and instrument carriage are seen at the far end of the tank.

171. The wave generator consisted of a vertical bulkhead 4.6 m (15 ft) wide and 7.0 m (23 ft) high mounted on a carriage which moved back and forth on rails to create the wave motion. The carriage was given oscillatory movement by arms 13 m in length (42 ft 9 in.), connected to two driving discs. Each disc was 5.8 m (19 ft) in diameter, weighed 12.7 tons, and was driven through a train of gears by a 510-hp variable speed electric motor. Wave periods between 2.6 and 24.8 sec could be generated by a gearing mechanism, and the maximum usable wave height at the standard operating depth was approximately 1.8 m (6 ft). Figure 3 gives a view of the wave generator, where the bulkhead is seen in the front of the picture and the two rotating discs are distinguished in the back. The experimental facility is further described by Raynor and Simmons (1964) and Kraus and Larson (1988a).

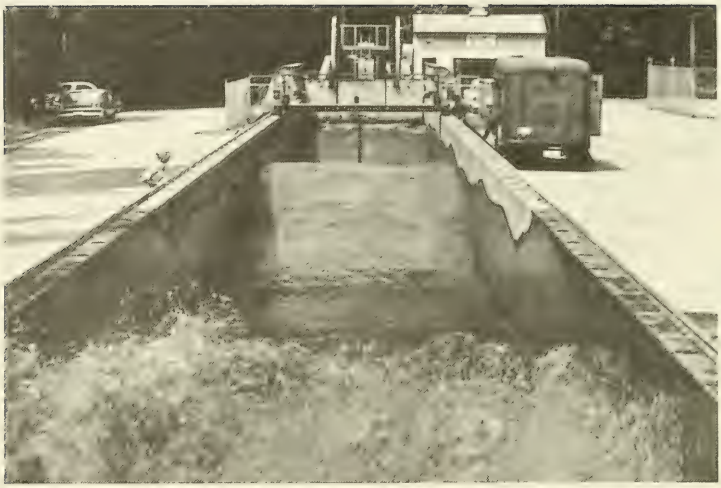

Figure 2. Tank for Large Waves at Dalecarlia Reservation

172. Eighteen distinct cases have been documented (see Kraus and Larson 1988a) of which all but two were started from a plane slope of 1:15. Approximately 1,500 $m^3$ of sand were needed to grade the plane initial slope, which was done with a small bulldozer. The wave parameters ranged from periods between 3.75 and 16.0 sec and generated wave heights between 0.55 and 1.68 m in the horizontal part of the tank. The wave height, wave period, and water depth were held constant during a run, except in one case for which the water level was varied to simulate a tide. The water depth ranged from 3.5-4.6 m in the different cases, and two grain sizes were used with median diameters of 0.22 and 0.40 mm. The 0.22-mm grain size was employed in the 1956-57 experiments, and the 0.40-mm grain size was used in the 1962 experiments. The specific gravity of the sand grains was 2.65. Waves were run until a stable beach profile had developed and no significant changes were detected, which normally occurred after 40-60 hr. The term "case" will be used to describe a

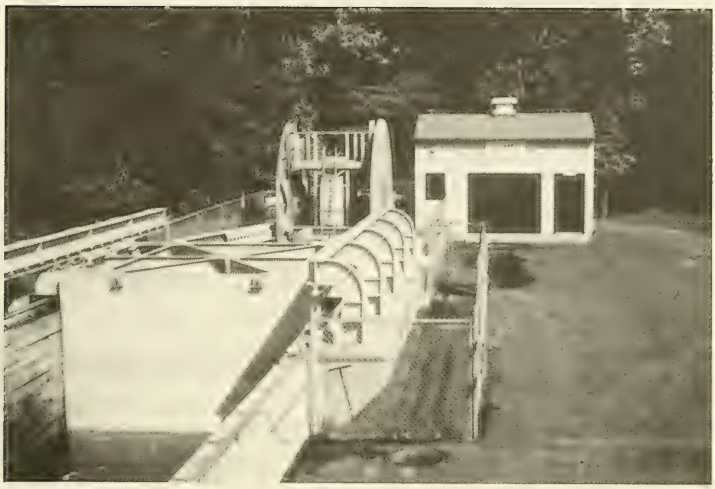

Figure 3. View of the wave generator in the LWT

collection of profile surveys for a unique combination of incident waves, beach slope, and grain size. A "run" is more loosely used to refer to either a case or an interval of wave action between two profile surveys.

173. Profile surveys were made intermittently during a run with shorter time increments in the beginning when large profile changes where expected. On the order of 10-15 profile surveys were made during a typical case, and the survey interval was 1.2 m (4 ft). For the initial cases with the 0.22-mm sand and all cases with the 0.40-mm sand, profiles were surveyed along three different lines in the tank*. Corresponding differences in depth between the three lines were small, and for the 0.22-mm sand only the survey along the center line was retained. However, for the 0.40-mm sand, although the cross-tank depth difference was small, surveys along three lines were made through

* Personal Communication, 1986, George W. Simmons, Former Engineering Technician, Beach Erosion Board, Dalecarlia Reservation, Washington, DC.

the entire experiment series, and the profile depths used in this report are an average of the three lines.

174. The numbering of the CE cases is discussed by Kraus and Larson (1988a) and essentially agrees with the system used by Hallermeier (1987). Table 1 summarizes the CE cases which started from a plane slope of 1:15, giving the wave and water level conditions. The deepwater wave steepness is also listed and was calculated using linear wave theory. Two cases not given in Table 1 were conducted from an initial profile that was irregular (Cases 510 and 610). Also, a repetition run was performed for Case 100 (Case 110), and satisfactory agreement was achieved between the two cases (Saville 1957). In Case 911 the water level varied stepwise in a sinusoidal manner, but the wave and sand parameters were identical to those in Case 901. The period of the water level variation was approximately 12 hr, the amplitude 0.45 m, and the mean water level 3.96 m.

175. The wave height was measured with a step resistance gage placed in a fixed position at the toe of the beach during the experiments. The incident wave was measured before any reflection occurred against the wave paddle. The accuracy of the wave measurements was about 3 cm (0.1 ft), and the wave period was quite accurately set due to the large stroke length of the wavemaker and fixed gear ratio. For most of the cases the breaking wave height and breaker location were estimated visually at specific times during a run.

CRIEPI experiments

176. The CRIEPI LWT is similar in size to the CE LWT, except that it is somewhat narrower (205 x 3.4 x 6 m). The experiment program consisted of 24 cases with wave periods ranging between 3.0 and 12.0 sec and generated wave heights between 0.3 and 1.8 m. A summary of the CRIEPI cases is given in Table 2, in which the numbering is identical to that used by Kajima et al. (1983b). All CRIEPI cases were performed with monochromatic waves and fixed water level. Many of the cases started from a plane beach slope (17 of the 24), but the initial slope was varied, ranging from 1:50 to 1:10 in individual cases.

177. As in the CE experiments, two different grain sizes were used, 0.27 mm and 0.47 mm. For the present study the CRIEPI profile survey was digitized from charts enlarged from those given by Kajima et al. (1983b) with

Table 1

CE Experiments: Wave Height, Wave Period, and Water Depth in the Horizontal Section of the Tank and Deepwater Wave Steepness

| Case No. | Wave Height m | Wave Period sec | Water Depth m | Deepwater Wave Steepness |
|---|---|---|---|---|
| | | 0.22-mm Sand | | |
| 100 | 1.28 | 11.33 | 4.57 | 0.0054 |
| 200 | 0.55 | 11.33 | 4.57 | 0.0023 |
| 300 | 1.68 | 11.33 | 4.27 | 0.0070 |
| 400 | 1.62 | 5.60 | 4.42 | 0.0351 |
| 500 | 1.52 | 3.75 | 4.57 | 0.0750 |
| 600 | 0.61 | 16.00 | 4.57 | 0.0011 |
| 700 | 1.62 | 16.00 | 4.11 (3.81)* | 0.0028 |
| | | 0.40-mm Sand | | |
| 101 | 1.28 | 11.33 | 4.57 | 0.0054 |
| 201 | 0.55 | 11.33 | 4.57 | 0.0023 |
| 301 | 1.68 | 11.33 | 4.27 | 0.0070 |
| 401 | 1.62 | 5.60 | 4.42 | 0.0351 |
| 501 | 1.52 | 3.75 | 4.57 | 0.0750 |
| 701 | 1.62 | 16.00 | 3.81 | 0.0028 |
| 801 | 0.76 | 3.75 | 4.57 | 0.0377 |
| 901 | 1.34 | 7.87 | 3.96 | 0.0129 |
| 911 | 1.34 | 7.87 | 3.96** | 0.0129 |

* Water level decreased after 10 hr.
** Mean of variable water level.

Table 2

CRIEPI Experiments: Wave Height, Wave Period, and Water Depth in the Horizontal Section of the Tank, Initial Beach Slope, and Deepwater Wave Steepness

| Case No. | Wave Height m | Wave Period sec | Depth m | Beach Slope | Deepwater Wave Steepness |
|---|---|---|---|---|---|
| | | | 0.47-mm Sand | | |
| 1-1 | 0.44 | 6.0 | 4.5 | 1/20 | 0.0082 |
| 1-3 | 1.05 | 9.0 | 4.5 | 1/20 | 0.0075 |
| 1-8 | 0.81 | 3.0 | 4.5 | 1/20 | 0.0607 |
| 2-1 | 1.80 | 6.0 | 3.5 | 3/100 | 0.0313 |
| 2-2 | 0.86 | 9.0 | 3.5 | 3/100 | 0.0058 |
| 2-3 | 0.66 | 3.1 | 3.5 | 3/100 | 0.0473 |
| | | | 0.27-mm Sand | | |
| 3-1 | 1.07 | 9.1 | 4.5 | 1/20 | 0.0074 |
| 3-2 | 1.05 | 6.0 | 4.5 | 1/20 | 0.0196 |
| 3-3 | 0.81 | 12.0 | 4.5 | 1/20 | 0.0029 |
| 3-4 | 1.54 | 3.1 | 4.5 | 1/20 | 0.108 |
| 4-1 | 0.31 | 3.5 | 3.5 | 3/100 | 0.0178 |
| 4-2 | 0.97 | 4.5 | 4.0 | 3/100 | 0.0335 |
| 4-3 | 1.51 | 3.1 | 4.0 | 3/100 | 0.107 |
| 5-1 | 0.29 | 5.8 | 3.5 | 1/50 | 0.0057 |
| 5-2 | 0.74 | 3.1 | 3.5 | 1/50 | 0.0533 |
| 6-1 | 1.66 | 5.0 | 4.0 | 1/10 | 0.0456 |
| 6-2 | 1.12 | 7.5 | 4.5 | 1/10 | 0.0125 |

a length increment of 0.5 or 1.0 m depending on the resolution necessary to distinguish principal features of the profile shape. The accuracy of the digitization is judged to be compatible with the profile surveys of the CE data, which is on the order of ± 1.5 cm in the vertical coordinate. No attempt was made to distinguish small-scale profile features such as ripples.

178. In the CRIEPI experiments wave height along the profile was measured from a vehicle mounted on rails on top of the tank. To confirm the two-dimensionality of the experiment, profiles were surveyed along three lines in the tank during the first few runs. Because the depth difference was small between the three survey lines, only the center line was surveyed in later cases (Kajima et al. 1983a). Wave measurements were usually carried out between profile surveys, and wave setup was determined. Plunging, spilling, and surging breaking waves were observed, although plunging breakers occurred in the majority of cases. Cases started from nonplanar bottom (in most cases the beach profile that remained from the previous test case) are not included in Table 2, namely Cases 1-2, 1-4, 1-5, 1-6, 1-7, 4-4, and 6-3.

Field data

179. At the Field Research Facility (FRF) of the Coastal Engineering Research Center (CERC) located at Duck, North Carolina, profile surveys are made regularly together with measurements of the wave and water level climate. During the period 1981-1984, four shore-normal profile lines (Lines 58, 62, 188, and 190) were surveyed approximately every 2 weeks with a typical spacing between survey points of 10 m (Howd and Birkemeier 1987).

180. Wave data are tabulated at 6-hr intervals based on a 20-min record at a wave gage (Gage 620) located at the end of the research pier, and data are simultaneously collected by a Waverider buoy off the end of the pier in 18 m of water (Gage 625). Water level is measured at 6-min intervals by a tide gage mounted at the end of the pier, and the record consists of the total change, including both tide and storm surge. Water level measurements used in the present study are averages over 1-hr intervals.

181. The profile change data set from the FRF is the most detailed known, encompassing profile surveys, water level, and wave data, and showing both seasonal and short-term changes in the beach profile. The FRF data set was primarily used for verifying the numerical model of beach profile change.

Summary

182. Use of two independent data sets from LWT studies is expected to increase reliability of relationships derived between the incident waves and features of the beach profile. Also, by restricting consideration to data from LWT experiments (as opposed to small-scale experiments), it is believed that scaling effects are eliminated and that the processes occurring during bar and berm formation in the field are closely reproduced in the wave tanks. Relationships developed from the LWT experiments can then be assessed for their applicability to the field by use of the quality FRF data set.

## PART IV: QUANTIFICATION OF MORPHOLOGIC FEATURES

183. The literature review presented in Part II revealed the remarkable fact that relatively few studies have been made to quantitatively characterize the shape of the beach profile. Even fewer studies have attempted to deterministically describe the response of the profile to the waves incident upon it. Development of a quantitative description of the observed dynamics of the profile in terms of the incident waves, therefore, appeared to be a valuable approach with which to begin this investigation, as well as a logical and necessary one in the path toward development of a predictive model of profile change. Precise knowledge of the morphology and dynamics of the profile is necessary both for understanding of the subject being studied and development of the predictive model.

184. As discussed in Part I, at this first stage of developing a quantitative deterministic description of the beach profile and its change, use of data obtained in experiments performed with large wave tanks was judged to be the best approach. The experiment condition of regular waves is considered an advantage for isolating the effect of breaking waves on the beach. The authors believe this to be the dominant process producing bar formation and much of the change in the beach profile under most environmental conditions. Solid understanding of profile change produced by breaking waves will further understanding of other possible contributing processes, since in nature all forcing agents act concurrently and their individual contributions are difficult to distinguish. Firm knowledge of one will aid in understanding the others.

185. The main purpose of the analysis described in this chapter is to establish the most important parameters governing beach profile evolution in terms of the wave and sediment characteristics. This procedure is expected to provide fundamental information on the response of the profiles and facilitate a physically based approach for development of the numerical model. The results are of interest in themselves in understanding beach profile response as well as for computation of cross-shore sand transport rates and profile change. Clear connections between cause (waves) and effect (profile change) as elucidated in the large wave tanks is expected to provide guidance for

applying a similar approach in analysis of field data where profile change is produced by the combination of a number of different forcing agents and is prone to ambiguity.

## Data Analysis Procedure

186. In this study, morphologic profile features of interest are formations created by wave action, directly or indirectly, during time scales much greater than the wave period. To numerically evaluate properties of morphologic features, the survey data were approximated by a set of cubic spline polynomials, producing on the order of 75-250 polynomials per profile. This representation allowed geometric properties such as volumes, distances, depths, and slopes to be determined analytically once the spline coefficients were calculated. Also, by using the interpolation polynomials, a continuous and accurate description of the profile depth with distance offshore was obtained from the discrete depth values at survey points.

187. A fundamental problem immediately encountered in quantitative analysis of a morphologic feature is specification of an unambiguous definition that will preserve the characteristics intuitively associated with it. For example, a bar is normally considered to be a subaqueous accretionary feature formed of sand redistributed and deposited along the profile. From observation of a natural barred beach profile it is easy to determine the crest of a bar and hence the approximate location of the bar, whereas it is much more difficult to define or agree upon the exact cross-shore length of a bar, a quantity which is needed if a volume calculation is to be done. Keulegan (1945) used the concept of a barless beach profile to which bar properties could be referenced. The barless profile is constructed by drawing lines joining maximum trough depths along the profile with the point of zero depth. Apart from the arbitrary nature of this definition, it is sometimes difficult to determine the seaward limit of the bar by this method.

188. Use of points where the second derivative (radius of curvature) is zero to define a bar is found to be convenient if applied on the shoreward side of a bar, where the curvature of the profile changes sign going from

trough to crest. However, often no such point exists on the seaward side of a bar since an immediate trough may not be present.

189. In the present study, it was found most natural and productive to define morphologic features with respect to the initial profile, since a time sequence of profiles was available. This procedure is, of course, not directly applicable to the field. Areas where sand accretes with respect to the initial profile constitute bar- or berm-like features, whereas areas where material erodes are trough-like in appearance. Figure 4a shows a definition sketch for a beach profile with representative bar and trough features, and Figure 4b illustrates the corresponding berm case. Nomenclature describing the geometric properties is given in the figures, and a typical wave height envelope is outlined in Figure 4a.

190. As a result of relating bar properties to the initial profile, some properties, such as bar volume, will depend on the initial profile slope. For example, two erosional profiles formed of sand of the same grain size and exposed to the same wave climate will show different equilibrium bar properties if the initial slopes differ. However, the inshore slopes of the equilibrium profile will still be similar (Kamphuis and Bridgeman 1975), but different amounts of material will be redistributed within the profile. In this respect, bar volume is a function of initial profile slope, which makes such a definition less useful in field data analysis for some bar properties.

191. Definition of morphologic features with respect to the initial profile does not affect net sand transport rate distributions, which only depend upon two consecutively surveyed profiles in time, as will be shown. Furthermore, the main objective of the data analysis is to identify the dominant factors of beach profile change, supporting development of the numerical model. These factors can be distinguished with any reasonable if arbitrary definition of the profile features if it is consistently applied through time. For example, the aforementioned bar definition of Keulegan (1945) would give different values of bar volume with time, but the trend of bar development toward equilibrium and the factors controlling its growth would be similar to those determined by the definition employed here.

192. Only those cases in the data base with an initially plane profile slope were used in calculation of morphologic features to more easily allow

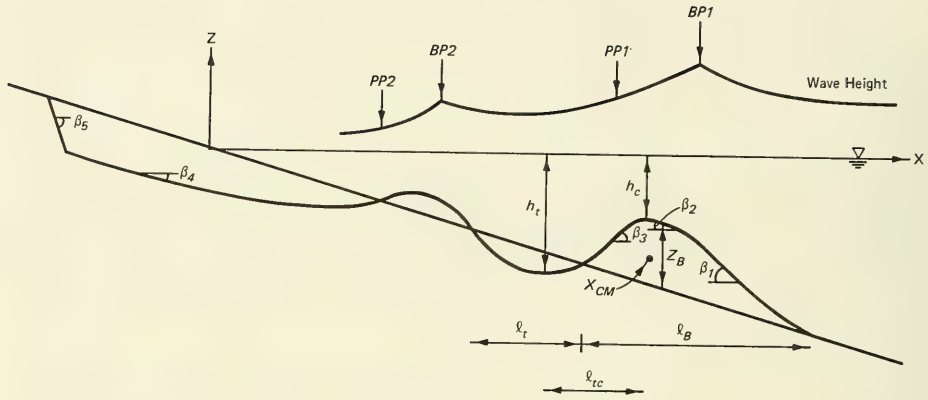


a. Bar profile

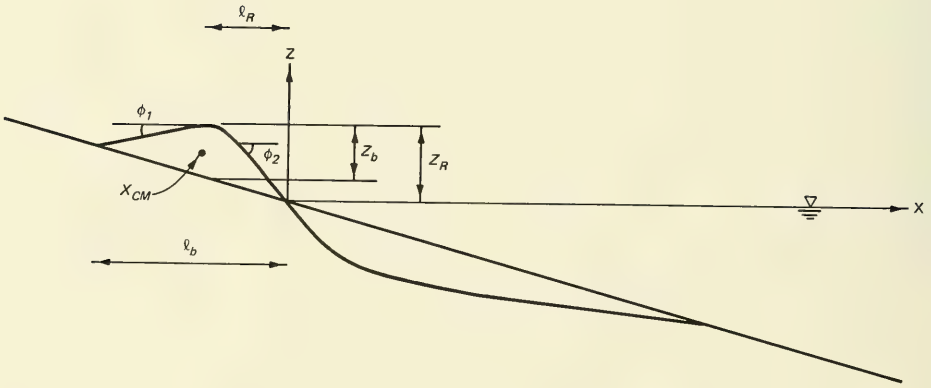


b. Berm profile

Figure 4. Notation sketch for beach profile morphology

comparison among various cases and to more clearly identify relationships between wave parameters and beach profile evolution. Definition of morphologic features with respect to the initial profile involves no limitations in characterizing the behavior of the features or understanding the fundamentals of profile response to wave action. Rather, a clear definition allows strict interpretation of where a bar, berm, or trough is located. Definition of a morphologic feature related to a specific profile has no meaning if a single profile is studied. The objective here is not to advocate a general definition of a bar or other feature applicable to an arbitrary beach profile but to employ a useful definition as a means for understanding the process of beach profile change and facilitating a quantitative description of the dynamic response of morphologic features.

193. An extensive correlation and regression analysis was carried out to investigate relations between geometric properties of the various morphologic features of the profile and the wave and sand characteristics. An overview of the statistical procedures used is given in Appendix A. The primary parameters used were: wave period $T$ or deepwater wavelength $L_o$, deepwater wave height $H_o$, breaking wave height $H_b$, water depth $h$, median grain size $D$, sand fall speed $w$, and beach slope $\tan\beta$. Also, various nondimensional quantities were formed, both for deepwater and breaking wave conditions, such as $H/L$, $H/wT$, $\tan\beta/(H/L)^{1/2}$, $D/H$, and $D/L$, in which $H$ and $L$ are the local wave height and wavelength, respectively.

## Concept of Equilibrium Beach Profile

194. A fundamental assumption in the study of beach profile change is the existence of an equilibrium profile which a beach will attain if exposed to constant wave conditions for a sufficiently long time. The idea is that the beach profile in its equilibrium state dissipates incident wave energy without significant net change in shape. If an equilibrium profile did not exist, the beach would continue to erode (or accrete) indefinitely if exposed to the same wave conditions and with no restrictions in the sand supply.

195. The concept of an equilibrium profile is an idealization that cannot be fully achieved in practice, since waves, water level, water tempera-

ture, and other conditions cannot be held perfectly fixed. Also, wave breaking and turbulence formed at the bottom and injected from the surface by wave breaking introduce randomness in the microscale sand motion, with resultant small continuous adjustments of the profile. Nevertheless, at a macroscale level, it has been demonstrated that an equilibrium profile can be approached, in which no significant systematic net sand transport occurs, although small perturbations still remain. Numerous laboratory studies (e.g., Rector 1954, Nayak 1970, Swart 1975) as well as the data used in this study support the equilibrium beach profile concept, since profile changes diminish with time and the beach profile approaches a stable shape.

196. From a theoretical viewpoint, it is of minor importance if the equilibrium profile is never realized in the field due to variable waves and water level, and complex three-dimensional hydrodynamic processes, as long as the concept is verified by experiment. Of course, from a practical point of view, it is of great significance if a natural beach of a certain representative grain size has a preferred shape under a given wave climate.

197. As an indicator of the approach of the beach to an equilibrium shape, cumulative change along the profile was calculated. Cumulative change was defined as the sum of the absolute differences in bottom elevation between initial profile and profile at a specific time (see also Shimizu et al. 1985). This quantity is plotted in Figure 5 for selected CE and CRIEPI cases.

198. The cumulative profile change will ideally approach a constant value under constant applied waves as the beach profile attains the equilibrium shape. The decrease in slope of the curves in Figure 5 is a measure of the rate at which equilibrium is approached. Some transport activity will always exist because of unsteadiness in experiment conditions, fluid turbulence, and random character of sand motion, and thus profile change will fluctuate about the equilibrium shape. Some cases exhibited cumulative change which had not completely leveled off at the end of the run, but the rate of change was still an order of magnitude smaller than the initial rate. Decreasing rates of accumulated profile change indicate an increasingly stable shape since less material was redistributed along the profile at later times.

199. A greater difference between initial profile and equilibrium profile for a specific wave climate and grain size implies that a greater

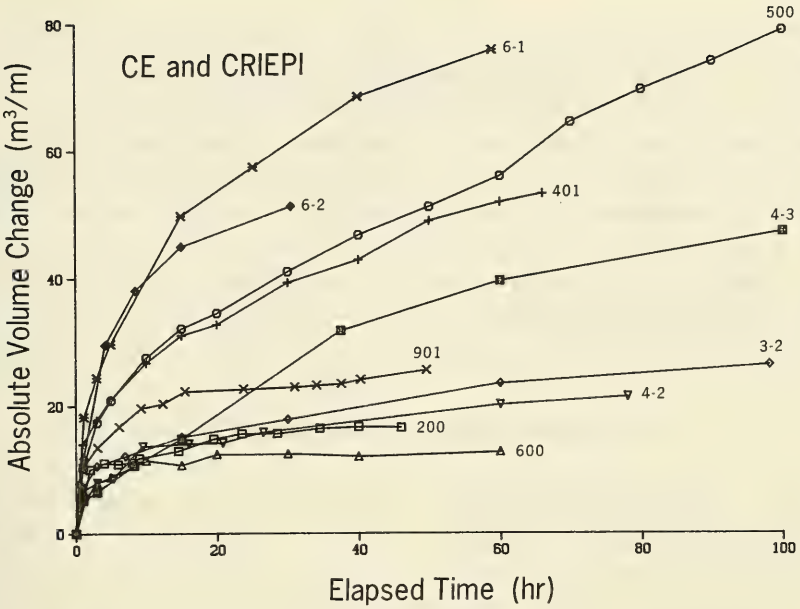


Figure 5. Absolute sum of profile change for selected cases

amount of sand must be redistributed in the process of reaching equilibrium. Dean (1977) derived a simple analytical expression for the beach profile shape in the surf zone based on the concept of a constant dissipation of wave energy per unit water volume. This expression agrees well with the relationship established by Bruun (1954) on empirical grounds from field data. The equilibrium beach profile shape may be written

$$h = Ax^{2/3} \tag{1}$$

where

h = water depth

A = shape parameter

x = cross-shore coordinate (directed positive in the seaward direction)

The shape parameter is mainly a function of grain size, in which a coarser grain size gives a larger value of A and a steeper beach (Dean 1977, Moore 1982). Dean (1987) recently reexpressed the curve of Moore (1982) in terms of

the dimensionless sediment fall speed $H/wT$, in which $H$ is the local wave height, $w$ is the sand fall speed, and $T$ is the wave period.

200. For an equilibrium profile developed during a storm, during which a bar normally forms in the vicinity of the break point, Equation 1 is expected to apply only to the portion of the surf zone shoreward of the bar, where strong turbulence is present and energy dissipation is related to the breaking wave height and water volume. If wave reformation occurs, several areas along the profile may exist in which profile change is controlled by energy dissipation per unit volume, and the profile in these areas is expected to be well approximated by Equation 1.

## Criteria for Distinguishing Profile Response

201. If a beach profile is not in equilibrium with the waves incident upon it, sand will be redistributed as the beach adjusts toward equilibrium shape. Depending on the wave conditions, existing profile shape, and sand properties, the cross-shore sand transport rate will be predominantly directed either offshore or onshore. Offshore transport results in erosion on the upper part of the profile and formation of a notable bar at the break point(s), whereas onshore transport leads to accretion of sand on the foreshore and berm buildup. These two types of profile response forming two distinctly different beach shapes are commonly known as bar/berm profiles (other descriptions are: winter/summer profile, storm/normal profile, erosional/accretionary profile, bar/step profile, bar/nonbarred profile, dissipative/reflective profile).

202. Criteria to distinguish bar and berm profiles have been developed by various authors, and Table 3 gives a summary of several criteria developed for distinguishing beach erosion and accretion or bar/berm profile response which will be discussed below. Note that the criteria of Rector (1954), Dean (1973), and Hattori and Kawamata (1981) originally referred to the direction of cross-shore transport.

Table 3

Criteria for Classifying Bar and Berm Profiles
Erosion and Accretion

| Author | Parameters* | Comments |
|---|---|---|
| Waters (1939) | $H_o/L_o$ | $H_o/L_o > 0.025$, bar<br>$H_o/L_o < 0.025$, berm |
| Rector (1954) | $H_o/L_o$, $D/L_o$ | $D/L_o < 0.0146(H_o/L_o)^{1.25}$, bar<br>$D/L_o > 0.0146(H_o/L_o)^{1.25}$, berm |
| Iwagaki and Noda (1963) | $H_o/L_o$, $H_o/D$ | Graphically determined |
| Nayak (1970) | $H_o/L_o$, $H_o/SD$ | Graphically determined |
| Dean (1973)<br>Kriebel, Dally, and Dean (1987) | $H_o/L_o$, $\pi w/gT$ | $H_o/L_o > A\pi w/gT$, bar<br>$H_o/L_o < A\pi w/gT$, berm<br>A = 1.7, mainly lab scale<br>A = 4-5, prototype scale |
| Sunamura and Horikawa (1975)<br>Sunamura (1980) | $H_o/L_o$, $D/L_o$, $\tan\beta$ | $H_o/L_o > C(\tan\beta)^{-0.27}(D/L_o)^{0.67}$ (bar)<br>$H_o/L_o < C(\tan\beta)^{-0.27}(D/L_o)^{0.67}$ (berm)<br>(C = 4, small-scale lab. regular waves; C = 18, field) |
| Hattori and Kawamata (1981) | $(H_o/L_o)\tan\beta$, $w/gT$ | $(H_o/L_o)\tan\beta > 0.5\ w/gT$, bar<br>$(H_o/L_o)\tan\beta < 0.5\ w/gT$, berm |
| Wright and Short (1984) | $H_b/wT$ | $H_b/wT > 6$, bar<br>$H_b/wT = 1$-6, mixed bar and berm<br>$H_b/wT < 1$, berm |
| Present Work | $H_o/L_o$, $H_o/wT$ | $H_o/L_o < M\ (H_o/wT)^3$, bar<br>$H_o/L_o > M\ (H_o/wT)^3$, berm<br>(M = 0.0007 regular waves in lab., or mean wave height in field) |

* Notation: $H_o$, deepwater wave height; $L_o$, deepwater wavelength; D, median grain size; S, specific gravity of sand; w, sand fall speed; g, acceleration of gravity; T, wave period; $\tan\beta$, beach slope; $H_b$, breaking wave height.

Regular waves

203. Examination of cross-shore transport rate distributions inferred from successive profile change (Part V) shows that development of a bar or a berm profile is closely related to the direction of net transport as offshore or onshore, respectively. Thus, a criterion for predicting bar or berm development can also be applied to predict the principal direction of net cross-shore transport. Typically, if a bar forms, the main direction of transport is offshore even if the bar receives a net contribution from the shoreward transport of material originating from areas seaward of the bar (in the situation of a relatively mild wave climate). A criterion which refers to onshore/offshore transport will, in most cases, predict offshore-directed sand movement if a bar is present and onshore-directed movement if a berm is present. However, profiles between bar and berm type may have complex transport distributions where a clear trend for onshore or offshore transport is not apparent. This more complex transport pattern and resultant profile change are left for future study and not pursued further here.

204. From his laboratory experiments performed at small scale, Waters (1939) (summarized in Johnson 1949) found that deepwater wave steepnesses $H_o/L_o$ greater than 0.025 produced a bar profile, whereas values less than 0.025 produced a berm profile. (Waters (1939) used the terminology storm/ordinary profile.) This convenient rule of thumb is still commonly applied to the field situation, but it is known to be incorrect for waves of prototype scale, as first pointed out by Saville (1957). Rector (1954) recognized the occurrence of a transition zone between bar and berm profiles defined by wave steepness values in the range of 0.016-0.025 (for small laboratory waves). Rector (1954) also developed an empirical equation for predicting cross-shore transport direction based on wave steepness and the ratio of median grain size to deepwater wavelength $D/L_o$ .

205. Kemp (1961) defined a "phase difference" parameter in terms of the uprush time (time for the wave to travel from the break point to the limit of uprush) and the wave period. The transition from a berm to a bar profile was considered to occur if the uprush time equalled the wave period. (Kemp (1961) used the terminology bar/step profile.)

206. Iwagaki and Noda (1963) used a combination of two nondimensional parameters, $H_o/L_o$ , and the ratio between deepwater wave height and median grain diameter, $H_o/D$ , to predict erosion and accretion (bar/berm formation). Nayak (1970) approached the problem in a fashion similar to that of Iwagaki and Noda (1963) but included the specific gravity in the denominator of $H_o/D$ .

207. Dean (1973) developed a popular heuristic model of sand transport in which most of the cross-shore transport in the surf zone is assumed to occur as suspended load, by which the sediment fall speed emerges as a significant parameter. The bar/berm predictive criterion developed by Dean (1973) is expressed in terms of $H_o/L_o$ and $\pi w/gT$ , in which $g$ is the acceleration due to gravity. Dean (1973) also introduced the dimensionless fall speed parameter $H/wT$ in a conceptual model of suspended sediment movement and developed it as an indicator of cross-shore transport direction. Gourlay (1968), Nayak (1970), and Kohler and Galvin (1973) also used the fall speed parameter as a descriptor of beach profile processes, based mainly on dimensional considerations.

208. Sunamura and Horikawa (1975) and Sunamura (1980) used three parameters in their criterion to predict erosion and accretion, $H_o/L_o$ , $D/L_o$ , and beach slope, $\tan\beta$ . Different values of the empirical coefficient in the equation delineating erosion and accretion (bar/berm profiles) were obtained for laboratory and field conditions, and it is of interest that the same functional form of the equation proved valid for both situations.

209. Hattori and Kawamata (1981) developed a criterion for onshore and offshore sand transport based on parameters essentially identical to those used by Dean (1973), except that the initial beach profile slope was combined with the wave steepness parameter.

210. In a milestone experiment using the first LWT in the world, Saville (1957) recognized that the deepwater wave steepness criterion of 0.025 was not accurate for distinguishing bar and berm profiles as produced by large waves in the field. For his LWT experiments, which used regular waves, bar profiles occurred at much smaller values of wave steepness (as small as 0.0028 in the CE experiments), whereas corresponding cases scaled down to 1:10 experienced marked berm buildup.

211. In a study of criteria for the occurrence of bar/berm profiles performed as part of the present work, the deepwater wave steepness $H_o/L_o$ and the dimensionless fall speed parameter $H_o/wT$ were found to be the most reliable parameters. Figure 6 is a plot of the LWT data on profile response as bar or berm (erosion or accretion) together with a line drawn by inspection to best separate the erosional and accretionary cases. This line defines an empirical criterion in terms of the two parameters given by the following equation:

$$\frac{H_o}{L_o} = M \left[ \frac{H_o}{wT} \right]^3 \tag{2}$$

in which the empirical coefficient $M = 0.00070$.

212. In classification of the different cases, only prominent features of the profile were considered. For example, a small berm which formed on the foreshore was ignored if a large bar also formed, since the main transport direction during the run was obviously offshore. In such a case, the profile was considered to be a bar profile. Similarly, a small bar may have formed close to the break point in a case where the main trend of transport was onshore by which large berm buildup occurred. The classification of the beach profile response determined here coincides with that used by Kriebel, Dally, and Dean (1987), except for two cases which were designated as mixed response by those authors but as berm type in this study. Similarity in classification indicates that results were not strongly influenced by subjectivity.

213. As an alternative to use of the dimensionless fall speed parameter, the parameter $H_o/D$ suggested by Iwagaki and Noda (1963) and formulated based on small-scale laboratory data was combined with the deepwater wave steepness to yield a criterion for bar and berm profiles for the prototype-scale data. Figure 7 shows that a clear distinction results between bar and berm profiles. The line of delineation between bar and berm profiles is given by

$$\frac{H_o}{L_o} = 4.8 \; 10^8 \left[ \frac{H_o}{D} \right]^{-3.05} \tag{3}$$

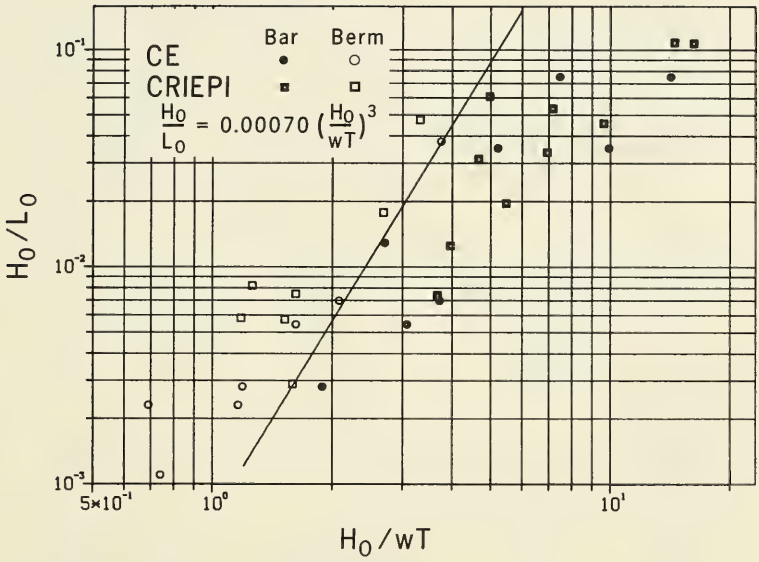


Figure 6. Criterion for distinguishing profile type by use of wave steepness and dimensionless fall speed parameter

214. Starting from the dimensionless fall speed parameter, Dean (1973) derived a criterion using $H_o/L_o$ and the parameter $\pi w/gT$ (Dean parameter). Figure 8 shows the CE and CRIEPI data classified according to these parameters. The equation of the separation line (Line B) is

$$\frac{H_o}{L_o} = 5.5 \frac{\pi w}{gT} \tag{4}$$

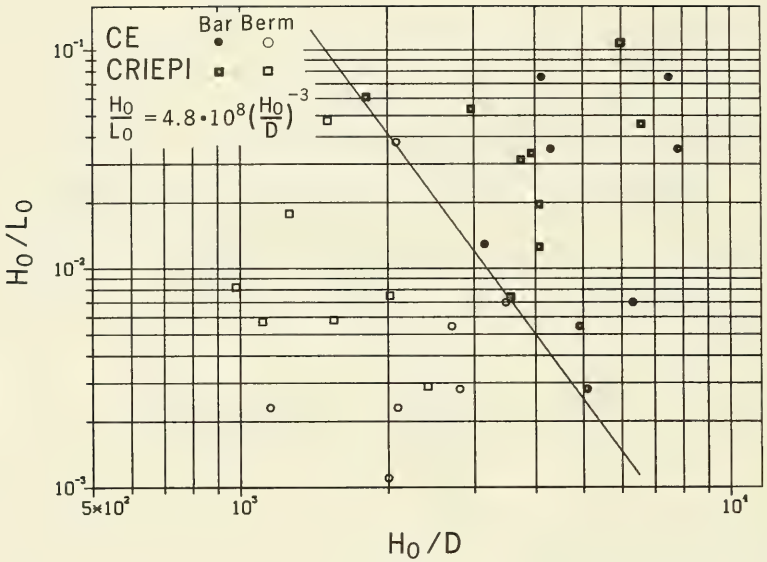


Figure 7. Criterion for distinguishing profile type by use of wave steepness and ratio of wave height to grain size

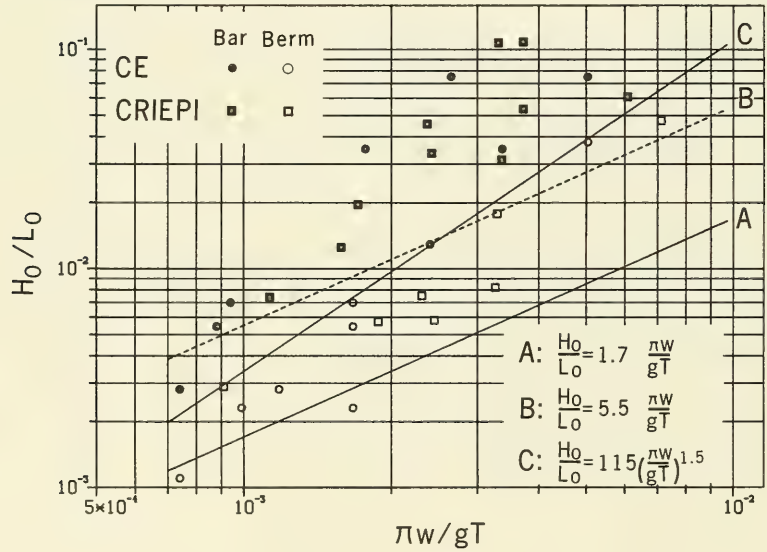


Figure 8. Criterion for distinguishing profile type by use of wave steepness and Dean parameter

215. The value of the empirical coefficient is 5.5 (Line B) and differs from the value of 1.7 (Line A) originally given by Dean (1973) as determined mainly from small-scale laboratory data. Kriebel, Dally, and Dean (1987) reevaluated this coefficient and obtained a band of values in the range of 4-5 using a portion of the CE and CRIEPI data set. It is, however, possible to achieve even a better delineation between bar/berm profiles if the Dean parameter is raised to an exponent (Line C) according to

$$\frac{H_o}{L_o} = 115\left[\frac{\pi w}{gT}\right]^{1.5} \tag{5}$$

Since $L_o \sim T^2$ , Equation 5 indicates a relatively weak dependence on wave period.

216. Sunamura (in press) proposed two somewhat different dimensionless quantities for classifying beach profile response involving breaking wave properties instead of deepwater wave conditions, namely $D/H_b$ and $H_b/gT^2$ . The second parameter is basically the inverse of the Ursell parameter $U = HL^2/h^3$ evaluated at breaking with linear wave theory. By using these two parameters, it was possible to obtain a good classification of profile type (Figure 9), although one point in the data set is located in the wrong area. The equation of the line separating bar/berm profiles is

$$\frac{D}{H_b} = 0.014\left[\frac{H_b}{gT^2}\right]^{0.68} \tag{6}$$

217. In summary, it is possible to obtain a clear distinction between bar profiles and berm profiles and, thereby, a predictor of overall erosion and accretion if the dimensionless quantities chosen to compose the criterion consist of parameters characterizing both sand and wave properties. Significant differences occur, however, in the values of the empirical coefficients in the criteria, depending on whether data from small-scale or prototype-scale experiments are used. Deepwater wave steepness appears in most criteria together with a parameter involving a quantity describing the sediment, such as the fall speed or grain size. In a theoretical sense, the sediment fall

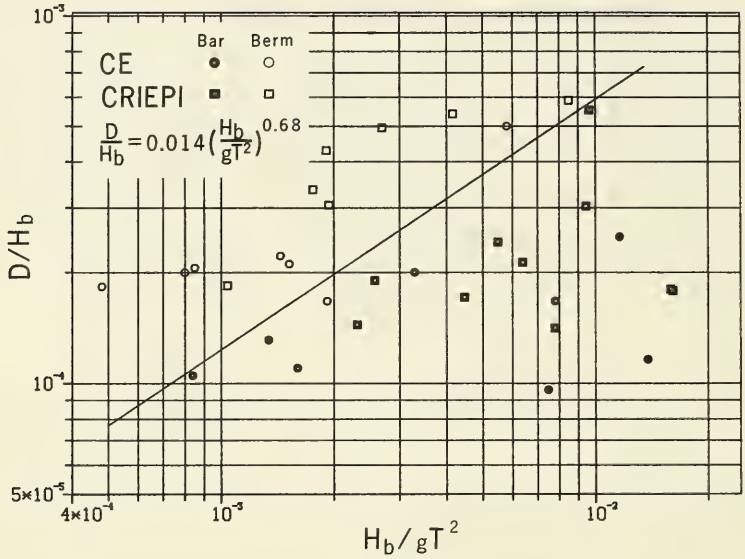


Figure 9. Criterion for distinguishing profile type by use of ratio of breaking wave height and grain size, and Ursell number at breaking

speed is superior to the grain size in development of profile classifications, as it incorporates both grain shape and fluid viscosity (water temperature).

218. An attempt was made to incorporate initial beach slope in the criteria for bar/berm profile classification using the LWT data set, but addition of this parameter did not increase predictability. In practice, determination of a representative beach slope on an irregular profile introduces some ambiguity, and a transitional slope would not be known in a predictive field application. A representative beach slope is implicitly contained in the fall speed (or grain size) because the equilibrium beach profile depends on this quantity (Moore 1982, Dean 1987). This implies that the existing beach profile should not be far from equilibrium for Equations 2-6 to be applicable, a condition expected to be satisfied at locations on the open coast and far from structures such as large jetties.

219. In the present study, use of the dimensionless fall speed as the sediment-related parameter gave a good delineation between bar/berm profiles, and this parameter has a sound physical basis, as first explained by Gourlay

(1968) and Dean (1973). Furthermore, in the process of quantifying morphologic features as described below, the dimensionless fall speed emerged in many of the developed empirical relationships. In most cases, the value of the dimensionless fall speed varies over the same order of magnitude for a wide range of sand and wave conditions, making it more appealing to use than, for instance, the parameter $H_o/D$. Thus, it is concluded that the parameters $H_o/L_o$ and $H_o/wT$ are the most basic and general for prediction of cross-shore beach change caused directly by large incident breaking waves. (Some researchers use the breaking wave height instead of the deepwater wave height in beach morphology descriptors, but this requires application of a breaking wave criterion to be useful in a predictive mode.)

220. The dimensionless parameters $H_o/L_o$ and $H_o/wT$ have distinct physical meanings. The wave steepness $H_o/L_o$ is a measure of the wave asymmetry, which influences the direction of fluid flow in the water column. The dimensionless fall speed $H_o/wT$ is a measure of the time that a sediment grain remains suspended in the water column (Dean 1973). Also, the wave height entering in the dimensionless fall speed directly introduces the magnitude of the wave height into the description of sediment motion (which is lacking in the wave steepness, as demonstrated by Saville 1957). The same argument is suggested for the wave period. Thus, although mathematically one power of $H_o$ could be cancelled in the numerators of both sides of Equation 2 (and, similarly, for $T$ in the denominators, since $L_o \sim T^2$), physically, the variables $H$ and $T$ enter on both sides of the equation for different reasons, on the left side for the wave asymmetry and the right side for the magnitudes of the wave height and wave period.

Irregular (field) waves

221. The criteria investigated above were developed for predicting tendencies for bars or berms to form (or for the profile to erode or accrete) under idealized laboratory conditions of regular waves and constant water levels in small and large wave tanks. The utility of such criteria has been questioned for applicability to the field situation (Seymour and King 1982, Seymour and Castel 1988). In the field, waves have a spread in height and period, implying potential differences in cross-shore sand transport produced directly by regular and irregular waves. Irregular waves may also be accom-

panied by long-period wave motion as surf beat and edge waves, modifying the transport regime that exists under purely regular waves. Other complicating factors include the change in water level with the tide and the ambiguity in specifying a representative grain size for the profile.

222. The literature provides guidance on the problem of the difference in transport under regular and irregular waves (see Kraus and Horikawa (1989) for a more complete discussion). Hattori (1982) found better correlation between the predicted cross-shore transport rate and the rate inferred from his field measurements if mean wave height was used in the predictive expressions instead of significant wave height. Mimura, Otsuka, and Watanabe (1987) compared profile change and transport direction and rate produced in a small wave tank in separate cases using regular and irregular waves. Among the many interesting results, they found that the Sunamura and Horikawa (1975) (Table 3) criterion of erosion and accretion was successful (with modified value of the empirical coefficient C) if mean wave height and period were used. Profile change also proceeded at a slower rate for the irregular waves, attributed to the presence of both "constructive" (accretionary) and "destructive" (erosional) wave components in the wave train.

223. To examine the applicability of Equation 2 for expressing profile type or erosion and accretion in the field, data sets published by Seymour (1985) and Sunamura (1980) were used. Seymour (1985) provides plots of the daily time history of contour movement between the berm and the approximately 1- to 2-m depth (relative to mean sea level) on three beaches--Santa Barbara and Scripps Beach, California, and Virginia Beach, Virginia--together with data on the significant wave height $H_s$ and peak spectral wave period $T_p$ at a nominal depth of 10 m, tidal range, and median sand size at the respective beaches. (It is noted that Figures 1 and 2 of Seymour (1985) should be interchanged.) Sunamura (1980) provides wave and sediment data on major erosion and accretion events in the literature and from his own field studies for a total of 10 beaches located on various coasts around the world.

224. The data of Seymour (1985) were censored to exclude days of minor contour change as based on the rate of change of the deeper contours. Deeper contours were used as the reference since the tidal range along the California beaches (approximately 1.5-2 m) and Virginia Beach (approximately 0.5-1 m)

indicates that large portions of the surveyed profiles were above water or in the swash zone most of the time. Criteria such as Equation 2 are applicable to the total surf zone profile extending from the berm to the main breakpoint bar and to prediction of major changes in it. In a strict sense, wading depth profiles do not provide a suitable data base for investigating beach erosion and accretion predictions since it is not known if sediment volume is conserved. Wave heights given by Seymour (1985) were shoaled to deep water using linear wave theory to provide a better estimate of the significant deepwater wave height $H_{so}$ than the value at the gage. Water temperatures, needed to calculate sand fall speed, were obtained from tables given in a University of California (1982) publication for the California beaches and from data available at the US Army Engineer District Norfolk, for Virginia Beach*. The data of Sunamura (1980) were used directly, with the given wave height interpreted as significant deepwater wave height.

225. The total field data set was tested using Equation 2, with the deepwater wave height taken as either the root mean square $H_{rms}$, mean $\bar{H}$, or significant wave height $H_{so}$. These wave heights were calculated using the relationships $H_{rms} = 0.706\ H_{so}$ and $\bar{H} = 0.626\ H_{so}$, derived under the assumption of a narrow banded wave frequency spectrum, for which the wave height follows a Rayleigh distribution (Longuet-Higgins 1952). Plots made using the three statistical wave heights showed that the data separated into two approximately distinct groups, similar to Figure 6 for regular waves. For the wave heights $H_{rms}$ and $H_{so}$, the values of $M$ in Equation 2 were different from 0.00070 found for regular waves. However, when $\bar{H}$ was used, Equation 2 with $M = 0.00070$ was found to separate the eroding and accreting cases reasonably well, as shown in Figure 10. The lines drawn in Figures 6 and 10 are identical, indicating that mean wave height is the appropriate statistical wave height to use in comparisons of erosion and accretion occurring in the field with that generated by prototype-scale regular waves.

226. As previously mentioned, the data of Seymour (1985) were censored to restrict analysis to times of larger rates of change of the profile. In the censored data set, some points remained which appear anomalous if viewed

---

* Personal Communication, 1988, Paul Bowen, Geologist, US Army Engineer District, Norfolk, VA.

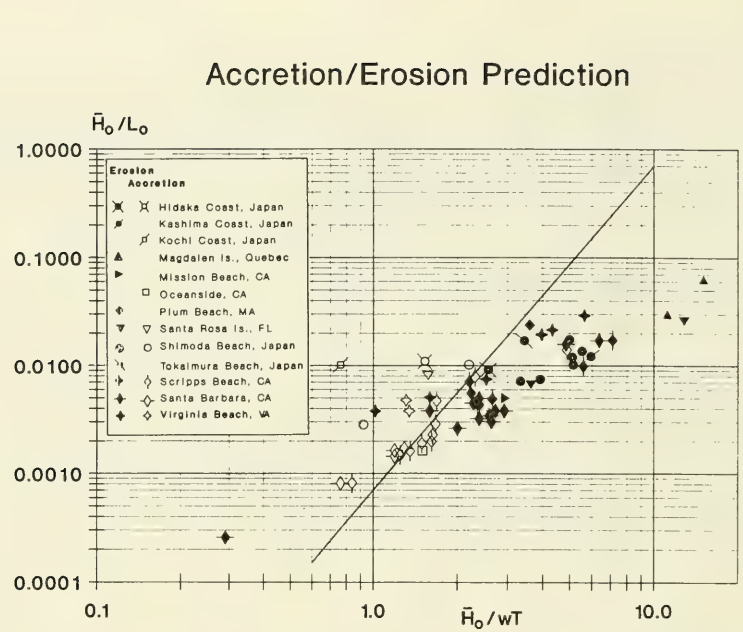


Figure 10. Classification of erosion and accretion events in the field using deepwater wave steepness and dimensionless fall speed, with wave height taken as mean wave height

within the context of the other plotted points. For example, day 1 of the Santa Barbara data described what would be considered as recovery waves with $H_{so}$ = 0.21 m and $T_p$ = 18 sec, yet the profile eroded. This point plotted at the bottom left side of Figure 10, far from other erosional events. Several mild accretionary events from the Scripps Beach data set plot on or near the erosion side of the separation line, suggesting that factors other than direct wave action contributed to produce the profile change and that the profile change may have been mixed. Kriebel, Dally, and Dean (1987) used a finite-width band rather than a single separation line to denote possible areas of mixed or ambiguous transport. In general, however, it is judged that the criterion given by Equation 2 is applicable to distinguish erosion and accretion events in nature for the more extreme events. Since engineering applications involving cross-shore sand transport, such as beach fill design, must consider extreme and not weak or mixed events, Figure 10 appears to be suitable as a first-order estimator for such purposes.

227. It is interesting to note that the erosion and accretion events plotted in Figure 10 are well separated by the simple criterion $\bar{H}/wT = 2$ . This value is of the same order of magnitude as that found by Wright and Short (1984) in use of their large field data set and the fall speed parameter evaluated at the breaker line (Table 3). The LWT data do not separate well (Figure 6) by use of only this single parameter, however, and additional unambiguous field data are required to further investigate this point. The profile surveys should encompass the full active profile to allow checking of sand conservation.

228. In succeeding sections, discussion and analysis are again directed toward profile change produced by regular waves in LWTs, unless noted otherwise.

Shoreline movement

229. If shoreline retreat/advance is analyzed instead of bar/berm profile type or global erosion/accretion, a less clear distinction is obtained when only dimensionless fall speed and deepwater wave steepness are used. In this case, incorporation of the initial beach slope increases predictability of the criterion because the initial slope is closely related to the amount of material that moves before equilibrium is attained. Also, a gentler slope dissipates more incident wave energy because the waves travel a greater distance in the surf zone before reaching the shoreline. Some CRIEPI cases showed that shoreline advance occurred for situations with a gentle initial slope even if considerable erosion took place in the surf zone to produce a distinct barred profile.

230. Figure 11 plots shoreline retreat and advance that occurred in the CE and CRIEPI experiments, together with a line distinguishing the two types of response. The initial profile slope was included in the numerator of the nondimensional fall speed to increase predictability. The equation of the line in Figure 11 is $H_o/L_o = 0.44\ (\tan\beta\ H_o/wT)^{2.08}$ .

Application to small-scale data

231. The dimensionless sediment fall speed and the deepwater wave steepness were also used to classify the data pertaining to small-scale laboratory profile change found in the experiments performed by Rector (1954), Iwagaki and Noda (1963), and Nayak (1970). As seen from Figure 12a, the

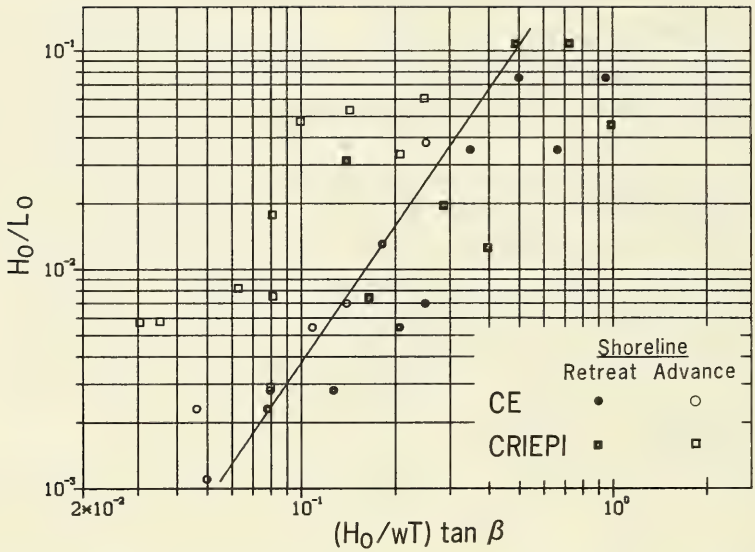


Figure 11. Criterion for distinguishing shoreline retreat and advance by use of wave steepness, dimensionless fall speed, and initial beach slope

criterion derived from the large-scale tests is not applicable to the small-scale data using the coefficients given in Equation 2. By modifying these coefficients it would be possible to obtain a crude delineation with the quantities in Equation 2. However, the dimensionless fall speed is probably of less significance in distinguishing bar/berm profile response in small-scale laboratory experiments than in prototype-scale experiments. This is attributed in great part to the mode of transport, the main transport mode probably being bed load in these types of experiments, with less significant contributions from suspended load as under higher waves as occur in the field.

232. Therefore, in small-scale laboratory experiments, use of the parameter $H_o/D$ instead of $H_o/wT$ should provide a better basis for profile classification since it expresses a relationship between the force exerted by the waves and the resistance offered by the grains (Nayak 1970). This interpretation is closely connected with the mechanism of bed load transport, where the main driving force is the horizontal component of the water particle

velocity near the bed. In contrast, in suspended mode, the upward transport of eddy momentum keeps sediment particles in the water column and available for transport by any current. Figure 12b illustrates the improvement obtained by using $H_o/D$ for classifying beach profile change produced in small-scale experiments. Although the points denoting bar and berm profile response overlap to some extent, the delineation obtained is somewhat better than in Figure 12a.

233. The effect of wave period in scaling is also emphasized through the significant difference between small-scale and prototype-size experiments in classifying beach response using the dimensionless fall speed.

## Form and Movement of Bars

### Bar genesis

234. Several theories have been advanced to explain the formation of longshore bars. Since a wide variety of bed forms has been classified as a bar-like feature by various authors, various mechanisms may presumably prevail in the formation process. Here, bar generation by depth-limited breaking waves is investigated, the "classical" viewpoint of bar genesis. As waves break near shore, energy is dissipated producing a turbulent fluid environment where sediment is entrained and maintained in suspension. Depending on the vertical profile of both the cross-shore fluid velocity field and the sediment concentration, the sediment will experience net onshore or offshore movement, resulting in a berm or bar profile. Sediment transported in the offshore direction will drop out of the water column to be deposited where the turbulence begins to decrease, somewhat seaward of the plunge point, where breaking waves undergo maximum energy dissipation (Miller 1976, Skjelbreia 1987). A berm is formed as material is transported onshore and deposited on the foreshore, for which the force of gravity and properties of the uprush bore determine the berm height (Bagnold 1940, Sunamura 1975). In the field, long-period (infragravity) wave motions, if present, may also influence and perhaps dominate foreshore development, since the energy of these waves is not depth limited, as is the case for short-period waves. However, no direct evidence

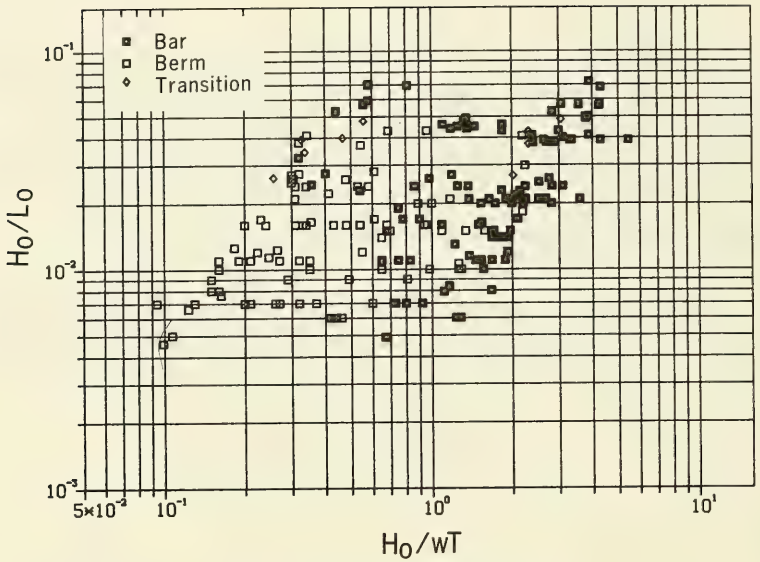


a. Dimensionless fall speed

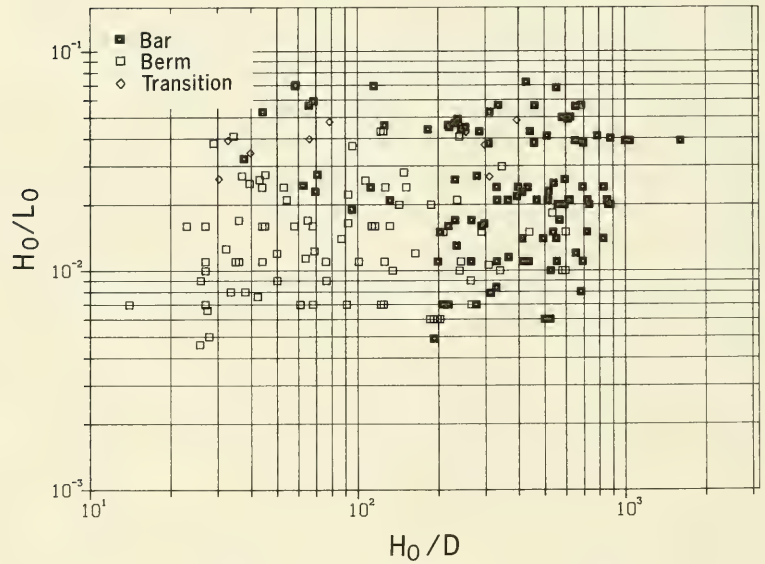


b. Ratio of wave height to grain size

Figure 12. Criteria for distinguishing profile type applied to small-scale laboratory data

of major bar or berm development by infragravity waves was found in the literature review.

235. The type of bars empirically investigated in this study are those formed by waves breaking on beaches exposed to moderate or high wave energy conditions with a moderate tidal variation (For a bar classification, see Greenwood and Davidson-Arnott 1979.) Waves approaching shore on a sloping beach increase in height due to shoaling until depth-limited breaking occurs. The condition for incipient breaking is a function of the local beach slope and the wave steepness (e.g., Weggel 1972, Singamsetti and Wind 1980). As breaking occurs, energy dissipation in the waves increases sharply, producing the necessary work to intensively entrain and transport sediment in the surf zone. The maximum in the cross-shore transport rate appears to be located in the vicinity of the plunge point where maximum energy dissipation occurs. Seaward of the point of maximum energy dissipation, the transport rate decreases, leading to deposition of sediment in this region and bar formation. As the bar grows, the waves break farther offshore and the break point and plunge point translate seaward, causing the location of the maximum transport rate and the bar to move offshore. Material needed to supply the bar is mainly taken from the region of the inner surf zone, resulting in erosion of the subaerial beach. This process continues until a stable beach profile is achieved which dissipates wave energy without significant changes in shape.

236. A broken wave may, after further travel, reach a stable wave height and reform, depending on the shape of the profile. Dissipation of energy decreases in the reformed waves, implying a corresponding decrease in the transport rate. Eventually, the reformed waves may shoal and break again closer to shore, resulting in a second but smaller bar in the same manner in which the more seaward main breakpoint bar was formed. The described mechanism is valid for both plunging and spilling breakers, both producing a trough in the profile shoreward of the break point (Sunamura in press), although the time scale of bar development will be longer under spilling breakers (Sunamura and Maruyama 1987). Figure 13 displays consecutive profiles in time for one of the CE cases (Case 500), showing a typical example of beach profile evolution with a main breakpoint bar and another smaller bar farther inshore.

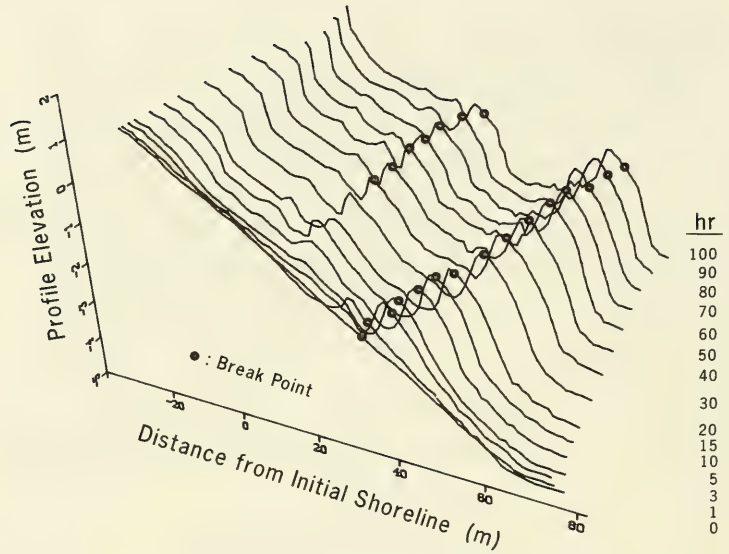


Figure 13. Growth and movement of breakpoint bar with elapsed time and location of break point

Average breaker locations are indicated in the figure for the profiles where such information was available.

237. Another mechanism for bar formation is long-period wave motion generated, for example, by reflection from the beach (Bowen 1980). Standing waves as a possible mechanism for bar formation have been investigated by Carter, Liu, and Mei (1973), Lau and Travis (1973), Short (1975a, b), and Mei (1985). An oscillating velocity field induces a steady mean current in the boundary layer close to the bed. If the oscillations are produced by purely progressive waves, the mean drift in the boundary layer will always be in the direction of the propagating waves. Partial reflection of the incident wave may cause the direction of mass transport in the lower part of the boundary layer to reverse if reflection is sufficiently large. (Theoretically the reflection coefficient should exceed 0.414, according to Carter, Liu, and Mei 1973.) A complete standing wave induces mass transport toward the nodes in the lower part of the boundary layer and toward the antinodes in the upper part of the boundary layer. Depending on the height to which the grains are

lifted in the water column when transported, the grains will experience a net drift and accumulate under the nodes or antinodes. This should depend on grain size to some extent (De Best and Bijker 1971). Holman and Bowen (1982) assumed that suspended sediment transport was dominant and used the average mass transport in the upper part of the boundary layer to calculate equilibrium shapes of beaches based on a Bagnold-type transport formula. Complex three-dimensional geometries were derived by superimposing progressive waves to obtain standing wave patterns alongshore and cross-shore.

238. In some of the CRIEPI cases which started from the steep plane slope of 1:10, considerable reflection was present (a reflected wave height of 0.4 m superimposed on the wave height distribution), but the effect of the reflected wave on the profile shape appeared to be very small (see Figure 14).

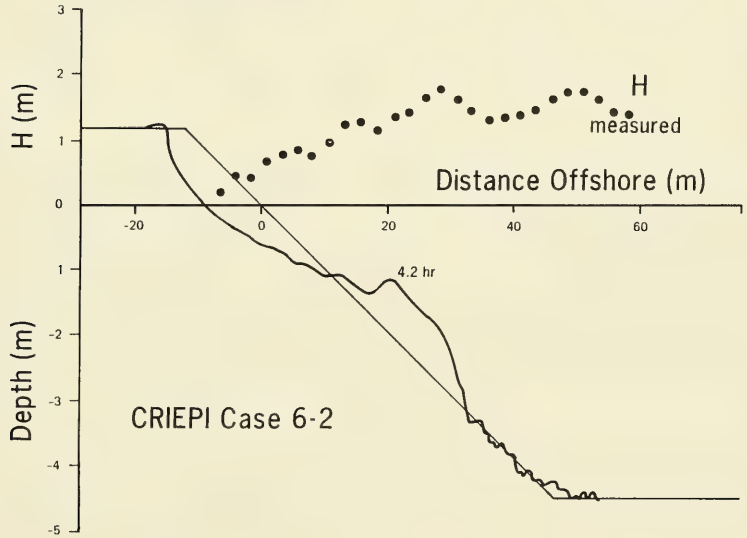


Figure 14. Profile measured after 4.2 hr together with the initial profile and wave height distribution

Actually, as the bar grew in size and the seaward slope became steeper, the bar should have promoted reflection, but it is surmised that the main effect

of reflection was to alter the breaking wave process somewhat since there is no evident feature in the surf zone profile attributable to reflected waves.

Equilibrium bar volume

239. As a bar moves offshore, it increases in volume to approach an equilibrium size. Figure 15 shows bar volume for the main breakpoint bar as a function of time for the CE and CRIEPI experiments, respectively. Some of the cases were not run sufficiently long to attain the equilibrium volume. The approach to equilibrium is typically smooth. If a breakpoint bar formed on a profile where onshore transport (accretion) dominated, equilibrium volume was reached rapidly and was relatively small. Examples are Cases 101, 301, and 801 from the CE data, and Case 2-3 from the CRIEPI data. Bar volume changed abruptly if the smaller seaward breakpoint bar merged with the main breakpoint bar. Often, further growth of the main breakpoint bar was hindered by this coalescence of bars, as shown in Case 300 (occurs at 15.0 hr). Profiles having only one bar showed a more regular development in time toward an apparent equilibrium volume.

240. Since equilibrium bar volume was not entirely reached in some cases, and in order to obtain an objective method for determining equilibrium bar volume, a simple expression of exponential type was least-square fitted to the data for each case. The chosen expression is often encountered in growth problems where an equilibrium state exists. The same expression was used by Kriebel and Dean (1985a) to characterize dune erosion. The bar volume $V$ is assumed to grow toward the equilibrium volume $V_{eq}$ according to

$$V = V_{eq} (1 - e^{-\alpha t}) \tag{7}$$

where $t$ is time, and $\alpha$ is an empirical temporal rate coefficient. Correlation analysis (25 cases evaluated) involving pertinent wave and beach profile parameters showed that equilibrium bar volume was most closely related to deepwater wave height, sand fall speed (or grain size), and initial beach slope, although the correlation coefficients (see Appendix A) were not high (0.6-0.7). A larger wave height implied a larger bar volume, a greater fall speed (or larger grain size) implied a smaller bar volume, and an initially steeper slope also produced a larger bar volume for a given grain size. Fall

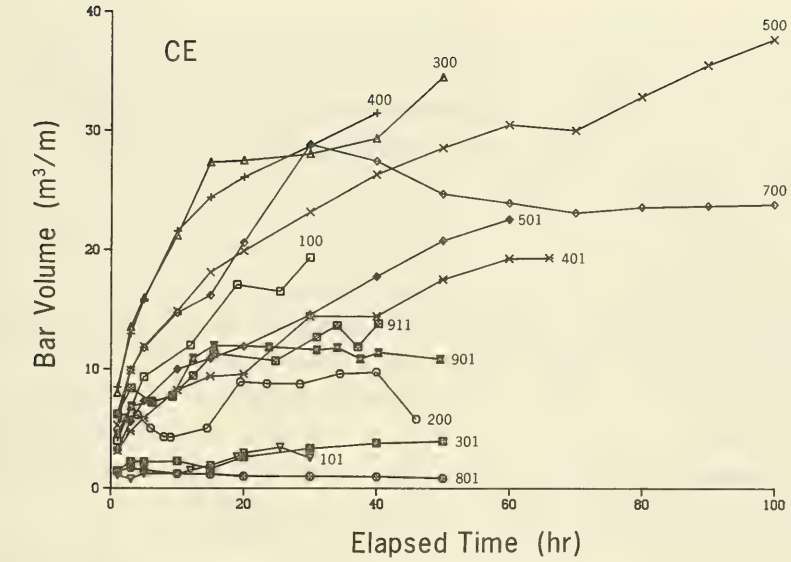


a. CE data

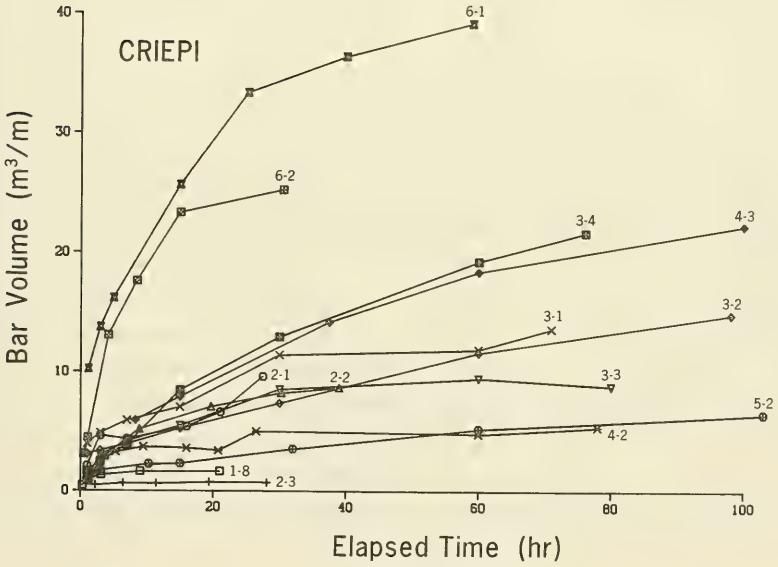


b. CRIEPI data

Figure 15. Growth of bar volume with elapsed time

speeds were calculated from an expression given by Hallermeier (1981) for the CRIEPI data, and in the CE cases fall speeds determined by Seelig (1983) were used. Fall speed depended on water temperature in the tank (Kajima et al. 1983b, Kraus and Larson 1988a). Under nonextreme water temperatures such as considered here, the fall speed is almost linearly dependent on grain size, resulting in similar correlation values for quantities expressed in terms of either the grain size or fall speed.

241. A stepwise regression analysis incorporating the aforementioned factors explained 70 percent of the variation in the data. Wave height was most important, accounting for 35 percent, followed by the fall speed which explained 30 percent. Wave period and initial beach slope together accounted for only 5 percent. If only bars formed on a profile which mainly experienced erosion (transport directed offshore), the explained variation increased to 80 percent, with the wave height and fall speed being most important. The dimensional regression relationship involving equilibrium bar volume $V_{eq}$, deepwater wave height, sand fall speed, and wave period for bars formed on erosional profiles is

$$V_{eq} = 0.088\ H_o^{2.26}\ w^{-1.36}\ T^{0.55} \tag{8}$$

242. It is desirable to use nondimensional quantities to obtain general relationships relating morphologic features to wave and sand parameters. From the regression equation describing equilibrium bar volumes on erosional profiles (Equation 8) dimensionless parameters were identified by dividing by the wave period raised to a suitable power. Equilibrium bar volume was normalized by the deepwater wavelength squared, and the independent parameters emerged as dimensionless fall speed and deepwater wave steepness. The coefficient of determination $r^2$ (see Appendix A), defined as the percentage of the sum of squares explained by the regression equation, will increase by incorporating the wave period in the parameters (from 75 percent without beach slope incorporated to 90 percent). The resultant regression equation is

$$\frac{V_{eq}}{L_o^2} = 0.028 \left[\frac{H_o}{wT}\right]^{1.32} \left[\frac{H_o}{L_o}\right]^{1.05} \tag{9}$$

243. Equation 9 is an inferior predictor of equilibrium bar volume compared with the original regression equation ($r^2$ decreased from 75 to 70 percent) formed by dimensional variables, since the least-square estimate will be more influenced by wave period which was found to be less important for determining equilibrium bar volume than wave height and sand fall speed. Thus, the advantage of nondimensional quantities is gained somewhat at the expense of predictability but will give a more general and physically-based relationship. Figure 16 displays a comparison between the predicted equilibrium volume according to Equation 9 and equilibrium volumes extrapolated from the measurements with Equation 7.

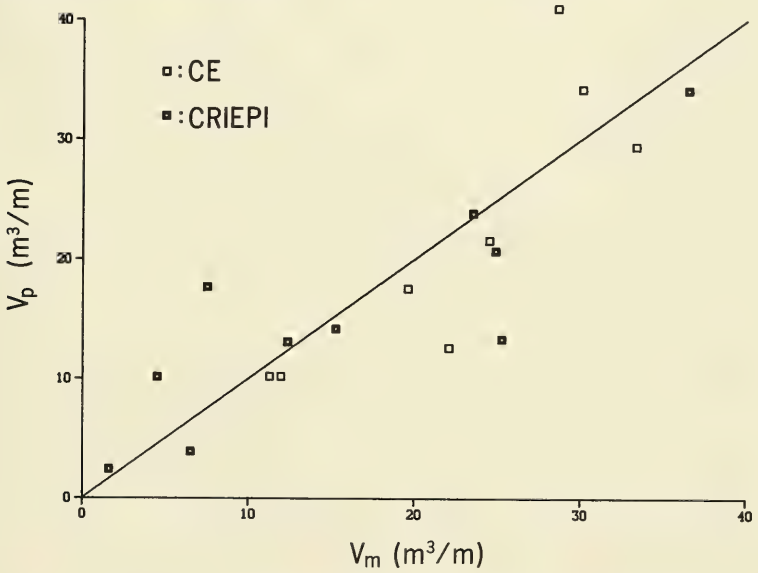


Figure 16. Measured equilibrium bar volume $V_m$ and empirical prediction $V_p$

244. The temporal rate coefficient $\alpha$ in Equation 7 controls the speed at which equilibrium bar volume is attained. Correlation between $\alpha$ and wave and beach profile properties was in general low (correlation coefficients less than 0.5). Qualitatively, $\alpha$ increased with fall speed (or grain size) and decreased with wave height and wave period. A large $\alpha$-value produces a rapid

response toward equilibrium. For larger wave heights, more wave energy is dissipated along the beach profile; that is, the bar becomes larger and forms farther offshore, causing more material to be moved before the equilibrium shape is reached (lower $\alpha$-values). Furthermore, greater wave energy is required to move larger (heavier) sediment particles, implying more rapid attainment of equilibrium (higher $\alpha$-values) for larger grain-size beaches.

Depth-to-bar crest

245. As a bar moved offshore, its height increased so that the depth to the crest $h_c$ was roughly constant during a run (except perhaps, at the very first profile surveys) (cf. Birkemeier 1985a, Dette and Uliczka 1987). In Figure 17(a and b), the minimum depth on the bar, called the crest depth, is plotted as a function of time for the CE and CRIEPI data. For some cases in which a bar formed on an accretionary profile, the bar remained stationary, or even moved slightly onshore, causing the crest depth to decrease. Also, if two bars joined together, the crest depth changed abruptly since the inner bar crest was located in more shallow water.

246. A comparison between Cases 901 and 911 shows that even though the equilibrium bar volume was almost the same (11.3 and 12.0 $m^3/m$, respectively), Case 911 experienced a considerably larger fluctuation in depth at the bar crest. Wave parameters and beach properties were identical for these two cases, the only difference being a stepwise sinusoidal water level change imposed in Case 911 to simulate a tide. Consequently, during cycles of increased water level in Case 911, the depth at the bar crest increased and the bar grew closer to the initial still-water (reference) level. During cycles of lower water level, the depth at the crest decreased and a portion of the bar eroded, causing the bar crest to move away from the initial location of the still-water level. There was no significant time lag between water level change and change in depth at the bar crest (see also Shepard 1950).

247. The average depth at the bar crest was calculated for all profiles comprising an individual case. This average was closely related to the breaking wave height and showed little dependence on wave period and grain size. If an inshore bar grew together with the main breakpoint bar, the most seaward bar crest was used in determining the depth at the bar crest. The

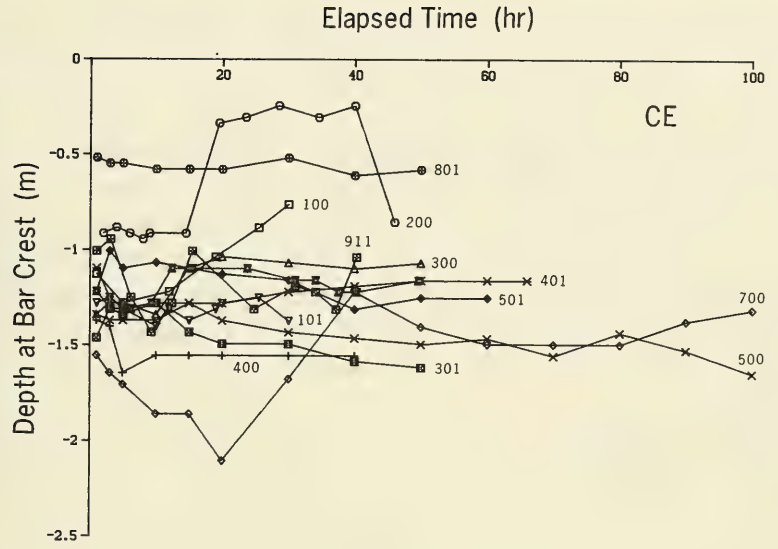


a. CE data

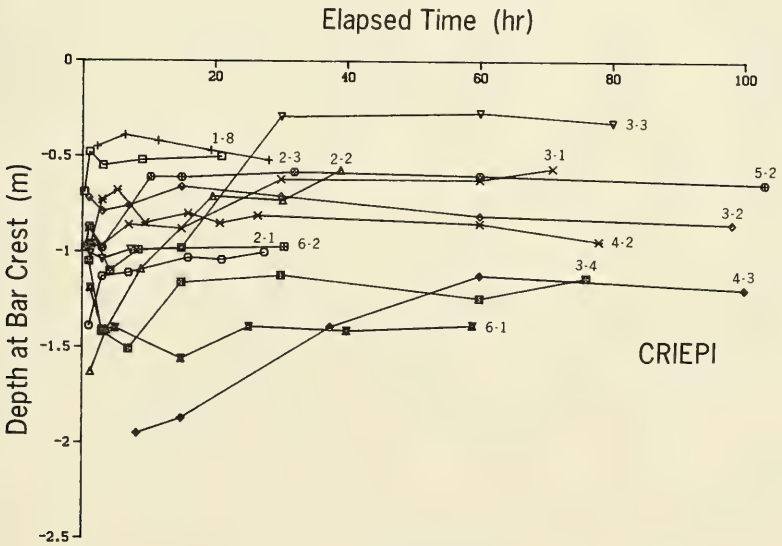


b. CRIEPI data

Figure 17. Evolution of depth-to-bar crest

following relationship with the breaking wave height was obtained:

$$h_c = 0.66\ H_b \tag{10}$$

Equation 10 is plotted in Figure 18. The coefficient of determination of the regression line was 70 percent.

248. For the cases where a small bar formed on an accretionary profile, the crest depth had a tendency to decrease slightly with time if onshore bar movement occurred, which contributed to the scatter in the data. Sunamura (in press) found a coefficient of 0.59 as opposed to 0.66 in Equation 10, based on small-scale laboratory wave tank data and some CRIEPI data.

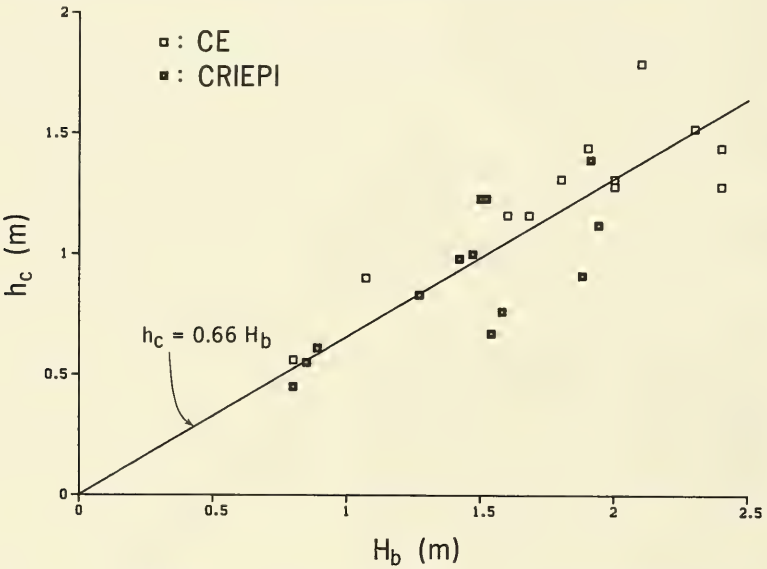


Figure 18. Depth-to-bar crest $h_c$ versus breaking wave height $H_b$

Ratio of trough depth to crest depth

249. The maximum depth occurring immediately shoreward of the bar was taken as the trough bottom in the analysis. This was considered as a natural and objective definition of trough position, although a trough was sometimes located in an area where material accreted with respect to the initial

profile. Keulegan (1945) studied the ratio of trough depth $h_t$ to bar crest depth $h_c$. He found an average value for $h_t/h_c$ of 1.69 for laboratory beaches and 1.65 for field beaches. Shepard (1950) found much lower ratios at the Scripps pier, with a mean value of 1.16 (referenced to mean sea level). The smaller value determined by Shepard is expected, since the tidal range is relatively large (order of 2 m) along the southern coast of California. Changing water level, combined with random and longer period waves in the southern California Bight, would act to smooth the profile.

250. In the present study, this ratio was calculated for 26 CE and CRIEPI cases and ranged between 1.26 to 2.16, with an average of 1.74 and standard deviation of 0.26. The ratio was calculated as an average for all profiles surveyed during a case and showed little change in time for most cases. However, for some cases the very first profile survey showed a markedly different value of $h_t/h_c$, typically much lower than the average, and these spurious values were excluded from the calculation of the average.

251. The ratio of trough depth to crest depth showed an inverse dependence on the wave period, as illustrated in Figure 19. The wave period accounted for 60 percent of the variation in the data using a regression relationship between $h_t/h_c$ and the wave period. Expressed as an empirical power law in terms of wave steepness, regression analysis gave

$$\frac{h_t}{h_c} = 2.50 \left[\frac{H_o}{L_o}\right]^{0.092} \tag{11}$$

252. Equation 11 had a coefficient of determination of 55 percent, slightly less than that found using only the wave period, but from a general point of view it is more attractive to use as a predictive relationship. Keulegan (1948) did not report a dependence on wave steepness.

253. Qualitative examination of the scattered data indicated that the ratio $h_t/h_c$ tended to increase with grain size for bars formed on erosional profiles, but decreased with grain size for bars formed on accretionary profiles. In erosional cases in general the profile for coarser grain sizes showed a steeper shoreward bar slope, allowing for a larger vertical distance between the bar crest and trough bottom. The breakpoint bar formed on an

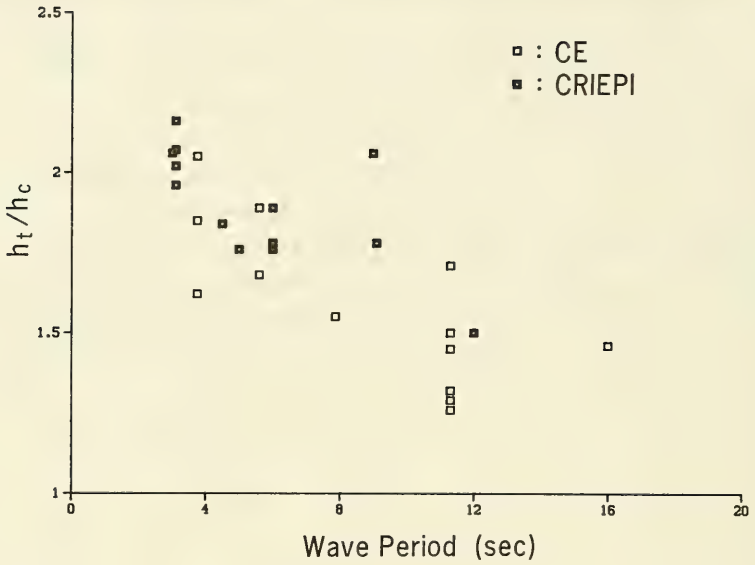


Figure 19. Ratio of depth-to-trough bottom and depth-to-bar crest $h_t/h_c$ as a function of wave period

accretionary profile was normally small, and its size decreased with increasing grain size, making the bar flatter with a smaller value of $h_t/h_c$ .

Maximum bar height

254. As a bar moved offshore, its maximum height defined with respect to the initial profile increased to approach an equilibrium value. Figure 20(a and b) shows maximum bar height $Z_B$ as a function of time for the CE and CRIEPI experiments. Bars formed on an accretionary profile achieved equilibrium height very rapidly, often during the first hour of the run (see Cases 101, 801, 2-3, 3-3). A coarser grain size produced a smaller equilibrium bar height for the same wave parameters, and a larger wave height produced a larger equilibrium bar height for fixed wave period and initial profile slope. The curves displayed in Figure 20(a and b) are readily approximated by an expression similar in form to Equation 7. (Some cases where a bar formed on an accretionary profile showed an almost constant bar height in time and thus were not used in the analysis.) Maximum bar height for all cases was esti-

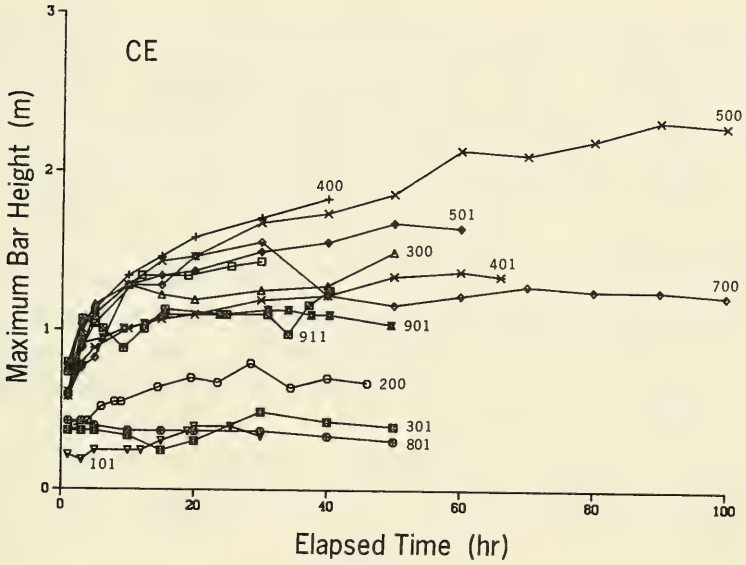


a. CE data

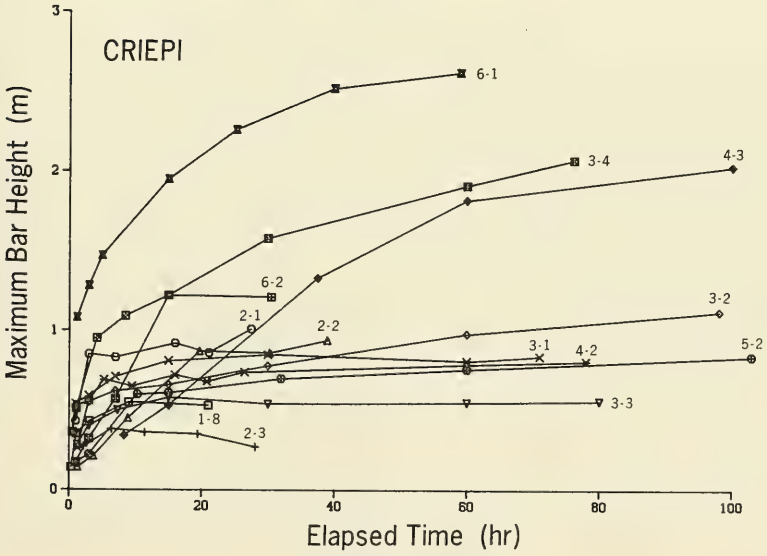


b. CRIEPI data

Figure 20. Evolution of maximum bar height

mated by least-square fitting of the data to an expression similar to that in Equation 7. Correlation analysis performed on the 24 values showed that the equilibrium bar height was most closely related to deepwater wave height and sand fall speed. If the wave height increased, the bar height increased, whereas a greater fall speed implied a smaller bar height. Equilibrium bar height was only weakly related to wave period, for which a longer period tended to produce a smaller bar height.

255. Regression analysis between the maximum equilibrium bar height and basic wave and beach parameters, preserving dimensions, accounted for 65 percent of the variation in the data. The deepwater wave height and the sand fall speed together accounted for 60 percent. If only bars that formed on erosional profiles were considered (19 values), the coefficient of determination increased considerably (80 percent), for which deepwater wave height and fall speed accounted for 75 percent. The dimensional regression equation for the erosional cases is

$$Z_B = 0.128\ H_o^{1.36}\ w^{-0.58} \tag{12}$$

256. From the regression relationship derived with dimensional quantities (Equation 12) it was possible to form nondimensional parameters by division with the wave period raised to a suitably chosen power. The maximum equilibrium bar height divided by the wavelength is a function of dimensionless fall speed and deepwater wave steepness. Wave period had little effect on bar height and, as mentioned previously, inclusion of the wave period may increase the coefficient of determination but not the predictability of the maximum equilibrium bar height. The regression equation is written

$$\frac{Z_B}{L_o} = 0.122 \left[ \frac{H_o}{wT} \right]^{0.59} \left[ \frac{H_o}{L_o} \right]^{0.73} \tag{13}$$

257. Use of nondimensional quantities in this case did not lower the coefficient of determination notably (from 80 percent to 75 percent) for predicting the maximum equilibrium bar height. Figure 21 shows a comparison

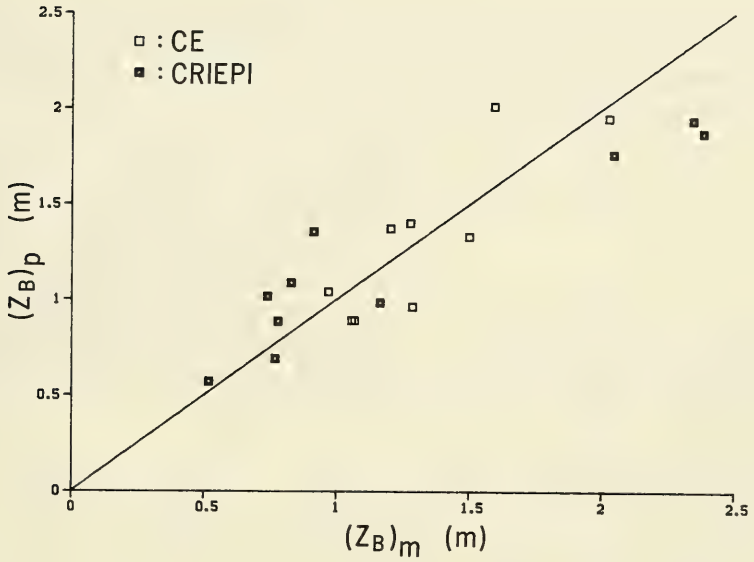


Figure 21. Comparison of measured equilibrium bar height $(Z_B)_m$ and empirical prediction $(Z_B)_p$

between the equilibrium bar height predicted by the regression model (Equation 13) and the measurements.

258. The temporal rate coefficients governing growth toward the maximum equilibrium bar height for bars formed on erosional profiles had highest correlation with sand fall speed. Similar to the situation for the rate coefficient governing bar volume growth, correlation coefficients were small (less than 0.5). However, a regression relationship between the rate coefficient and wave period, deepwater wave height, and sand fall speed gave a relatively high coefficient of determination of 70 percent. This relationship was considerably larger than any obtained for the rate coefficient pertaining to bar volume growth. The sand fall speed and deepwater wave height accounted for 60 percent of the variation in the data, giving

$$\alpha = 34.1\ H_o^{-1.43}\ w^{1.98}\ T^{1.23} \qquad (14)$$

259. From the dimensional regression equation, Equation 14, the dimensionless fall speed was identified as an important quantity. By normalizing with wave period, the quantity thus obtained was related to the dimensionless fall speed according to

$$\alpha T = 117 \left[ \frac{H_o}{wT} \right]^{-2.30} \tag{15}$$

260. The coefficient of determination was only 55 percent, but Case 700 contributed to more than half of the sum of the residuals. The reason is probably due to a decrease in wave height that occurred between 20-30 hr during the run, strongly affecting buildup of the bar.

Bar location and speed of movement

261. Movement of a bar during wave action is perhaps most accurately characterized by its center of mass $x_{CM}$ . The bar crest, which is the most convenient measure of bar location, especially in the field, is not as accurate a measure since the shape of the bar changes during the course of its growth, influencing the location of the crest more than the center of mass. In general, the mass center of the bar moved offshore on an erosional profile unless a more shoreward bar grew together with the main breakpoint bar. Actually, if a secondary bar merged with the main bar, further clear movement of the bar conglomerate was absent. On an accretionary profile, the small bar that formed moved somewhat onshore or was stationary.

262. In Figure 22(a and b), the horizontal location of the mass center is shown as a function of time for the CE and CRIEPI experiments. Distance was measured from the intersection of the initial profile and the still-water level. Bars formed on a beach composed of coarser grains in general moved less than those on beaches composed of finer grains under the same wave conditions (compare Cases 400-401 and 500-501). Case 911, which involved a sinusoidally varying water level, showed back-and-forth movement of the bar in response to the change in water level, an effect not observed in control Case 901 (fixed water level).

263. It was difficult to detect trends in the movement of the vertical position of the bar center of mass. For bars formed on accretionary profiles,

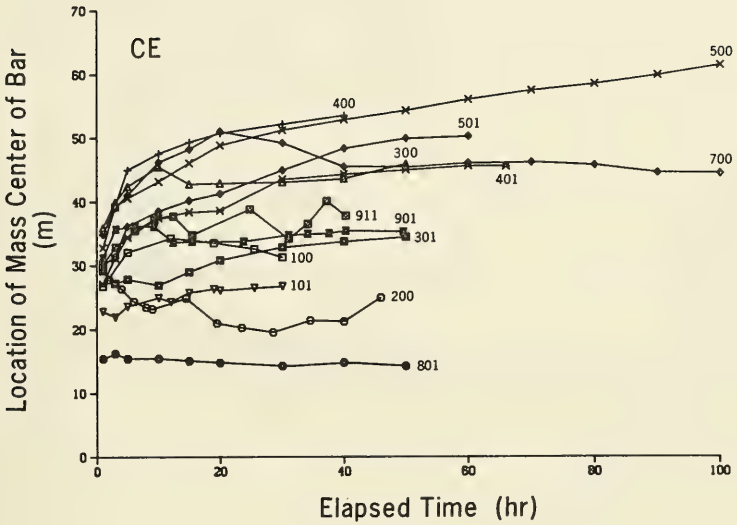


a. CE data

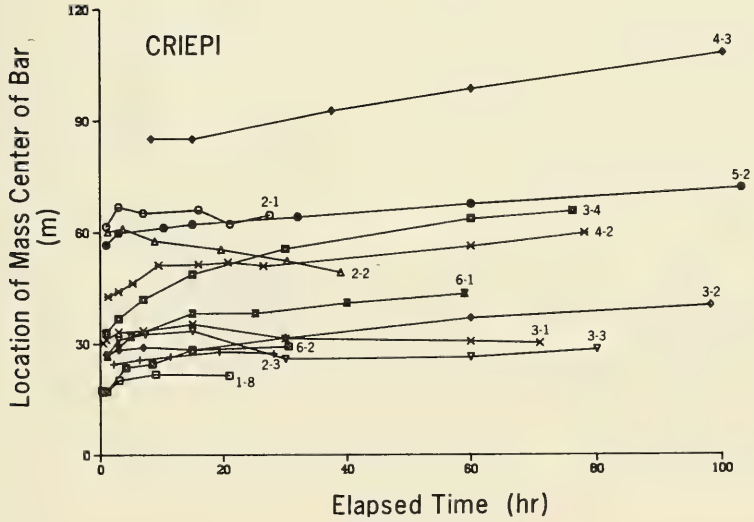


b. CRIEPI data

Figure 22. Horizontal movement of bar center of mass

vertical position of the mass center was relatively constant since the equilibrium bar volume was attained rapidly, and horizontal movement of the bar was limited. However, the overall trend for bars formed on erosional beach profiles was for the vertical distance to the bar mass center to increase with time.

264. As expected, bars appeared to be initiated at the same location along the profile for the same wave conditions and initial beach slope, irrespective of beach grain size. However, the bar center of mass at later times was usually located farther offshore and in deeper water for finer grain-sized beaches.

265. The locations of both the bar crest and the bar center of mass were used as reference points to calculate the speed of bar migration. Evolution of bar speed had the same characteristic features for both references. Only bars formed on erosional profiles were included in analysis of migration speed, since bars on accretionary profiles were almost stationary (see Figure 22). Furthermore, if an inner bar grew together with the main breakpoint bar, only the seaward portion of the bar conglomerate was considered to eliminate spurious instantaneous shoreward displacements of the center of mass resulting from coalescence of the bars. Figure 23(a-d) displays speed of bar migration. Positive speeds of bar migration indicate movement directed offshore. The main trend was similar for all cases and independent of definition (reference point), exhibiting a high initial speed of bar migration which slowed as the profile approached the equilibrium shape.

266. Case with a simulated tide. Case 911 from the CE experiment, which had a cyclical variation in water level, showed cyclical onshore and offshore bar movement, i.e., negative bar speeds as the water level dropped. The main purpose of Case 911 was to demonstrate that a variation in water level would produce a more gently sloping bar*. A negative speed of bar migration also occurred if bar shape changed considerably during a run, particularly if the location of the crest were used as the reference point. For example, Case 100 showed a negative bar speed after about 20 hr, as the

* Personal Communication, Thorndike Saville, Former Technical Director, Coastal Engineering Research Center, Ft. Belvoir, VA.

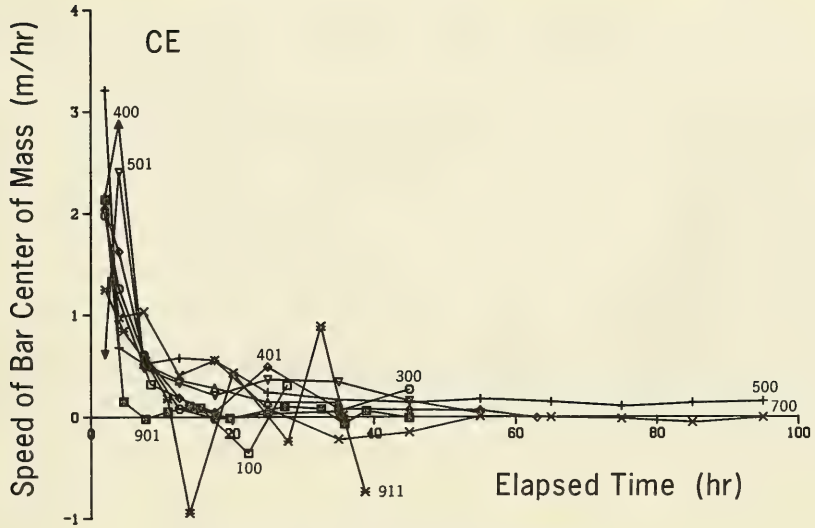


a. CE data, bar center of mass

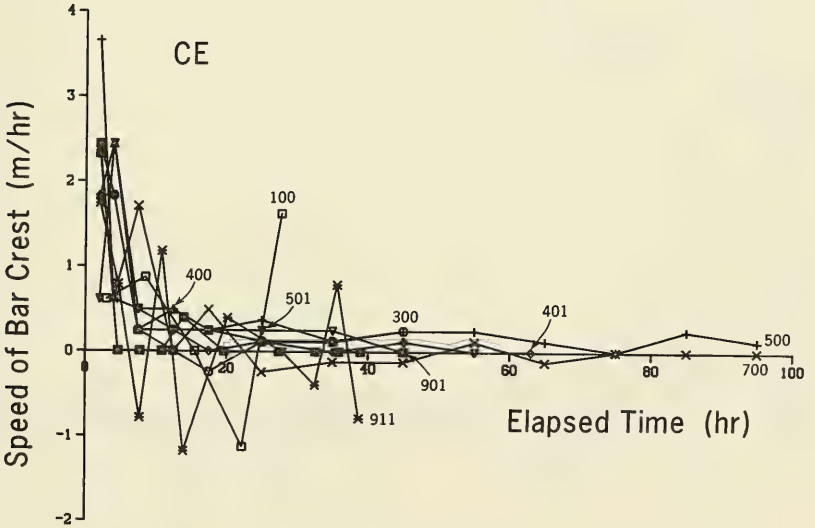


b. CE data, bar crest

Figure 23. Speed of bar movement with elapsed time (Continued)

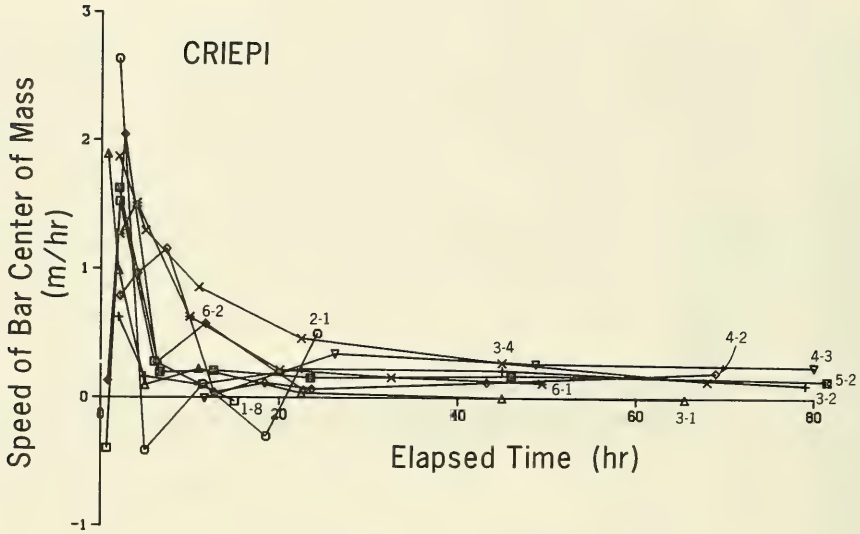


c. CRIEPI data, bar center of mass

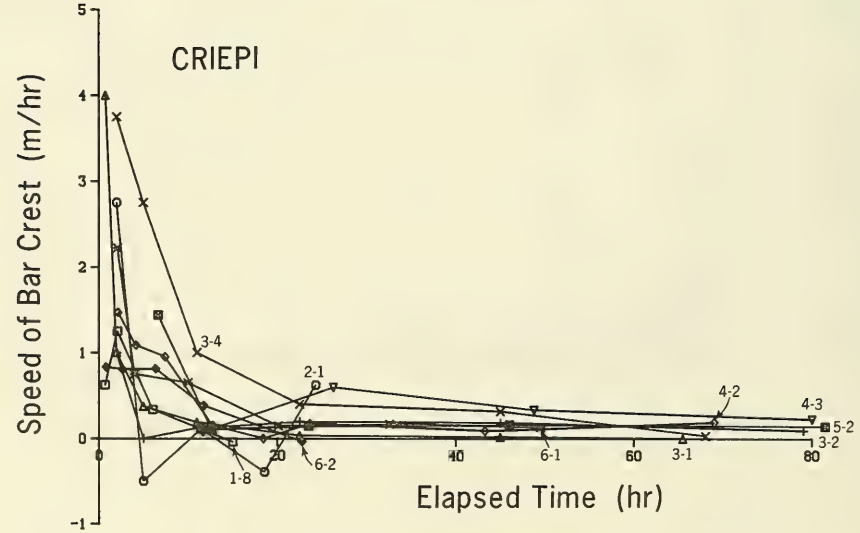


d. CRIEPI data, bar crest

Figure 23. Concluded

beach eroded back to the end of the tank and marked reflection started to occur, influencing bar shape.

267. Comparison with a field measurement. Initial speeds of bar movement in the LWTs had the same magnitude as observed in the field measurements of Sallenger, Holman, and Birkemeier (1985) made during a storm at CERC's FRF at Duck, North Carolina. In general, morphologic features of the profile in the field showed rapid response to changing wave conditions, in qualitative agreement with profile response generated in the LWTs. The bar crest at Duck had an average offshore speed of 2.2 m/hr during the initial phase of one storm (6-hr average) and a speed of 1.4 m/hr for another storm which had smaller waves. Migration speeds measured by Sallenger, Holman, and Birkemeier (1985) were close to those obtained in the CE and CRIEPI studies for the cases showing strong erosion (Figures 23b and 23d).

268. The distance between the location of the maximum trough depth and the bar crest was approximately constant during cases with a well-developed trough. Coarser grained beaches tended to have greater distances between trough bottom and bar crest. Larger waves also caused the distance from the bar crest to the trough bottom to increase for a specific grain size. For a typical unibarred profile, the vertical distance between maximum trough bottom and bar crest appeared to increase slightly with time up to the equilibrium value.

Distance from break point to trough bottom

269. According to the (small-scale) wave tank results of Miller (1976), the trough located shoreward of a breakpoint bar is initiated where the breaking waves completely disintegrate. Sunamura (in press) made the observation that this process is valid not only for plunging breakers but also for spilling breakers, although the trough is not so marked and takes longer to form under spilling breakers. The distance between break point and plunge point may thus be generalized to include both plunging and spilling breakers to yield a plunge distance. Galvin (1969) noted through small-scale and prototype-scale experiments that this distance was equal to about $4H_b$ . For the CRIEPI data, Sunamura (in press) related the distance between trough bottom and break point to bottom slope and wave steepness at breaking. In the relationship, distance was normalized by deepwater wavelength, which gives the

impression of a stronger correlation between parameters than is the case.

270. In the present study, the CRIEPI data set, which contains comprehensive wave information, was used to determine the distance $\ell_{tc}$ between the break point and the maximum trough depth normalized by the deepwater wavelength. This quantity was best correlated with the ratio of the breaking wave height to the deepwater wave height and to the local slope just prior to breaking. Evaluation of the slope was somewhat subjective, and it was defined as the average for the region of approximately one-half the local wavelength seaward of the break point. Consideration was also given to characteristics of the cross-shore distribution of wave height to determine the region of considerable shoaling and thus where wave properties were greatly influenced by profile shape. The regression relationship derived is

$$\frac{\ell_{tc}}{L_o} = 0.12\ (\tan\beta)^{-0.44} \left[\frac{H_b}{H_o}\right]^{-2.36} \tag{16}$$

271. The coefficient of determination for Equation 16 is 65 percent for 110 values. Only profiles having a distinct trough were used in the analysis. Figure 24 displays predicted normalized plunge point distances (subscript p) and measurements (subscript m). The location of the maximum trough depth was inferred to be closely related to the location of the maximum cross-shore transport rate. A bar typically formed immediately seaward of the trough as an accretionary feature resulting from the seaward decrease in cross-shore transport rate.

Bar slopes

272. The growth of a bar is ultimately restricted by the maximum slope that sand grains can maintain without moving under the action of gravity. If this limiting slope is exceeded, avalanching will occur and the sand will be redistributed to attain a more gentle slope which is stable. Allen (1970) recognized these two different slopes and called them the angle of initial yield and residual angle after shearing, respectively. From his experiments with natural sand (diameters ranging from 0.27 to 3.17 mm in the experiments), he obtained an angle of about 48 deg to cause avalanching and an angle of about 33 deg as the stable slope after avalanching had ceased.

273. In the LWT experiments, as a bar approached equilibrium, its shoreward face appeared to approach the angle of initial yield, followed at later profile survey times by intermediate lower values. This alternating behavior in bar angle supports the concept of a continuous steepening of the

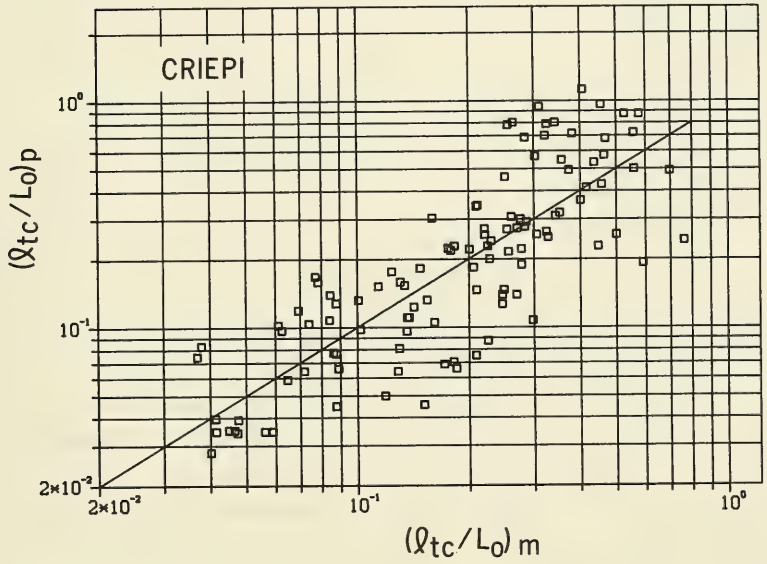


Figure 24. Comparison of measured and predicted nondimensional horizontal distance between break point and trough bottom

shoreward slope to a limiting angle followed by avalanching which adjusts the slope to a lower value. Figure 25 shows the behavior of the average shoreward slope of a bar $\beta_3$ with time for Cases 401 and 501, increasing at first and then having smaller values after a certain initial maximum slope was reached. However, the number of profile surveys is too small to obtain reliable information about the avalanching process apart from circumstantial evidence that it appeared to occur.

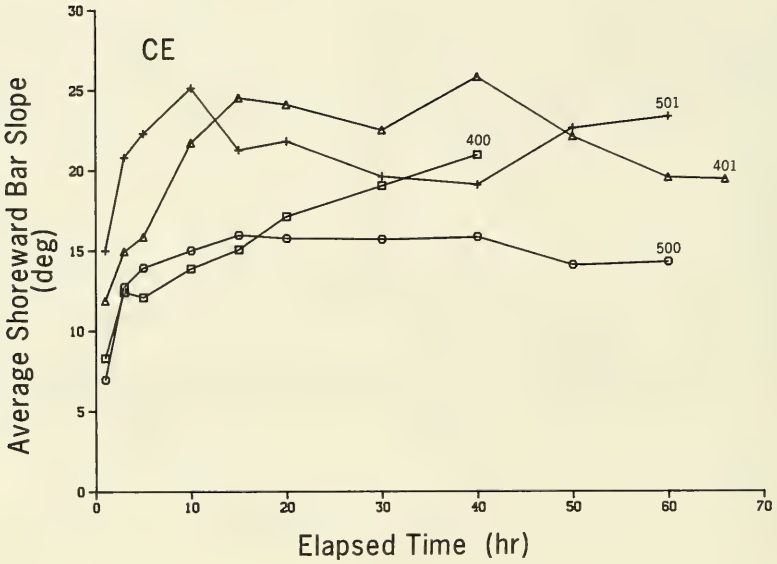


Figure 25. Evolution of shoreward slope of main breakpoint bars

274. In general, the average shoreward bar face slope generated in the LWT experiments increased with time, and the angle of initial yield was apparently not achieved (see Cases 400 and 500 in Figure 25). In particular, for the finer grain sizes, steepening of the shoreward face slope appeared to be slower even though the angle of initial yield should be approximately independent of grain size for the range of material studied.

275. If a second bar formed immediately shoreward of a main breakpoint bar, steepening of the shoreward slope of the main bar was usually hindered, and the slope sometimes decreased. The maximum bar face slope on the shoreward side of a bar was 35 deg (Case 4-3), which is considerably less than Allen's (1970) limiting value. A smaller maximum slope under wave action is logical because of the turbulent fluid environment existing in the surf zone, which is considerably different from the laminar flow conditions under which Allen performed his experiments. The expected result of turbulent flow is increased destabilization of the sand grains, thus lowering the maximum stable slope, which is in agreement with the trend of the observations. Evaluation

of the 14 cases where the angle of initial yield appeared to have been attained indicated that the maximum slope on the shoreward bar face was in the range of 20-35 deg, with an average of 28 deg. In each of the cases, the angle of initial yield should be somewhat larger than the value determined as the maximum slope. An estimate of bar face slope after avalanching occurred may be obtained by examining the minimum shoreward bar face slope after the angle of initial yield had apparently been exceeded. The slope thus calculated (10 cases showing clear minima) was in the range of 20-25 deg, with an average of 22 deg. These values should be somewhat higher than the actual residual angle after shearing since some steepening of the slope probably occurred between the times of avalanching and the profile survey.

276. The average seaward bar face slope was fairly constant through time, sometimes exhibiting a slight increase during the first hours of the run. Figure 26 shows the seaward bar face slope as a function of time for representative cases. The average slope was typically in the range of 8-12 deg, although local slopes reached 20 deg. The variation in average seaward bar face slope was small and appeared to be independent of grain size, but weakly related to wave period, with longer periods giving a more gentle slope.

277. The seaward face of the bar was in many cases well approximated by two or three planes having distinctly different slopes. The upper part of the bar face seaward from the crest had a slope $\beta_2$ ranging from 4-8 deg, whereas the slope of the lower part of the bar $\beta_1$ was in the range of 8-18 deg. In some cases, the very end of the bar could be approximated by a third line of constant slope, often with a magnitude smaller than that of the two shoreward slopes. The location of the intersection between the upper and lower seaward face slopes approximately coincided with the location of the break point in many cases (see Figure 14). This triplaned nature of bars formed under regular waves does not seem to have been noted before. Although such a configuration would probably not be exhibited in the field because of varying waves and water level, its manifestation under regular waves indicates the existence of a small and subtle regime of hydrodynamic forces in the region under prebreaking waves which acts on a wave-by-wave basis whether or not it is observed in macroscale profile surveys in the field.

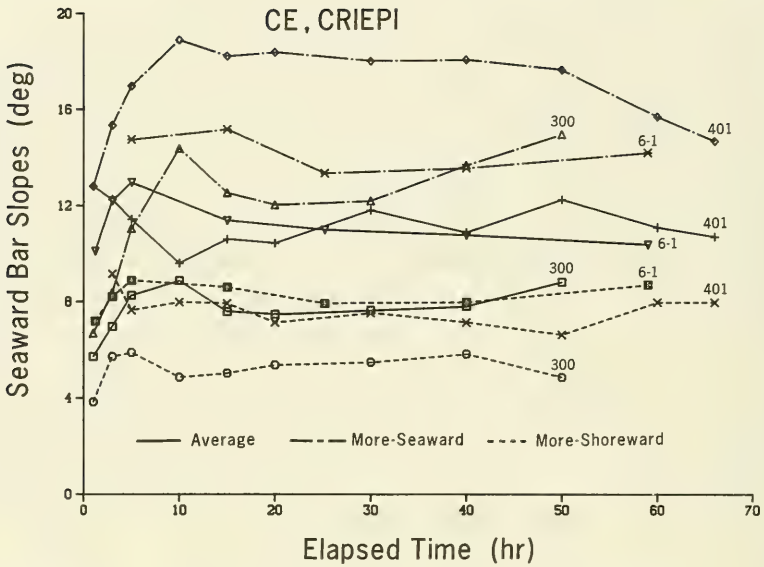


Figure 26. Evolution of seaward slopes of main breakpoint bars

278. Since average shoreward and seaward bar face slopes were considerably different, the bars were asymmetric in shape. The average shoreward bar slope was always steeper than the corresponding average seaward slope, making the bar positively skewed.

279. Bar face slopes encountered in the field are, in general, milder than slopes in the CE, CRIEPI, and other tank studies involving regular waves and constant water levels. Under laboratory situations, the smoothing effect on the profile of random waves and varying water level which normally exist in nature (e.g., Keulegan 1948) is absent. For example, Hands (1976) found that maximum bottom slope was less than 10 deg for numerous measurements of Lake Michigan bars (varying waves but constant water level). On the basis of frequent and repetitive high-accuracy surveys on an Atlantic Ocean beach over 5 years, Birkemeier* found that steepest shoreward bar slopes of approximately

* Personal Communication, 1987, William Birkemeier, Hydraulic Engineer, Coastal Engineering Research Center, Vicksburg, MS.

10 deg occurred when bars moved onshore during the profile recovery process after a high wave event, not when bars moved offshore. Seaward bar faces rarely exceeded 10 deg.

280. Within the context of this study, the difference between present and field results for bar face slopes can be attributed in great part to the action of random waves and varying water level, which would widen the breaker zone and smooth profile features in the field. Another factor is that steady wave conditions are usually not of sufficient duration in the field for bars to reach equilibrium form.

Step and terrace slope

281. In the LWT experiments, when erosion occurred the beach profile retreated to produce a characteristic scarp or step immediately landward of the still-water level. This scarp developed concurrently with a gentle terrace slope that was milder than the slope of the initial profile. The slope of the step increased with time and sometimes reached the angle of initial yield, exhibiting the same tendency of alternating maxima and minima, similar to the behavior of the shoreward slope of breakpoint bars as discussed above. If the initial slope was mild, the retreat of the shoreline was small; and the shoreline sometimes advanced somewhat even if a breakpoint bar formed offshore. In this latter case most of the material in the bar was taken from the surf zone rather than from the foreshore. If the waves were not too severe (erosive) in these cases, the bar may have also received a net contribution of material by onshore transport from the area located seaward of it. However, if the waves were severe, a step formed even if the slope were relatively gentle since the surf zone was not wide enough to dissipate all of the incident wave energy, thereby resulting in strong wave attack and erosion of the foreshore.

282. Figure 27 illustrates the average slope of the step $\beta_5$ as a function of time for selected cases in which considerable erosion of the foreshore took place. Time development of the average terrace slope $\beta_4$ immediately seaward of the step is also presented. For a coarser grain size, steepening of the step slope proceeded more slowly (Case 401) and may have achieved an equilibrium value before the angle of initial yield was reached. The slower response of the coarser grains is probably due to their greater

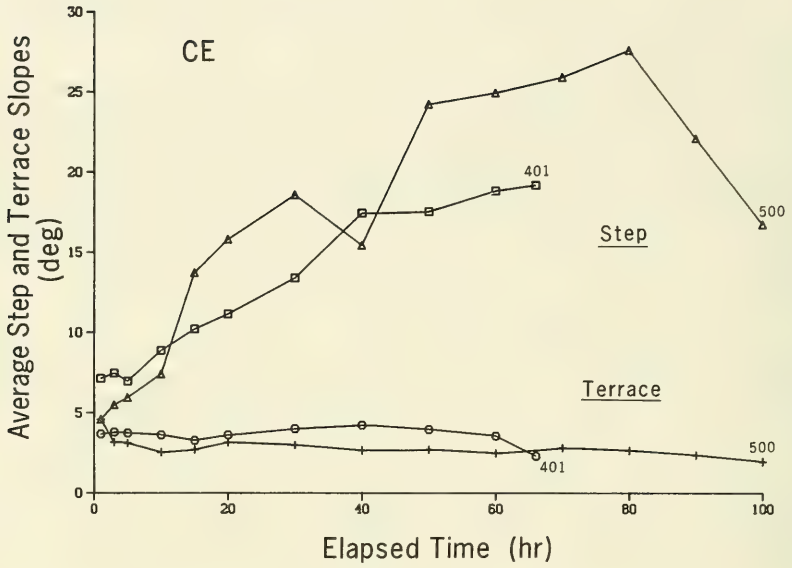


Figure 27. Evolution of representative step and terrace slopes

stability against dislodgement and transport by the bore. The terrace slope was more gentle than the initial slope and appeared to be almost independent of grain size, with finer grain sizes showing a slight tendency to form gentler slopes.

## Form and Movement of Berms

### Berm genesis

283. As wave steepness becomes smaller (e.g., as a storm wanes and the wave height decreases), the transport direction changes from offshore to onshore and material builds up on the foreshore, a process documented by Hayes and Boothroyd (1969), Sonu (1970), and Kriebel (1987). A berm forms which is a function of local wave and water level movement on the foreshore and sediment properties. In this study, the berm was defined as the volume of material accreted on the foreshore with reference to the initial plane slope (Figure 4b). This is a natural definition since a berm is intuitively thought

of as an accretionary feature. The berm typically forms above the still-water level but may extend below the water surface and move the shoreline position slightly seaward as it grows with time. The vertical extent of the berm is closely related to the runup limit, whereas its shoreward extent in the equilibrium state is mainly determined by how the grains move under gravitational force. The point on the foreshore where berm formation is initiated mainly depends on the runup limit where a larger runup implies berm initiation further shoreward. Runup is essentially a function of local beach slope, wave period, and breaking wave height for both regular waves in the laboratory (Hunt 1959, Savage 1959) and irregular waves in the field (Holman and Sallenger 1985).

284. No information about runup was available from the CRIEPI experiments and only little information from the CE experiments. In the CE experiments, runup was measured in most cases, typically for the first 10-20 waves (Kraus and Larson 1988a). There were only five CE cases which had berm build-up and measurement of runup. However, an indication of the relationship between berm formation and runup may be obtained by viewing Figure 28 where the distance to the mass center of the berm is plotted as a function of the runup length $\ell_r$ , all quantities referenced to the initial still-water level. The runup length is the average of all runup measurements, and the first profile survey (typically performed after about 1 hr of wave action) was used to calculate the distance to the berm center of mass. The distance to the center of mass was roughly half the runup length which, if the berm is considered to be approximately symmetrical, indicates that the runup length was close to the shoreward end of the berm, as would be expected. All berms in the previously-mentioned five cases were formed on profiles showing a strong tendency for onshore transport during the full duration of the run, although a small breakpoint bar may have been present.

285. In cases where a berm was present but the transport rate was more variable in direction both along the profile and in time, the berm was often small and sometimes formed with its center of mass below the still-water level. Equilibrium properties of the berm on such profiles (berm volume, maximum berm height) were reached very rapidly, typically prior to the time of the first profile survey.

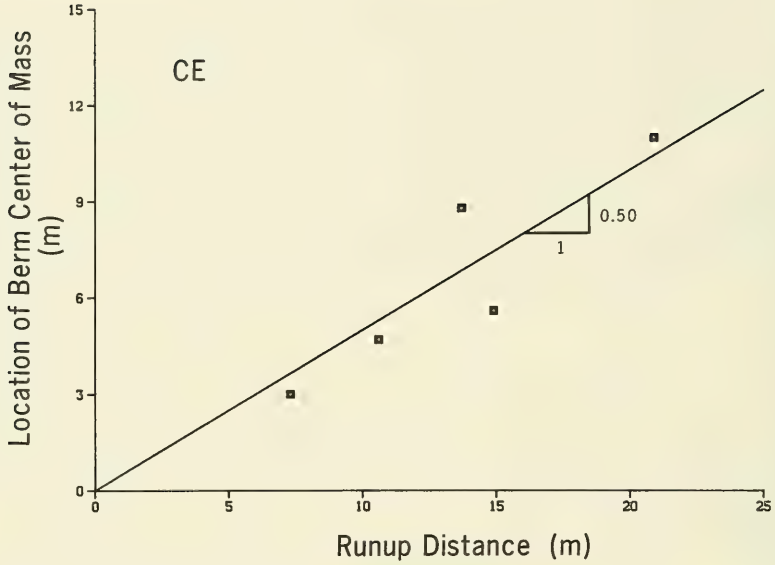


Figure 28. Relation between berm center of mass and wave runup

286. For most berms, the horizontal movement of their center of mass was small, indicating that the berm grew uniformly in time over its length. If the berm showed a net movement of its center of mass, it was always in the shoreward direction. The length of the berm at equilibrium appeared to depend mainly on breaking wave height and little on wave period (Bagnold 1940, Sunamura 1975, Takeda 1984).

Active profile height

287. A quantity $Z_R$ was defined as the maximum subaerial elevation of the active profile above still-water level for either bar or berm profiles (Figure 4b). An empirical equation was obtained from the LWT data by relating this quantity to the surf similarity parameter, $\tan\beta/(H_o/L_o)^{1/2}$ (Battjes 1975). The surf similarity parameter was evaluated using the initial beach slope, resulting in the empirical equation

$$\frac{Z_R}{H_o} = 1.47\left[\frac{\tan\beta}{\sqrt{H_o/L_o}}\right]^{0.79} \quad (17)$$

The coefficient of determination was 75 percent for 32 cases for which the height of the active profile could be distinguished.

Equilibrium berm volume

288. In the LWT experiments, volume of the berm increased with time to approach an equilibrium value attained when the profile was in balance with the incident waves, thereby dissipating wave energy without significant changes in shape. Seventeen cases exhibiting some kind of foreshore buildup were identified in the CE and CRIEPI data sets. However, only eight of these cases showed strong berm buildup with onshore transport occurring during most of the run. In some CRIEPI cases, accretion on the foreshore started to occur only at the very last few profile surveys, and equilibrium was reached almost immediately (for example, Cases 4-2 and 5-2). Profiles of this type were erosional, but these cases had a moderate wave climate and a gentler initial slope, allowing for a small amount of onshore transport on the foreshore as the breakpoint bar system approached equilibrium. In Figure 29(a and b), the berm volume as a function of time is displayed for the CE and CRIEPI experiments.

289. To estimate equilibrium berm volume, an expression similar to Equation 7 was least-squares fitted to the data for the eight cases. The number of cases was too small to derive reliable empirical relationships between berm volume and wave characteristics and beach profile properties. Some tendencies noted may be of interest for indicating which factors appear to control equilibrium berm volume. Berm volume showed the greatest dependence on sand fall speed, with a greater fall speed implying a larger berm volume. This phenomenon seems reasonable because the tendency for onshore transport increases with greater fall speed for the same deepwater wave steepness (Figure 6). Within the range of grain sizes used in the experiments, coarser material often experienced more marked onshore transport than the finer material. In contrast, the finer material, for the cases where berm buildup occurred, had a less dominant transport direction, thus resulting in

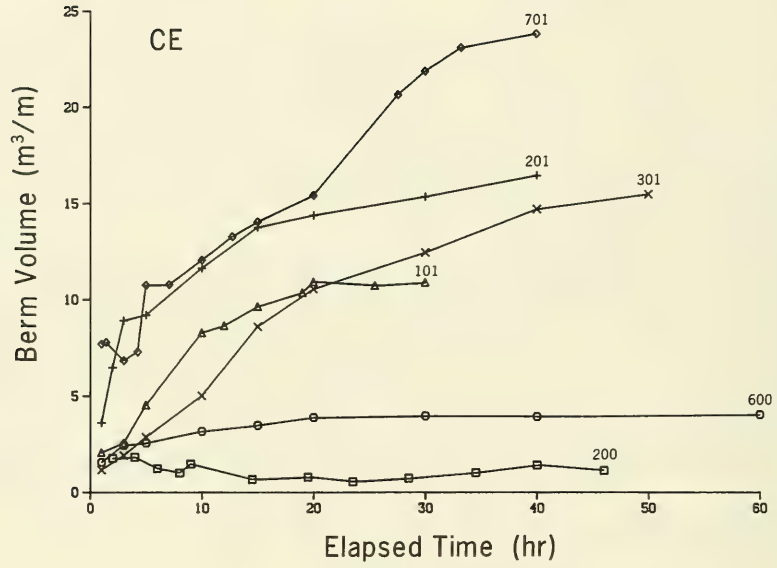


a. CE data

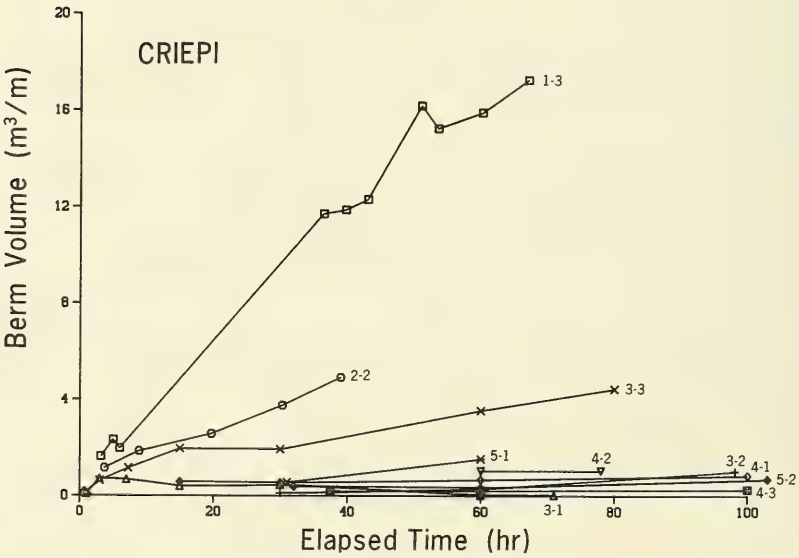


b. CRIEPI data

Figure 29. Growth of berm volume with elapsed time

smaller equilibrium berm volumes. An increase in wave height produced a larger berm volume, whereas wave period seemed to be a negligible factor. However, wave period influenced the rate at which equilibrium berm volume was reached, with a longer wave period producing more rapid berm buildup.

Maximum berm height

290. Maximum berm height $Z_b$ defined with respect to the initial profile showed development with time similar to berm volume. Figure 30(a and b) shows the growth of maximum berm height as a function of time. If accretion on the foreshore occurred in cases with predominant offshore transport, equilibrium berm height was attained quickly, as seen in Cases 200, 3-1, and 4-2. Equilibrium maximum berm height was estimated from a least-squares fit of the data from each case (eight cases used in total), with an expression of the form of Equation 7. Grain size emerged as an important variable for the same reasons as discussed for equilibrium berm volume. Breaking wave height appeared as a considerably more decisive factor than deepwater wave height, probably because runup is more closely related to breaking wave height. The ratio between maximum equilibrium berm height and breaking wave height had a relatively small range. The average value of the ratio was 0.5, ranging from 0.3 to 0.8 for the eight cases analyzed. The standard deviation was 0.16.

291. Berm height, normalized by some appropriate length scale (wave height or wavelength), showed no correlation with dimensionless sand fall speed. This occurrence is not surprising since this quantity is generally believed to characterize suspended transport which is not the dominant transport mode on the foreshore. For a specific grain size, berm height divided by breaking wave height was found to be weakly dependent on the surf similarity parameter, but a clear overall relationship could not be obtained. Runup height is usually expressed in terms of the surf similarity parameter (see Hunt 1959), so this dependence is expected; however, the present data sets on berm growth are too limited to conclusively verify such a relationship.

Berm slopes

292. If a berm formed on the foreshore, its seaward face slope steepened and a positive slope developed on its shoreward face. Average seaward berm face slope was relatively constant, with a slight tendency to increase

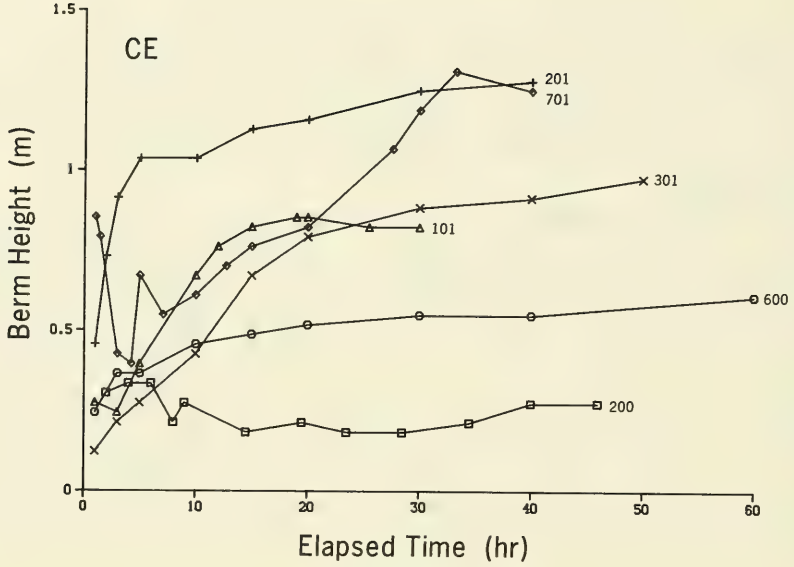


a. CE data

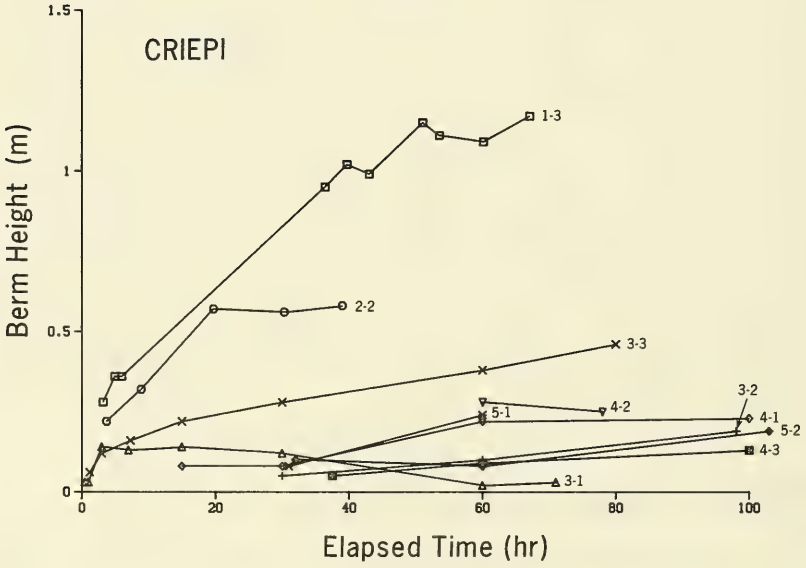


b. CRIEPI data

Figure 30. Growth of maximum berm height with elapsed time

with time. Figure 31 shows the time change of the average shoreward berm face slope $\phi_1$ and seaward slope $\phi_2$ changed during two typical cases (Cases 300 and 1-3) with berm buildup. The seaward berm slope was approximately independent of grain size and ranged between 6-8 deg.

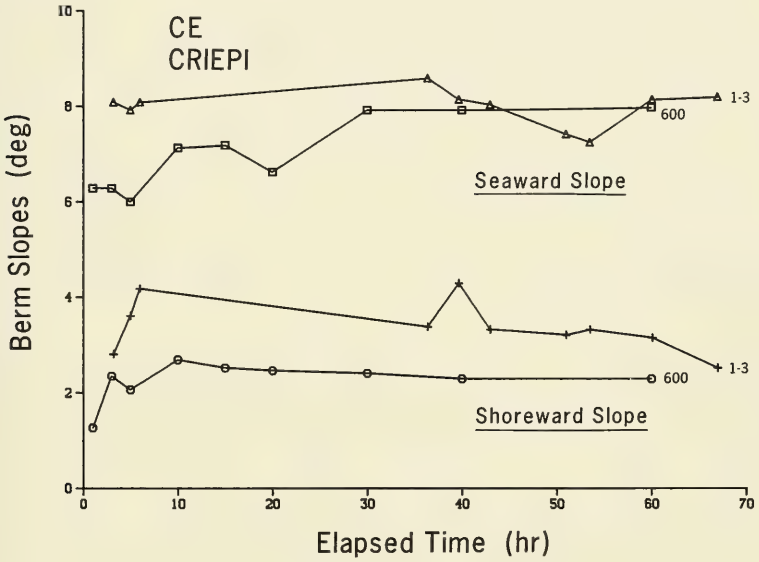


Figure 31. Growth of representative berm slopes with elapsed time

293. If a well-developed shoreward berm face slope was present, it was considerably more gentle than the seaward face slope. Typical values of the average shoreward berm face slope were 2-4 deg, although steeper slopes occurred. The average shoreward berm face slope also appeared to be independent of grain size and constant in time, except for one case (Case 201) which showed an increase with time toward an equilibrium value of about 15 deg. In this case the grain size was coarse, and the wave height and wave steepness were relatively small. The waves were probably breaking very close to the shoreline, one of the few cases where no breakpoint bar appeared along the profile, strongly affecting the shape of the berm.

## Summary

294. Numerous morphologic features of beach profiles generated under breaking waves in large wave tanks were quantitatively described in this chapter. Selected morphologic parameters are presented in Tables 4 and 5, together with the breaking wave height. Under steady, regular waves and constant or slowly varying water level, the evolution of bars and berms was found to be regular, exhibiting clear growth and equilibrium properties that were readily described by simple regression expressions. The dimensionless sand fall speed $H_o/wT$ emerged as an important parameter in predicting both profile response and geometric properties of various major morphologic features. The strong relationship between wave and sand characteristics and morphologic features suggests the possibility of quantitatively predicting the evolution of macroscale features of the profile.

295. The effect of scale was made apparent through the different values of empirical coefficients in the criteria for erosion and accretion (bar/berm formation) for small-scale and prototype-scale wave and beach conditions. Interestingly, most criteria held for both small- and prototype-scale experiments provided that empirical coefficients were modified. It was found that use of mean wave height with field data allowed the same criterion to be used (Equation 2) as found for the LWT experiments involving regular waves, with no change of the empirical coefficient.

296. In general, profile response in the LWT experiments, apart from effects related to use of regular waves, was considerably in agreement with what is observed on a natural beach. Irregular waves as occur in the field are expected to give a smoother character and slower rate of change of morphologic features.

Table 4

CE Experiments: Values of Selected Quantities

| Case No. | Bar $V_{eq}$ $m^3/m$ | Bar $h_c$ m | Bar $(h_t/h_c)_{avg}$ | Bar $H_b$ m | Berm $V_{eq}$ $m^3/m$ | Berm $Z_b$ m | Berm $Z_R$ m |
|---|---|---|---|---|---|---|---|
| 100 | 18.5 | 1.16 | 1.45 | 1.68 | ---- | ---- | ---- |
| 200 | 8.2 | 0.90 | 1.50 | 1.07 | ---- | ---- | 0.89 |
| 300 | 30.1 | 1.31 | 1.71 | 2.00 | ---- | ---- | 1.56 |
| 400 | 28.6 | 1.52 | 1.68 | 2.30 | ---- | ---- | 1.50 |
| 500 | 33.3 | 1.44 | 1.84 | 1.90 | ---- | ---- | 1.05 |
| 600 | ---- | ---- | ---- | 1.15 | 3.8 | 0.53 | 0.88 |
| 700 | 24.5 | 1.79 | 1.46 | 2.10 | ---- | ---- | 1.81 |
| 101 | 3.7 | 1.31 | 1.26 | 1.80 | 11.7 | 0.88 | 1.29 |
| 201 | ---- | 1.18 | 1.32 | 1.90 | 14.9 | 1.17 | 1.45 |
| 301 | 2.9 | 1.44 | 1.29 | 2.40 | 18.3 | 1.01 | 1.36 |
| 401 | 19.6 | 1.28 | 1.89 | 2.40 | ---- | ---- | 1.48 |
| 501 | 22.1 | 1.16 | 2.05 | 1.60 | ---- | ---- | 0.72 |
| 701 | ---- | ---- | ---- | 1.95 | 23.1 | 1.14 | 2.56 |
| 801 | ---- | 0.56 | 1.62 | 0.76 | ---- | ---- | 0.47 |
| 901 | 11.3 | 1.28 | 1.55 | 2.00 | ---- | ---- | 0.97 |
| 911 | 12.0 | ---- | ---- | ---- | ---- | ---- | 1.26 |

Table 5

CRIEPI Experiments: Values of Selected Quantities

| Case No. | Bar | | | | Berm | | |
|---|---|---|---|---|---|---|---|
| | $V_{eq}$ $m^3/m$ | $h_c$ m | $(h_t/h_c)_{avg}$ | $H_b$ m | $V_{eq}$ $m^3/m$ | $Z_b$ m | $Z_R$ m |
| 1-1 | ---- | 0.47 | 1.89 | 0.95 | ---- | ---- | 0.37 |
| 1-3 | ---- | ---- | ---- | 1.40 | 27.7 | 1.12 | 1.31 |
| 1-8 | 1.6 | 0.55 | 2.06 | 0.85 | ---- | ---- | 0.24 |
| 2-1 | 7.5 | 1.12 | 1.78 | 1.94 | ---- | ---- | 0.23 |
| 2-2 | 8.7 | 0.67 | 2.06 | 1.54 | 7.3 | 0.60 | 0.52 |
| 2-3 | 0.7 | 0.45 | 1.96 | 0.80 | ---- | ---- | 0.14 |
| 3-1 | 12.4 | 0.91 | 1.78 | 1.88 | ---- | ---- | 0.75 |
| 3-2 | 15.3 | 0.76 | 1.76 | 1.58 | ---- | ---- | 0.55 |
| 3-3 | 9.1 | 1.00 | 1.50 | 1.47 | 5.0 | 0.43 | 0.98 |
| 3-4 | 24.9 | 1.23 | 2.16 | 1.50 | ---- | ---- | 0.48 |
| 4-1 | ---- | ---- | ---- | 0.50 | ---- | ---- | 0.21 |
| 4-2 | 4.5 | 0.83 | 1.84 | 1.27 | ---- | ---- | 0.37 |
| 4-3 | 23.5 | 1.23 | 2.07 | 1.52 | ---- | ---- | 0.34 |
| 5-1 | ---- | ---- | ---- | 0.63 | ---- | ---- | 0.36 |
| 5-2 | 6.5 | 0.61 | 2.02 | 0.89 | ---- | ---- | 0.43 |
| 6-1 | 36.5 | 1.39 | 1.76 | 1.91 | ---- | ---- | 1.66 |
| 6-2 | 25.3 | 0.98 | ---- | 1.42 | ---- | ---- | 1.19 |

## PART V: CROSS-SHORE TRANSPORT RATE

297. If a beach profile is not in equilibrium with the existing wave climate, sediment will be redistributed along it to produce an equilibrium profile shape in which state the incident wave energy will be dissipated without causing further significant net sediment movement. It has been established that as sediment is transported across the shore certain characteristic net transport rate distributions occur, and these distributions have specific properties in time and space. Regularity in transport rate distributions is anticipated since the previous chapter showed that the shape of the beach profile changed regularly through time.

298. The objective of this chapter is to describe properties of the cross-shore sand transport rate and relate them to wave parameters, sand characteristics, and beach profile shape. Quantitative knowledge of cross-shore transport provides the necessary foundation for the numerical modeling component of this investigation.

299. Keulegan (1948) appears to have been the first to measure cross-shore sand transport along the profile. He used traps mounted in a small wave tank and found that the maximum transport rate was located at the point of impending wave breaking where the front of the wave was almost vertical near the crest. He noted a correlation between the sand transport rate and total displacement of the water surface, and he recognized the existence of a critical wave height for sand transport to occur.

300. Several early papers concerned development of criteria for predicting the predominant direction of the transport (onshore or offshore). Rector (1954) used deepwater wave steepness and ratio between median grain size and deepwater wavelength. Ippen and Eagleson (1955) studied the movement of individual particles on a plane slope under shoaling waves and found net motion to result from inequality of hydrodynamic drag and particle weight. Their criterion for distinguishing between onshore and offshore motion contained three nondimensional parameters: wave steepness, ratio of wave height and water depth, and ratio of sediment fall speed and wave celerity.

301. Van Hijum (1975, 1977) determined the distribution of the cross-shore transport rate on a beach of coarse material by comparing consecutive

beach profiles in time. The equation of mass conservation was integrated from successive beach profile surveys, and an average net transport rate over the studied time interval was obtained. The technique of determining the distribution of the net cross-shore transport rate from consecutive profile surveys has been employed in other studies (for example, Hattori and Kawamata 1981; Watanabe, Riho, and Horikawa 1981; Shimizu et al. 1985). A classification of transport rate distributions for LWT results was proposed by Kajima et al. (1983a) based on a beach profile classification by Sunamura and Horikawa (1975) who used data from experiments with a small tank.

302. By determining the transport rate from profile change, an average net distribution of the cross-shore transport rate is obtained for the elapsed time between two surveys. An alternative method of acquiring information on the transport rate is measurement of the sediment concentration and fluid velocity field. Sawaragi and Deguchi (1981) and Deguchi and Sawaragi (1985) measured sediment concentrations in small-scale laboratory experiments and obtained concentration profiles at selected locations across the beach profile. Vellinga (1986) and Dette and Uliczka (1987b) made similar measurements of concentration profiles in experiments performed with large tanks and waves of prototype scale.

303. The average net cross-shore transport rate may be obtained by integrating the equation of mass conservation between two beach profiles in time. The transport rate $q(x)$ across the profile is thus calculated from the mass conservation equation written in difference form with respect to time as

$$q(x) = \frac{1}{t_2 - t_1} \int_{x_o}^{x} (h_2 - h_1)\, dx \tag{18}$$

where

$t_1$ , $t_2$ = times of profile surveys

$x_o$ = shoreward location of no profile change, where $q(x_o) = 0$

$h_1$ , $h_2$ = profile depths at survey times 1 and 2

304. To evaluate the transport rate numerically, measured profiles used in this study where approximated by a set of cubic spline polynomials (see

Part IV). Subsequent calculations used in the analysis were carried out from a point on the shoreward end of the profile where no change occurred during the run to a seaward point where there was no movement of material (typically, to the horizontal part of the tank beyond the toe of the beach).

305. In Equation 18, sand porosity has been incorporated in $q$, the cross-shore transport rate, implying that the porosity is independent of time and space. Qualitatively, it was noted during the CE experiments that the foreshore sand tended to compact, whereas sand at the flanks of the breakpoint bar tended to be looser (Kraus and Larson 1988a). The error introduced by assuming constant porosity is believed to be negligible.

306. Errors may be introduced through limitations in accuracy of the profile surveys or due to long time interval between surveys. A small systematic error in profile depth measurements may give a finite contribution if summed over the profile length and could give rise to an apparent transport at the seaward boundary of the profile where no transport actually occurred. In particular, the CE surveys, having a 1.2-m (4-ft) spatial interval, were in some cases not taken frequently enough to indicate negligible transport at the seaward boundary. Therefore, in these cases, to proceed with the analysis, one of the profiles was displaced vertically to achieve the condition of zero transport at the boundary. The vertical displacement was in general small (less than 1 cm) and less than the measurement accuracy of the profile survey ($\pm$1.5 cm). A small displacement of one of the profiles exerts some influence on the magnitudes of maximum and minimum transport rates but only slightly changes the shape of the transport rate distribution.

## General Features of Cross-Shore Transport

307. Distributions of the net cross-shore transport rate were determined for both the CE experiment (18 cases) and the CRIEPI experiment (24 cases). However, in most of the analyses a subset comprising 33 cases was used which encompassed those cases starting from an initial plane slope. Profile behavior was thereby more readily isolated, and the added complexity of an arbitrary initial profile shape avoided. Between 5 and 10 transport rate distributions were calculated for each case, depending on the number of

profiles surveyed. Information about the specific cases, such as wave conditions, sand grain size, and initial profile slope are summarized in Tables 1 and 2.

308. Figure 32 shows the beach profile at consecutive times for CE Case 300, which is an example of a bar profile with transport mainly directed offshore. Two bars appeared, and the shoreline receded considerably with a pronounced scarp or step formation. Seaward of the step, the foreshore eroded with a slope more gentle than the initial slope (1:15). In Figure 33 are shown the calculated distributions of the cross-shore sand transport rate associated with Case 300. Transport directed offshore has a positive sign; the coordinate system originates from the position of the initial still-water shoreline. Decay of the transport rate with time is clear from Figure 33, and the maximum transport rate calculated from the final two surveys is more than one order of magnitude smaller than the maximum from the first two surveys.

309. The peak in the transport rate distribution translated seaward with the break point, and thus the bar moved seaward. The first maximum in the transport rate occurred shoreward of the first break point, close to the plunge point and slightly seaward of the location of the trough bottom. Another, smaller maximum in the transport rate was present further inshore, and this maximum also moved slightly seaward with time. For the transport rate distributions at later times, the shape was flatter and no maxima were prominent, indicating that material was mainly conveyed from the inner to the outer part of the profile. Seaward of the first maximum, the transport rate decreased rapidly with an approximate exponential shape.

310. CE Case 101 is an example of a case of mainly onshore transport, resulting in deposition on the foreshore and creation of a berm. Figure 34 shows surveyed profiles at consecutive times, with an initial slope of 1:15. Although a large berm formed on the foreshore, a small bar was also present just shoreward of the break point. The bar was created mainly during the first hours of the run, and it rapidly reached an equilibrium volume. The trough shoreward of the bar became less pronounced as the berm grew.

311. In Figure 35 distributions of the transport rate pertaining to Case 101 are shown (negative transport rate implies onshore transport). The transport rate decreased with time as the profile approached equilibrium

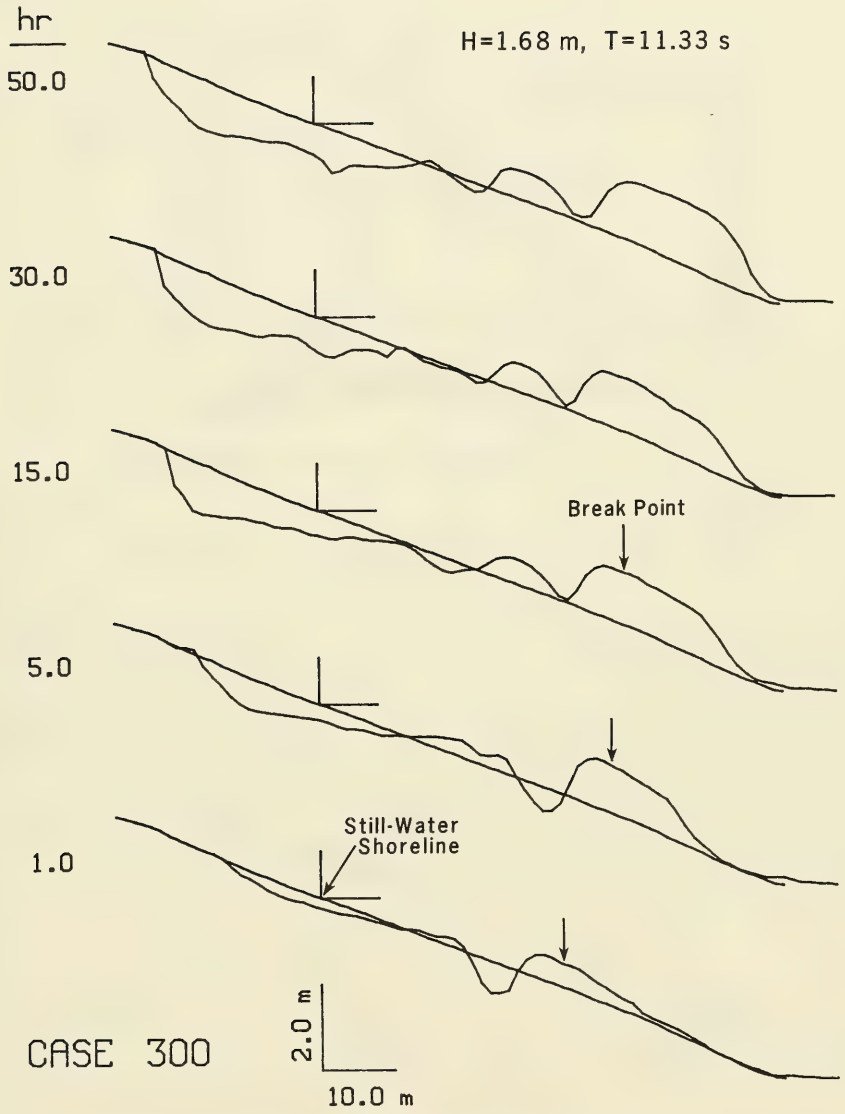


Figure 32. Evolution of beach profile under constant incident wave conditions for an erosional case (Case 300)

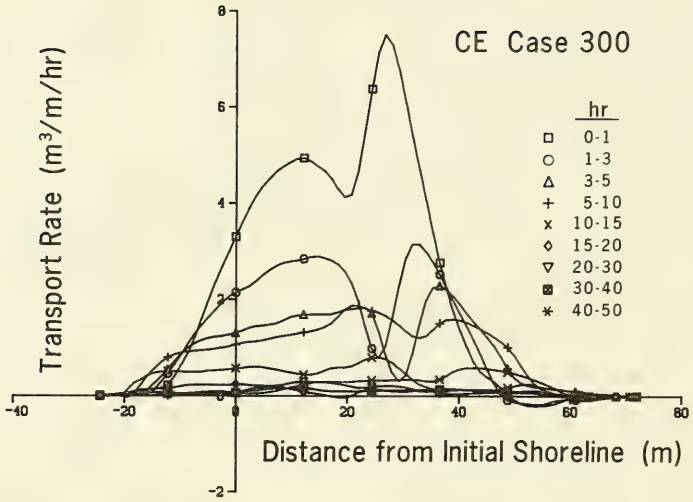


Figure 33. Calculated distributions of the net cross-shore sand transport rate for an erosional case (Case 300)

shape. Initially, the transport rate distribution showed a clear negative peak, but the shape of the distribution became smoother as the breakpoint bar approached equilibrium volume. Material was thus transported shoreward over the bar and deposited on the foreshore. The breakpoint bar was formed mainly by onshore transport and is seen as the minimum occurring in the first transport rate distribution. Similar to Case 300, the seaward part of the transport rate distribution may be well approximated with an exponential function decaying with distance in the offshore direction.

## Classification of Transport Rate Distributions

312. Depending on wave conditions and sand size, the distribution of the cross-shore transport rate took a specific shape. Since the transport rate in this study is determined from consecutive profile surveys, calculated distributions represent an average net response of the profile and not the instantaneous transport rate. If the initial and final profiles from a

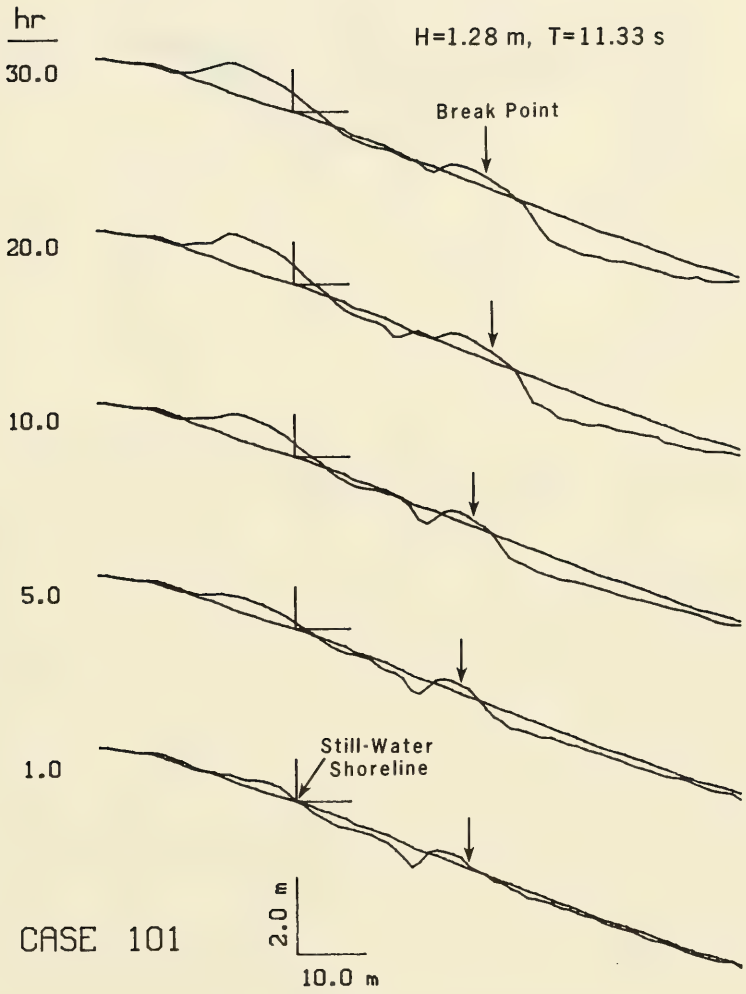


Figure 34. Evolution of beach profile under constant incident waves for an accretionary case (Case 101)

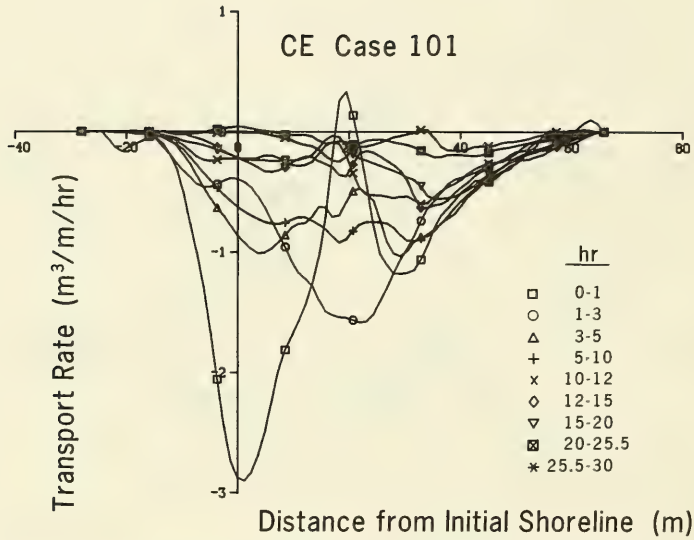


Figure 35. Calculated distributions of net cross-shore sand transport rate for an accretionary case (Case 101)

specific case are used to calculate the distribution of the transport rate, an overall picture of the profile response is obtained. The distribution determined from the initial and final profile surveys will be termed the "equilibrium distribution," although it is recognized that the final profile survey only approximates the actual equilibrium configuration and the time weightings are not equal between cases.

313. Based on this so-defined equilibrium distribution, a classification of net transport rate distribution shapes is more easily performed than if consecutive profiles in time are used. This description also indicates where the sand originated which supplied the bar and berm. For example, depending on the wave and sand properties, a bar may be formed from sand supplied from either its shoreward side or its seaward side or from both sides.

314. From the equilibrium transport rate distributions, three main shapes were identified, although general trends in the distributions often exhibited small perturbations. Figure 36(a-c) illustrates the three principal

distribution shapes calculated for three cases, CE Cases 300 and 101, and CRIEPI Case 3-2. Note that the cases shown from the CE data are identical to those presented in Figures 33 and 35, where the distributions of the net transport rates were given corresponding to consecutive survey times and not as equilibrium forms. The classification of transport rate distribution is closely related to criteria for distinguishing bar and berm formation (erosion and accretion). A barred profile is generally associated with erosive conditions, implying offshore transport, whereas a profile with berm buildup mainly experiences onshore transport. However, in some cases where a bar formed, even though much of the material composing the bar was eroded from the foreshore, onshore transport from the region seaward of the bar also contributed.

315. The equilibrium transport rate distribution, illustrated by Case 300, is called Type E (Erosional) and is characterized by transport in the offshore direction along the full extent of the active profile. A positive derivative in the transport rate with respect to the cross-shore coordinate indicates local erosion of the profile, whereas a negative derivative indicates local deposition. At locations where the derivative is zero, the depth was constant and material was simply conveyed through the point. A minimum or maximum in the equilibrium distribution of the transport rate pertains to a morphologic feature along the beach profile. Cases where the transport was directed offshore along the entire profile are by definition subject to strong erosion, giving rise to one or more breakpoint bars. For larger grain sizes, the width of the peak of the equilibrium transport rate distribution decreased for the same wave conditions, indicating that the major part of the sand movement was concentrated in a narrow portion of the profile. This concentration is caused by the requirement for greater energy dissipation to achieve the equivalent transport condition for beaches composed of larger sand grains.

316. For the second main type of equilibrium transport rate distribution, exemplified by Case 101 and called Type A (Accretionary), transport is directed onshore along the full extent of the active profile. The distribution is in essence the mirror image, through the cross-shore coordinate axis, of the Type-E distribution. In general, however, any secondary minimum in the

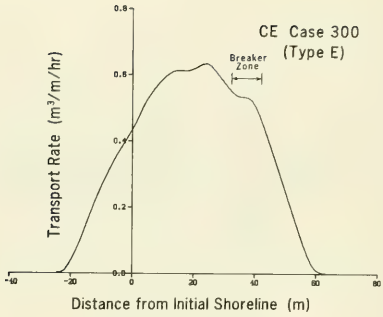


a. Type E, Erosional

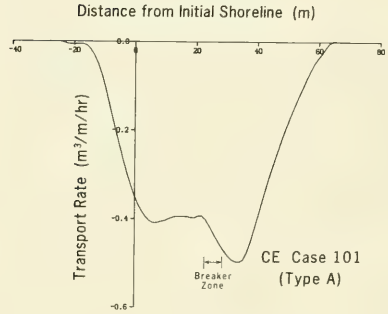


b. Type A, Accretionary

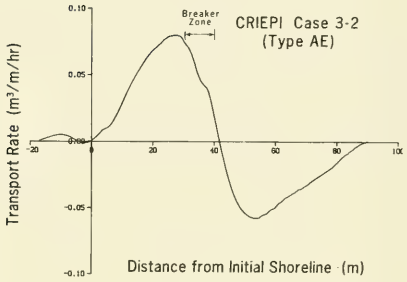


c. Type AE, Mixed Accretionary and Erosional

Figure 36. Net cross-shore sand transport rate distributions

transport rate distribution is more pronounced than for Type E, related to the small bar frequently present and located slightly shoreward of the break point on accretionary profiles. The onshore-directed transport gives rise to a berm on the foreshore.

317. The third main type of equilibrium transport rate distribution, Type AE, and typified by Case 3-2, is characterized by one peak with offshore-directed transport occurring on the foreshore and another peak with onshore-directed transport located seaward of the break point. Thus, the bar receives contributions of material from both offshore- and onshore-directed transport. The Type-AE equilibrium transport rate distribution is characteristic of bar profiles which were closer to the dividing line between bar/berm profiles than profiles associated with Type-E distributions. Figure 37 illustrates profile evolution for CRIEPI Case 3-2, which is a typical example resulting from mixed accretionary and erosional (Type AE) transport distributions.

318. Of the 33 cases examined, 29 were easily classified as having Type A, E, or AE equilibrium transport rate distributions (15 E-type, 10 A-type, and 4 AE-type). In some cases, particularly when the change in beach profile was small (i.e., the beach profile almost stable under the incident waves), the distributions take on a more complex form with multiple peaks for onshore- and offshore-directed transport appearing along the profile. If the beach profile is close to an equilibrium shape under the incident waves, it is expected that the transport rate distribution will not show such a strong net overall trend as compared to a profile that is far from equilibrium with the imposed waves. Distributions rarely occurred having a peak for onshore-directed transport on the foreshore and a peak for offshore-directed transport located more seaward, and then only if minor changes in the profile occurred.

319. Kajima et al. (1983a) proposed a classification, similar to that developed in this study, in which three basic distribution types and two subdivisions were defined. One of their main distributions differs from that presented here. Their distribution corresponding to Type AE has a peak with onshore-directed transport located shoreward of the peak with offshore-directed transport which is opposite to the present classification. The two subdivisions each contain three peaks, varying in direction onshore and offshore. Sawaragi and Deguchi (1981) derived distribution shapes from

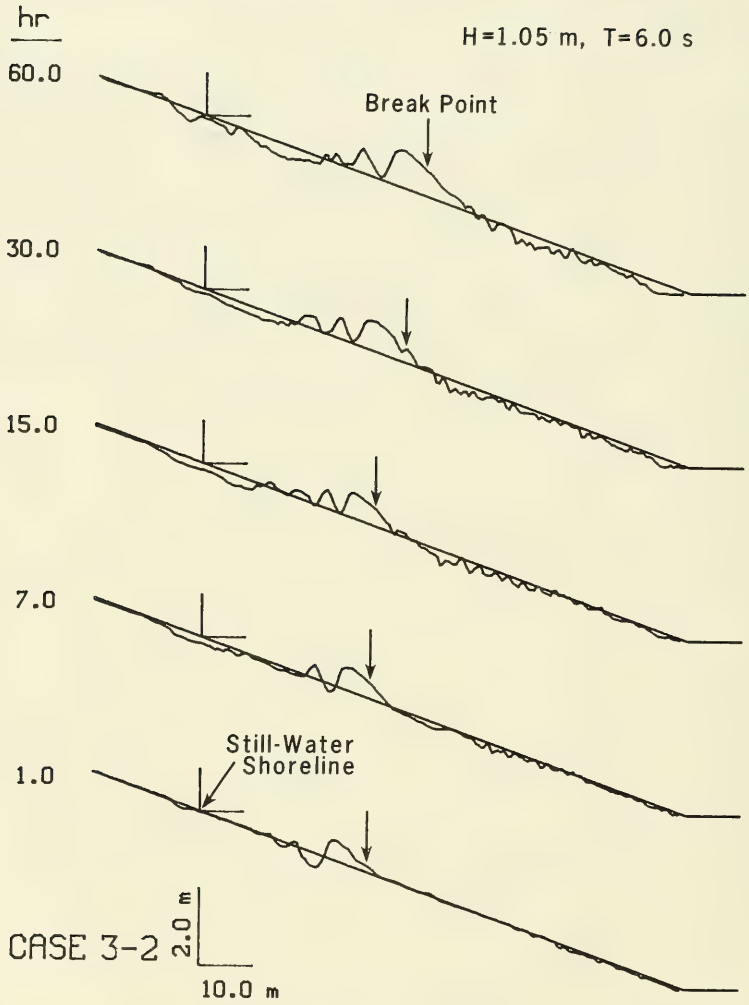


Figure 37. Evolution of beach profile under constant incident wave conditions for a mixed accretionary and erosional case (Case 3-2)

schematic profile shapes identified by Sunamura and Horikawa (1975). Their classification is also similar to the two mentioned above.

320. A factor that may influence profile development and net transport rate distribution is the limited depth in the horizontal section of the tanks in the CE and CRIEPI experiments. The effect is judged to be relatively minor since the depth in the horizontal section was at least 2-3 times the wave height in that part of the tank. Nevertheless, it is probable that some amount of onshore transport would have occurred if the depth and movable bottom had not been limited for those cases having transport distribution Type E. In any case, such a contribution would probably be small compared to the amount of material eroded from the foreshore.

321. Aubrey (1979) studied long-term exchange of material across the profile in the field. He applied empirical eigenfunction analysis to determine characteristic bar and berm profiles (prevalent during the winter and summer, respectively) and discovered two pivotal points where the profile depth was effectively constant. One pivotal point occurred for the studied beach at 2 to 3-m depth and the second one at 6-m depth below mean sea level. The seasonal volume exchange over the two pivotal points had a relation of 1 to 5, with the largest exchange taking place over the pivotal point closest to shore. This occurrence indicates that, in a long-term perspective during which weak onshore movement of sand may give a finite contribution, material exchange in deeper water is much less than that in the nearshore. For a single storm event giving rise to bar formation simulated in the LWT experiments, the ratio between the sand transport rate from the seaward and shoreward sides of the bar should be small.

## Approach to Equilibrium

322. As a beach profile approaches an equilibrium shape dictated by the incident waves, the net cross-shore transport rate decreases to approach zero at all points along the profile. By studying a relevant quantity related to the transport rate distribution at consecutive times, a picture of the approach to equilibrium can be attained. The peak onshore or offshore transport rate along the profile is a candidate quantity which might be

considered for examining the decay of the transport rate distribution with time. However, since the shape of the transport rate distribution also varies with time, a peak transport rate may not be the best overall indicator. Instead, the average absolute transport rate $Q_A$ along the profile was used since it provided a better measure of all transport activity along the profile. The average absolute transport rate was calculated as

$$Q_A = \frac{1}{x_1 - x_o} \int_{x_o}^{x_1} |q| \, dx \tag{19}$$

where $x_1$ is the seaward limit of profile change.

323. Figure 38(a and b) shows the decay of $Q_A$ with time for the CE and CRIEPI experiments. The general trend was for rapid decay during the first 10 hr, followed by a slower decrease with elapsed time. The approach to zero transport was slow at longer elapsed time since small adjustments in the profile occurred even if the profile had attained a near-equilibrium shape.

324. In many of the CRIEPI cases, $Q_A$ was small from the beginning of the run, since the initial beach profile was close to the equilibrium shape. The maximum occurring for one of the CE cases (Case 700), just before 20 hr, approximately coincided with a decrease in wave height that took place during the experiment (Kraus and Larson 1988a), forcing the profile toward another equilibrium condition. The general conclusion made based on Figure 38(a and b) is that the equilibrium concept is valid and that a numerical model developed for simulating realistic beach profile change must include this property.

Peak offshore transport

325. To quantify the time decay of the transport rate distribution as a function of wave parameters and sand size, the peak onshore or offshore transport rate is a good target quantity since the peak rate has a clear physical meaning. Figure 39 plots the peak transport rate as a function of time for 16 of the CE cases. For cases with strong erosion, decay with time of the peak offshore transport rate was much more pronounced than for cases with mainly accretion on the foreshore. If onshore transport prevailed, the

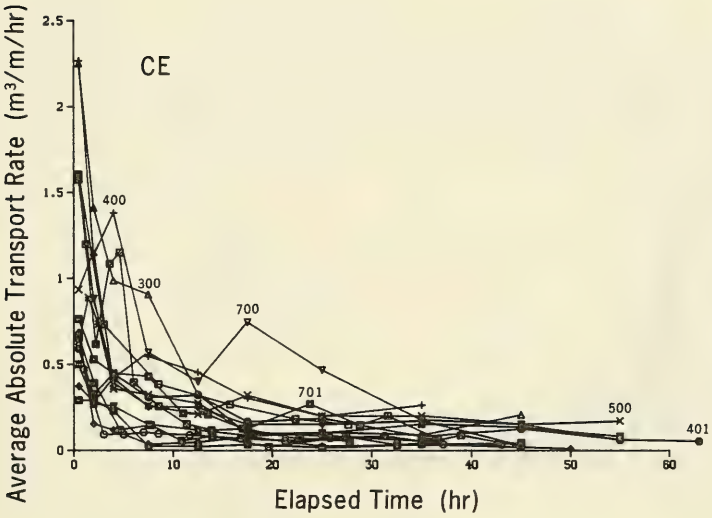


a. CE data, 16 cases

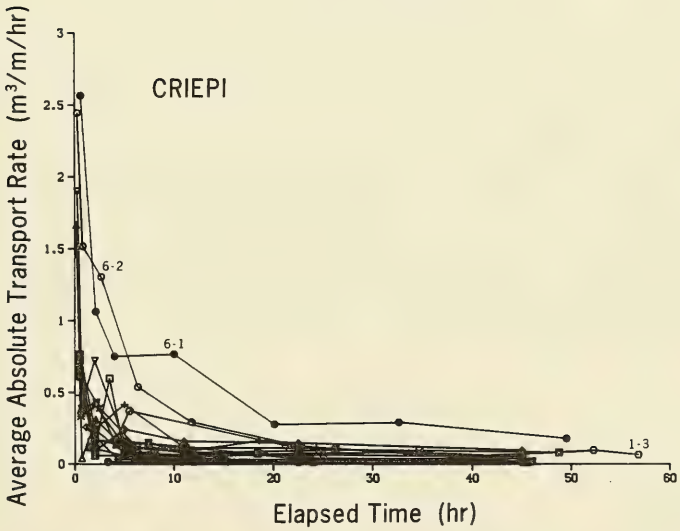


b. CRIEPI data, 17 cases

Figure 38. Decay of net cross-shore sand transport rate

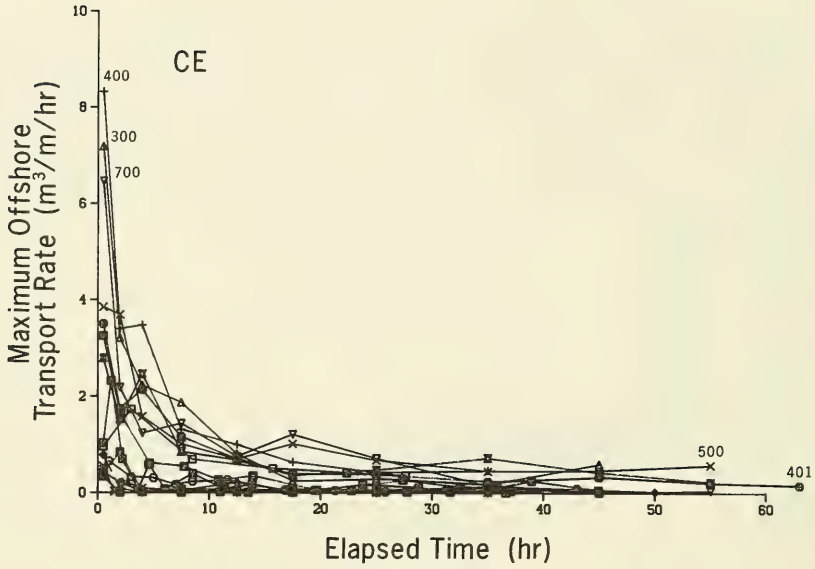


Figure 39. Evolution of peak offshore net sand transport rate for 16 CE cases

peak offshore transport rate was usually small or sometimes even zero through most of the run (see Figure 35).

326. Various trial empirical expressions to describe time decay of the peak offshore transport rate were least-squares fitted for cases having strong offshore transport in the combined CE and CRIEPI data set (12 cases). The best general agreement was obtained with an inverse dependence of the maximum transport rate on time according to

$$q_m = \frac{q_{mo}}{1 + \alpha t} \tag{20}$$

where

$q_m$ = peak transport rate

$q_{mo}$ = peak transport rate at time $t = 0$

$\alpha$ = rate coefficient of decay of peak transport rate

The rate coefficient $\alpha$ controls the time rate of decay of the peak offshore transport rate.

327. Figure 40 displays the peak offshore transport rates from Case 300 and the least-squares fitted line according to Equation 20 (solid line). The agreement is very good and the regression equation explained over 90 percent of the total variation.

328. The average value of $\alpha$ was 0.91 $hr^{-1}$, and the standard deviation was 0.48 $hr^{-1}$ for the 12 cases. To relate the decay coefficient to wave and sand properties, a correlation analysis was carried out, although the data set was small. The decay coefficient showed the strongest correlation to wave period ($r = 0.60$) and the initial maximum transport rate ($r = 0.65$); that is, a longer wave period or a larger initial peak offshore transport rate (profile far from equilibrium shape) resulted in faster decay in the peak offshore transport rate. Correlation with grain size (or fall speed) was very weak, and no dependence on wave height could be found. Furthermore, it was not possible to arrive at a regression equation with an acceptable coefficient of determination by using any wave or sand parameters.

329. Among the trial functions examined was also an exponential decay with time, but this expression gave an inferior fit compared to Equation 20, especially at longer elapsed times, as there was a tendency for the peak offshore transport rate to have a small but still significant value at the end of a case. The exponential decay function approached zero too fast to accurately reproduce this feature. Kajima et al. (1983a, b) developed a conceptual model of beach profile change assuming that the peaks in the transport rate distribution decayed exponentially with time. Sawaragi and Deguchi (1981) also used an exponential decay to derive a time-dependent transport relationship.

330. An exponential decay is expected on general theoretical grounds, since the response of the profile should be proportional to the departure from equilibrium. However, microscale processes and, possibly, nonconstant forcing conditions evidently alter the time decay to a more gradual approach to equilibrium, causing a deviation of the profile response from the expected exponential idealization based on linear concepts.

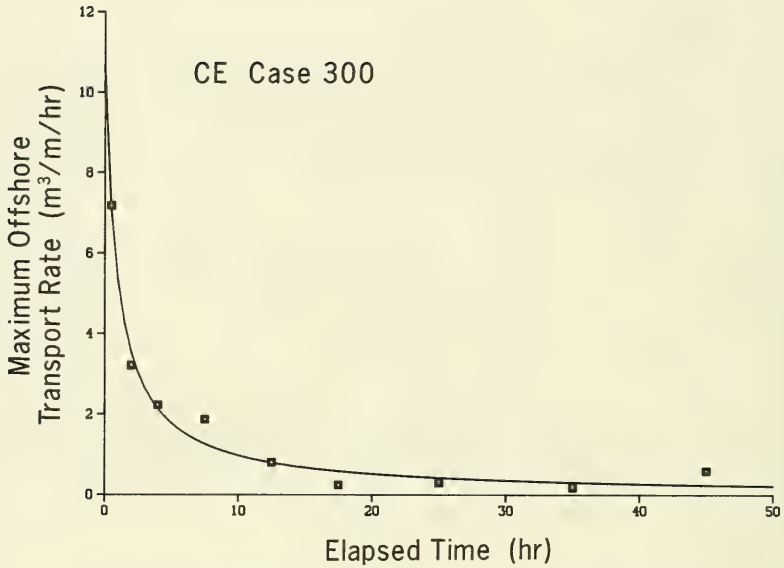


Figure 40. Decay of peak offshore sand transport rate and a best-fit empirical predictive expression

Peak onshore transport

331. The same analysis as for the peak offshore transport rate was carried out for the peak onshore rate, which encompassed 13 cases with strong onshore transport conditions. Figure 41 shows time decay of the peak onshore transport rate for the CE experiments. Similar to the behavior of the peak offshore rate, the initial peak onshore transport rate decayed rapidly, when the profile was far from its equilibrium shape, and then more slowly at the end of the run. Equation 20 was used to obtain an empirical expression to describe the decay with time by least-squares fitting. Figure 42 shows the agreement for a typical case (Case 101) between the peak onshore transport rate calculated from the profile surveys and Equation 20 (solid line). In this case also the regression equation explained over 90 percent of the total variation.

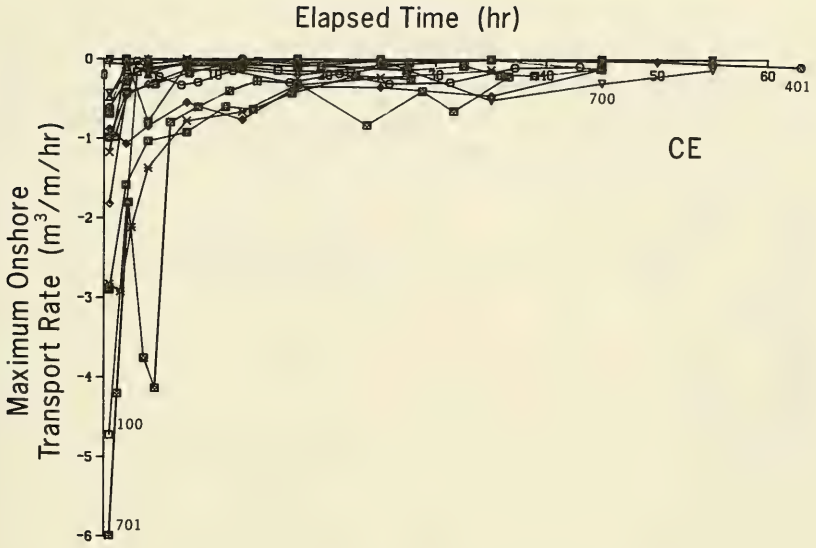


Figure 41. Evolution of peak onshore net sand transport rate for 16 CE cases

332. The average temporal rate coefficient in Equation 20 was $\alpha$ = 1.42 $hr^{-1}$ for the studied cases, with standard deviation of 2.50 $hr^{-1}$. Thus, decay in the peak onshore transport rate was more rapid than for the peak offshore rate. This finding is in agreement with observations made by Sawaragi and Deguchi (1981) from laboratory experiments in which they noted that the onshore transport decayed faster with time than the offshore transport. It is hypothesized here that the peak onshore transport rate decays more rapidly than the peak offshore rate because of the retarding force of gravity on onshore sand motion on a sloping beach.

333. Also, in the present case, there is a wider range in values of the rate coefficient for the peak onshore transport rate compared to the peak offshore rate, as illustrated by the larger standard deviation. The rate coefficient showed a lower correlation with wave period (r = 0.50) than did that for offshore transport but still a rather high correlation with the initial peak onshore transport rate (r = 0.75). No significant correlation of peak onshore rate with wave or sand parameters was found.

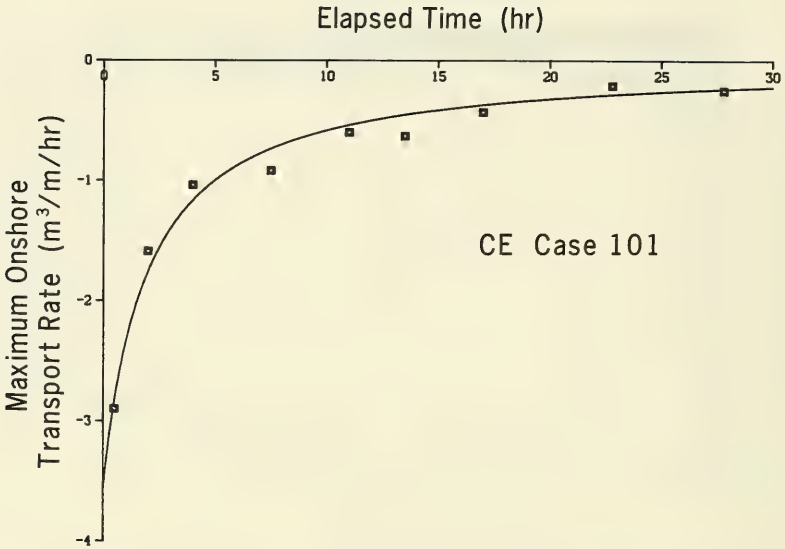


Figure 42. Decay of peak onshore sand transport rate and a best-fit empirical predictive equation

Magnitude of Net Cross-Shore Transport Rate

334. In the LWT experiments, breaking waves caused sand movement that changed the shape of the beach profile. Depending on the wave properties, characteristics of net cross-shore sand transport are expected to vary in various regions along the profile, at least in a morphological sense (Keulegan 1948). In regions of breaking waves, wave energy dissipation is large, maintaining grains in suspension, and more material is transported than in regions of nonbreaking waves. Also, the swash zone is governed by quite different dynamics than the surf zone, even if breaking waves prevail in both zones. Keulegan (1948) identified three regions where "the laws of transportation of sand" were expected to be different: from the point of impending wave break to the point where wave reformation occurs, from the point of impending wave break and seaward, and from the point of wave reformation to the shoreline.

335. A similar division was developed in this study to more closely relate transport rate properties to local wave characteristics. Figure 43 is a definition sketch illustrating division of the profile into four zones. Wave breaking in the surf zone (excluding the swash zone) can be separated into two hydrodynamic regions according to the scale and intensity of the induced vortices, as described by Miller (1976), Svendsen, Madsen, and Buhr Hansen (1979), Basco (1985), Jansen (1986), and others. Svendsen, Madsen, and Buhr Hansen called the region extending shoreward of the wave breaking point for a distance of several breaker depths the "outer or transition region." The more seaward region of the surf zone was called the "inner or quasi-steady state region." The outer region is characterized by large vortices and splash-jet motions, whereas the inner region is characterized by bore-like movement and more gradual change in internal fluid motion. The aforementioned studies showed this classification to be valid for both spilling and plunging breakers, with the intensity of the process being less for spilling breakers. Thus, when waves break, either by spilling or plunging, there is a certain distance between the incipient break point and the location where the waves are fully broken (where the energy dissipation achieves a maximum or near-maximum). Sunamura (in press) similarly hypothesized a plunge point for spilling breakers in analogy to that for plunging breakers. Skjelbreia (1987) conducted a detailed laboratory study of reproducible breaking solitary waves. He reviewed the literature of the wave breaking process and defined four zones of shoaling wave transformation as gradual shoaling, rapid shoaling, rapid decay, and gradual decay. These zones are similar to those developed in the present work based on considerations of cross-shore sand transport, discussed next.

## Transport Regions

336. Various regions having distinct sand transport relationships were defined based on generally accepted concepts of nearshore wave dynamics, in accordance with Figure 43. One region, known as prebreaking, extends from the seaward limit of significant profile change to the break point, denoted as Zone I. In the prebreaking region the transport rate is influenced by trans-

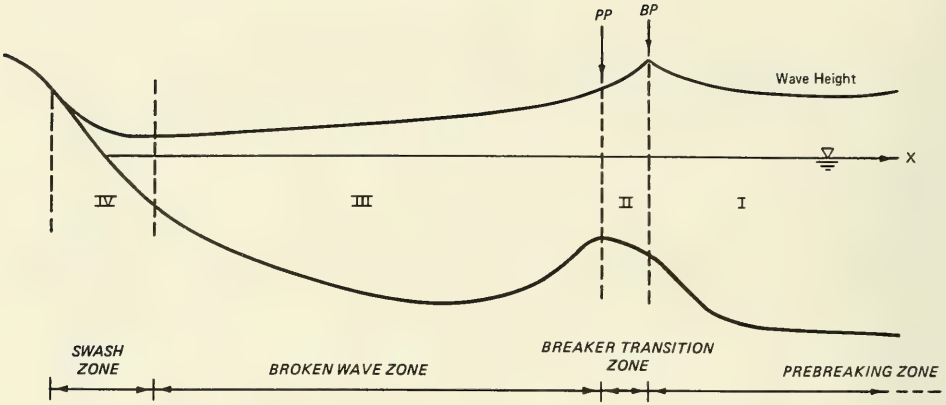


Figure 43. Definition sketch for four principal zones of cross-shore sand transport

port in the zone of wave breaking through the sediment flux at its shoreward boundary, but the governing transport processes on either side of the boundary are quite different. Zone II corresponds to the breaker transition region and is located between the break point and the plunge point. From the location of the plunge point to the point of wave reformation, one specific region, Zone III, is defined where the waves are fully broken and gradually decay (inner region in hydrodynamic terms). In this region the energy dissipation of the waves due to breaking becomes fully developed. If several break points occur with intermediate wave reformation, several zones of type II and III will be present along the profile.

337. Transport conditions in the swash zone differ from those in the surf zone, making it logical to define a fourth transport region, Zone IV. Cross-shore sand transport in the swash zone is expected to depend mainly on properties of the runup bore, local slope, and sediment characteristics. The runup limit approximately constitutes the shoreward boundary for cross-shore transport by waves. In regions between zones of breaking and fully broken waves, where wave reformation occurs, the transport conditions are regarded as similar to what prevails in the region seaward of the main breakpoint.

338. In summary, the four transport zones are located as follows:

a. Zone I: From the seaward depth of effective sand transport to the break point (prebreaking zone).

b. Zone II: From the break point to plunge point (breaker transition zone).

c. Zone III: From the plunge point to the point of wave reformation or to the swash zone (broken wave zone).

d. Zone IV: From the shoreward boundary of the surf zone to the shoreward limit of runup (swash zone).

339. The division of the profile into different transport regions is not immediately recognized viewing the net transport rate distributions (see, for example, Figure 33) since the transport regions interact, and the long-term average represented by the calculated distributions has a smoothing effect. Nevertheless, from a physical point of view it is attractive and productive to divide the beach profile into regions with different governing transport relationships. In the following, net transport rate conditions are investigated in the transport zones and in three zones related to wave and sand characteristics. Empirically-based relationships for the net transport rate are formulated for the different regions based on physical considerations and observations from the data.

Zone I: Net transport rate seaward of the break point

340. The net cross-shore transport rate seaward of the break point has probably been the most intensively studied of all regions on the profile, both in the field and in the laboratory. Transport in the prebreaking zone is in many cases governed by ripple dynamics (e.g., Inman 1957, Dingler and Inman 1977, Nielsen 1979, Sunamura 1981a). Sophisticated transport rate formulas have been developed based on laboratory experiments (e.g., Madsen and Grant 1977, Sato and Horikawa 1987), but these empirically-based formulas must also be supplemented by other information for their application. Such formulas describe sand transport on spatial and temporal microscales which are not compatible with the present approach of quantifying large-scale profile features over intervals of tens of minutes.

341. As a wave approaches the point of breaking, its velocity field becomes more asymmetric with high, narrow peaks of onshore-directed flow and broad troughs of flow directed offshore. This motion could cause material to move either onshore or offshore depending on the elevation in the water column at which a grain is suspended in relation to the duration of the on/offshore

flow. Sorting of material is thus expected along the profile, with coarser material migrating closer to shore (Ippen and Eagleson 1955).

342. Erosional cases. For erosional profiles, in the vicinity of the break point it is expected that diffusion in the seaward direction of sand that was set in suspension by the breaking waves dominates over material moved along the bottom by oscillatory wave forces. As seen from Figure 33, the shape of the net transport rate distribution is well approximated by an exponential decay with distance from a point somewhat seaward of the location of the maximum transport rate. This point is located in the vicinity of the break point, and the transport rate $q$ in Zone I may accordingly be written

$$q = q_b e^{-\lambda(x - x_b)} \tag{21}$$

where

$q_b$ = transport rate at the break point

$\lambda$ = spatial decay coefficient

$x_b$ = location of breakpoint

343. In analysis of the distribution of the net transport rate seaward of the break point, cases involving mainly onshore transport and offshore transport were studied separately. Equation 21 was least-squares fitted through the data for 12 cases showing mainly erosion and for 13 cases showing mainly accretion. Each case typically comprised 5-10 transport rate distributions for which a spatial decay coefficient was obtained. For a specific transport rate distribution a high coefficient of determination was always obtained (above 90 percent). The estimated decay coefficient $\lambda$ was quite stable and showed only a slight tendency to decrease with time. Figure 44 illustrates the spatial decay coefficient as a function of time for four of the erosional CE cases.

344. To obtain an overall estimate of the spatial decay coefficient for a specific erosional case, the transport rate for each distribution during a run was normalized with the $q_b$-parameter as given by the least-squares fit for the individual distribution. Figure 45 illustrates, for CE Case 500, the decay of the normalized transport rate from the break point and seaward for consecutive transport rate distributions (indicated by various symbols)

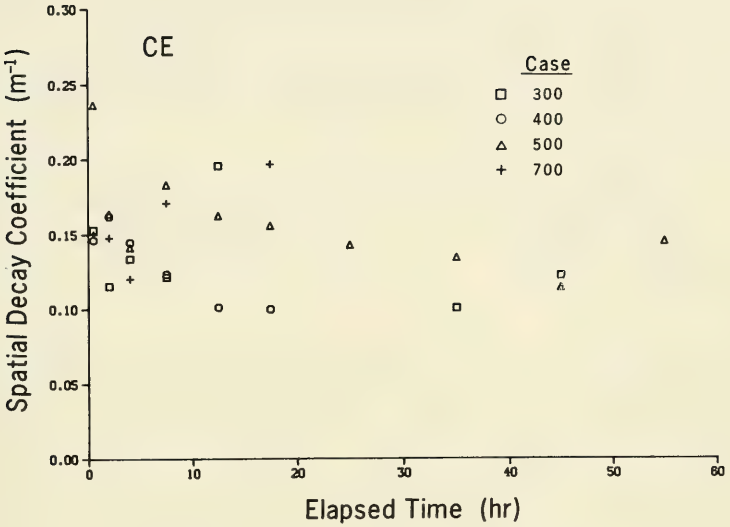


Figure 44. Spatial decay rate coefficient seaward of the break point

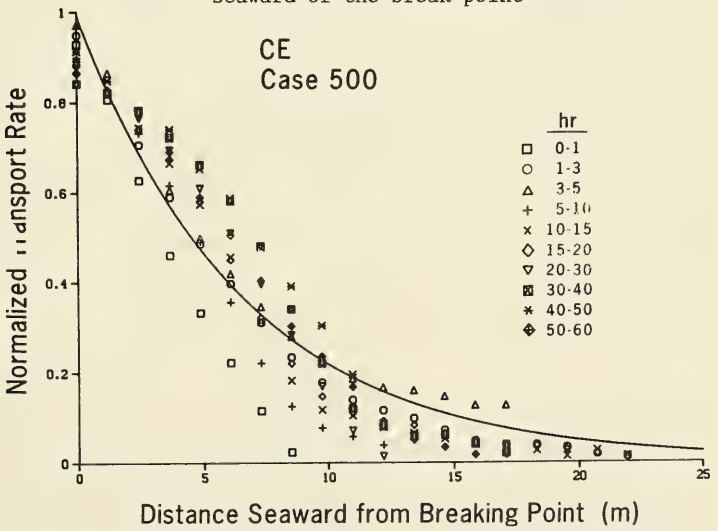


Figure 45. Comparison of net offshore sand transport rates seaward of the break point and an empirical expression

through time, together with a solid line showing the least-squares estimate of the exponential decay. The coefficient of determination in this case was 92 percent. The difference between averaging the individual estimates of the spatial decay coefficient and obtaining an overall estimate by using normalized transport rates was small.

345. The average spatial decay coefficient for erosional cases was calculated for each case and related to wave properties and sand characteristics. The overall average value of the decay coefficient was 0.18 $m^{-1}$ with a standard deviation of 0.06 $m^{-1}$. Values ranged from a minimum of 0.12 $m^{-1}$ to a maximum of 0.34 $m^{-1}$.

346. Correlation analysis showed an inverse dependence of the spatial decay coefficient on the breaking wave height and a direct dependence on the grain size (correlation coefficients of -0.70 and 0.75, respectively). In principle, a larger breaking wave height, for a specific grain size, would stir up more sand and thus allow more of the entrained grains to disperse seaward from the break point implying a more gradual decay in the transport rate. For constant breaking wave height, larger sand grains are less likely to be put into suspension and the transport rate distribution decays more rapidly seaward of the break point. This intuitive picture is supported by the correlation analysis.

347. The spatial decay coefficient showed only a weak inverse dependence on the wave period, giving a small correlation coefficient. Regression between the decay coefficient and the breaking wave height and the grain size explained 70 percent of the variation in the data. The regression equation is

$$\lambda = 0.40 \left[ \frac{D}{H_b} \right]^{0.47} \tag{22}$$

In Equation 22 the units of $D$ are millimeters and the units of $H_b$ are meters.

348. Figure 46 illustrates decay coefficients calculated from the data compared with values predicted by Equation 22. Note in Figure 46 that one of the points influences the regression and correlation analysis considerably.

The regression relationship given by Equation 22 contains a coefficient (0.40) which is dimensional, since the units of $\lambda$ are $m^{-1}$. Effort was made to form a nondimensional quantity involving $\lambda$ and a relevant wave or sand property, but no significant dependence was achieved.

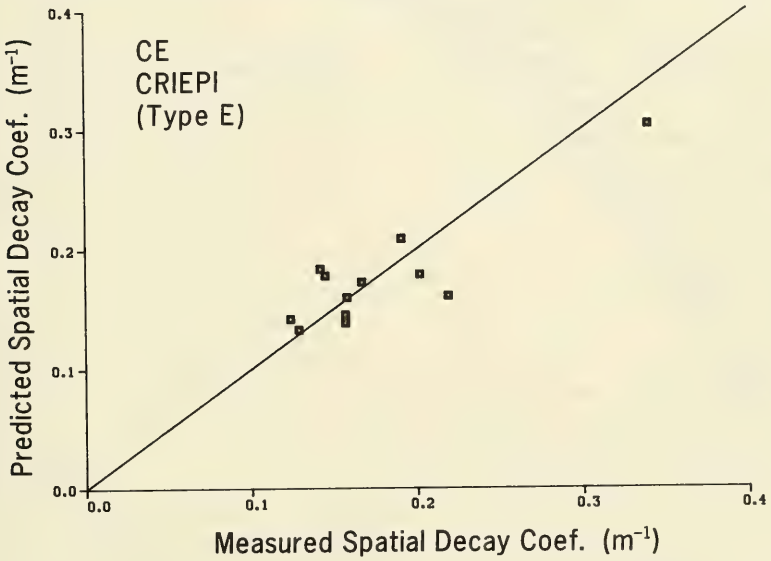


Figure 46. Comparison of spatial decay rate coefficients and an empirical predictive expression

349. Accretionary cases. A similar analysis of the decay of the transport rate for the zone seaward of the break point was carried out for cases which showed mainly onshore transport. Coefficients of determination obtained by least-squares fitting of an exponential decay function were in almost all cases greater than 90 percent for the individual transport rate distributions. Figure 47 illustrates, in analogy with Figure 45, the decay in the transport rate seaward of the break point and the corresponding calculated result from the regression equation (coefficient of determination 95 percent) for a typical case (Case 101). Transport was directed onshore at all times.

350. Spatial decay coefficients for accretionary cases were in general smaller than for erosional cases, indicating that a larger portion of the profile seaward of the break point was affected by the waves for the accre-

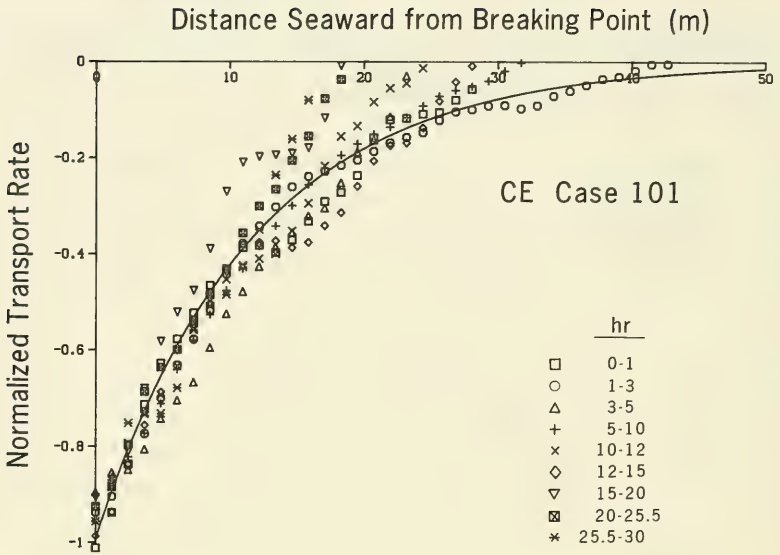


Figure 47. Comparison of net onshore sand transport rates seaward of the break point and an empirical predictive equation

tionary cases. The average value of $\lambda$ for all accretionary cases studied (13 cases exhibiting mainly onshore transport) was 0.11 $m^{-1}$, with a standard deviation of 0.02 $m^{-1}$. There was significantly less spread in the values of $\lambda$ for accretionary cases, indicated by the smaller standard deviation and the more narrow range between minimum and maximum values (0.08-0.16 $m^{-1}$). Contrary to the erosional cases, the spatial decay coefficient could not be related with any significance to wave and sand properties.

351. Secondary Zone I transport. The above analysis concerned Zone I, the region from the break point and seaward, in the absence of multiple break points. If wave reformation occurred and waves broke again closer to shore, the region seaward of the second breaker appeared to show transport rate characteristics similar to those in the region immediately seaward of the first breaker line. Only a few of the cases had a second breaker, and often the second breakpoint bar formed during the initial part of the run, rapidly

reaching an equilibrium volume. However, the main breakpoint bar had to develop to a certain size before the trough shoreward of the bar was sufficiently deep to allow the waves to reform. Formation of a second bar was manifested in the transport rate distribution as a local minimum, indicating that material was deposited shoreward of this point, implying a negative derivative of the transport rate. A local minimum in the transport rate was typically found only in the first few transport rate distributions of a run, since the second breakpoint bar soon attained equilibrium.

352. The present data sets do not provide sufficient information to determine reliable quantitative empirical relationships for the net transport rate in areas of wave reformation. Some qualitative observations may be made from the data with regard to the shape of the transport rate. The transport rate decayed in the seaward direction from a point located somewhat shoreward of the second break point, and the spatial decay in the net transport rate appeared to be more gradual than for the region seaward of the main breakpoint bar. It is speculated that even though breaking ceases, more turbulence is generated or convected in areas of reformation than in the area seaward of the main breakpoint, thus making the decay of the transport rate in wave reformation zones more gradual.

Zone II: Net transport rate between break point and plunge point

353. Waves must propagate shoreward a certain distance from the break point before breaking fully develops and energy dissipation reaches a maximum (Miller 1976; Svendsen, Madsen, and Buhr Hansen 1979; Basco 1985; Jansen 1986; Basco and Yamashita 1987; Svendsen 1987). This distance appears to be approximately equal to the plunge distance for plunging breakers and provides the basis for a definition of an equivalent plunge distance for a spilling breaker. The shape of the main breakpoint bar was in many cases well approximated by two linear slopes on the seaward side of the bar (see Part IV). The break in slope was located in the vicinity of the break point, indicating that the properties of the net transport rate were different in regions seaward and shoreward of the break point.

354. It proved too difficult to determine quantitative characteristics of the net transport rate in the region between the break point and the plunge point. This region is of small spatial extent. Furthermore, the breaker

transition zone moves together with the bar during the course of wave action, which makes analysis problematic, as the transport rate calculations are based on average profile changes that occurred over a relatively long time. However, from a conceptual point of view, it is important to recognize this region as being different from neighboring areas.

355. Some distributions provided insight into the nature of the net transport rate in Zone II, particularly during later times of a run, when changes in the beach profile shape were more gradual. Figure 48 illustrates the transport rate distribution in the region between the break point and the location of the maximum transport rate for selected cases and times. The transport rate decreased in the offshore direction at a lower rate than in the region seaward of the break point. Analysis of a small data subset where Zone II transport could be distinguished (as in Figure 48) indicated that an exponential decay was a reasonable approximation, with the spatial decay coefficient approximately 0.20-0.25 of the value of the spatial decay coefficient governing transport seaward of the break point.

Zone III: Net transport rate in broken waves

356. Breaking and broken waves produce turbulent conditions that put grains into suspension and make them available for transport across the profile (Watts 1953, Fairchild 1973, Kana 1977, Kraus and Dean 1987). Thus, it is plausible to assume that the magnitude of the transport rate is closely related to wave energy dissipation (Dean 1977). Different models of wave height decay in the surf zone based on energy dissipation have been developed (e.g., Dally 1980; Mizuguchi 1981; Svendsen 1984; and Dally, Dean, and Dalrymple 1985a, b).

357. The CE data set did not include detailed measurements of the wave height distribution across the profile, whereas the CRIEPI data set provided wave height data for most of the cases with a resolution of 2.5 m. The wave height distribution was usually measured between profile surveys, making the exact beach profile shape unknown for the time of the measurement. To obtain a picture of the relationship between the cross-shore transport rate and local wave parameters in broken wave zones, the CRIEPI data set was used, although the number of cases that contained significant profile change and corresponding measurements of wave height across-shore was limited. Only four cases

allowed thorough analysis of the correlation between local wave properties and transport rate at consecutive times during a run.

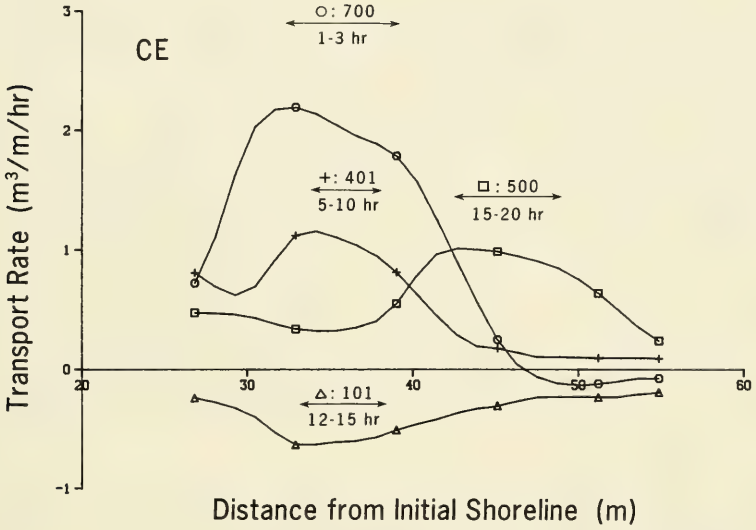


Figure 48. Net cross-shore sand transport rate distributions between break point and plunge point

358. Energy dissipation is related to the change in wave energy flux along the profile. The energy flux F may be written using shallow-water wave theory as

$$F = \frac{1}{8} \rho g H^2 \sqrt{gh} \tag{23}$$

where $\rho$ is the density of water. The energy dissipation is given by $dF/dx$ .

359. Due to the relatively low resolution in the wave height measurement, evaluation of the derivative and transport proved sensitive to individual measurement values. To obtain a better estimate, the wave decay model of Dally (1980) was least-squares fitted through discrete values of each measured wave height distribution from the point of breaking shoreward until wave reformation occurred or the water depth became small (approximately 20 cm).

The wave model is presented in Part VI, where the analytic solution which was used in the least-square fit is given (Equation 29). It is noted that a change in broken wave height is not completely indicative of wave energy dissipation; energy reordering may also occur, as discussed by Svendsen, Madsen, and Buhr Hansen (1979).

360. The empirical coefficient relating stable wave height to water depth employed in the Dally model (still-water depth without setup) was determined from wave height measurements by examining the ratio between wave height and water depth in the proximity of areas of wave reformation. An average stable wave height coefficient was calculated for each case and values ranged from 0.3-0.5, showing a marked dependence on the beach slope (compare with Dally, Dean, and Dalrymple 1985b). Steeper beach slopes yielded larger values of the stable wave height coefficient. The wave decay coefficient was then least-squares estimated, giving values in the range of 0.15-0.3. In most cases, there was a tendency for the wave decay coefficient to decrease with time as the inshore slope became more gentle.

361. At first, both empirical parameters in the wave decay model (stable wave height and wave decay coefficient) were least-squares estimated (cf. Part VI). However, the minima of the sum of squares were located in a very flat region, causing differences between optimum parameter combinations and neighboring values to be small. To achieve a certain increase in the energy dissipation, either the wave decay coefficient could be increased or the stable wave height coefficient decreased (or a combination of these adjustments). Thus, in the optimization process, since the region surrounding the minimum was very flat, almost the same agreement could be obtained with a small value of the stable wave height coefficient and a large value of the wave decay coefficient, or the opposite situation. In some cases the optimum parameter values gave unrealistically low coefficients of stable wave height, such as 0.2. For this reason, the stable wave height was fixed as described in the previous paragraph and only a least-squares estimate of the wave decay coefficient was made, giving a sum of squares deviating only slightly from the mathematically optimum value.

362. Dissipation in wave energy flux was determined from the wave decay model, calculated starting at the location of the maximum transport rate,

somewhat shoreward of the break point, and ending where the wave decay model calculation was arbitrarily stopped. For each case, various quantities connected with the energy flux dissipation were correlated with the cross-shore sand transport rate in Zone III for all distributions obtained during a run. The net cross-shore transport rate showed good correlation with energy flux dissipation per unit water volume for all cases studied (correlation coefficients of 0.7-0.8), which was higher than the correlation resulting from tests using only the energy flux dissipation per unit area of beach. Figure 49 shows the transport rate plotted against the energy flux dissipation per unit volume as evaluated for Case 6-1.

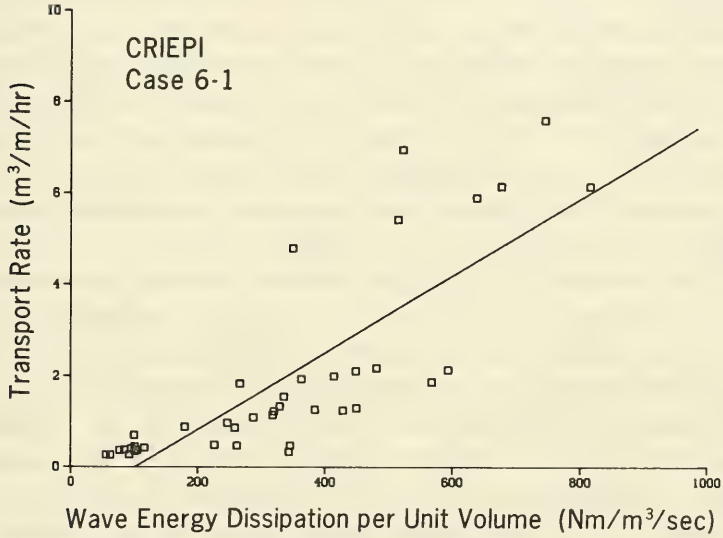


Figure 49. Net cross-shore sand transport rate versus calculated wave energy dissipation per unit volume in broken wave region

363. Correlation was in general higher for individual transport rate distributions than if all values from a specific case were used. Other parameters pertaining to the geometry of the beach profile, such as beach slope and wave characteristics, were also correlated with the transport rate. To determine geometric parameters of the beach profile, the average profile

calculated from surveys taken before and after the measurement of the wave height distribution was used. No significant correlation was found that was consistent for all cases between any other parameter studied and the transport rate. For some cases, there was a positive correlation between transport rate and beach slope.

364. A linear regression equation relating the transport rate to energy dissipation per unit volume and local beach slope was least-squares fitted to the data. The regression relationship explained about 50-70 percent of the total variation in the data for the different cases studied, in which local beach slope accounted at most for 10 percent of the total variation.

365. Kriebel and Dean (1985a) assumed that the cross-shore sand transport rate was proportional to the excess energy dissipation per unit volume over a certain equilibrium value of energy dissipation, which was defined by the amount of energy dissipation per unit volume a beach with a specific grain size could withstand (cf. Part VI). From the regression analysis between wave energy dissipation per unit volume and transport rate, it was possible to obtain an estimate of the transport rate coefficient corresponding to the proportionality constant used by Kriebel and Dean (1985a).

366. For the four cases intensively studied, the average value of the transport rate coefficient was determined from regression analysis to be $1.1\ 10^{-6}\ m^4/N$, which is approximately half the value originally obtained by Moore (1982). Moore developed a numerical model of beach profile change using a transport equation for the cross-shore sand movement in which the transport rate was proportional to wave energy dissipation per unit volume. He arrived at a transport coefficient of $2.2\ 10^{-6}\ m^4/N$ by calibration using profile change measured in one CE case and field measurements from Santa Barbara, California.

367. Two major causes are believed responsible for the difference in values obtained. First, Moore (1982) inferred the transport coefficient by comparison of simulated profile change and measurement, not directly between wave energy dissipation per unit volume and measured transport rate as done here. Second, considerable smoothing of the calculated transport rate was used in Moore's model. By smoothing the energy dissipation along the profile, a larger value of the transport rate coefficient is needed to achieve the same

beach profile response as compared to a simulation with no smoothing. A more thorough discussion of values of the transport rate coefficient is given in Part VII describing application of the numerical model.

368. It was not possible to relate the transport rate coefficient to wave or beach properties. In a numerical model the transport rate coefficient functions largely as a calibration parameter to give the proper time scale of profile change.

369. In the regression analysis between transport rate and energy dissipation per unit volume, other beach and wave parameters were added to quantify their influence. For the cases where the local beach slope showed some influence on the transport rate, the coefficient in the regression equation was typically small, on the order of 0.0006 $m^2/sec$. The equilibrium energy dissipation was determined from the constant term in the regression equation and varied considerably between the runs evaluated, although the grain size was the same for the studied cases. This variation was probably due to the scatter in the data relating transport rate to energy dissipation, making the least-squares estimate of the constant in the regression equation less reliable. However, two of the cases resulted in equilibrium energy dissipations that were somewhat smaller than the values given by Moore (1982), who used natural beach profiles to determine this parameter (108 and 134 $Nm/(m^3sec)$ from the present data compared to Moore's value of 170 $Nm/m^3sec$).

370. The purpose of the previous analysis was to emphasize the close relationship between wave energy dissipation per unit volume and magnitude of the transport rate in zones of broken waves. Although the number of satisfactory cases for obtaining quantitative information about wave height and associated sand transport rate distribution was small, the relationship between the two quantities was clearly evident. All of the studied cases encompassed beach profiles which experienced erosion of the foreshore and bar formation in the vicinity of the break point. It is expected that profiles with accretion on the foreshore will also exhibit transport rates that are related to the energy dissipation per unit volume, although it was not possible to directly confirm this assumption by means of the present data.

Zone IV: Net transport rate on the foreshore

371. The net transport rate in the swash zone is expected to be a function of local beach slope, sediment characteristics, and properties of the bore propagating upon the beach. No wave or bore information was available for this study, except for some runup measurements from the CE data. Consequently, it was not possible to derive a relationship connecting the net transport rate on the foreshore to local wave properties and other factors. However, some qualitative observations were made of the shape of the net transport rate distribution on the foreshore. The region discussed in this section extends approximately from the runup limit seaward to some specific depth corresponding to the point of maximum retreat of the waves in the swash. This depth is a function of the incident waves which cause setup at the shoreline roughly proportional to the breaking wave height. Swash oscillates about the mean shoreline elevation with a range dependent mainly on wave height and surf similarity parameter, even in the field (Guza and Thornton 1982, Holman 1986).

372. For some cases, the net transport rate showed a fairly complex spatial dependence on the foreshore, in particular at the early stages of the experiments. However, the net rate had an almost linear decay with distance for a majority of the cases, both for onshore and offshore transport conditions. Figure 50 gives a representative example of the transport rate distribution over the foreshore for CE Case 300, in which different consecutive distributions in time are plotted. The slope of the transport rate decreased with time as the profile approached equilibrium, but the shape of the distribution roughly maintained a linear form. In Case 300, the profile retreated shoreward as the foreshore eroded during the run. (The location of the still-water shoreline is indicated by vertical lines for the various distributions in time.) A linear decay in the transport rate implies that an equal amount of material is eroded at all points along the foreshore up to the runup limit (compare field observations of Seymour 1987).

373. As the foreshore eroded, a step formed extending approximately from the still-water shoreline to the runup limit. The slope of the step may have increased until the angle of initial yield was exceeded (Allen 1970) and avalanching occurred, thereby adjusting the slope to a lower value (residual

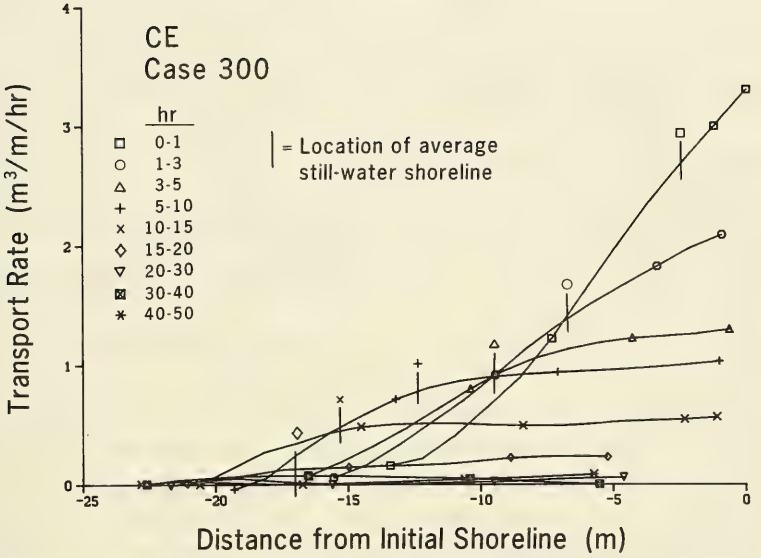


Figure 50. Time behavior of net cross-shore sand transport rate distribution on the foreshore

angle after shearing). Sediment transport produced by slope failure is expected to occur very rapidly and would produce a transport rate distribution of a quadratic shape since the step rotates at a fixed angle around some point along its face. Averaging of the net transport rate smooths over the process of avalanching. Also, the progress of avalanching is probably not ideal with a pure and constant steepening of the step face; rather, transport is probably greater at the base of the step, undermining it.

## Summary

374. Calculated distributions of the net cross-shore transport rate from profile change measured over intervals on the order of hours displayed very regular and smooth properties despite the random character of the grain-by-grain movement that actually took place. It therefore appears possible to estimate the net cross-shore sand transport rate with sufficient reliability

to predict the development of main morphologic features of the beach profile. Available equilibrium distributions of the net transport rate could be classified almost exclusively into three main types, two types of which correspond to either onshore or offshore transport along the profile. Transport distributions with one onshore and one offshore peak were not common and occurred mainly for cases which fell close to a derived line delineating bar profiles and berm profiles. As a result, the assumption of a unidirectional transport rate along the profile should give a reasonable first approximation in most cases for describing the overall profile response to incident short-period waves.

375. Division of the profile into four zones with different transport properties, based in part on general observations of nearshore wave dynamics, proved to be a fruitful approach both from the conceptual and predictive points of view. The net transport rate in zones of broken waves, where the most active transport is expected to occur, showed good correlation with the wave energy dissipation per unit water volume. The net transport rate in the prebreaking zone decayed exponentially with distance offshore. On the foreshore, the net transport rate showed an approximately linear behavior decreasing in the shoreward direction from the end of the surf zone. More data on the transport rate in the foreshore are needed to better understand physical processes there.

376. Quantitative information on the net cross-shore transport rate is difficult to obtain in the field due to the limited resolution in time and space of profile surveys, number of instruments that can be deployed, contaminating effects of longshore sand transport, and changing wave conditions. In this respect, data from large wave tanks provided valuable insight into the behavior of the net cross-shore transport rate and enhanced the possibility of modeling beach profile change. Although monochromatic waves were used in the large wave tank experiments, it is expected that the main features of the transport rate are representative of processes associated with random waves in the field. This hypothesis is tested in Part VII where model predictions are compared with field observations.

## PART VI: NUMERICAL MODEL OF BEACH PROFILE CHANGE

377. Quantitative prediction of the response of the beach profile to wave action and changes in water level is an important goal of coastal engineering. The capability to quantitatively estimate dune erosion, beach response to large storms, and the initial adjustment and long-term evolution of a beach fill is necessary to design and make economic evaluations of shore erosion and flood protection projects. A numerical model can be an efficient tool to evaluate various design alternatives while easily incorporating detailed process data, such as time series of waves and water level.

378. Many attempts have been made to develop numerical models of beach profile change. The authors are not aware of any existing model, however, which can be applied to an arbitrary beach profile exposed to variable wave and water level conditions to reproduce bar formation and movement in addition to overall change in the profile. It was a major goal of this investigation to model the growth and movement of bars as part of the beach profile response, since these features constitute natural protection for a beach exposed to severe erosional conditions. Furthermore, for long-term simulations, a predictive model must necessarily incorporate events producing onshore transport and berm buildup, which no known engineering model can simulate. Development of such a model would allow simulation of seasonal changes in the profile as produced by cross-shore sediment transport.

379. This chapter describes the numerical model developed in this study for simulating beach profile change. An important feature possessed by the model is the capability to reproduce main morphologic features of the profile, in particular, bars and berms. Many of the assumptions and relationships used in development of the model were founded on observations presented in previous chapters of this report. The numerical model is aimed at reproducing macro-changes of the beach profile in a deterministic fashion, neglecting small-scale features such as ripples and avoiding the extreme complexity associated with detailed specification of the fluid flow and sediment concentration.

380. The model is formally based on the equation of mass conservation, for which mathematical expressions for the cross-shore transport rate are required. Any type of theoretical or empirical transport rate formula can be

used in the model. Therefore, as knowledge of cross-shore fluid flows and sediment transport improves, the model is sufficiently general and flexible to allow inclusion of these advances to supplement the transport rate formulas developed in this study. Under the assumption of linear superposition, contributions from driving forces other than short-period breaking waves can be added if the transport rate relations are known. Examples for future inclusion would be transport by undertow and long-period wave motions.

381. In Part IV, a clear connection was found between macrofeatures of the beach profile and wave and sand characteristics. Reliable prediction of the net cross-shore sand transport rate distribution on the spatial scale of meters and time frame of minutes was demonstrated in Part V. Thus, all preparatory work supports the feasibility of developing a predictive engineering numerical model for simulating macroscale changes in the beach profile.

## Methodology

382. At the present state of knowledge, it is clear that any type of numerical model of beach profile change to be used in engineering practice must be based on semi-empirical relationships derived from measurements. The model presented here was developed using data from experiments carried out in LWTs involving waves of prototype size.

383. Dally (1980) and Birkemeier et al. (1987) presented criteria to judge the suitability of a numerical model of beach profile change. In the present work, the following properties were considered to be fundamental. The model should:

a. Accurately simulate time evolution of a profile of arbitrary shape subjected to changes in water level and incident wave parameters.

b. Calculate an equilibrium configuration if all model parameters and input values are held constant.

c. Simulate formation and movement of main morphologic profile features such as bars and berms.

d. Reproduce erosional and accretionary beach change.

e. Be verified for a wide range of realistic conditions.

384. A short description of the capabilities of existing numerical models is contained in the literature review in Part II. Of the various

numerical models proposed prior to the present work, that of Kriebel (1982) (see also Kriebel and Dean 1985a, Kriebel 1986) comes closest to satisfying the five criteria listed above. The Kriebel model was critically evaluated and determined to be the best available tool for estimating erosion on U.S. coasts (Birkemeier et al. 1987). The Kriebel model satisfies criteria a. and b., and, in part e., but not criteria c. and d. The model was originally developed and verified using cases from the CE data set, as well as an erosional event associated with Hurricane Elena, and has since been used in engineering studies (Kriebel and Dean 1985b, Kraus et al. 1988). Development of the present model was stimulated by the success of the Kriebel model.

385. In the following, a short overview of the structure of the numerical model is given as an introduction before its various components are discussed in detail. Changes in the shape of the beach profile are assumed to be produced by breaking waves; therefore, the cross-shore transport rate is determined from local wave, water level, and beach profile properties. The equation expressing conservation of beach material is solved to compute profile change as a function of time.

386. The wave height distribution is calculated across the shore by applying small-amplitude wave theory up to the point of breaking, and then the breaker decay model of Dally (1980) is used to provide the wave height in regions of breaking waves. The profile is divided into specific regions according to the wave characteristics at the given time-step for specification of transport properties. The distribution of the cross-shore transport rate is then calculated from semi-empirical relationships valid in different regions of transport. At the shoreward end of the profile, the runup limit constitutes a boundary across which no material is transported, whereas the seaward boundary is determined by the depth at which no significant sediment motion occurs. Once the distribution of the transport rate is known, profile change is calculated from the mass conservation equation. The described procedure is carried out at every time-step in a finite-difference solution scheme using the current incident wave conditions and water level, and updating the beach profile shape.

387. First, the wave model is described and calculations compared with measurements from the CRIEPI data set. Then the various transport relations

are developed for use in the profile change model. The next section gives a description of the numerical solution scheme and the associated boundary conditions. Finally, calibration and verification of the profile change model with the LWT data set are made. Applications of the model, including sensitivity analyses and tests of predictions with field data, are given in Part VII.

## Wave Model

388. As waves approach shore over a gently sloping bottom, they increase in height and decrease in length due to shoaling. It will be assumed that the waves are incident normal to the coast, i.e., that refraction can be neglected. The increase in wave height continues until some critical ratio is reached between wave height and water depth, at which point the waves break. The wave height distribution across the shore is calculated by linear wave theory. In initial model development, the nonlinear shoaling laws proposed by Shuto (1974) were used in an effort to provide an improved description of the increasing nonlinearity of waves as they approach breaking. However, in comparison of predictions of the nonlinear wave model against wave height measurements from the CRIEPI data set, the predicted height increased too steeply before breaking for longer-period waves. In simulations involving development of a prominent breakpoint bar through time, the wave height just prior to breaking was overestimated. It was thus decided to use linear wave theory in all regions of the shoaling calculation and leave the problem of nonlinear wave shoaling to the future.

### Breaking criterion and breaker height

389. The ratio of wave height to water depth at breaking (called the breaker index) was evaluated using the CRIEPI data set. Only those cases with an initially plane slope were used and, if no profile survey was taken at the time of the wave height measurement, the depth at breaking was determined by interpolation from the two profiles bracketing the wave measurement in time. In total, 121 pairs of wave height and depth values were obtained from 17 cases having different wave conditions and initial beach slopes. The average breaker index (wave height to water depth at breaking) was 1.00, with a

standard deviation of 0.25. As shown in Figure 51, the distribution of the breaker indices was somewhat positively skewed, and values ranged from 0.58 to 1.79. The steep slope that developed on the seaward side of the growing bar caused the breaker index to increase with time, allowing the wave to break in more shallow water.

390. To evaluate this effect, results were compared with small-scale laboratory data tabulated by Smith and Kraus (1988) for experiments made with fixed plane bottom slopes typically more gentle than the seaward bar faces in the CRIEPI cases. Figure 52 shows the distribution of the breaker index for the small-scale experiment data, in analogy with Figure 51. Because of the more gentle slopes, the average breaker index for the small-scale data was only 0.82 (135 values), with a standard deviation of 0.18. If the beach slope grows steep seaward of the break point, the breaker index should accordingly be increased to account for the bottom slope effect on wave breaking.

391. Correlation analysis showed that the breaker index depended mainly on the slope before breaking and the deepwater wave steepness (see Galvin 1969, Weggel 1972, Singamsetti and Wind 1980, Sunamura 1981b). The slope was evaluated as an average over that part of the beach profile seaward of the break point where waves showed a marked increase in height due to shoaling (typically in the range of 10-20 m). The breaker index increased with an increase in bottom slope and decreased with an increase in wave steepness. For profiles exhibiting bar development during a run, the average seaward slope in general showed an increase with time (Part IV), causing an increase in breaker index. Regression analysis between the aforementioned variables explained 55 percent of the variation and indicated that the beach slope and deepwater wave steepness could be combined to form the surf similarity parameter $\tan\beta/(H_o/L_o)^{1/2}$ (Battjes 1975) without loss of predictability. The regression equation obtained is

$$\frac{H_b}{h_b} = 1.14 \left[ \frac{\tan\beta}{\sqrt{H_o/L_o}} \right]^{0.21} \tag{24}$$

where $\tan\beta$ is the local beach slope seaward of the breakpoint.

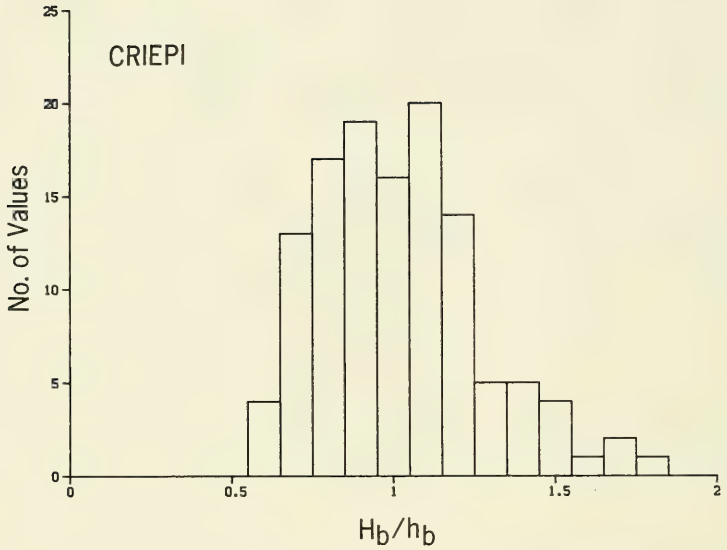


Figure 51. Distribution of breaker ratio for the CRIEPI data

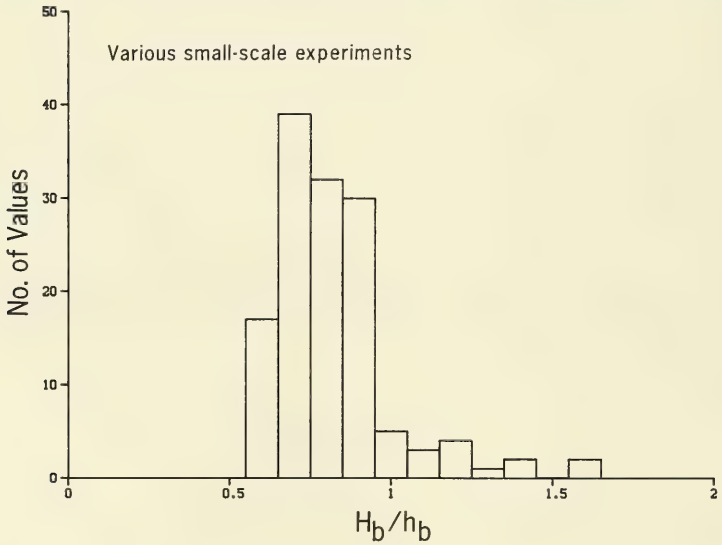


Figure 52. Distribution of breaker ratio for small-scale laboratory data

392. Values of the empirical multiplicative coefficient and exponent in the regression equation are very similar to those obtained by Battjes as reported by Singamsetti and Wind (1980) and Sunamura (1981b) based on small-scale laboratory data. In Figure 53, data from the CRIEPI experiments are plotted together with Equation 24. The wave model uses Equation 24 to predict the breaking condition, for which the bottom slope is evaluated over a distance one third of the local wavelength seaward of the break point.

393. The breaking wave height on the movable bed bottoms of the CE and CRIEPI experiments normalized by the deepwater wave height was related to the deepwater wave steepness. An average breaking wave height was used for each case, making up a total of 32 cases for the analysis. Regression analysis with the deepwater wave steepness explained 80 percent of the variation in the data, leading to the equation

$$\frac{H_b}{H_o} = 0.53 \left[ \frac{H_o}{L_o} \right]^{-0.24} \tag{25}$$

394. Inclusion of initial beach slope in the regression equation did not improve predictability, probably due to the significant change in slope that occurred seaward of the break point during the course of wave action. Figure 54 illustrates the prediction from Equation 25 and the data points from the studied cases. Data points associated with different initial slopes have been plotted with different symbols. Note that the value of the empirically determined exponent in Equation 25 is close to that which is obtained with linear wave theory for shoaling of normally incident waves from deep water to breaking (-0.20; see Komar and Gaughan 1973).

Breaker decay model

395. Several numerical models have been developed for describing wave height decay in the surf zone (e.g., Battjes and Janssen 1979, Dally 1980, Mizuguchi 1981, Svendsen 1984). All contain empirical parameters whose values have to be established by calibration against measurements. The wave model proposed by Dally (1980) and further discussed by Dally, Dean, and Dalrymple (1985a, 1985b) was chosen for use here since it has been verified with both laboratory data (Dally 1980) and field data (Ebersole 1987). Furthermore, the

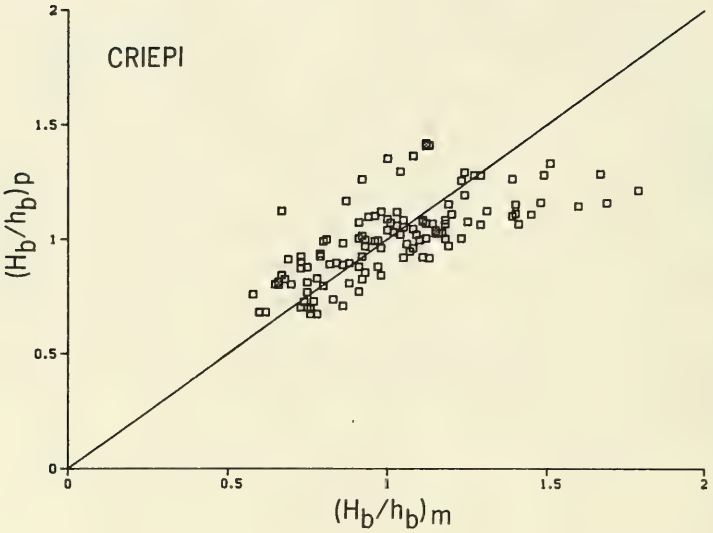


Figure 53. Comparison between measured and predicted breaker ratio

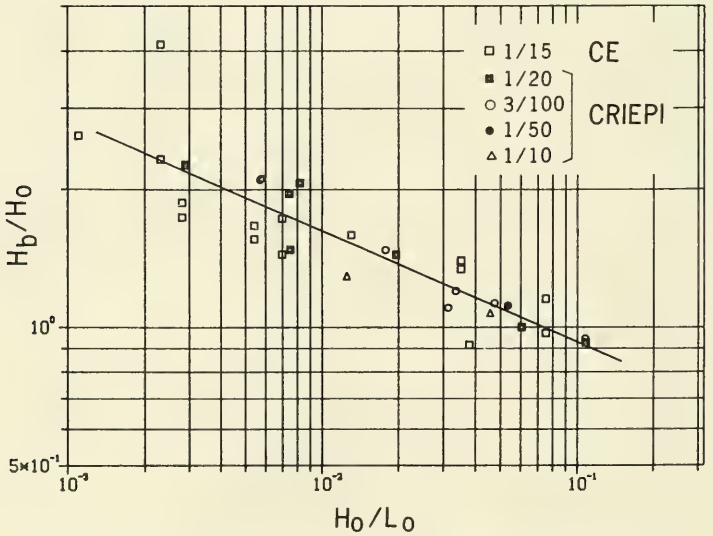


Figure 54. Ratio between breaking and deepwater wave height as a function of deepwater wave steepness

breaker decay model allows for wave reformation to occur, which is an essential feature for modeling profiles with multiple bars. The governing equation for the breaker decay model is written in its general form as

$$\frac{dF}{dx} = - \frac{\kappa}{h} (F - F_s) \tag{26}$$

where

$\kappa$ = empirical wave decay coefficient

$F_s$ = stable wave energy flux

In this equation, the cross-shore coordinate $x$ has its origin at the break point and is directed positive shoreward.

396. The assumption behind Equation 26 is that the energy dissipation per unit plan beach area is proportional to the difference between the existing energy flux and a stable energy flux below which a wave will not decay. By using linear wave theory, the energy flux in shallow water is

$$F = \frac{1}{8} \rho g H^2 \sqrt{gh} \tag{27}$$

397. The stable energy flux is generally considered to be a function of the water depth (Horikawa and Kuo 1967), and a coefficient $\Gamma$ is used to express the ratio between the local wave height and water depth at stable conditions according to

$$H_s = \Gamma h \tag{28}$$

398. Measurements of the wave height distribution from the CRIEPI experiments were used to evaluate performance of the breaker decay model and to estimate values of the two empirical parameters ($\kappa$ and $\Gamma$) in the model. As described in Part V, the breaker decay model was least-squares fitted to wave height data from the breakpoint shoreward to the end of the surf zone. The solution of Equation 26 for a beach with an arbitrary shape, applying linear wave theory, is given by

$$H = \left[ \frac{1}{\sqrt{h}} \left( H_b^2 \sqrt{h_b}\ e^{-\kappa} \int_0^x \frac{dx}{h} + e^{-\kappa} \int_0^x \frac{dx}{h}\ \kappa\ \Gamma^2 \int_0^x h \sqrt{h}\ e^{\kappa} \int_0^x \frac{dx}{h}\ dx \right) \right]^{1/2} \qquad (29)$$

where, as previously mentioned, the cross-shore coordinate axis originates at the break point. Figure 55 shows a typical fit between results of the breaker decay model and measured wave heights in the surf zone. The symbols connected by straight lines denote the model result for different times, whereas the corresponding single points are the measured wave heights. The breaker decay model was in this case least-squares fitted against all wave height distribution measurements made during one run. To evaluate parameters of the breaker decay model simultaneously for various distributions, wave height was normalized with the incipient breaking wave height, and cross-shore distance and water depth were normalized with depth at incipient breaking.

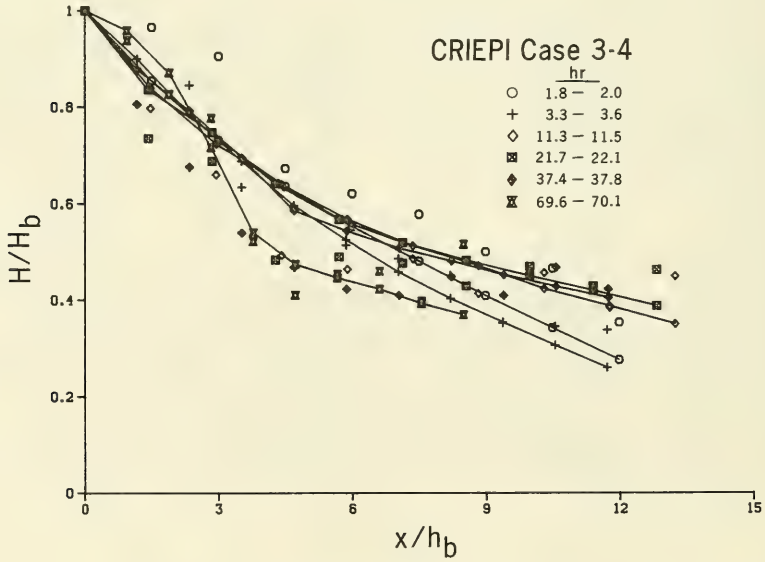


Figure 55. Measured and calculated wave heights

399. Wave setup and setdown are incorporated in calculation of the wave height distribution and determined by solving the following differential equation together with Equation 26 (Longuet-Higgins and Stewart 1963)

$$\frac{dS_{xx}}{dx} = -\rho g(h + \eta) \frac{d\eta}{dx} \tag{30}$$

where

$S_{xx}$ = radiation stress component directed onshore

$\eta$ = wave setup

400. The radiation stress is, using shallow-water approximations,

$$S_{xx} = \frac{3}{16} \rho g H^2 \tag{31}$$

Setdown in the first calculation cell is determined from the analytical solution to Equation 30 seaward of the break point, assuming no energy losses.

$$\eta = \frac{-\pi H^2}{4L \sinh\left[\frac{4\pi h}{L}\right]} \tag{32}$$

By calculating the wave height distribution across shore at every time-step in the model, a quasi-stationary approach is implied in which it is assumed that the input wave height changes at a time scale significantly longer than the wave period.

401. Energy dissipation by bottom friction is calculated in the model as done by Dally (1980) using linear wave theory to determine the horizontal component of the wave orbital velocity at the bottom and assuming a shear stress proportional to the horizontal velocity component squared. After the waves break, energy dissipation greatly increases due to the generation of turbulence. In the surf zone, energy dissipation produced by breaking is considerably larger than dissipation due to bottom friction.

## Transport Rate Equations

402. The distribution of the transport rate was calculated using relationships developed for the four different zones of the profile described in Part V. In the surf zone, i.e., the region of breaking and broken waves, the distribution of the transport rate is mainly a function of the energy dissipation per unit volume. Seaward and shoreward of the surf zone, semi-empirical relationships derived from the LWT experiments are applied to calculate the transport rate distribution. The magnitude of the transport rate in all transport zones is governed by that calculated for the part of the surf zone where broken waves prevail (Figure 43, Zone III).

403. The direction of net cross-shore transport is determined in the model by the criterion described in Part IV, which is based on the deepwater wave steepness and the dimensionless fall velocity (Equation 2). Although the criterion was developed to predict formation of bar and berm profiles, examination of associated cross-shore transport rate distributions showed that this relation was applicable to predict the direction of net transport as well. Onshore transport is predominant if a berm profile is formed, whereas offshore transport is predominant if a bar profile is formed. According to the criterion, material is transported offshore or onshore along the full length of the active profile at a specific instant in time. This is a good approximation if the profile is not too close to the equilibrium shape for the existing incident waves, in which case the transport rate would tend to be mixed, i.e., both onshore and offshore transport might occur along different regions of the profile at the same time. If the model is applied to field conditions, the mean wave height should be used to determine the direction of transport by Equation 2. (As discussed below, significant wave height should be used to calculate the breaking waves and transport rate.)

404. Both Moore (1982) and Kriebel (1982) used transport rate formulas for the surf zone in which the rate was proportional to the excess energy dissipation per unit volume over an equilibrium energy dissipation which the beach profile could withstand without changing shape significantly. Dean (1977) showed that an equilibrium profile derived from the concept of a constant energy dissipation per unit water volume from the break point and

onshore corresponded to a shape governed by a power law with an exponent of 2/3 (Equation 1). The relationship between excess energy dissipation per unit volume and transport rate in zones of broken waves was verified in Part V using wave and profile change data from the CRIEPI experiments.

405. In the profile change model, a transport relationship similar to that used by Moore (1982) and Kriebel (1982) is applied in a region of fully broken waves (Zone III) with a term added to account for the effect of local slope. A steeper slope is expected to increase the transport rate down the slope. The modified relationship for the transport rate $q$ is written

$$q = \begin{cases} K\left(D - D_{eq} + \frac{\epsilon}{K}\frac{dh}{dx}\right) & D > D_{eq} - \frac{\epsilon}{K}\frac{dh}{dx} \\ 0 & D < D_{eq} - \frac{\epsilon}{K}\frac{dh}{dx} \end{cases} \tag{33}$$

where

$K$ = empirical transport rate coefficient

$D$ = wave energy dissipation per unit volume

$D_{eq}$ = equilibrium energy dissipation per unit volume

$\epsilon$ = transport rate coefficient for the slope-dependent term

The energy dissipation per unit volume is given from the change in wave energy flux (Equation 27) as

$$D = \frac{1}{h}\frac{dF}{dx} \tag{34}$$

406. Equation 33 indicates that no transport will occur if $D$ becomes less than $D_{eq}$, corrected with a slope-dependent term. $D$ can become less than $D_{eq}$ due to a variation in water level. For example, if a well-developed bar forms, waves will break seaward of the bar crest, but a water level increase would make the depth inshore sufficiently large to decrease $D$ below $D_{eq}$ without wave reformation occurring. In this case, $q$ becomes zero.

407. As previously described, the transport direction is determined by an empirical criterion (Equation 2) and the magnitude by Equation 33. If $D$ were allowed to become less than $D_{eq}$, Equation 33 would predict a reversal

in sand transport, which might be in conflict with the imposed criterion specifying transport direction. Furthermore, in such a case, the magnitude of sand transport would increase as $D$ decreased to reach a maximum if no energy dissipation occurred. This is an incorrect description of what is expected to occur, since a cutoff energy dissipation exists under which no sand transport takes place. (See Kraus and Dean (1987) and Kraus, Gingerich, and Rosati (1989) for empirical evidence of an effective cutoff in longshore sand transport in the surf zone.) Consequently, the logical decision is to set q to zero if $D$ falls below $D_{eq}$. Also, from Figure 48 it can be inferred that the transport rate is small if $D$ approaches $D_{eq}$ (the situation distant from the break point).

408. Physically, the equilibrium energy dissipation represents a state in which the time-averaged net transport across any section of the beach profile is zero. The equilibrium energy dissipation may be expressed in terms of the beach profile shape parameter A in the equilibrium profile equation (Equation 1) according to

$$D_{eq} = \frac{5}{24} \rho g^{3/2} \gamma^2 A^{3/2} \tag{35}$$

where $\gamma$ is the ratio between wave height and water depth at breaking (breaker index, $H_b/h_b$). In the derivation of Equation 35, Dean (1977) assumed that the wave height existed in a fixed ratio with the water depth in the surf zone.

409. From Equation 34 it may be deduced that $D$ inherently contains a term proportional to the beach slope. The reason for incorporating an explicit slope dependent term in the transport relationship (Equation 33) is that regression analysis showed a dependence of q on slope for some of the cases analyzed in Part V. Also, numerical stability of the model was improved by inclusion of this term, as will be discussed below. Dean (1984) also modified the equilibrium energy dissipation by reducing it depending on the ratio between the local beach slope and the limiting slope for the sand surface, thus including a further slope dependence (cf. Watanabe 1985).

410. As discussed in Part V, the value of the transport rate coefficient K determined by comparison of calculated energy dissipation per unit

volume from measured wave heights and inferred or "measured" transport rates from the LWT data was about 1.1 $10^{-6}$ $m^4/N$. In contrast, Moore (1982) and Kriebel (1982) obtained a value of 2.2 $10^{-6}$ $m^4/N$ by making comparisons between calculated and measured profile change. This value was revised by Kriebel (1986) to become 8.7 $10^{-6}$ $m^4/N$. The coefficient $K$ is not entirely comparable between the models, since the structures of the models are different. The value of $\epsilon$ was found to be on the order of 0.0006 $m^2/sec$ (Part V).

411. The equilibrium energy dissipation was determined by Moore (1982) by fitting Equation 1 to 40 field and laboratory profiles. Beach material ranged in size from boulder (30 cm) to fine sand, and $D_{eq}$ was related to the mean sand diameter. Moore's analysis provided the best fit to profiles both with and without bars. These values were used in the numerical model and found to give reasonably accurate estimates of $D_{eq}$ in regions of broken waves. However, in the present study, in order to obtain optimal agreement between model simulations and measured profile change, values of $D_{eq}$ as specified by Moore had to be reduced by 25 percent, as discussed later.

412. By adding the slope term in Equation 33, the shape of the equilibrium profile will be somewhat gentler, since a profile with a specific grain size will be able to withstand a lower energy dissipation per unit volume. The shape of the equilibrium profile, derived from Equation 33 in analogy to Dean (1977), may be written

$$h\sqrt{h} + \frac{\epsilon}{K}\frac{24}{5\rho g^{3/2}\gamma^2} = A^{3/2}\,x \tag{36}$$

413. In Equation 36 water depth is an implicit function of the cross-shore distance. The effect of incorporating beach slope is only noticeable close to the shoreline for the values of $\epsilon$ used in the model. Further seaward the profile agrees with Dean's (1977) equilibrium profile.

414. In the numerical model, regions of fully broken waves are identified at each time-step, and transport rates are determined from Equation 33. Waves are considered to be fully broken from the plunge point to the shoreward end of the surf zone or to the point where wave reformation occurs. The location of the plunge point is defined with respect to the break point to

give the "plunge length." Galvin (1969) estimated the plunge length $\ell_p$ to be about four times the breaking wave height, showing a dependence upon beach slope $\tan\beta$, where a steeper beach implied a shorter plunge length for the same breaking wave height. The equation given by Galvin (1969) is

$$\frac{\ell_p}{H_b} = 4.0 - 9.25 \tan\beta \tag{37}$$

415. Equation 37 was tested for predicting the plunge length but gave unrealistically short distances for steep bar face slopes. Therefore, in the numerical model an overall value of three times the breaking wave height is used to estimate the plunge distance (see Singamsetti and Wind 1980, Svendsen 1987).

416. For the region seaward of the break point, the transport rate distribution is well approximated by an exponential decay with distance (Equation 21). For offshore transport the spatial decay coefficient is a function of the breaking wave height and grain size (Equation 22), whereas for onshore transport the decay coefficient is effectively constant.

417. For the relatively short region extending from the break point to the plunge point, an exponentially decaying transport rate is also used but with a smaller value of the spatial decay coefficient. Analysis of available data from the LWT experiments indicated the value of the spatial decay coefficient to be approximately 0.20-0.25 that of the spatial decay coefficient applicable seaward of the break point. A multiplicative factor of 0.20 is used in the numerical model to compute the spatial decay coefficient in the zone between the break point and the plunge point. The magnitude of the transport rate at the plunge point is determined from Equation 33, and seaward from this point the transport rate is calculated from the exponential decay functions.

418. The transport rate distribution on the foreshore is approximated by linear decay with distance from the end of the surf zone (Part V). The slope of the transport rate distribution on the foreshore decreases with time as the profile approaches equilibrium shape in the surf zone. Profiles generated in the LWT that either eroded or accreted exhibited this linear

behavior, implying a foreshore which receded or accreted uniformly along its full length. In the model, the transport rate is linearly extended from the end of the surf zone to the runup limit. (The surf zone is arbitrarily ended at a depth of 0.3-0.5 m.) However, as the foreshore erodes, the slope steepens and a pronounced scarp or step develops. Eventually, if erosive waves act for a sufficiently long time, the slope of the step will exceed the angle of initial yield (Allen 1970). In Part IV, time evolution of profile slopes was analyzed and indications of avalanching were found if profile slopes exceeded a value of 28 deg on average. This value is used in the numerical model to limit the growth of slopes along the profile.

419. Since the transport relationships do not explicitly describe avalanching, an algorithm was developed to simulate avalanching if the profile slope steepened excessively. If the angle of initial yield is exceeded, the profile slope decreases to a lower, stable value known as the residual angle after shearing (Allen 1970). Inspection of the LWT profiles indicated that a stable slope appeared to be reached at a value somewhat smaller than 22 deg on average. In the numerical model the residual angle after shearing was therefore set to 18 deg. The reason for this ambiguity was the difficulty of determining the residual angle after shearing from the profile data; instead, Allen's experimental results were used where the dilatation angle (difference between angle of initial yield and residual angle after shearing) was found to be in the range of 10-15 deg for sand. A dilatation angle of 10 deg was chosen, implying a residual angle after shearing of 18 deg.

420. If avalanching occurs in the numerical model, that is, if the angle of initial yield is exceeded, sand is redistributed into neighboring cells so that the slope adjusts to the residual angle after shearing. Once avalanching has started in one cell, it proceeds along the grid until a point is reached where the slope is less than the residual angle after shearing. A definition sketch is shown in Figure 56 illustrating a number of calculation cells and one cell where the angle of initial yield is exceeded (cell 1). Depths after avalanching, denoted with a prime in Figure 56, can be determined once the change in depth in the cell where avalanching is initiated is known. The change in depth in the first cell is given by

$$\Delta h_1 = -\left[\frac{N-1}{N}\right] h_1 + \frac{1}{N} \sum_{i=2}^{N} h_i + \frac{1}{2}(N-1)\Delta h \qquad (38)$$

where

$h_1$ = depth in the first cell where angle of initial yield is exceeded

$N$ = number of cells where sand is to be redistributed

$h_i$ = depth in cell i

$\Delta h$ = difference in depth between two neighboring cells as given by the residual angle after shearing

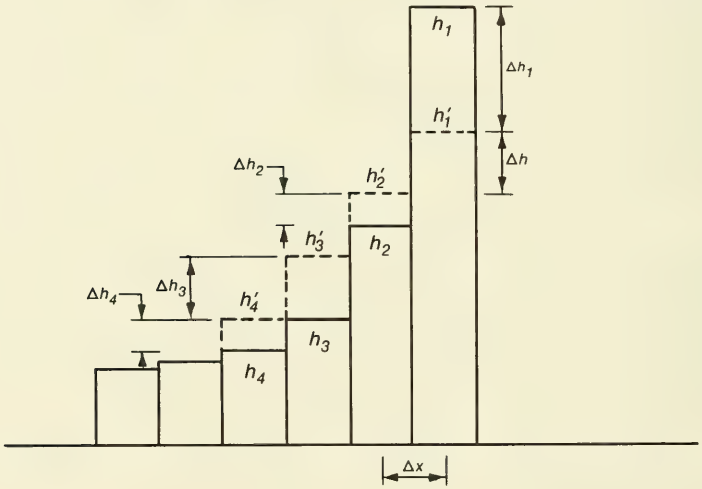


Figure 56. Definition sketch for describing avalanching

421. After the depth change in the first cell has been determined according to Equation 38, depth changes $\Delta h_i$ in neighboring cells are given by the following expression

$$\Delta h_i = h_1 + \Delta h_1 - h_i - (i-1)\,\Delta h \qquad (39)$$

where the index i refers to the cell number counting consecutively from the starting point of the avalanching in the direction of avalanching. The number of cells N that the avalanching will affect is not known a priori and has to be determined iteratively as more cells are incorporated in the calculation until the slope between cells N and N+1 is less than the residual angle after shearing. The avalanching routine limits the growth of the step and prevents the shoreward slope of a bar from becoming too steep.

## Profile Change Model

422. Changes in the beach profile are calculated at each time-step from the distribution of the cross-shore transport rate and the equation of mass conservation of sand. The equation of mass conservation is written as

$$\frac{\partial q}{\partial x} = \frac{\partial h}{\partial t} \tag{40}$$

423. Standard boundary conditions in the model are no sand transport shoreward of the runup limit and seaward of the depth where significant sand movement occurs. The runup height is determined from an empirical expression, Equation 17, derived from the LWT experiment data relating the height of the active profile to the surf similarity parameter and the deepwater wave height. The depth of significant sand movement is determined through the exponential decay of the transport rate with distance seaward from the break point. If the transport rate decreases to a small predetermined value, the calculation stops, and the transport rate is set to zero at the next cell, making that cell the seaward boundary. An expression presented by Hallermeier (1984) for the seaward limit depth was investigated for use in the model. However, this equation failed to predict what were considered to be reasonable closure depths on a wave-by-wave basis, evidently because the formula was developed for extreme annual events. Also, apparently because of the limited range of values from which the equation was derived, the closure depth was found to be too shallow for profiles exposed to the very steep waves that were used in some of the LWT cases.

424. In calculation of the wave height distribution across shore at a specific time-step, the beach profile from the previous time-step is used, and the transport rates are calculated explicitly. The mass conservation is written in difference form as

$$\frac{h_i^{k+1} - h_i^k}{\Delta t} = \frac{1}{2}\left[\frac{q_{i+1}^{k+1} - q_i^{k+1}}{\Delta x} + \frac{q_{i+1}^{k} - q_i^{k}}{\Delta x}\right] \tag{41}$$

where $k$ denotes the time level and $i$ the cell number over which the discretization is carried out.

425. The equation of mass conservation is discretized over two time levels using transport rates evaluated at the present and previous time-step. To obtain a realistic description of the wave height distribution across highly irregular profiles exhibiting bar formations, a moving average is used to obtain representative depth values. Averaging of the profile depth, carried out over a distance of three breaking wave heights as determined from Equation 25, was found to make the model numerically more stable. If the wave calculations are not based on a beach profile which has been filtered to some degree, the wave height will respond in an unrealistic manner to small changes in the profile. The beach profile generated with the moving average scheme is used only for calculation of the wave height distribution, and no changes in the profile itself are made.

426. Since the transport rate distribution is determined using various relationships in various regions of the profile, the derivative of the transport rate may be discontinuous at inter-region boundaries. To obtain a smoother transport rate, a three-point weighted filter is applied to the calculated transport rates. The wave height distribution is calculated explicitly in a manner similar to that of Dally (1980), proceeding from the most seaward cell onshore until the end of the surf zone is detected. The advantage of using an explicit solution scheme is that it easily allows description of initiation of breaking, switching to the breaker decay model, and reformation of broken waves. Use of an implicit solution scheme would considerably complicate the calculation and require an iterative procedure

since the location of the break point and any point where wave reformation occurs are not known a priori.

427. The slope-dependent term in Equation 33 improves numerical stability of the model. Some simulations performed omitting this term experienced numerical oscillation at the shoreward bar face as the slope grew steep and the trough became more pronounced. The slope-term tends to flatten the trough, since the transport rate at the shoreward bar face is reduced.

428. The numerical scheme proved to be very stable under a wide range of conditions in spite of the irregular bathymetry that occurs if bars are formed. Typical length and time-steps used in the model are $\Delta x$ = 0.5-5.0 m and $\Delta t$ = 5-20 min. The length step has to be chosen so as to resolve the main morphologic features. A shorter length step requires a correspondingly shorter time-step to maintain numerical stability. An effort was made to derive an explicit stability criterion but was not successful. Therefore, at the present time, trial and error must be used to determine appropriate values of $\Delta x$ and $\Delta t$ for the particular application.

429. For a beach profile exposed to constant wave and water level conditions, the profile shape predicted by the model approaches a steady-state, resulting in an equilibrium profile. The approach to equilibrium is controlled by the rate at which energy dissipation in the surf zone attains the equilibrium value $D_{eq}$ . A bar, if formed, causes the break point to translate in the seaward direction as it grows, making the offshore boundary of the surf zone move accordingly. At equilibrium, the break point is stationary and the energy dissipation per unit water volume is constant throughout the surf zone, being approximately equal to $D_{eq}$ , corrected by the slope-dependent term in Equation 33.

## Calibration and Verification

430. The numerical model was applied to simulate beach profile evolution for a number of erosional cases from the LWT experiments. As an objective criterion for judging agreement between the simulated and measured beach profile, the sum of squares of the difference of measured and calculated depths was formed according to

$$R = \sum_{i=1}^{N_p} (h_i^m - h_i^c)^2 \tag{42}$$

in which the superscripts m and c refer to measured and calculated profile depths, respectively, and $N_p$ is the number of data points. Values of different model parameters were varied to minimize the sum of the squares. In the calibration process, equal weight was placed on all measurement points along the profile without bias toward bars or eroded areas on the foreshore. Furthermore, the model was restricted to generating one breakpoint bar to limit the effort to reproducing the main breakpoint bar in the calibration. The volume of the main breakpoint bar was always at least ten times greater than that of any secondary inshore bar, thus being significantly more important for determining the wave height distribution across shore.

431. In simulation of beach and dune erosion, it is considered most important to predict the evolution of the main breakpoint bar, since this feature serves as a natural defensive response for reducing incident wave energy that would otherwise arrive at the beach face. Only a small amount of information was available from the LWT data set to quantify the net cross-shore transport rate in zones of wave reformation. As an exercise of the model, simulations to reproduce the inshore bar are presented below. It was necessary to make assumptions on the net transport rate between zones of fully broken waves for these simulations.

432. It is desirable to relate empirical parameters in the model directly to physical quantities or assign them a constant value to minimize the degrees of freedom in the calibration process. For instance, values recommended by Dally (1980) were used in the breaker decay model, i.e., a stable wave height coefficient of $\Gamma = 0.40$ and a wave decay coefficient of $\kappa = 0.17$. (The optimum value of the wave decay coefficient was modified slightly by Dally, Dean, and Dalrymple (1985a) to 0.15.) Although parameters in the breaker decay model showed a qualitative dependence on average beach slope in breaking wave data from the CRIEPI experiments, the above-mentioned constant values were used in the calibration. The number of parameters available for adjustment in the calibration process was thereby reduced with

little loss of accuracy in determining an optimal calibration, since the minimum of the sum of squares in most cases was located in a rather flat region.

433. Based on preliminary calibration runs, the coefficient expressing the slope dependence of the transport rate ($\epsilon$ in Equation 33) was set to 0.001 $m^2$/sec. A smaller value of $\epsilon$ will allow the trough to be locally somewhat more pronounced, whereas a higher value will flatten the trough. The angle of initial yield was set to 28 deg according to slope behavior inferred from the LWT experiments, and the residual angle after shearing was set to 18 deg. A larger angle of initial yield will allow the profile slope to become steeper before avalanching occurs. During simulation of an erosional event in the LWT data, avalanching typically takes place on the foreshore step or on the shoreward side of the bar.

434. At the initial stage of model calibration, both K and $D_{eq}$ in the transport equation (Equation 33) were used in the calibration procedure. The transport rate coefficient K was varied together with $D_{eq}$ for 10 erosional cases. Although it was considered desirable to avoid using $D_{eq}$ as a calibration parameter and instead determine its value from the design curve given by Moore (1982), it was found that in order to achieve best agreement between numerical model simulations and tank measurements, the value of $D_{eq}$ had to be reduced. The equilibrium energy dissipation controls the amount of sand that is eroded before the equilibrium profile is attained. Moore's relationship was derived by a least-squares fit of a power curve (Equation 1) to beach profiles in general, making this method not entirely compatible with the concept of regions with different transport rate relationships used in the present numerical model. In most cases, the parameter combination which gave the minimum sum of squares was located in the vicinity of an equilibrium energy dissipation value of about 75 percent of that obtained by Moore's relationship. This fixed reduction (0.75) of the equilibrium energy dissipation was applied in all cases, and the optimal value of the transport rate coefficient K was determined by minimizing the sum of the squares of depths.

435. Values of the transport rate coefficient for the 10 cases simulated which gave the best agreement between measured and simulated profiles varied in the range of 0.3 - 2.2 $10^{-6}$ $m^4$/N, with an average of 1.4 $10^{-6}$ $m^4$/N

for 10 separate optimizations. Most of the cases, however, had a value of K in the range of 1.1 - 1.9 $10^{-6}$ $m^4/N$. The sum of squares was minimized with respect to all profiles measured during the particular case, typically encompassing 5-10 profile surveys per case. Figure 57 shows a representative calibration run with the numerical model and a comparison with the measured beach profile from the last profile survey of the simulated case (Case 6-1). Beach profiles at selected time-steps from the model calculations are shown together with the wave height distribution calculated at the last time step. The optimal K-value for this case was 1.9 $10^{-6}$ $m^4/N$. As seen in Figure 57, bar formation (size and location) and the amount of erosion on the foreshore were well described by the numerical model. The small inshore bar was purposefully neglected in the calibration simulation. This feature appeared in the LWT experiment after 40 hr of run time, just prior to the last profile survey. Measured wave heights are shown across the profile, indicating that the wave height distribution was satisfactorily reproduced by the breaker decay model.

436. Transport rate distributions calculated at selected times are shown in Figure 58. The magnitude of the transport rate decreased with time as the profile approached an equilibrium shape in accordance with the behavior of transport rate distributions directly inferred from the profile survey data in Part V. Occasionally, the transport rate increased in the vicinity of the break point compared with previous distributions, caused by movement of the break point. As the break point moved offshore, energy dissipation increased because of the decrease in depth occurring at the plunge point, and the transport rate increased accordingly.

437. It was not possible to relate K obtained from individual calibrations to wave or sand characteristics with any significance for the number of cases available for study. Qualitatively, the transport rate coefficient seemed to decrease with increasing grain size and increase with decreasing wave period. A wave period dependence of the profile time response was also shown in the analysis in Part V of peak net cross-shore transport rates calculated from the LWT data.

438. Since it was not possible to relate the transport rate coefficient to any physical property, it was desirable to achieve an optimal estimate of

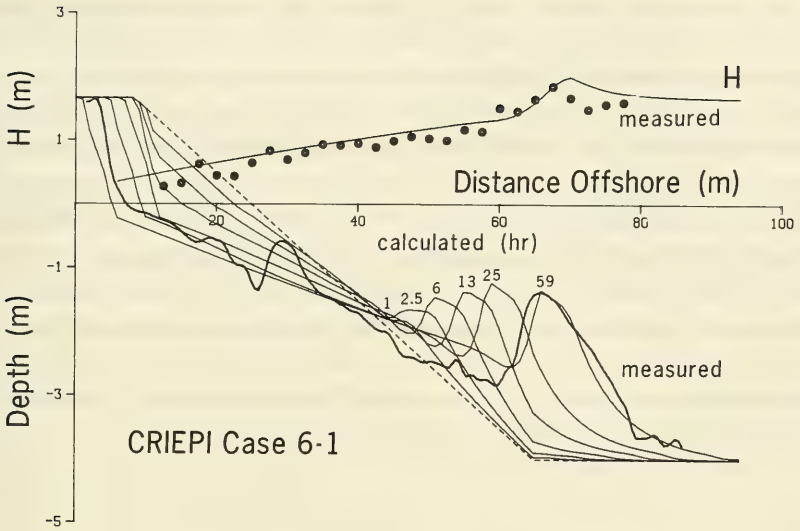


Figure 57. Calibration of numerical model

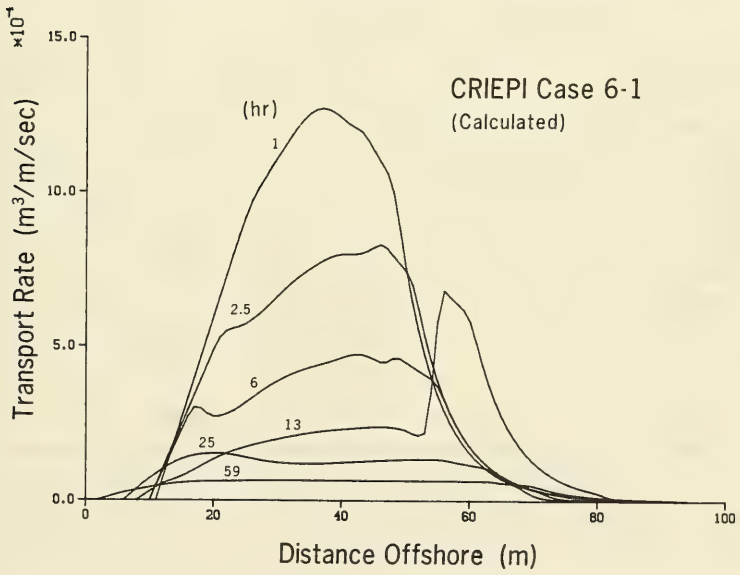


Figure 58. Net cross-shore transport rates at selected times

K for use in simulating all cases. To obtain best overall agreement between simulated and measured profiles with constant K , the model was calibrated for seven of the cases with respect to the total sum of squares. After the optimal value had been determined for K , the model was verified through use of two independent cases. One case (Case 700 with K = 0.3 $10^{-6}$ $m^4/N$) was eliminated from the overall calibration process since water was released from the tank during the run (probably to reduce wave overtopping), lowering the water level by 0.3 m, thus contaminating the case for the purpose here (see Kraus and Larson 1988a). The sum of squares of the difference in depth between measured and simulated beach profiles was calculated for all profile surveys for all seven cases. Figure 59 illustrates the total sum of squares for all cases as a function of the transport rate coefficient. A minimum occurred around the coefficient value 1.6 $10^{-6}$ $m^4/N$.

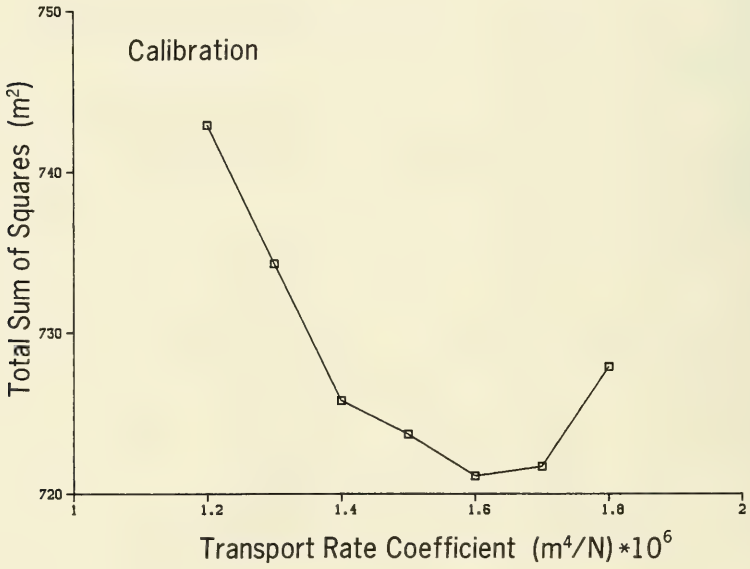


Figure 59. Optimization for model calibration

439. Two cases, one from the CE data set (Case 400) and the other from the CRIEPI data set (Case 6-2), were used to verify the applicability of the numerical model with parameter values obtained from the calibration. Figure 60(a and b) shows the results of the verification runs, illustrating the development in time of the beach profile together with a comparison with the measured profile at the last time-step. The wave height distribution across shore at the last time-step is also shown. The volume of the main breakpoint bar and the amount of erosion on the foreshore are rather well predicted by the numerical model. However, the crests of the bars are located somewhat too far seaward, whereas the trough is not deep enough for Case 400. In general, the trough is not well reproduced in the numerical model, being less pronounced than for the measurements, since the slope term in the transport equation (Equation 33) counteracts the seaward transport of sand on the shoreward side of the bar. Elimination of the slope term, however, seriously affects numerical stability, resulting in a much shorter allowable time-step in relation to the length step.

## Summary

440. The developed numerical model was calibrated and verified to simulate erosional (bar-type) profiles with relatively little ambiguity in determining values of the required empirical coefficients. In particular, the time rate of growth, volume, and location of the main breakpoint bar were well reproduced. The location of the shoreline and the steep slope of the foreshore step were also well simulated. Inclusion of avalanching was needed to restrict bottom slopes to within measured angles, and an explicit slope-dependent contribution to the transport rate was found to greatly improve stability of the model.

441. Importantly, in all tests run with constant incident wave conditions and water level, the calculated profile approached an equilibrium form. This property is highly desirable to represent the proper time scale of profile change and to use the model in an arbitrary situation without the problem of numerical stability. Sensitivity analysis of the model is described in the next chapter.

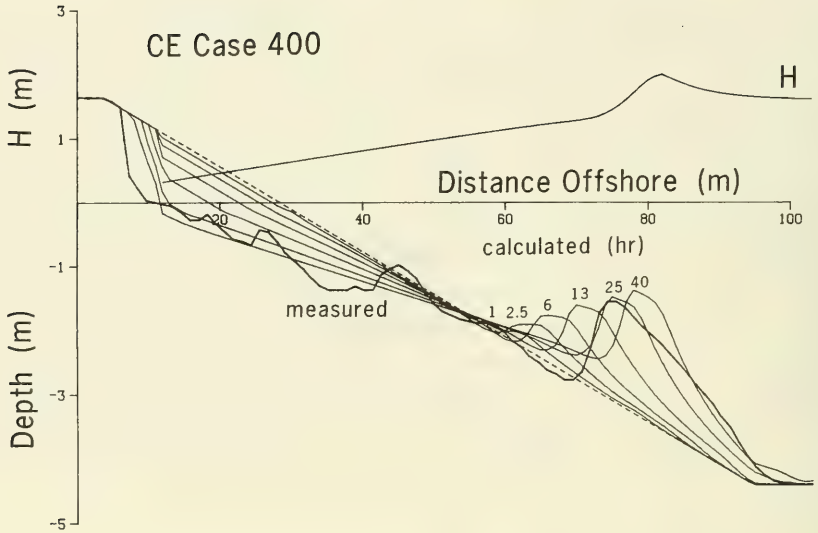


a. Case 400

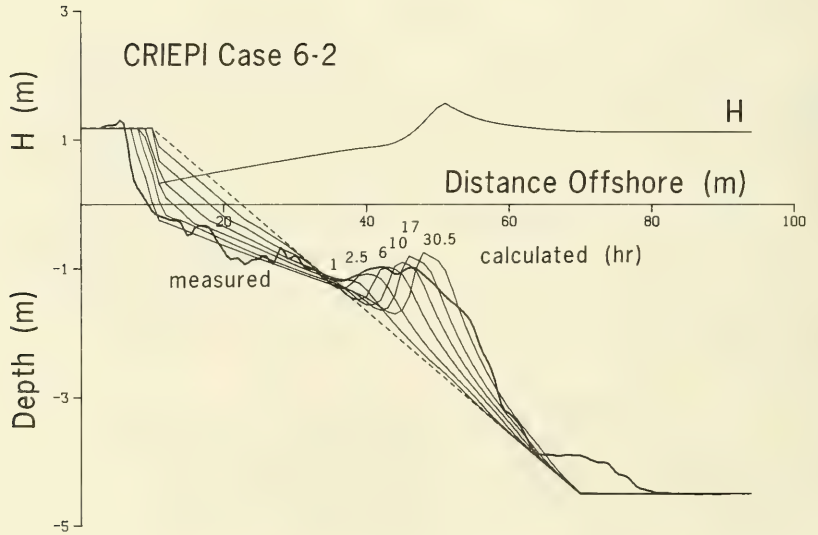


b. Case 6-2

Figure 60. Verification of numerical model

# PART VII: APPLICATIONS OF THE NUMERICAL MODEL

442. The numerical model developed in this study and its calibration are described in Part VI. The model was calibrated by comparison to the large data base of LWT experiment results obtained by using constant waves and water level. In this chapter, sensitivity analysis is conducted with respect to a number of model parameters to evaluate their influence on the calculated results. Predictions of the model are examined for a variety of hypothetical cases, including varying wave and water level conditions. Consideration is also given to simulation of multiple bars. The model is then put to the severe test of reproducing beach profile change, in particular, bar movement in the field. Example applications of the model are made to investigate the effect of a vertical seawall on beach profile development, as well as initial adjustment of beach fill. Comparison with an existing model, the Kriebel model (Kriebel 1982), is made for a number of hypothetical conditions to evaluate the importance of bar formation on beach erosion. Finally, model simulations are made to qualitatively reproduce onshore sand transport and berm buildup.

## Sensitivity Analysis of Model Parameters

443. A sensitivity analysis was performed to quantify the influence of various model parameters and empirical coefficients on simulation results. Sensitivity analysis gives valuable information about the physical implications of the model parameters and their relative effects on the result. It is important to explore the predictions of the model beyond the range in which it was calibrated to determine if expected and intuitively reasonable trends are obtained. In the following, the influence of principal model parameters on beach evolution is discussed mainly by reference to bar properties. To this end, the change in shape and size of the bar is investigated for a specific case (Case 401) under perturbations of optimal values of model parameters as determined by the calibration.

Influence of K

444. The empirical transport rate coefficient K (Equation 33) primarily governs the time response of the beach profile. A smaller value gives a longer elapsed time before equilibrium is attained, whereas a larger value produces more rapid evolution. However, K also influences equilibrium bar volume, as seen in Equation 36. Although Equation 36 was derived assuming uniform energy dissipation per unit volume everywhere in the surf zone and not just in zones of fully broken waves, it gives important qualitative information about the influence of K and $\epsilon$ . A smaller K-value implies a flatter equilibrium beach profile with correspondingly more sand to be moved from the inshore for a fixed initial profile slope before equilibrium is attained.

445. Figure 61 illustrates the growth of bar volume with time for different values of the transport rate coefficient. For $K = 2.2\ 10^{-6}\ m^4/N$, more than 90 percent of the equilibrium bar volume was reached after 20 hr, whereas for $K = 0.4\ 10^{-6}\ m^4/N$ only approximately 30 percent of the final bar volume was reached. The dependence of equilibrium bar volume on K is introduced through the slope term in the transport equation. Without this term the shape of the equilibrium beach profile would be independent of K , and this coefficient would only influence the time response of the profile.

446. Calculated maximum bar height (defined with respect to the initial plane beach profile) as a function of time is shown in Figure 62 for various K-values. Maximum equilibrium bar height was insensitive to the value of K . However, as expected, time evolution of the bar height is controlled by K , showing a more rapid change for larger values. The location of the mass center of the bar was only slightly influenced by the value of K , with the mass center somewhat displaced shoreward when the value of K was decreased.

Influence of $\epsilon$

447. The empirical coefficient $\epsilon$ in the slope term in Equation 33 mainly influences equilibrium bar volume and thus the amount of sand that is redistributed along the profile to reach equilibrium. Profile response was similar for quite different values of $\epsilon$ during the initial phase of the simulation and differed only after longer elapsed times (Figure 63). Equation 36 indicates that a smaller $\epsilon$-value implies a steeper equilibrium beach profile and less sand to be moved before a state of equilibrium occurs. The effect of the slope term on maximum bar height was weak, where a change in

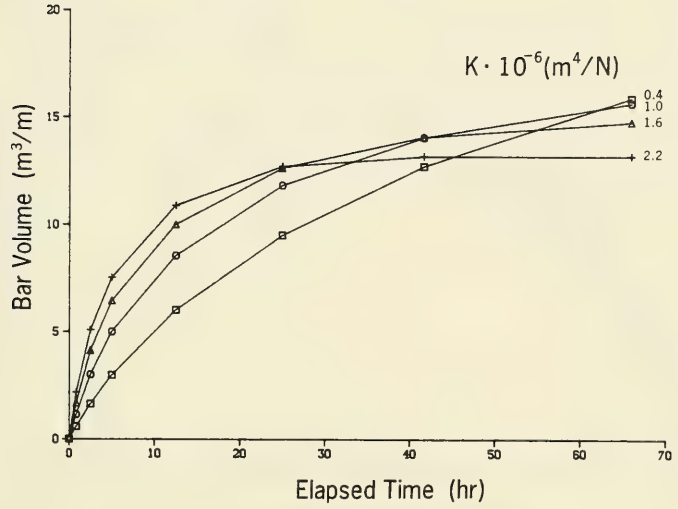


Figure 61. Effect of K on bar volume

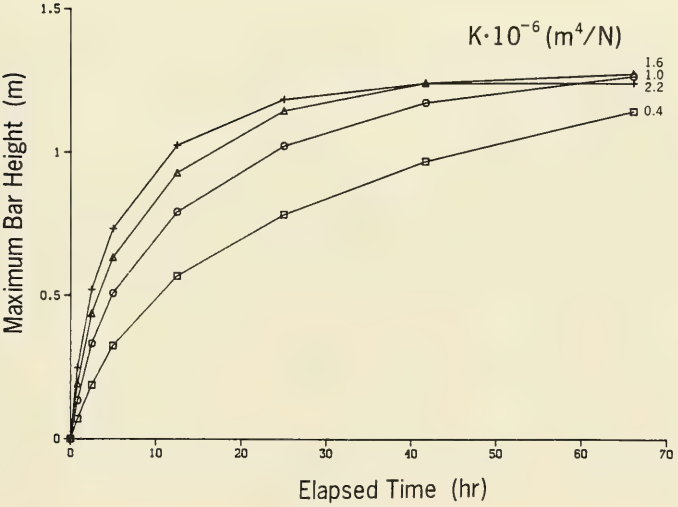


Figure 62. Effect of K on maximum bar height

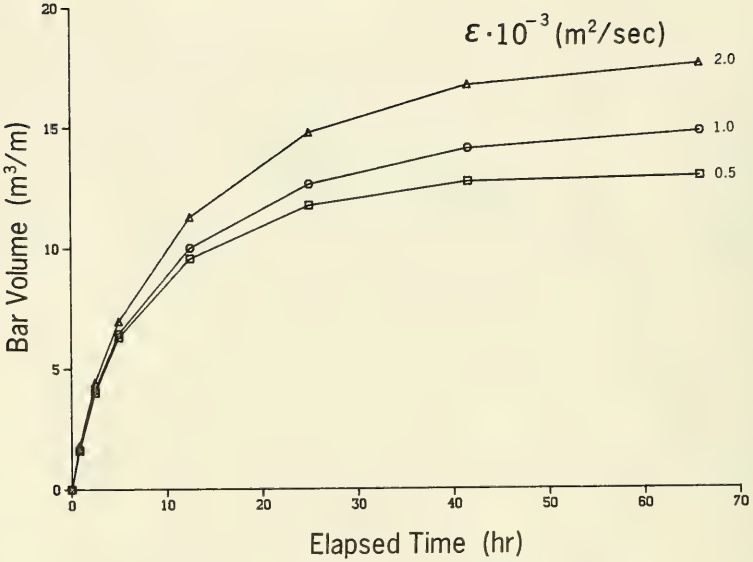


Figure 63. Effect of $\epsilon$ on bar volume

$\epsilon$ by a factor of four gave a corresponding change in the equilibrium maximum bar height of less than 10 percent. Similarly, the location of the bar mass center was found to have a weak dependence on changes in $\epsilon$ .

Influence of wave model parameters

448. Parameter values in the breaker decay model were specified in the calibration procedure as suggested by Dally (1980). To quantify the importance of variations in the wave height calculation, the wave decay coefficient $\kappa$ in Equation 26 was varied. Figure 64 illustrates the growth of bar volume as a function of time for various values of $\kappa$ . A smaller value of $\kappa$ implied a larger equilibrium bar volume, although the time responses were similar at the very beginning of a simulation. As theoretical background it proves valuable to digress and examine the shape of the equilibrium beach profile exposed to a wave height distribution which fulfills the breaker decay model developed by Dally (1980).

449. Dally, Dean, and Dalrymple (1985a, b) presented analytical solutions for the cross-shore distribution of wave height for simple beach profile

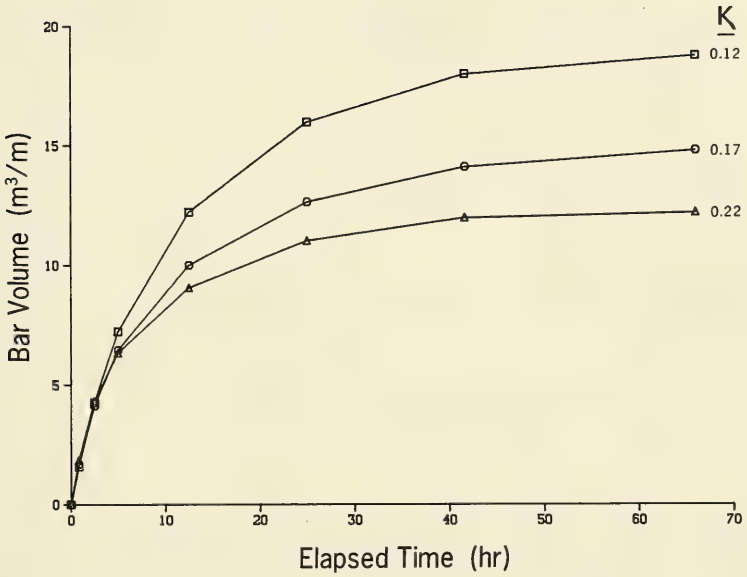


Figure 64. Effect of $\kappa$ on bar volume

shapes. However, these solutions did not fulfill the Dean criterion of equal energy dissipation per unit volume for equilibrium conditions to prevail on a beach. If the slope-dependent term in the transport equation (Equation 33) is dropped, it is possible to solve the coupled problem of requiring constant energy dissipation per unit volume subject to the Dally breaker decay model. The coupled system of equations consists of Equations 26 and 33, for which the slope term is neglected and $D$ is set equal to $D_{eq}$ according to

$$\frac{1}{h}\frac{dF}{dx} = D_{eq} \tag{43}$$

$$\frac{dF}{dx} = \frac{\kappa}{h}(F - F_s) \tag{44}$$

Note that here the x-axis originates from the shoreline, making Equation 44 differ in sign from Equation 26.

450. The depth of the beach profile is obtained as an implicit function of the location across shore according to

$$\left[ \frac{2}{\kappa} + \frac{5}{3} \frac{\Gamma^2 \rho g^{3/2}}{8 D_{eq}} \sqrt{h} \right] h = x \tag{45}$$

The corresponding wave height distribution is given by

$$H = \left[ \frac{8 D_{eq}}{\kappa \rho g^{3/2}} h^{3/2} + \Gamma^2 h^2 \right]^{1/2} \tag{46}$$

451. As seen from Equation 45, a smaller value of the wave decay coefficient $\kappa$ gives a flatter shape of the equilibrium beach profile and thus requires redistribution of a greater amount of sand before equilibrium is attained. On the other hand, a smaller value of the stable wave height coefficient $\Gamma$ gives a steeper equilibrium beach profile, resulting in a smaller equilibrium bar volume, since less material has to be moved from the inshore to attain equilibrium.

452. Figure 65 shows the effect on bar volume of varying the stable wave height coefficient, supporting the qualitative result as predicted by Equation 45. The influence of changes in parameter values in the breaker decay model on maximum bar height was less pronounced compared with the effect on bar volume. The stable wave height coefficient affected the equilibrium maximum bar height only slightly, and the development in time was very similar during the initial phase of a simulation. The wave decay coefficient had a somewhat greater influence on the equilibrium maximum bar height, in which a smaller value implied a larger bar height.

Influence of equilibrium energy dissipation

453. Equation 45 also reveals the importance of the magnitude of the equilibrium energy dissipation, which was shown to be a function of grain size by Moore (1982). A change in grain size causes a marked change in the shape

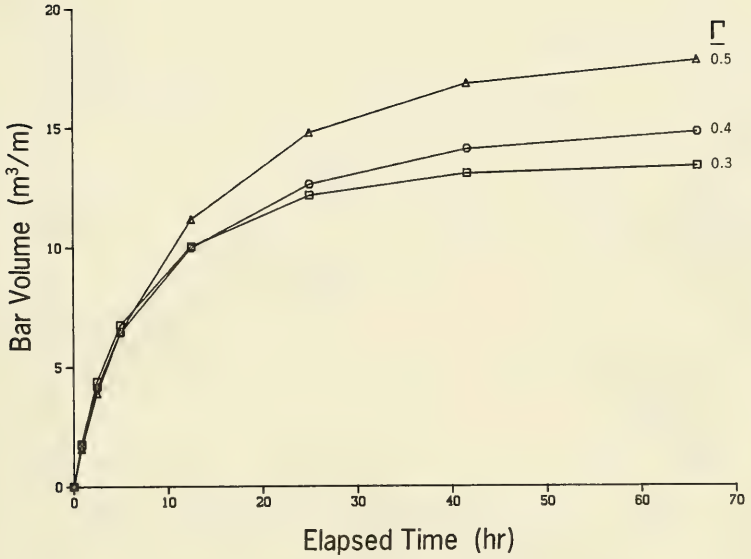


Figure 65. Effect of Γ on bar volume

and size of the bar, which is more pronounced for finer material. A smaller value of $D_{eq}$, occurring for finer grain sizes, corresponds to a flatter equilibrium beach profile, thus requiring more sand to be moved before equilibrium is attained.

454. Sensitivity of model predictions on grain size was investigated. Since equilibrium energy dissipation decreases rapidly with grain size (Moore 1982), bar volume correspondingly increases, as illustrated in Figure 66. (Values of $D_{eq}$ used to obtain the curves in Figure 66 are 0.75 the value of those obtained by Moore (1982), according to the results of the model calibration in Part VI.)

455. Changing the median grain size from 0.50 to 0.40 mm increased the equilibrium bar volume by about 20 percent, whereas a decrease in median grain size from 0.40 to 0.30 mm gave an increase of about 90 percent. Corresponding changes in values of $D_{eq}$ were 10 percent and 70 percent, respectively. Changes in maximum bar height were also significant as the grain size was decreased, although not as great as for bar volume.

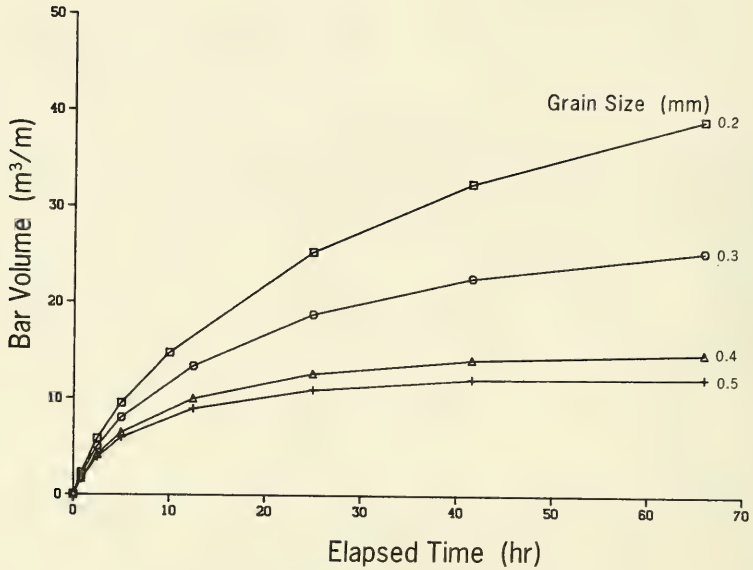


Figure 66. Effect of D on bar volume

456. Equilibrium maximum bar height increased by percentage values about half those of bar volume for the same changes in grain size. Movement of the bar center of mass was only slightly affected by changes in most model parameters. However, change in grain size did have a significant influence on the location of the center of mass, as seen in Figure 67. Initiation of bar formation occurred roughly at the same place, independent of grain size; however, after initiation, bar movement was considerably greater for the finer grain sizes.

457. Grain size also influences the spatial decay coefficient for the transport rate seaward of the break point (see Equation 22). The decay coefficient increases with grain size, implying that the transport rate decreases more rapidly, moving sand less seaward.

Influence of wave period and height

458. So far in the sensitivity analysis, only parameters which are expected to be effectively constant for a specific beach have been investigated. Since the driving force in the numerical model is wave breaking, it

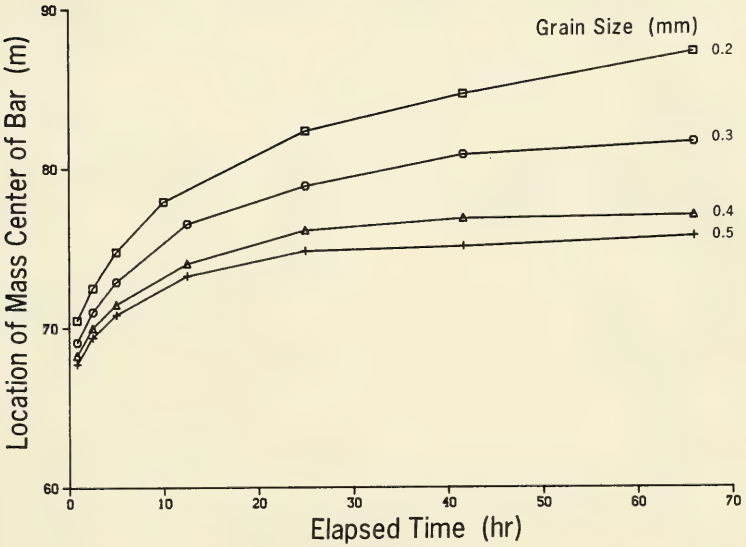


Figure 67. Effect of D on bar center of mass

is of considerable interest to analyze the response of the beach profile to changes in wave input parameters. Therefore, wave height and period were varied to investigate the sensitivity of the numerical model to changes in wave input.

459. An increase in wave period resulted in an increase in bar volume. Figure 68 shows the evolution in time of bar volume for various wave periods. Since small-amplitude wave theory for shallow-water conditions is applied in the numerical model, wave period does not enter explicitly in the shoaling calculation within the grid, but through shoaling from deep water to the seaward boundary of the grid and through the breaking wave criterion (Equation 24) (and, of course, in the criterion determining direction of transport, Equation 2). A longer wave period will allow a specific wave to shoal further inshore before it breaks, producing greater energy dissipation and moving more sand before equilibrium is attained. Maximum bar height was influenced by wave period in the same manner as bar volume; an increase in period gave a larger maximum bar height.

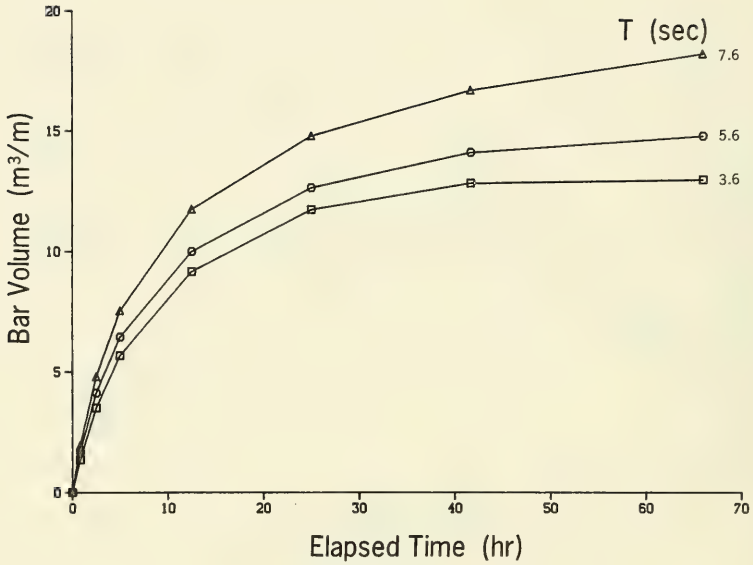


Figure 68. Effect of T on bar volume

460. The effect of an increase in wave height on bar properties is readily understood, since a larger wave height involves a larger amount of wave energy for the beach profile to dissipate in a state of equilibrium. Both equilibrium bar volume and equilibrium maximum bar height increased significantly as wave height increased.

Influence of runup height

461. The location of the shoreward boundary in the model is closely related to the runup height and can be predicted by an empirical relationship (Equation 17). Since Equation 17 contains the slope of the beach, a difficult parameter to quantify in a field application, it is of significance to estimate the influence of runup height on the simulation result. Figure 69 illustrates growth of bar volume with time for various runup heights calculated through Equation 17. Evolution of bar volume was only slightly affected by the considerable variation in runup height. Consequently, even a significant error in estimation of the runup height will not notably degrade the

representation of the time evolution of the bar. However, model prediction of the amount of erosion occurring on the foreshore may be substantially in error.

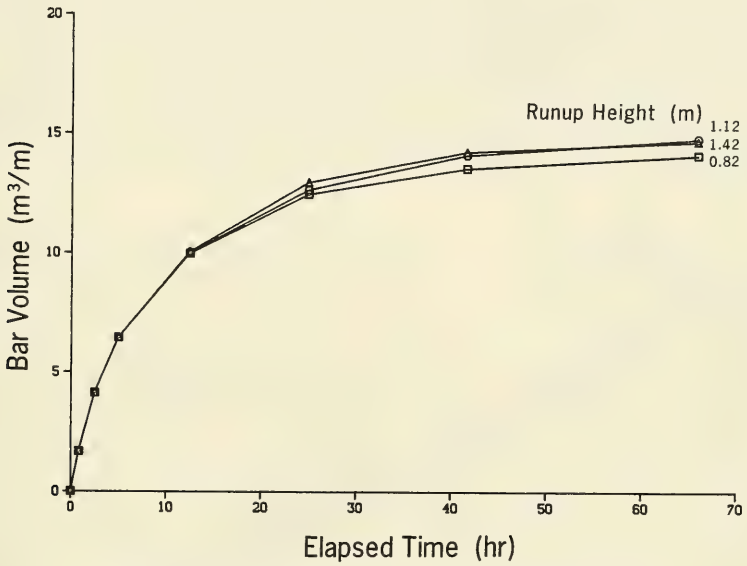


Figure 69. Effect of runup height on bar volume

Effect of Time-Varying Water Level and Waves

462. In the preceding calibration, verification, and sensitivity analysis, all simulations were conducted with a fixed water level and constant wave conditions. However, in one of the LWT experiments (Case 911), water level was varied in a sinusoidal manner to simulate the influence of a tidal variation on beach profile evolution. This case provided an opportunity to evaluate model predictions of profile change induced by constant incident waves with a realistic variation in water level. The water level variation had an amplitude of 0.45 m and a period of 12 hr. Optimal model parameters obtained in the overall calibration were used in the simulation of Case 911.

463. Figure 70 illustrates the result of the model run and a comparison with the measured beach profile at the end of the tank experiment. Develop-

ment of the beach profile as predicted by the numerical model was as follows. The first increase in water level resulted in the formation of an almost stationary emergent bar, as observed in the first few profiles. As water level dropped, the break point rapidly moved seaward, and the bar correspondingly moved in the seaward direction. When the water level increased at later cycles and a well-developed bar existed at the seaward end of the profile, waves passed over the bar and broke inshore creating a small second feature just shoreward of the main breakpoint bar.

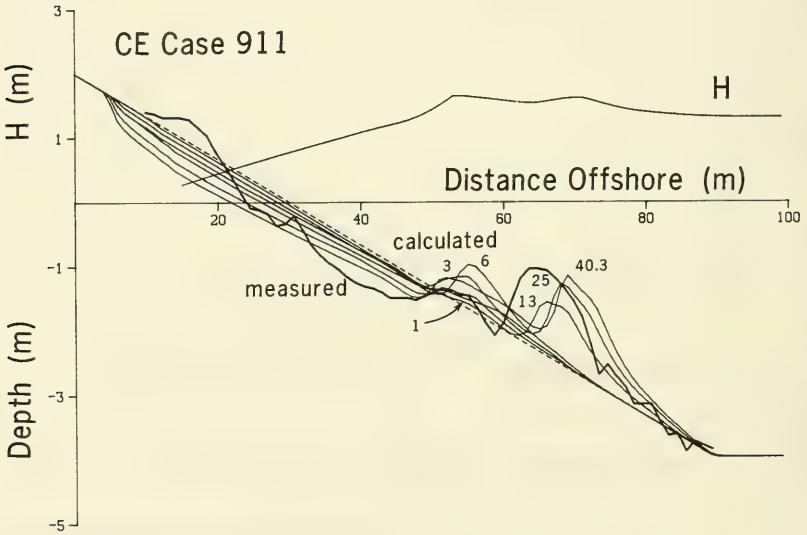


Figure 70. Verification for case of varying water level

464. As observed on the measured profile, a small berm formed on the foreshore during the latter part of the run which was not described by the model. Otherwise, the model reproduced the main shape of the beach profile, that is, a main breakpoint bar with a smaller bar-like feature inshore, separated by a distinct trough. Locations of calculated bars were somewhat farther seaward compared with those of the measured profile, but bar volume was reasonably well predicted.

465. It was possible to obtain better agreement between simulated and measured bar locations by changing model calibration parameters. However, it was not possible to simulate berm buildup on the foreshore because the empirical criterion for the transport direction (Equation 2) predicted seaward-directed transport during the entire run. Wave and sand parameters for Case 911 are such that the intersection of quantities involved in the criterion determining transport direction is very close to the line separating bar and berm profiles. This may explain the somewhat mixed response of the profile.

Water level, wave height, and wave period

466. To qualitatively evaluate model performance for varying water level, wave height, and wave period, a number of hypothetical cases were simulated. In all cases, the initial beach profile consisted of a dune with a steep face having a plane slope (1:5) joined to a more gentle plane slope (1:15) at the still-water shoreline. The cycle of the variation for wave period, wave height, and/or water level was set at 200 time-steps ($\Delta t$ = 5 min), and the simulation was carried out for 1,000 time-steps.

467. The effect of a varying wave period was investigated first, where the deepwater wave height was chosen as 2.0 m and the water level was fixed. The wave period was varied sinusoidally between 6 and 10 sec with the previously-mentioned time cycle. Figure 71 shows the simulated beach profile at selected time-steps and the wave height distribution at the last time-step. The shape of the bar is somewhat more gentle than for a fixed wave period (see Watts 1954) and changes in the profile decrease with time, approaching a near-equilibrium state, even though the wave period continues to change. The direction of bar movement was seaward during the entire simulation period.

468. Beach profile change produced by a sinusoidally varying water level showed features similar to those in the Case 911 simulation. The simulated example had a water-level amplitude of 1 m, a wave height of 2 m, and a wave period of 6 sec. Figure 72 shows the calculated beach profile at selected time-steps and the wave height distribution across-shore at the last time-step. As the water level increased, the bar was stationary or even moved some what shoreward, whereas during the decline in water level the bar moved rapidly seaward. Once the bar formed, a rise in water level allowed waves to

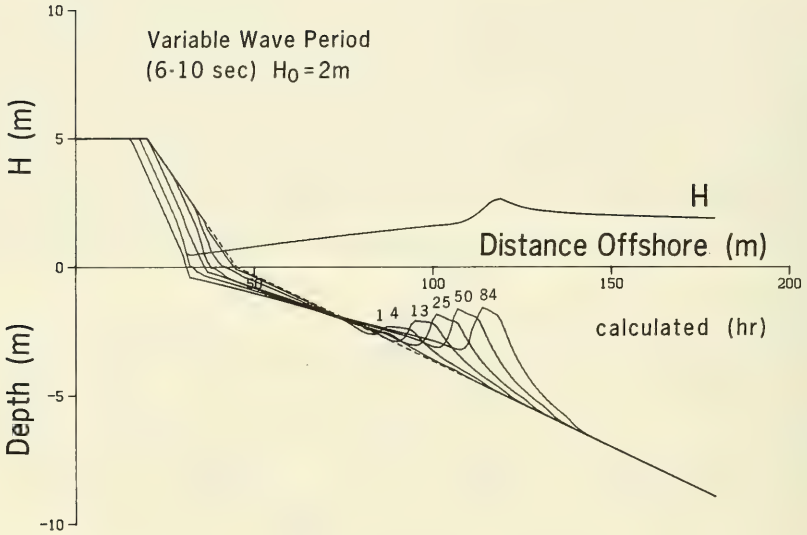


Figure 71. Simulation with varying wave period

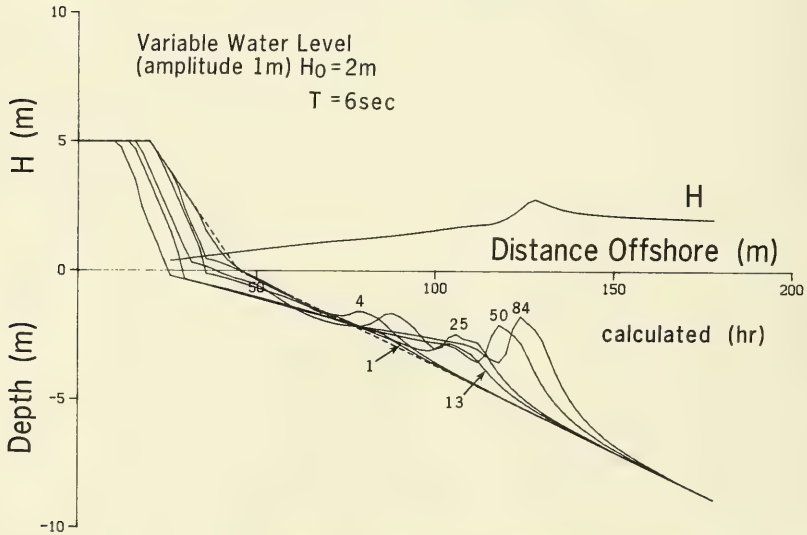


Figure 72. Simulation with varying water level

pass over the main bar and break inshore, causing deposition of sand shoreward of the bar. The flat portion of the bar was a result of waves breaking shoreward of the bar crest. The seaward peak of the bar was created from waves breaking at the bar crest when water level was at a minimum.

469. Somewhat similar profile development occurred when wave height was varied sinusoidally. As an example, deepwater wave height was varied between 1 and 3 m, with the wave period fixed at 10.0 sec and the water level constant. In Figure 73, selected profiles predicted by the model are displayed at consecutive times, together with the calculated wave height distribution at the last time-step. The bar had a flat shape initially, but a pronounced peak formed after a number of wave height cycles had been completed.

470. The constant supply of sand from the dune as the wave height changed, together with the movement of the break point, prevented the inshore from developing a characteristic monotonic shape. However, if the wave height is held constant, the beach profile would approach an equilibrium shape with a concave inshore profile.

471. As an example of the shape of the net cross-shore transport rate, distributions associated with Figure 73 are plotted in Figure 74. The peak of the transport rate distribution moved across-shore with movement of the break point as wave height varied. At some time-steps, a small peak appeared at the foreshore (not shown in Figure 74, but seen in Figure 58), particularly if avalanching took place on the dune slope. In this case, sand accumulated in the foreshore cells as the slope adjusted to the residual angle after shearing. The corresponding decrease in depth produced a larger energy dissipation per unit volume in those cells, resulting in a greater transport rate. Figure 74 also shows that the transport rate distribution exhibited a more complex shape at later times, when the depth was not monotonically decreasing.

472. A hypothetical case was also numerically simulated for concurrent sinusoidal variations of water level (±1 m) and wave height (2 m ±1 m). Variation of the two parameters was in phase with a period of 200 time-steps ($\Delta t$ = 5 min). The total simulation time was 1,000 time-steps, and the wave period was 8 sec. As seen from Figure 75, the bar is higher and wider than in previous examples. Also, the dune face retreated more than for the example with only wave height variation, since the waves could attack higher on the dune because of the water level variation

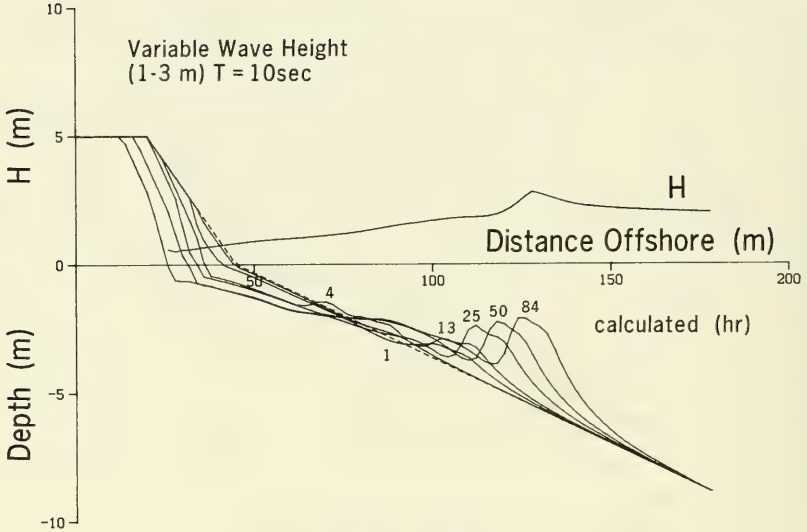


Figure 73. Effect of varying wave height

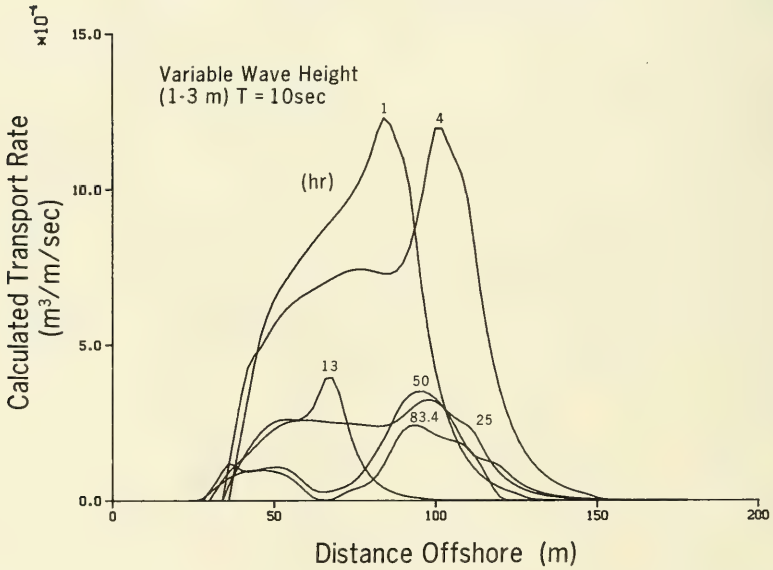


Figure 74. Transport rate distributions for varying wave height

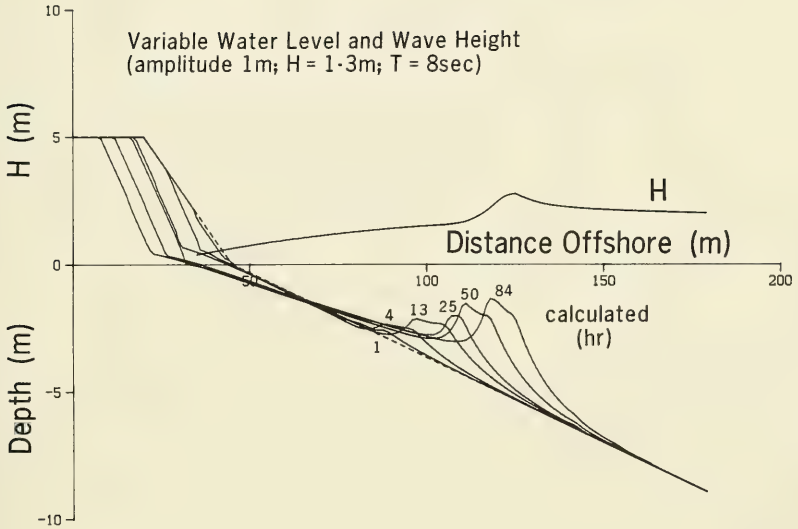


Figure 75. Simulation with varying water level and wave height

## Multiple Barred Profiles

473. If the water level varies simultaneously with the wave height, waves may reform as they pass over the trough. The reformed waves will break further inshore and create another bar, thus producing a multiple barred profile. The shape and properties of the net transport rate in zones of broken waves, seaward of the break point, and on the foreshore were investigated in Part V, whereas in zones of wave reformation less empirical information was available for analysis and deduction. However, some conclusions of a qualitative nature can be made from observations of transport rate distributions obtained from the LWT studies.

474. Formation of a second bar inshore is recognized in the transport rate distribution as a local minimum, with monotonically decreasing transport rates seaward and shoreward of this point. Since calculated net transport

rate is obtained from profile surveys separated by several hours, the inshore peak of the distribution was sometimes not clear. Also, the number of cases studied in which wave reformation occurred was limited. This made information scarce about the net transport rate in zones of wave reformation, and choice of the shape of the transport rate distribution became somewhat arbitrary.

475. It is reasonable to assume that the transport rate in zones of wave reformation is a function of the transport characteristics in the bordering zone of broken waves, since mobilization and transport are expected to be most intense in the broken wave zone. It is therefore assumed that the magnitude of the transport rate at the boundary of the broken wave zone determines the magnitude of the transport rate in the wave reformation zone. Then, only information about the functional form of the decay of the transport rate to the point of minimum transport and the location of this minimum are required to completely specify the transport rate distribution in the wave reformation zone. The magnitude of the minimum transport rate in the wave reformation zone is given by a decay function once the location of the minimum is specified.

476. Various trial functions were investigated to find a suitable description of the transport rate distribution in the wave reformation zone, focusing on exponential and power functions. A qualitatively acceptable representation of beach profile evolution was obtained by an exponential decay from the point of wave reformation shoreward to the point of minimum transport. From the second break point seaward to the point of minimum transport, a power law was applied to describe the transport rate. By introduction of these empirical functions, additional parameters are introduced in the model, and their magnitudes must be determined through calibration against measurement. The two empirical transport relationships used to describe the transport rate $q$ in zones of wave reformation are

$$q = q_r \, e^{-\nu(x_r - x)} \qquad x_m \leq x < x_r \tag{47}$$

and

$$q = q_b + (q_m - q_b) \left[ \frac{x - x_b}{x_m - x_b} \right]^n \qquad x_b < x < x_m \tag{48}$$

where

$q_r$ = transport rate at wave reformation point

$\nu$ = spatial decay coefficient

$x_r$ = location of wave reformation point

$x_m$ = location of minimum transport rate

$q_b$ = transport rate at second break point

$q_m$ = minimum transport rate in wave reformation zone (determined from Equation 47)

$x_b$ = location of break point

n = exponent determining spatial decay in transport rate

477. To investigate the possibility of modeling wave reformation and multiple bar formation, one of the CE cases was used for which measurements of a second break point were made (Case 500). Since the wave height in the surf zone approaches the stable wave height $\Gamma$ asymptotically as the waves progress onshore (Horikawa and Kuo 1967, Dally 1980), wave reformation will not occur in the model for a beach with monotonically decreasing depth in a surf zone that is exposed to constant wave conditions and water level. As a bar grows in size, the trough becomes more pronounced, but the slope-dependent term in the transport equation (Equation 33) will not allow the trough to become sufficiently deep to initiate wave reformation.

478. One method of forcing waves to reform in the model is by turning off breaking at a predetermined level somewhat higher than the value of the stable wave height coefficient (see Dolan 1983, Dolan and Dean 1984). A physical argument for a higher value is that an asymptotic decay toward the stable wave height is unrealistic in nature, and wave reformation is initiated through a delicate balance between competing processes close to stable conditions. Consequently, by forcing wave reformation to occur, the phenomenon is included in the model, although the details of the process are simplified.

479. In this particular simulation, a stable wave height coefficient of $\Gamma = 0.4$ was used in all simulations, whereas breaking was turned off at a value of $\Gamma = 0.5$ to initiate wave reformation. A typical simulation result is displayed in Figure 76. Simulated beach profiles at consecutive times are

given together with the measured beach profile at the last time-step. The wave height distribution across-shore for the last time-step is also shown.

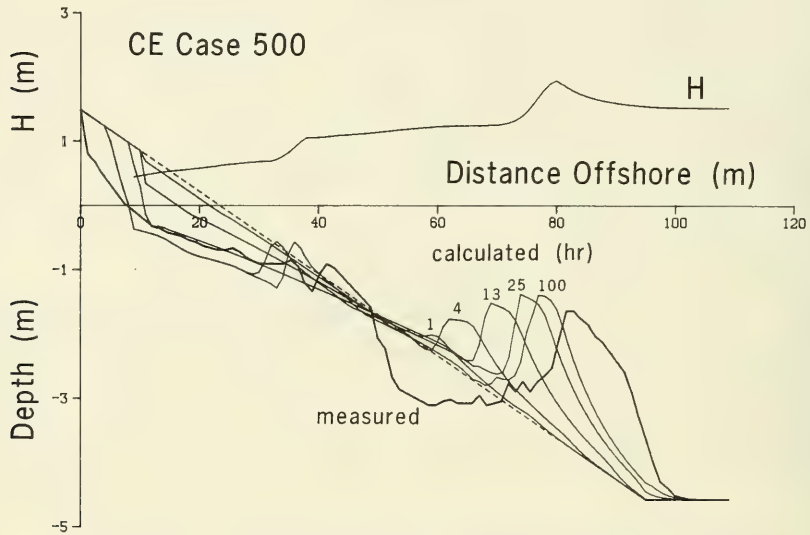


Figure 76. Reproduction of the second breakpoint bar

480. Locations of the two bars and the amount of erosion on the foreshore were well described by the model, whereas the distinct trough shoreward of the main break point was not reproduced. When the second bar appeared, sand transport to the main breakpoint bar was hindered in the model and growth of the main bar slowed.

481. As previously mentioned, between the shoreward break point $x_b$ and the point where the transport rate attains a minimum in the reformed wave zone $x_m$ , a power function was used to describe the decrease in transport rate. An exponent of 0.5 proved adequate, although the calculation was not sensitive to changes in this value. Changes in the exponent did not affect the shape or size of the outer bar but did influence somewhat the location of the inner bar. A larger value of the exponent caused the inner bar to move farther seaward, whereas a smaller value hindered seaward bar movement. From the point of wave reformation $x_r$ shoreward, an exponential decay was used, thus introducing another spatial decay coefficient $\nu$ . Typical coefficient

values were around 0.10 $m^{-1}$ between those found for the main breakpoint bar from the plunge point to the break point and from the break point seaward (Part V).

482. The location of the minimum transport rate $x_m$ must be specified to completely determine the transport rate distribution in the wave reformation zone. Once this point is known, the transport rate is calculated from the exponential decay starting from the wave reformation point. The power curve then connects the minimum transport rate thus determined with the transport rate at the second break point. As waves reform, turbulence is advected onshore with the waves, keeping grains in suspension and making them available for transport. However, because the generation of turbulent motion through wave energy dissipation decreases considerably, the transport rate decreases correspondingly. Closer to the second break point on the seaward side, the transport rate is expected to increase again, caused by the large energy dissipation shoreward of the break point. Since the sand transport capacity of a reformed wave is probably larger than for waves in the zone immediately seaward of a break point, the point of minimum transport should probably be located closer to the second break point than the point of wave reformation. In the model, the location of the minimum transport rate in zones of wave reformation was arbitrarily placed seaward of the second break point one third the distance to the wave reformation point.

483. In initial simulations of multiple bar formation, the inshore bar typically formed too close to the main breakpoint bar, compared with measured beach profiles from the LWT experiments. This was caused by rapid shoaling in the model after wave reformation, making the break point form too far seaward, since wave energy dissipation drastically changed as waves reformed and shoaling became dominant. Because wave reformation is a gradual phenomenon, it was believed that successive turn-off of energy dissipation would provide a more adequate representation of what actually happens in this zone. The turn-off is implemented in the numerical model by decreasing the wave decay coefficient $\kappa$ exponentially with distance from the wave reformation point. A decay coefficient of 0.025 $m^{-1}$ in the exponential damping function proved sufficient to accurately describe the location of the second bar.

## Simulation of Field Profile Change

484. The numerical model was used to simulate beach profile change measured at the FRF in Duck, North Carolina. The FRF is operated by CERC at the US Army Engineer Waterways Experiment Station. Beach profile surveys along four shore-normal lines and associated wave and water level measurements have been obtained regularly for more than 4 years at the FRF. Measurement procedures and a listing of the data are given by Howd and Birkemeier (1987). Surveys are carried out at approximately 2-week intervals, statistical wave parameters are calculated from gage data every 6 hr, and water level is recorded every 6 min.

485. Five time periods were chosen for model simulation, each distinguished by two profile surveys between which erosional conditions prevailed (storm events). Erosional conditions were characterized by offshore movement of one or two bars, whereas shoreline position in most cases was very stable and no retreat was noted. Anomalous stability of shoreline position is characteristic of the FRF beach and may be caused in part by the presence of coarser sediment that produces an armoring effect on the foreshore, thus requiring a larger amount of wave energy to move the material.

486. Figure 77 shows the sediment size distribution across the profile on 17 March 1981 as given by Howd and Birkemeier (1987). The median grain size was more than an order of magnitude greater on the foreshore compared to the seaward region. Because of the large grain size, the slope of the foreshore at the FRF is usually very steep, allowing waves to break directly on the beach face.

487. Although profile data from the FRF are unsuitable for evaluating shoreline change and the prediction of eroded subaerial volume, movement of the bar may still be simulated with reasonable confidence. Furthermore, beach changes may be highly three-dimensional in the field, making it essential to identify profile change in the record for use here that was likely minimally affected by longshore transport and rip currents. Howd and Birkemeier (1987) documented a wave event 821013 - 821015 (notation: year-month-day) during which time closely spaced profiles showed very different responses, with a bar moving onshore on one survey line and offshore on the other line, illustrating

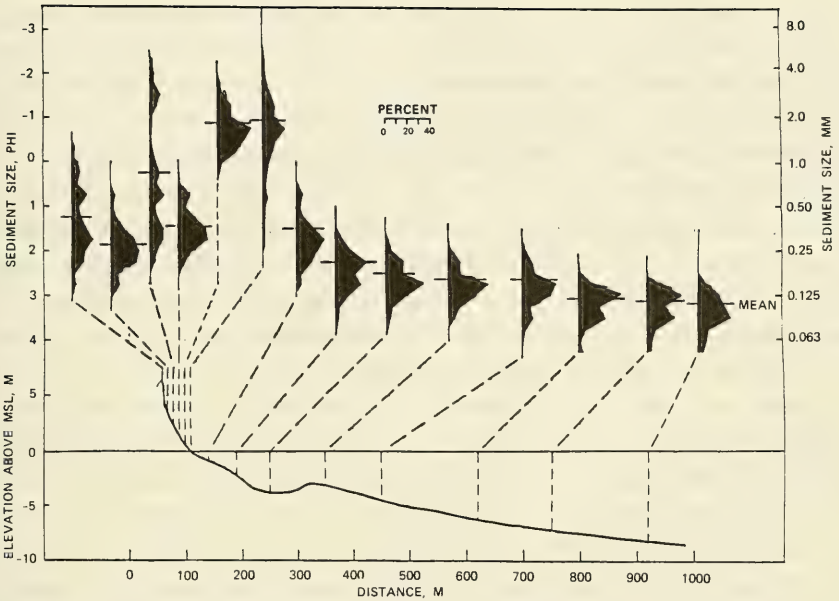


Figure 77. Distribution of grain size across profile line 188 (from Howd and Birkemeier 1987)

the importance of choosing events which show similar profile response alongshore. Therefore, in the present study time intervals were selected during which adjacent profile lines displayed similar development.

Data set

488. Survey line 188 (Howd and Birkemeier 1987) located southeast of the FRF pier was selected for profile simulation. The survey line is beyond the influence of the pier and located in an area of characterized by nearly straight and parallel bottom contours. To minimize the effect of longshore variability in profile change in selecting storm events for simulation, the response of line 188 was compared with line 190, located less than 100 m away. Five events were selected for which profile evolution was similar for the two survey lines, making it reasonable to believe that beach changes were predominantly two-dimensional during the storm events. However, for most events used, mass was not rigorously conserved in comparison of consecutive surveys, indicating that longshore effects influenced profile response to some degree.

489. Measured wave height and period were available every 6 hr and water level every hour. Since a shorter time-step (typically, $\Delta t$ = 20 min; $\Delta x$ = 5.0 m) was used in the numerical model, cubic spline interpolation was used to provide input values for time-steps between measurements. The energy-based wave height $H_{mo}$ was determined from the wave spectrum as four times the standard deviation, which corresponds to the significant wave height if a Rayleigh distribution of the wave height is assumed. Wave period was given as the peak period of the spectrum. Wave input data were obtained from gage 620, located in 18 m of water directly seaward of the pier. The height was then transformed using linear wave theory to the beginning of the model calculation grid, located at a depth of about 8 m below mean sea level.

490. The tide gage is located at the end of the pier and measures the total water level variation with respect to mean water level. Thus, water level measurements include both storm surge and tidal variation, the latter being semidiurnal (two high and two low waters in a tidal day).

491. Profile surveys were made at an average interval of 2 weeks, with more frequent surveys when greater profile change took place. Although profile data from the FRF represent one of the most detailed and accurate data sets on profile change, horizontal spacing between measurement points along a profile line is typically tens of meters. Small features along the profile are not resolved, and the general shape has a more smoothed character than actually exists. However, the data set is highly suited to the present application.

Calibration of numerical model with field data

492. Parameter values given by calibration with the LWT data sets were initially used in simulation of the field profile change data. However, it became apparent that values of some empirical coefficients would have to be modified to achieve agreement between measured and calculated profiles. Four storm events (811022 - 811103; 811110 - 811116; 840210 - 840216; and 840403 - 840406) were chosen for calibration of the numerical model, and one event (821207 - 821215) was used for verification. Calibration was performed by minimizing the total sum of squares of the difference between calculated and measured depths. The optimum transport rate coefficient K obtained for the four events was smaller than the value obtained for the LWT data. As

previously described (Part VI), the optimum K-value for the LWT calibration was determined to be 1.6 $10^{-6}$ $m^4/N$. For the field data, a value of 0.7 $10^{-6}$ $m^4/N$ proved to give the best agreement. Three cases had a best fit for 0.9 $10^{-6}$ $m^4/N$, whereas the remaining case gave 0.4 $10^{-6}$ $m^4/N$.

493. A smaller value of the transport coefficient is not unexpected since the coefficient showed an inverse dependence on wave period for the LWT experiments, and wave periods in the field data were somewhat longer than in the LWT data set. Calibration of K using the LWT data set is somewhat biased toward shorter period waves. Use of the K-value determined from the LWT data caused the beach profile to respond too quickly and the bar to become too pronounced, not having the smooth character of the field measurements. Transport induced by irregular waves that exist in the field, i.e., wave heights and periods varying above and below the representative monochromatic (but time-varying) waves used in the model, is also expected to alter the value of the transport coefficient, as both transport thresholds and mean rates will be different (Mimura, Otsuka, and Watanabe 1987). From these considerations, the amount of change in K between LWT and field calibrations is surprisingly small.

494. Values of other empirical coefficients appearing in the various transport rate relationships were kept at the values given by the LWT calibrations. In the breaker decay model, the stable wave height coefficient was set to $\Gamma = 0.4$ as for the LWT calibration, whereas a wave decay coefficient of $\kappa = 0.13$ gave better agreement between measured and simulated profile evolution. A smaller wave decay coefficient is expected for the FRF data compared to the LWT data since this coefficient depends slightly on beach slope (Part V), and the field profiles had more gentle slopes than the LWT profiles. The stable wave height coefficient was also varied, but the simulation was insensitive to changes in this parameter.

495. The breaking criterion developed from the LWT data caused waves to break too far offshore, creating a bar farther seaward than found in the measurements. Instead, a constant value of the breaker ratio of 1.0 was applied, which gave a better description of the bar location. In the breaker criterion derived from the CRIEPI data set, the slope seaward of the break point was used. At the seaward side of the bar the slope was normally

relatively steep, making the breaker ratio correspondingly high. Beach profiles from the FRF data set showed more gentle slopes than the CRIEPI experiment, causing the predicted breaker ratio to become lower, and the waves to break farther offshore. As a result, the relationship derived from the LWT data produced a slope dependence which appears not to apply to the more gently sloping bars found in the field.

496. The energy-based significant wave height was used in the numerical model to determine the wave height distribution across shore. On a field beach, the break point constantly moves back and forth due to random variation in wave parameters. A problem is to find a measure of the wave height that will on the average reproduce properties of the random breaking waves. As an alternative to the significant wave height, the mean wave height $\bar{H}$, determined by assuming a Rayleigh distribution, was used in some simulations. Since $\bar{H}$ is smaller than $H_{mo}$, the waves broke farther inshore but moved less sand. However, better agreement was not achieved using $\bar{H}$, in contrast to what was reported by Mimura, Otsuka, and Watanabe (1987) based on their small tank experiments.

497. The nonlinear shoaling law derived by Shuto (1974) was also tested in some field data simulations. It seemed to overestimate shoaling just before breaking, as was the case for the LWT experiments. Longer period waves calculated by the nonlinear theory markedly increased in height in shallow water, creating a bar too far offshore. Consequently, linear wave theory was judged to be more satisfactory and was used throughout.

498. Median grain size probably varied across the beach profile (see Figure 77) with a notably larger grain size on the foreshore. To represent this variation in the model, two different grain sizes were used along the profile. A larger grain size (2.0 mm) was specified on the foreshore to a distance approximately 130 m from the baseline, and a finer grain size (0.15 mm) was employed from this point and seaward. The larger grain size requires larger equilibrium energy dissipation with correspondingly more wave energy needed to move material. As for the LWT simulations, the equilibrium energy dissipation design curve of Moore (1982) was reduced by a factor of 0.75. Additional variation in median grain size across shore somewhat improved the fit of the model in trial simulations but was considered to be

unrealistic because of the added complexity and because the movement and mixing of individual grains are not simulated in the model.

Results

499. Calibration. Figure 78(a and b) illustrates the result of a typical calibration for one event (840403-840406) together with the wave and water level data. The initial measured profile is displayed together with the measured and calculated final profiles. Movement of the bar was rather well predicted by the model regarding location, but the amount of material moved was underestimated, and the trough was not sufficiently pronounced. Also, even though a larger equilibrium energy dissipation was used on the foreshore corresponding to the measured 2-mm grain size, the simulated shoreline still receded somewhat, whereas this did not occur in the field. One reason for this retreat was transport produced by small waves that passed over the bar and broke immediately on the beach face. Indeed, wave breaking at the step is commonly observed at the FRF; nevertheless, little shoreline movement takes place. Application of the concept of cross-shore transport being proportional to energy dissipation may be questionable if a surf zone is absent and waves break directly on the beach face. Lack of shoreline movement at the FRF is anomalous, and model results cannot be interpreted in this region based on the data.

500. Verification. Optimum parameter values determined from the calibration were used to simulate an independent storm event (821207-821215), and thus evaluate the applicability of these values for an independent erosional case. The result of the model verification is shown in Figure 79(a and b), together with the input wave height, wave period, and water level. The initial beach profile exhibited two bars, with the outer bar having a very smooth shape. The model simulation reproduced the main changes of the beach profile in that both bars moved offshore. However, the amount of material moved was underpredicted as in the calibration, and the calculated shoreline receded farther than the measured. Movement of the inner bar was overestimated by the model, whereas the outer bar was located correctly but with less volume than measured. Also, the long, smooth trough located shoreward of the outer bar was not produced in the model simulation, and only a small amount of material was eroded from this region.

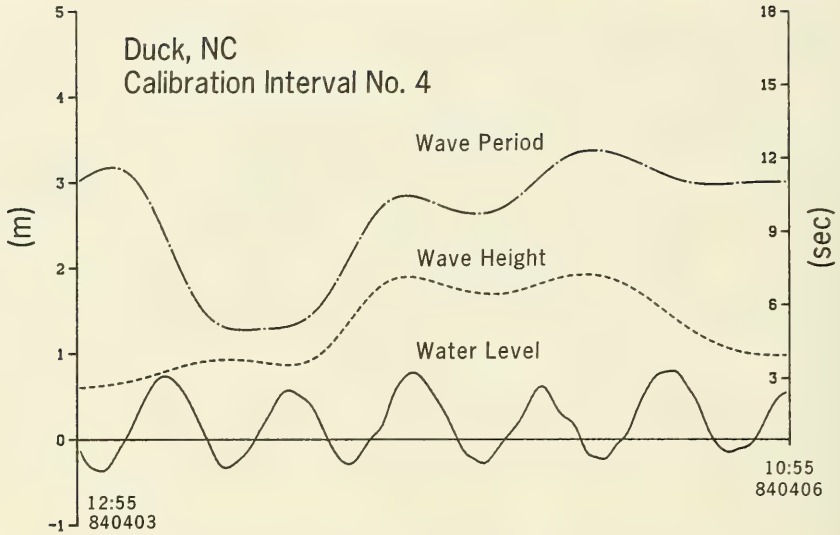


a. Input measured wave height, wave period, and water level

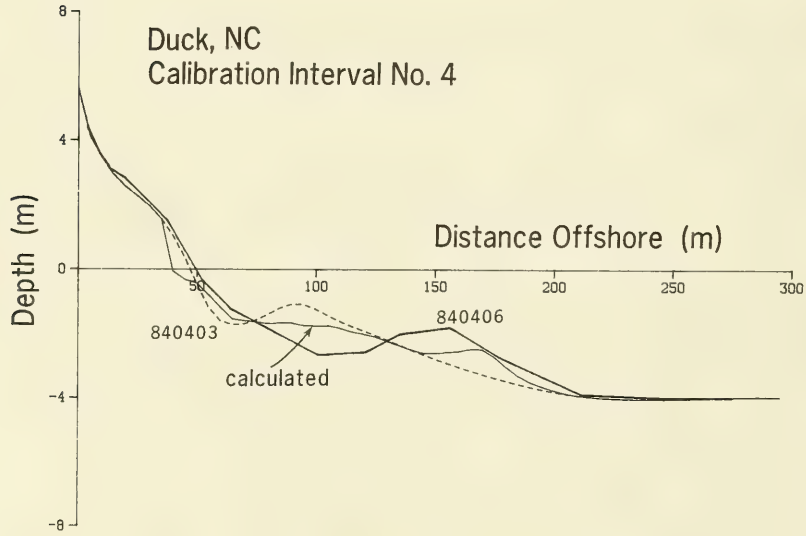


b. Result of simulation

Figure 78. Field calibration, event 840403-840406

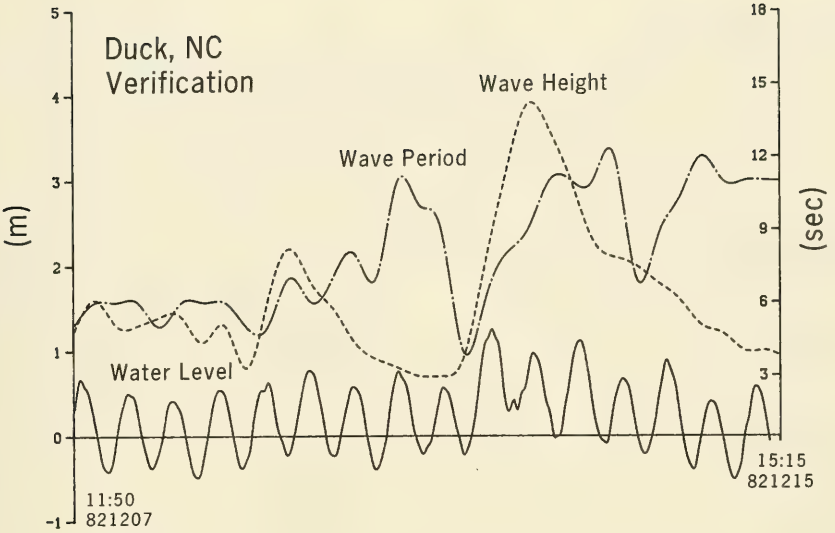


a. Variation of wave height, wave period, and water level

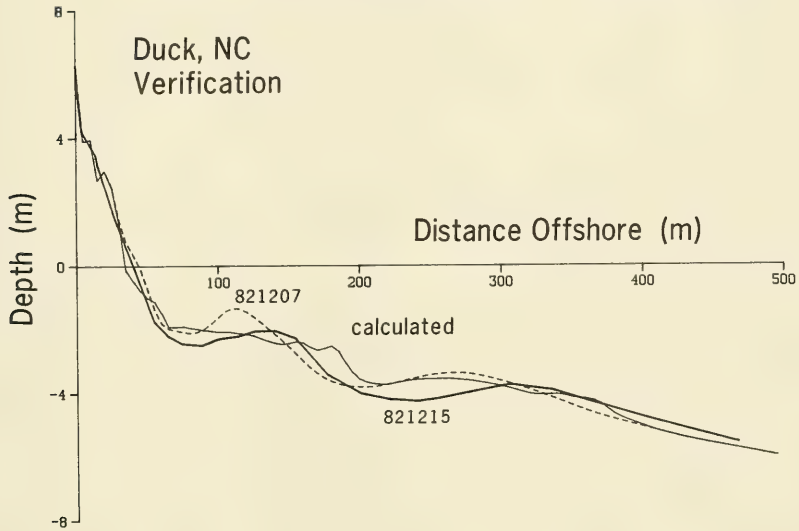


b. Result of simulation

Figure 79. Field verification, event 821207-821215

Sensitivity tests

501. To determine the influence of input wave and water level conditions and to put the results in perspective, variant simulations using the verification case 821207-821215 were performed. Since calibration was not carried out for this case, changes in wave parameters and water level better reflect model sensitivity to these input data. Parameter values given from calibration were used in these simulations. First, the extent to which changing water level improves or degrades model results was investigated.

502. In one simulation, water level variation was neglected completely, and neither the storm surge nor the tidal variation were represented. Figure 80 compares the measured 821215 profile and the simulated profile obtained by omitting water level changes. A constant water level implied that only wave height and period would determine the location of the surf zone and the amount of energy dissipation. Comparison with Figure 79b shows that the bar closest to shore developed a double-peaked shape. The most seaward bar was smaller and not as smooth as the corresponding bar formed under a varying water level. The sum of squares of the difference between measured and calculated profiles was smaller for the case including the water level variation, thus giving a better objective measure of agreement with the actual profile change. However, the constant water level simulation showed less shoreline retreat, which is artificial since the waves did not attack the beach as high as in the variable water level case as would take place in the field.

503. In another simulation, both wave height and period were kept constant at their average values for the verification period, and the water level was fixed at its mean position. The calculated result is shown in Figure 81, together with the measured initial and final profiles. The shoreward bar grew very steep and pronounced due to the constant wave and water level conditions. Also, the seaward bar did not move, since, without higher waves, all waves broke further inshore. This oversimplification of the input wave parameters and water level variation did not adequately represent the main features of the driving forces. When wave height and period were held constant, but water level was allowed to vary, a pronounced bar developed. The main difference compared with the constant water level case was a smoother bar and greater retreat of the shoreline.

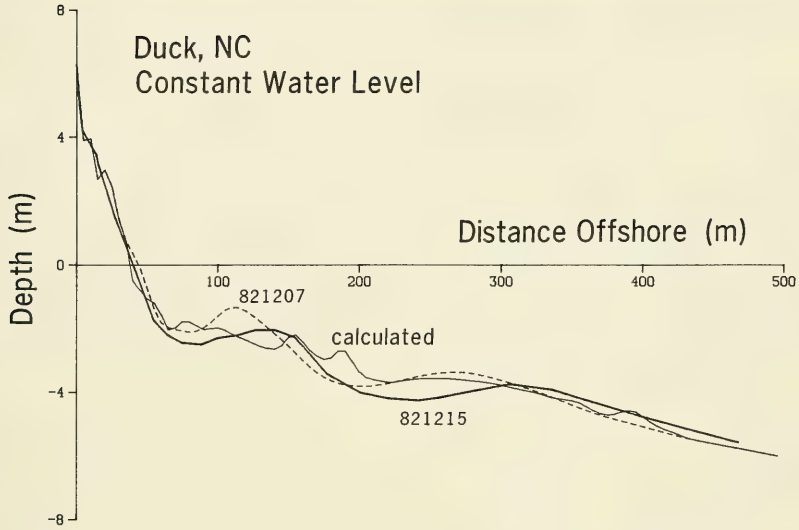


Figure 80. Field verification omitting water level variation

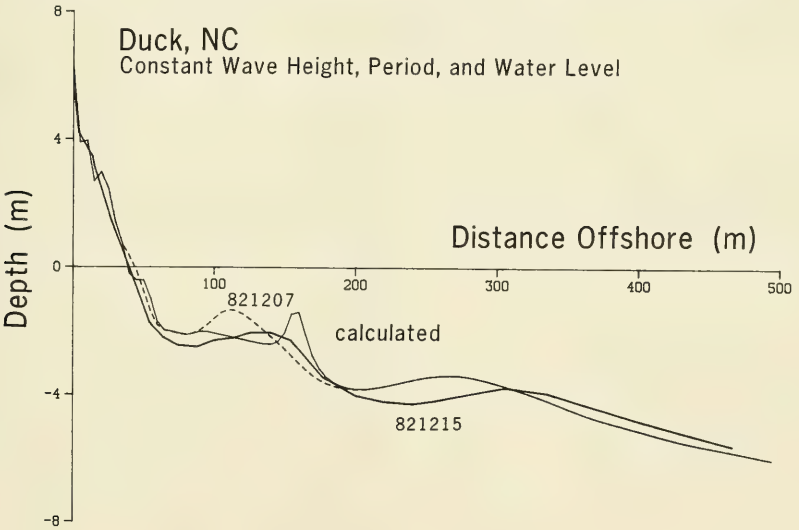


Figure 81. Field verification with fixed wave height, wave period, and water level

Discussion of field simulation

504. The numerical model best reproduced the measured response of the beach profile with the most detailed, realistic input of wave height, wave period, and water level variation. To correctly simulate the behavior of the profile under changing forcing conditions, the variation in the input data should have a time scale compatible with the profile response. Changes between individual waves is not necessary or meaningful for use of the present model, but differences occurring at a time scale of about an hour should be represented for best results. Constant wave and water level conditions will produce bars that are too steep and do not exhibit the smooth character usually encountered in the field.

505. The concept of breaking waves as a major cause of bar movement was verified by the model simulation of the field profile change. Locations of the bars were surprisingly well predicted considering the great variability in water level during the modeled storm events. A mass conservation check between measured initial and final profiles showed that none of the cases simulated were free from three-dimensional effects. In Figure 79b the difference in beach volume between initial and final volume was 45 $m^3/m$ (a loss in beach volume constituting 25 percent of the total absolute volume moved across the profile). This difference is attributed mainly to differentials in longshore sand transport, and, possibly, to limitations in the surveys (spacing and accuracy). It is speculated that incorporation of longshore sand transport in the numerical model might produce a more pronounced trough because a maximum in the longshore sand transport rate is believed to occur somewhat shoreward of the break point.

506. Although the model was developed using laboratory data from situations with constant wave parameters, the capability to generalize and simulate profile change on natural beaches with variable wave and water level conditions was demonstrated. The steep foreshore and bar slopes produced in the large wave tanks and well simulated by the numerical model were a product of regular waves and constant water level. However, the important effects on the profile of variable wave and water level could be represented fairly well by superimposing regular waves with time changing height and period and stepwise changes in water level. Thus, a single regular wave and fixed water level

serve as elemental conditions that can be combined in a time series of varying conditions to approximately replicate natural conditions.

## Comparison with the Kriebel Model

### Overview

507. Presently, there is only one other known numerical model available to the engineering community that allows simulation of time-dependent changes in beach profile produced by breaking waves, the model developed by Kriebel (1982, 1986) and Kriebel and Dean (1985a). Simulations were performed with the present model and the Kriebel model for hypothetical cases to evaluate differences in calculated profile response. The Kriebel model does not simulate bar formation and, a priori, is expected to produce more erosion than the present model. Furthermore, the Kriebel model was developed to simulate profile behavior during erosional conditions, particularly dune erosion, with no capability for simulating berm buildup in its original formulation.

508. Since the two models differ in structure and purpose and contain different parameters, direct comparison using identical parameter values is not possible. For example, in the present model wave height is calculated at grid points across the shore, requiring specification of two empirical parameters. In the Kriebel model, wave height is assumed to be related to water depth in a fixed ratio. To facilitate comparison, parameter values were used as given by calibration against the LWT data for the respective models. Parameter values for the Kriebel model were taken from Case 300 which was used for calibration (Kriebel 1986).

### Calibration

509. Parameter values in the present model were identical to those obtained from calibration against seven of the LWT cases. Even though the transport relationships are similar in the two models, values of the transport rate coefficient K resulting from the calibration were quite different (in the present model, $K=1.6\ 10^{-6}\ m^4/N$; in the Kriebel model, $K=8.7\ 10^{-6}\ m^4/N$). The transport rate coefficient is basically a calibration parameter determining the time scale of profile change, and its value is affected by the amount of smoothing applied in the model. Also, incorporation of a bottom

slope-dependent term in the transport rate equation in the present model increases the transport rate on positive slopes. By calculating the wave height distribution in the surf zone with a wave decay model, a more realistic description of surf zone wave properties is obtained. Such calculation also produces a difference in values of the optimum transport rate coefficient.

Comparisons of model simulations

510. A hypothetical beach profile with a dune having a slope of 1:4, no distinct berm, and a foreshore slope of 1:15 to 0.6-m depth was used in the model comparison. Seaward of 0.6 m, an equilibrium profile shape according to Bruun (1954) and Dean (1977) (Equation 1) was used, where the shape parameter A was determined from the design curve of Moore (1982) corresponding to a median grain size of 0.25 mm. Water level was varied sinusoidally to go through a maximum in a manner similar to a storm hydrograph and with a half-period of 24 hr, and wave conditions were held constant with a wave height of 3 m and period of 10 sec. (see Figure 86 for an example surge hydrograph.) Figure 82a shows that both numerical models produced similar amounts of erosion. Figure 82b gives a detailed view of the dune and foreshore.

511. The main difference between model results for this particular case is the area over which material was deposited. The Kriebel model distributed eroded material approximately evenly over the beach profile, whereas the present model tended to deposit sand closer to the toe of the dune. Experiments performed by Vellinga (1982) with a large wave tank showed time evolution of the profile qualitatively in agreement with the present model, but for a shorter surge hydrograph.

512. The dune face of the eroded profile was steeper for the present model, whereas the Kriebel model produced direct translation of the initial profile. Only a low-relief bar feature developed at the seaward end of the profile in the present model because of the varying water level, which caused the break point to move first shoreward and then seaward as the surge rose then receded. Since the break point was not stationary, movement of the transport rate maximum did not give the bar sufficient time to evolve.

513. Wave period does not directly enter in the Kriebel model, but it is of importance for the shoaling, breaking, and runup of waves in the present model. Therefore, wave period was changed in the test case to 14 sec to

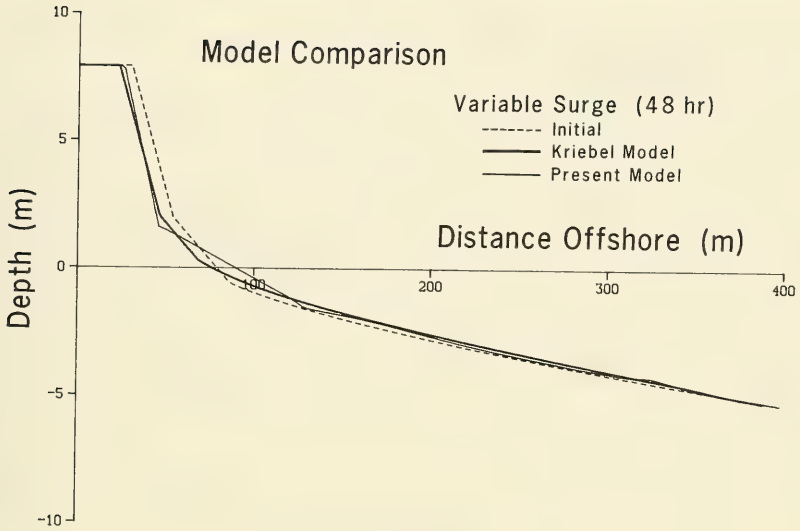


a. Full simulated profile

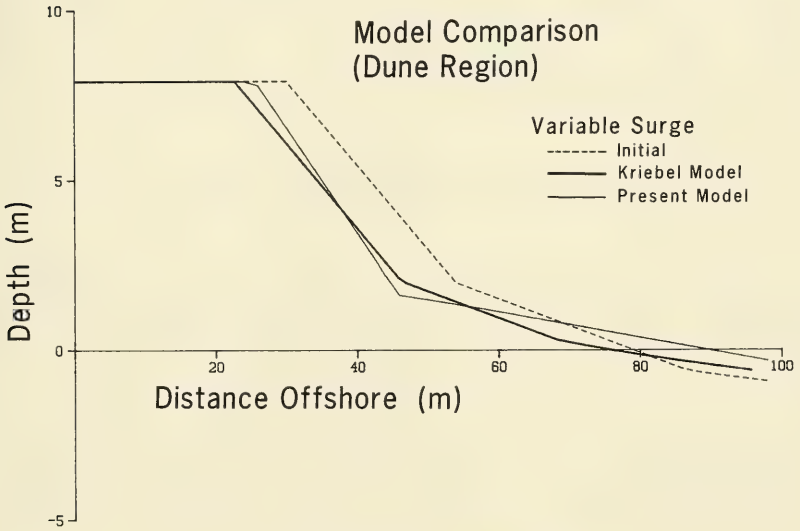


b. Details of dune region

Figure 82. Comparison of present model and Kriebel model for a surge case

evaluate its effect on the simulation. The result with the present model was formation of a gently sloping, wide bar of low height; the amount of dune erosion was approximately the same for both models.

514. To illustrate the difference between model predictions, another example was simulated in which the water level variation was contrived to promote bar formation. The same initial beach profile and wave conditions were used as in the previous case, but the water level variation consisted of an instantaneous rise of 2 m (surge) at the start of the simulation. The simulation period was 48 hr, and the result is displayed in Figure 83(a and b). A distinct bar was developed by the present model, reducing the incident wave energy at the dune and thus reducing the amount of dune erosion compared with the Kriebel model. The shoreward slope of the bar is quite steep due to constancy of the incident wave conditions.

515. Summary. In general, the two models produce similar dune erosion if wave and water level conditions are such that bar development is limited. However, if conditions allow a bar to form, the present model will predict a smaller amount of nearshore erosion than the Kriebel model. The beach profile shape seaward of the dune toe is probably more realistically described in the present model where the area of material deposition is more concentrated, implying a narrower surf zone as the water level increases.

## Simulation of Beach Profile Accretion

### Background and review

516. Most development work with the numerical model was focused on simulating beach profile response to erosional waves and water levels, since prediction of erosion is of immediate engineering importance. Although berm construction was discussed in the data analysis and geometric properties of the berm quantified, initial model development was not primarily directed toward simulating accretionary stages of a beach. Transport rates from the LWT experiments that resulted in berm buildup were determined from profile surveys, together with some associated characteristics of the transport rate distribution. However, due to lack of suitable test cases having sufficient information of the wave height distribution across the shore, it was not

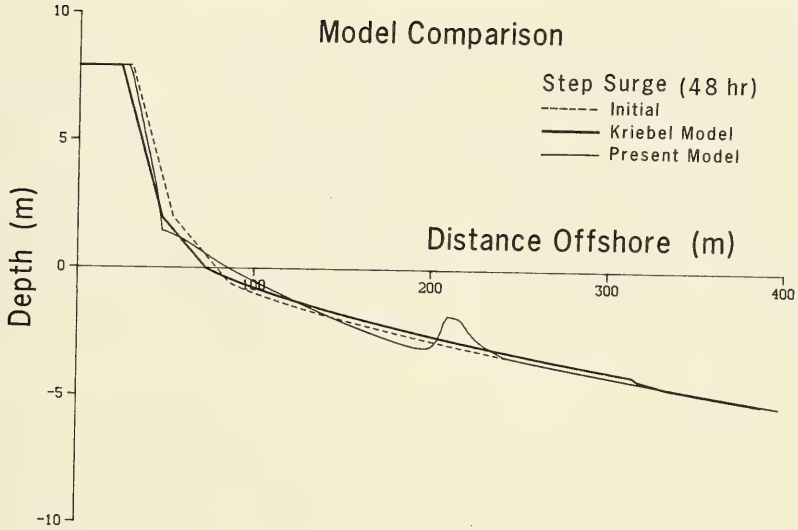


a. Full simulated profile

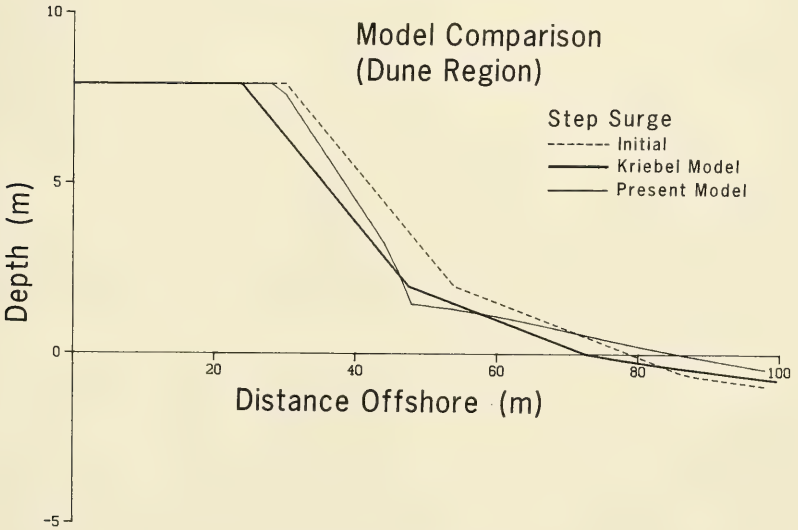


b. Details of dune region

Figure 83. Comparison of present model and Kriebel model for a step increase in water level

possible to derive an empirical transport relationship for the surf zone specifically applicable to onshore-directed transport.

517. The net direction of cross-shore transport may be predicted using Equation 2 in terms of the deepwater wave steepness and dimensionless fall speed. As the grain size increases for given waves, the tendency for onshore-directed transport also increases. By consideration of the dimensionless fall speed, Dean (1973) explained the tendency for onshore transport to occur in terms of the relation between the elevation to which a particle is suspended and the distance it falls during wave passage. A hydraulically heavy particle falls to the bottom during the onshore portion of the wave motion because of the greater settling speed, resulting in net movement onshore.

518. The criterion for distinguishing bar and berm formation is closely related to the transport direction and used in the model to determine transport direction, as discussed previously. The same basic transport relationship (Equation 33) is used whether onshore or offshore transport occurs. A beach that is not in equilibrium with the waves and unable to dissipate incident wave energy uniformly over its length will experience transport until equilibrium is attained if exposed to the same wave climate for a sufficiently long time. For onshore transport, the net transport rate in the model is assumed to be proportional to the energy dissipation per unit volume, similar to the situation for offshore transport. Also, the term which modifies the net transport rate due to the local bottom slope is incorporated. Seaward of the break point, exponential decay (Equation 21) of the transport rate is imposed with a spatial decay coefficient as given from the LWT experiments. The same value of the spatial decay coefficient, 0.11 $m^{-1}$, is applied independently of wave and sand parameters.

519. Both the location of the plunge point and the value of the spatial decay coefficient between the break point and plunge point are determined in the same manner for both accretionary and erosional profiles. Since the magnitude and direction of the transport rate seaward of the plunge point depend on the transport rate in the surf zone, the transport will be onshore if the transport is directed onshore in the surf zone. On the foreshore, a linearly decreasing transport rate is applied to the runup limit with the decay starting from the shoreward end of the surf zone. This shape is

identical to that chosen for the transport rate distribution on the foreshore for erosional transport. The linear shape of the transport rate on the foreshore was supported by the data analysis for both onshore and offshore transport.

520. Parameter values used in the breaker decay model are identical to the ones applied for erosional conditions, and these values are considered to be representative averages for various slopes. Also, the same criterion for incipient breaking is applied for both erosional and accretionary transport conditions, although this was primarily derived from cases showing erosion and having a distinct breakpoint bar.

Berm simulation

521. Case 101 from the LWT experiments was used to qualitatively evaluate the capability of the model to simulate beach profile accretion. As shown in Figure 84, a berm rapidly formed on the foreshore by onshore transport from breaking waves, and material was deposited up to the limit of runup. As sand was transported onshore, the surf zone and offshore eroded, increasing the depth along this portion of the profile. The increase in depth caused the break point to move onshore and, at about the same time, the berm retreated somewhat at the shoreline while its seaward slope became steeper. Continuous onshore movement of the break point made the surf zone become narrower through time, restricting the onshore transport to a smaller area of the profile. The seaward berm slope steepened because of the continuing transport, limited only by the angle of initial yield. The angle of initial yield had to be reduced somewhat on the foreshore to achieve a less steep slope, considered realistic because of the strong turbulent conditions. A large region of erosion appeared immediately seaward of the foreshore, where a deep trough developed, allowing waves to break at the beach face.

522. The profile approached equilibrium, exhibiting a well-formed berm together with a deep seaward trough. The measured and simulated berm volume and location are in good agreement. However, the seaward slope of the berm grew too steep in the numerical simulation, and the profile shape in the surf zone was not well reproduced. The small bar that developed slightly shoreward of the breakpoint in the wave tank was not obtained with the model. The main

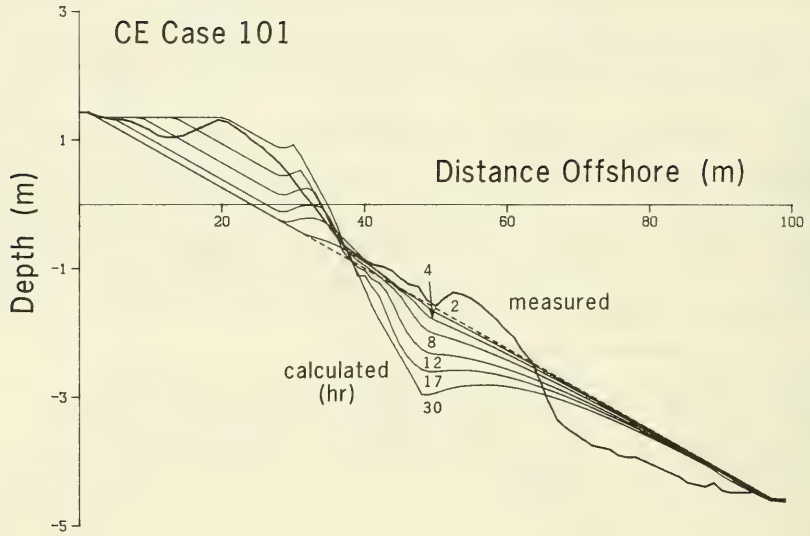


Figure 84. Simulation of berm formation and growth

zone of erosion in the tank occurred more seaward than the location predicted by the numerical model.

523. In other model simulations of accretion, the zone of fully broken waves became very narrow as the break point moved onshore and the waves directly struck the berm or foreshore. The length of the broken wave zone eventually decreased to only one calculation cell, and a transport rate equation based on energy dissipation per unit volume was no longer realistic. In these cases, the transport rate calculated from the energy dissipation was reduced. If no reduction was employed, very local erosion and accretion occurred in the vicinity of the shoreline, giving rise to numerical instability. The value of the reduction factor was typically around 0.2 in these cases. This problem might have been circumvented by using extremely small spatial and temporal steps.

## Influence of a Seawall and Beach Fill

524. The numerical model has the capability of simulating the influence of a seawall on beach profile evolution. The shoreward boundary of the calculation grid is located at the seawall preventing transport of material across this cell. The seawall only affects changes in the beach profile if it is exposed to incident waves. Overtopping is not simulated by the model, and it is assumed that the height of the seawall exceeds the runup height (or local wave height).

### Profile with seawall

525. A hypothetical example was modeled to evaluate the effect of a seawall on beach profile evolution during storm conditions. The initial profile and wave data from CE Case 400 (Figure 60a) were used, and a seawall was placed on the foreshore, approximately at the still-water shoreline, protecting the subaerial part of the profile from wave attack. The simulation result is displayed in Figure 85, which shows the calculated beach profile at selected time-steps with a seawall on the foreshore and the beach profile at the last time-step without a seawall. The wave height distribution across shore is shown at the last time-step for the seawall calculation.

526. The evolution and size of the bar were similar in the simulation with and without the seawall, the bar being somewhat larger and located more seaward for the case without the wall. The main difference was the amount of material eroded in front of the seawall and shoreward of the bar. With the seawall present, the width of the surf zone was much shorter, requiring more material to be moved before an equilibrium beach shape developed. The subaerial eroded volume for the case without the seawall approximately agreed with the extra volume eroded in front of the seawall.

527. The approach to equilibrium was more rapid for the seawall case, indicated by the slightly more gentle inshore profile slope. The longer time elapsed before equilibrium was obtained for the case without the seawall was caused by the larger extent of the profile involved in redistribution of sand. Since the depth in front of the seawall was greater than for the case without the wall at the corresponding location, the height of the broken waves was larger (compare with wave height distribution in Figure 60a).

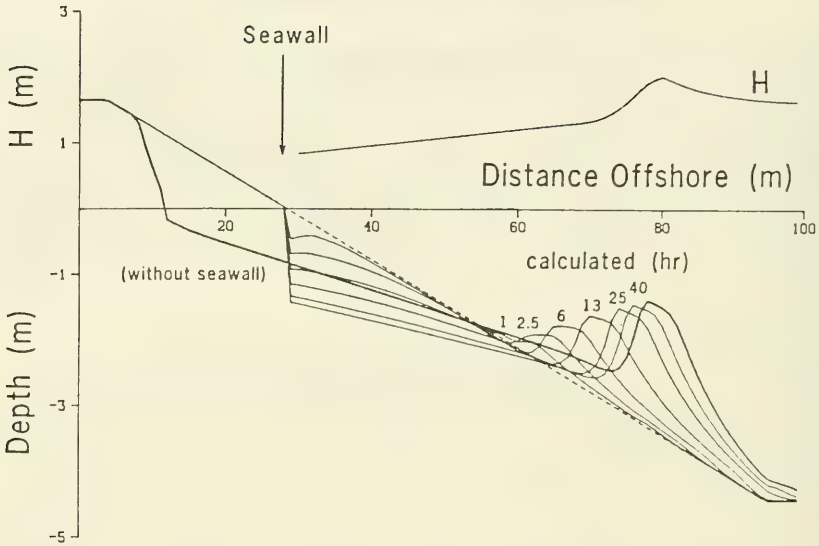


Figure 85. Simulation with and without seawall

Profile with seawall and beach fill

528. To evaluate the performance of the model for more complex conditions, a simulation was carried out for a time period involving both mildly erosive or accretionary waves, a storm event, and a recovery period. Furthermore, a seawall was located in the subaerial part of the profile, and beach profile response was calculated both with and without beach fill. Two different beach fill schemes and grain sizes were evaluated, one case where material was added as an artificial berm above the still-water level and another case where the material was spread out mainly below the still-water level according to the equilibrium shape associated with the natural sand. The wave height and water level of the simulated event are illustrated in Figure 86 (note that the time scale is distorted).

529. During the first 21 days of the simulation, the wave height was 0.5 m and the wave period 8 sec, producing mildly erosional or accretionary conditions depending on the grain size. The beach profile was thus allowed to attain its equilibrium shape for the prevailing wave conditions. At day 21, a

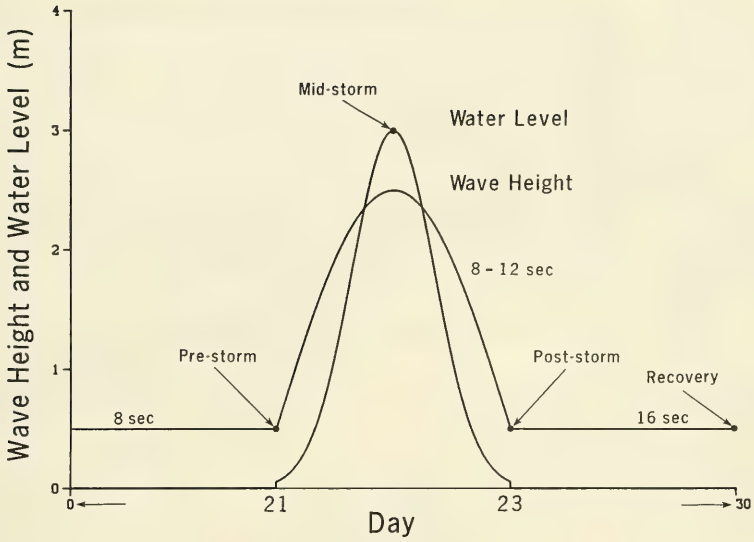


Figure 86. Wave height and water level for beach fill simulations

storm was imposed which lasted 3 days, during which the wave height increased sinusoidally up to a maximum of 2.5 m. Simultaneously, a storm surge occurred with a Gaussian shape, raising the water level to a maximum of 3 m above the still-water level. The wave period varied sinusoidally between 8 and 12 sec during the storm with the maximum period occurring at the same time as the maximum wave height. After the storm, accretionary conditions were imposed with long-period swell of height 0.5 m and period 16 sec, producing beach recovery.

530. Original profile. At first, model simulations were performed without adding fill for the two grain sizes 0.25 and 0.40 mm. The initial profile consisted of two linear slopes to a depth of 0.5 m, joining to an equilibrium profile shape (Equation 1). Figure 87(a and b) shows the beach profiles at selected times during the simulated time period; just before the storm (Day 21, prestorm), during the storm (middle of Day 22, midstorm), after the storm (Day 23, poststorm), and at the end of the simulation period (Day 30, recovery).

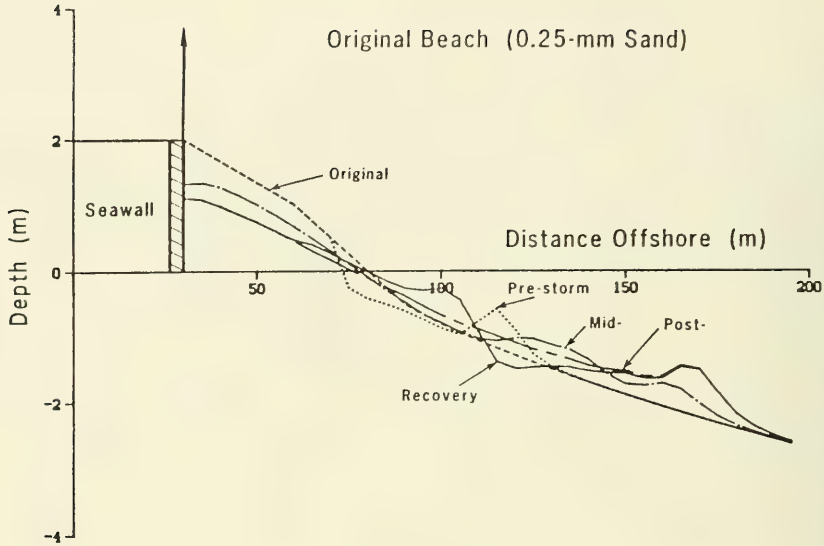


a. 0.25-mm beach

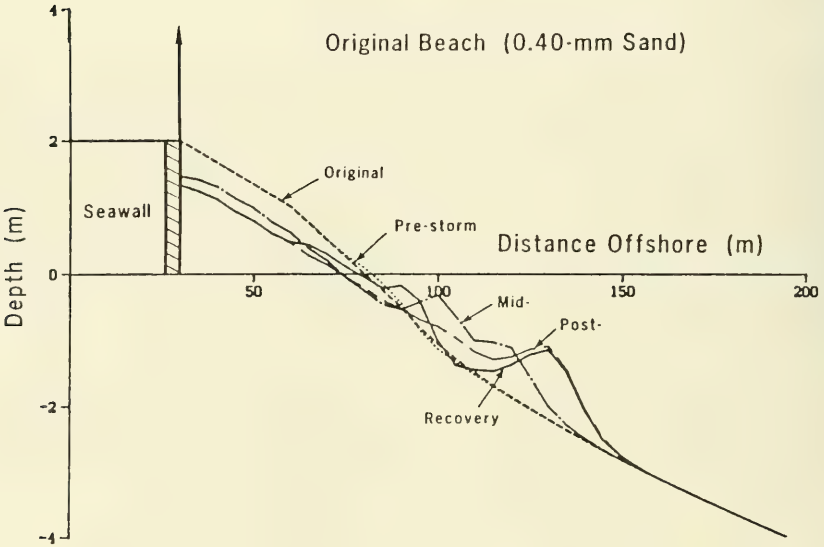


b. 0.40-mm beach

Figure 87. Response of original beach to the storm event

531. Initial wave conditions produced erosion for the 0.25-mm grain size (Figure 87a), and a small bar developed offshore with the shoreline receding somewhat. As water level increased during the storm, the beach in front of the seawall was submerged, and considerable erosion occurred. The high seawall prevented the beach from retreating. A long flat bar developed during the peak of the storm which moved offshore with the break point as the water level decreased. After the storm, the inshore portion of the profile partly recovered, producing buildup on the foreshore and a bar-like feature just below the still-water level. The main part of the bar, however, did not contribute material for the recovery process since it was located too deep and too far seaward of the breaking waves.

532. The equilibrium profile of the 0.40-mm sand was much steeper than the 0.25-mm beach (Figure 87b) because of the grain-size dependence of the A-parameter in Equation 1. Mild waves arriving during the initial part of the simulation period produced onshore transport and a small berm. During the storm surge, the amount of subaerial erosion was similar to that in the 0.25-mm profile example, but the bar did not migrate as far offshore. The recovery of the 0.40-mm beach did not produce such a marked trough seaward of the bar-like feature as did the 0.25-mm beach.

533. Artificial berm. The first type of beach fill evaluated was an artificial berm consisting of approximately 85 $m^3/m$ of material placed on the subaerial portion of the beach. In simulations with the beach fill, it was assumed that the fill material was identical to the natural beach sand. A small bar formed before the storm, much in agreement with the case without the fill but closer to shore. During the storm, a large part of the fill eroded and was deposited offshore. Figure 88(a and b) illustrates simulation results for the 0.25- and 0.40-mm grain sizes. Although significant recovery occurred for the 0.25-mm beach, a large amount of material was trapped offshore. The eroded material from the artificial berm for the 0.40-mm beach was deposited closer to shore, and during the recovery phase the entire bar moved slightly onshore.

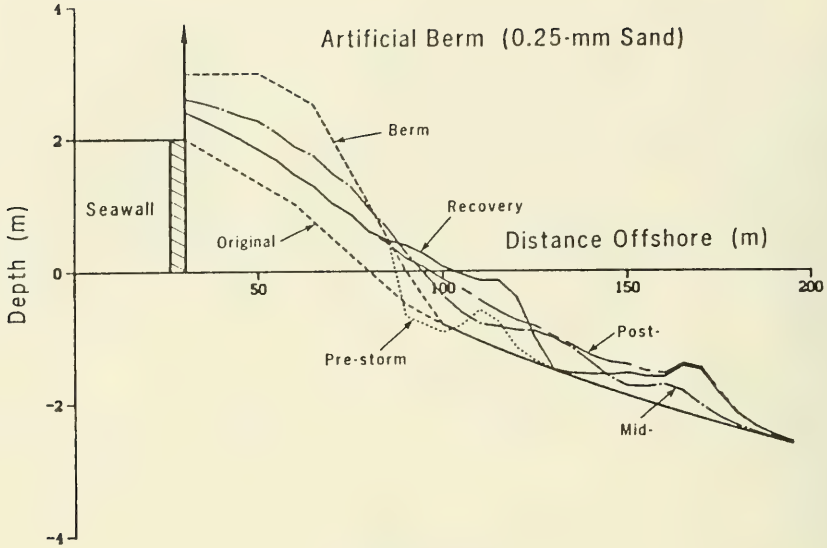


a. 0.25-mm beach

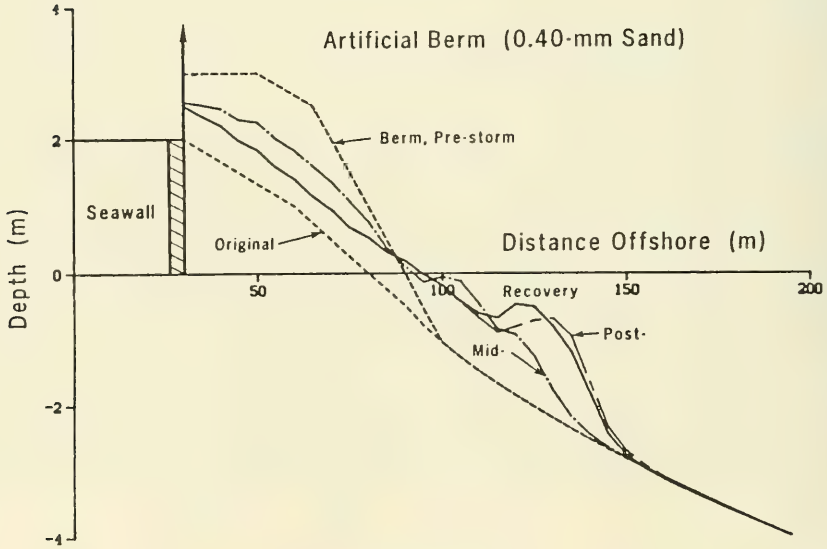


b. 0.40-mm beach

Figure 88. Response of artificial berm to the storm event

534. Bruun fill. In the second fill alternative, material was deposited mostly along the subaqueous portion of the profile in accordance with the equilibrium shape of the beach (called a Bruun beach fill). Bruun (1988) has advocated "profile nourishment," as opposed to placing fill material only on the upper part of the profile, under the concept that the beach can best resist erosive wave action in its most natural shape. The fill volume was 85 $m^3/m$, the same as for the artificial berm. Figure 89(a and b) shows the simulation result for the two grain sizes studied. The amount of subaerial erosion was reduced significantly even though the entire profile was submerged during much of the storm surge. Bar development was less pronounced for the 0.25-mm beach compared to the artificial berm case, whereas the 0.40-mm beach showed stronger bar formation.

535. Summary. The numerical model provided qualitatively reasonable results in calculation of the response of hypothetical beach cross sections to storm events. In the examples, the Bruun fill provided better overall protection of the subaerial beach according to the numerical model, and less material was redistributed along the profile during the storm surge compared to the artificial berm design. Examples given in this section are described further by Kraus and Larson (1988b). Larson and Kraus (in press) extend the analysis further to consider model predictions for erosion of various cross sections to a synthetic hurricane and a synthetic extratropical storm with return periods of approximately 2-5 years.

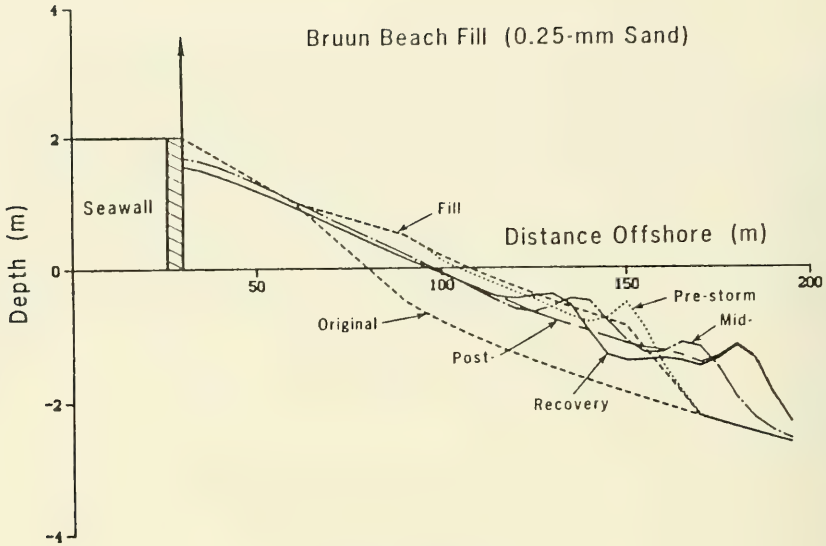


a. 0.25-mm beach

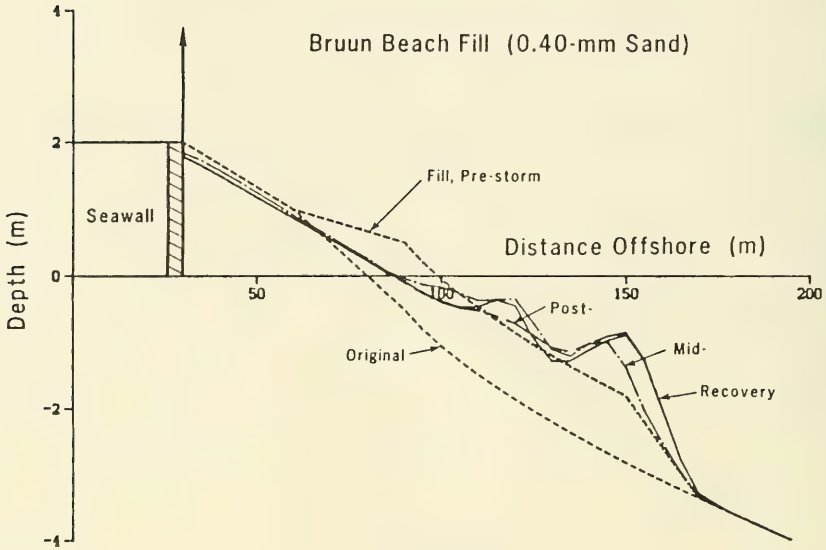


b. 0.40-mm beach

Figure 89. Response of the Bruun fill to the storm event

## PART VIII: SUMMARY AND CONCLUSIONS

536. The ultimate objective of this study was to develop an engineering numerical model of beach profile change having the capability of simulating formation and movement of major morphologic features of the profile, particularly bars and berms. Beach profile response produced by severe storm or hurricane events, with large erosion and possible dune retreat, was the principal target problem of the study, although profile change occurring on longer time scales, such as adjustment of beach fill, which involves accretionary as well as erosional processes, was also of interest. A basic assumption underlying this work was that major morphologic change occurring in and around the surf zone is produced by breaking and broken waves.

537. Data from two LWT experiments were used in development of the numerical model; one experiment performed by the US Army Corps of Engineers (CE) and the other carried out by the Central Research Institute of Electric Power Industry (CRIEPI), Japan. In total, these experiments encompassed 42 cases having different values of wave height, wave period, water level, grain size, and initial profile slope or shape. The CRIEPI experiment also included measurements of wave height along the profile from prebreaking through the surf zone.

538. Extensive analysis of morphologic features of the profile was conducted to provide the foundation for the numerical model, but the analysis also produced functional relationships between geometric characteristics of the profile and wave and sand properties. Geometric properties of the profile that were quantified were bar volume, bar height, depth-to-bar crest, ratio of depth-to-bar trough and depth-to-bar crest, distance between break point and trough bottom, movement of mass center of bar, bar migration speed, bar slopes, active profile height, step and terrace slopes, berm volume, berm height, and berm slopes. This type of analysis is expected to stimulate corresponding analysis of field profiles and provide guidance for collecting analogous field data.

539. Regression relationships were established between a number of geometric characteristics of the profile and wave and sand properties. In this process, the dimensionless fall speed $H_o/wT$ emerged as an important

parameter together with the deepwater wave steepness $H_o/L_o$ . Quantities that could be related to either $H_o/wT$ , $H_o/L_o$ , or both parameters were bar volume, ratio of trough depth to crest depth, bar height, and active profile height, respectively normalized with various wave or sand properties. Distance between break point and trough bottom, normalized with deepwater wavelength, was determined to be a function of the local slope seaward of the break point and $H_b/H_o$ . Average depth to bar crest proved to be directly proportional to the breaking wave height. Profile properties derived from the LWT data sets were found comparable to those in the field, which supported the possibility of generalizing observations from the LWT experiments to field application. The validity of the equilibrium beach profile concept was confirmed by the LWT experiments, which clearly showed a systematic decrease in profile change as time elapsed.

540. A criterion (Equation 2) was developed to delineate between formation of bar and berm profiles in terms of $H_o/wT$ and $H_o/L_o$ . Although several well-known criteria were evaluated using the LWT experiments, the criterion developed in the present study appeared to be the most attractive from a physical point of view and gave a good delineation between bar and berm profiles. The criterion was closely related to the predominant direction of cross-shore transport. A bar formed under mainly offshore-directed transport and a berm formed under mainly onshore-directed transport. The criterion was tested with field data and found to be valid with the same value of the empirically determined coefficient when the deepwater wave height appearing in the criterion was taken to be the mean wave height.

541. Profile slopes were analyzed for the seaward and shoreward side of the bar, seaward and shoreward side of the berm, inshore step, and terrace. Circumstantial evidence was found for the process of avalanching to occur on the shoreward bar face and on the inshore step as the slopes grew beyond a critical angle. An average estimate of this angle of initial yield was 28 deg, and the slope appeared to reach a stable value of around 20 deg. The average slope on the seaward bar face was typically in the range 8-12 deg and was, in many cases, well approximated by two linear slopes, possibly signifying the occurrence of two somewhat different sediment transport processes. Bar slopes for the LWT experiments were considerably steeper than correspond-

ing slopes found in the field, attributed to the monochromatic waves and constant water level used in the experiments. Berm face slopes were typically in the range of 6-8 deg on the seaward side and 2-4 deg on the shoreward side.

542. Properties of the cross-shore transport rate were investigated by integrating the mass conservation equation between consecutive profiles in time. This methodology provided a picture of the net average transport rate distribution between two surveys. The magnitude of the net transport rate distribution decreased with time as the profile approached an equilibrium shape and less material moved along the profile. Decrease of peak transport rates was best described by a function which showed an inverse dependence with elapsed time, not with an expected exponential decay with time. This difference was attributed to randomness of microscale processes and slight unsteadiness in forcing conditions, which produce a perturbation on the idealized mean behavior. Decrease of the peak transport rate was more rapid for accretionary profiles than erosional profiles.

543. By comparing the initial and final profile surveys, an "equilibrium transport distribution" was defined and calculated, which indicated how sand was redistributed along the profile to achieve an equilibrium configuration. Equilibrium distribution could be classified into three characteristic shapes in a majority of the experimental cases; Erosional (Type E), Accretionary (Type A), and mixed Accretionary-Erosional (Type AE). Type E distributions showed transport directed offshore along the entire profile, whereas Type A distributions showed transport directed onshore along the entire profile. Type AE distributions were characterized by a mixed response with offshore transport along the shoreward portion of the profile and onshore transport along the seaward portion of the profile.

544. The profile was divided into four different zones to interpret and quantify properties of the cross-shore transport rate distribution, in analogy with recent findings from nearshore wave dynamics. These zones were: prebreaking zone (I), breaker transition zone (II), broken wave zone (III), and swash zone (IV). For Zone I, the LWT experiments showed that the net transport rate was well approximated by an exponential decay with distance from the break point, with a spatial decay coefficient (average value of 0.18 $m^{-1}$) proportional to the ratio of the grain size to the breaking wave height for

erosional conditions. Exponential decay proved to be valid for onshore transport as well, but the spatial decay coefficient was almost constant, with an average value of 0.11 $m^{-1}$.

545. For Zone II, which extends over the narrow range from the break point to the plunge point, it was difficult to extract information on the transport characteristics from the LWT experiments. However, an exponential decay with distance offshore showed good agreement with transport rate data inferred from the small number of available cases, with a spatial decay coefficient about 0.20 of the value of the spatial decay coefficient applicable to Zone I. Zone III encompasses the main part of the surf zone, and the transport rate was demonstrated to be closely related to the energy dissipation per unit volume, based on the CRIEPI experiment results involving wave height distributions and profile change. Values of empirical coefficients in the transport equation found through regression analysis were similar to values found by other authors through more indirect numerical modeling.

546. In Zone IV, the region dominated by runup and backrush, the transport rate is governed by swash dynamics. A transport rate expressed in terms of physical quantities could not be developed for this zone due to lack of measurements of swash wave properties. However, the transport rate showed an approximately linear behavior for both offshore and onshore transport for a wide range of conditions. The extent of Zone IV decreased if the profile eroded and a step evolved, and the transport rate simultaneously decreased with time.

547. A numerical model of profile response was developed on the basis of quantitative analysis of the LWT wave and profile change data. The domain of model extends from the depth of significant net cross-shore sediment movement, located seaward of the largest breaking waves, to the limit of runup on the beach face. The model calculates the wave height distribution across-shore at each time-step with linear wave theory up to the break point, and thereafter with a breaker decay model in the surf zone. The break point is determined from an empirical criterion, derived from the CRIEPI data set, relating the breaker ratio to the surf similarity parameter defined by the deepwater wave steepness and the local slope seaward of the break point. A nonlinear shoaling theory was applied initially but found to overestimate the

breaking wave height, not producing as good agreement as linear wave theory in comparisons with the LWT data.

548. In the numerical model, the net cross-shore sediment transport rate distribution is determined by using local wave properties along the profile. The profile is divided into four zones according to findings from the LWT data sets, and the respective transport relationships are used to determine the transport magnitude. Transport direction is determined from an empirical criterion derived from the LWT data sets, which predicts bar or berm profile development. Changes in the profile are determined from the mass conservation equation. The model proved to be numerically stable over a wide range of conditions, and simulated profiles approached an equilibrium configuration if exposed to constant waves and water level.

549. The model was calibrated against seven cases from the CE and CRIEPI experiments showing foreshore erosion and bar formation. The optimal value of the empirical rate coefficient for the transport relationship applied in zones of broken waves was $1.6\ 10^{-6}\ m^4/N$. The model was then verified against two independent cases from the CE and CRIEPI experiments with the parameter values given by the calibration. Good agreement was obtained between calculated and measured profiles regarding both the amount of foreshore erosion and the movement and size of the main breakpoint bar. The bar trough was less well reproduced, and smaller features inshore of the main breakpoint bar were omitted in the simulations. The model was also tested with one CE case which included a water level variation simulating a tide, and this case was also satisfactorily reproduced.

550. A number of hypothetical cases were simulated with the numerical model to evaluate the influence of variations in incident wave height, wave period, and water level. Sensitivity analyses were performed for a large number of model parameters to establish their influence on bar formation. Simulation for a hypothetical example which included a seawall on the foreshore showed that the size of the bar was approximately the same as for simulations without the seawall, but the area immediately seaward of the seawall experienced more erosion. Simulations of beach fill adjustment for use in storm protection design were also performed as an example of the utility of the model.

551. The process of multiple bar formation was simulated and compared with one case from the CE data set where two bars developed. Multiple bars could be generated in the numerical model by allowing wave reformation and the appearance of multiple break points. Data from the LWT experiments gave little guidance about the cross-shore transport properties in zones of wave reformation. The transport rate in this zone was determined through simple functional relationships based on qualitative observations from the experiments.

552. The model was also used to simulate onshore transport and berm formation by using one CE case. The size of the berm was well reproduced; however, the model failed to adequately describe the seaward berm face slope and inshore profile shape. The seaward berm face slope is only limited by the angle of initial yield in the model because of the crude description of transport in the swash zone.

553. A comparison between the present model and the Kriebel (1982, 1986) model was conducted to evaluate how bar formation would affect beach erosion. One hypothetical case involved a variation in water level which prevented bar development; both models gave similar predictions of erosion. The description of the profile at the dune toe was more realistically described by the present model, based on experience with the LWT and other experiments, than by the Kriebel model, which distributed the eroded material more evenly over the surf zone. Another comparison case involved bar development, giving a significant difference in dune retreat, for which the Kriebel model produced a larger amount of erosion than the present model, as expected.

554. The numerical model was also used to simulate bar movement in the field at CERC's FRF in Duck, North Carolina. Four different storm events showing erosive profile response and offshore bar movement were used in the calibration, and another independent event was used for verification of the model. Some empirical model parameters determined with the LWT data had to be modified somewhat to achieve agreement with measured field profiles. In particular, the transport rate coefficient took a smaller value for the field simulation than for the LWT cases, with an overall best value in a least-square sense of $0.7\ 10^{-6}\ m^4/N$.

555. Bar movement and location of bar crest were well reproduced by the model both for the field calibration and verification runs. However, bar troughs were not pronounced enough in the model, and bar size was underestimated. Although bar face slopes produced by the model were steep for the LWT cases simulated, in agreement with the physical experiment data, model simulations for the field data with variable input waves and water level produced more gentle slopes in agreement with the field measurements. This finding supports the assumption of superposition implicit in the numerical model, whereby the effect of a random wave field can be simulated as the effect of a number of consecutive individual waves of different height and period.

556. In conclusion, this study validated the methodology of obtaining quantitative information on beach profile response in prototype-sized facilities and generalizing the information to field conditions. The developed numerical model successfully reproduced beach profile change both in large tanks and in the field. The approach of focusing on macroscale profile features such as bars and berms proved highly productive, both for providing a thorough and quantitative understanding of beach profile change to wave action and for promoting development of numerical models for simulating coastal processes aimed at engineering use.

## REFERENCES


Allen, J. R. 1970. "The Avalanching of Granular Solids on Dune and Similar Slopes," Journal of Geology, Vol 78, No. 3, pp 326-351.

Aubrey, D. G. 1978. "Statistical and Dynamical Prediction of Changes in Natural Sand Beaches," unpublished Ph.D. thesis, University of California, San Diego, CA.

_____. 1979. "Seasonal Patterns of Onshore/Offshore Sediment Movement," Journal of Geophysical Research, Vol 84, No. C10, pp 6347-6354.

Aubrey, D. G., Inman, D. L., and Nordstrom, C. E. 1977. "Beach Profiles at Torrey Pines, California," Proceedings of the 15th Coastal Engineering Conference, American Society of Civil Engineers, pp 1297-1311.

Aubrey, D. G., Inman, D. L., and Winant, C. D. 1980. "The Statistical Prediction of Beach Changes in Southern California," Journal of Geophysical Research, Vol 85, No. C6, pp 3264-3276.

Aubrey, D. G., and Ross, R. M. 1985. "The Quantitative Description of Beach Cycles," Marine Geology, Vol 69, pp 155-170.

Bagnold, R. A. 1940. "Beach Formation by Waves; Some Model-Experiments in a Wave Tank," Journal of the Institution of Civil Engineers, No. 1, pp 27-52.

_____. 1963. "Mechanics of Marine Sedimentation," In: The Sea, Vol 3, ed. M. N. Hill, Interscience, NY, pp 507-528.

_____. 1966. "An Approach to the Sediment Transport Problem from General Physics," Geological Survey Professional Paper 422-I, Washington D.C.

Bailard, J. A. 1982. "An Energetics Total Load Sediment Transport Model for a Plane Sloping Beach," Naval Civil Engineering Laboratory, Report No. TN-1626, Port Hueneme, CA.

Bailard, J. A., and Inman, D. L. 1981. "An Energetics Bedload Model for a Plane Sloping Beach: Local Transport," Journal of Geophysical Research, Vol 86, No. C3, pp 2035-2043.

Balsillie, J. H. 1984. "A Multiple Shore-Breaking Wave Transformation Computer Model," Florida Department of Natural Resources, Beaches and Shores Technical and Design Memorandum No. 84-4, Tallahassee, FL.

Basco, D. R. 1985. "A Qualitative Description of Wave Breaking," Journal of Waterway, Port, Coastal and Ocean Engineering, Vol 111, No. 2, pp 171-188.

Basco, D. R., and Yamashita, T. 1987. "Toward a Simple Model of the Wave Breaking Transition Region in Surf Zones," Proceedings of the 20th Coastal Engineering Conference, American Society of Civil Engineers, pp 955-970.

Bascom, W. N. 1951. "The Relationship Between Sand Size and Beach-Face Slope," Transactions American Geophysical Union, Vol 32, No. 6, pp 866-874.

Battjes, J. A. 1975. "Surf Similarity," Proceedings of the 14th Coastal Engineering Conference, American Society of Civil Engineers, pp 466-480.

Battjes, J. A., and Janssen, J. P. F. M. 1979. "Energy Loss and Set-Up Due to Breaking of Random Waves," Proceedings of the 16th Coastal Engineering Conference, American Society of Civil Engineers, pp 569-587.

Berg, D. W., and Duane, D. B. 1968. "Effect of Particle Size and Distribution on Stability of Artificially Filled Beach, Presque Isle Peninsula, Pennsylvania," Proceedings of the 11th Conference on Great Lakes Research, International Association of Great Lakes Research, pp 161-178.

Birkemeier, W. A. 1985a. "Time Scale of Nearshore Profile Changes," Proceedings of the 19th Coastal Engineering Conference, American Society of Civil Engineers, pp 1507-1521.

_____. 1985b. "Field Data on Seaward Limit of Profile Change," Journal of Waterway, Port, Coastal and Ocean Engineering, Vol 111, No. 3, pp 598-602.

Birkemeier, W. A., Kraus, N. C., Scheffner, N. W., and Knowles, S. C. 1987. "Feasibility Study of Quantitative Erosion Models for Use by the Federal Emergency Management Agency in the Prediction of Coastal Flooding," Technical Report CERC-87-8, Coastal Engineering Research Center, US Army Engineer Waterways Experiment Station, Vicksburg, MS.

Boczar-Karakiewicz, B., and Davidson-Arnott, R. G. D. 1987. "Nearshore Bar Formation by Non-Linear Wave Processes - A Comparison of Model Results and Field Data," Marine Geology, Vol 77, pp 287-304.

Bowen, A. J. 1980. "Simple Models of Nearshore Sedimentation; Beach Profiles and Longshore Bars," In: The Coastline of Canada, ed. S. B. McCann, Geological Survey of Canada, Paper 80-10, pp 1-11.

Bruun, P. 1954. "Coast Erosion and the Development of Beach Profiles," Technical Memorandum No. 44, Beach Erosion Board, Coastal Engineering Research Center, US Army Engineer Waterways Experiment Station, Vicksburg, MS.

_____. 1962. "Sea-Level Rise as a Cause of Shore Erosion," Journal of the Waterways and Harbors Division, American Society of Civil Engineers, Vol 88, No. WW1, pp 117-130.

_____. 1988. "Profile Nourishment: Its Background and Economic Advantages," Journal of Coastal Research, Vol 4, No. 2, pp 219-228.

Buhr Hansen, J., and Svendsen, I. A. 1975. "Laboratory Generation of Waves of Constant Form," Proceedings of the 14th Coastal Engineering Conference, American Society of Civil Engineers, pp 321-339.

Caldwell, J. M. 1959. "Shore Erosion by Storm Waves," Miscellaneous Paper No. 1-59, Beach Erosion Board, Coastal Engineering Research Center, US Army Engineer Waterways Experiment Station, Vicksburg, MS.

Carter, T. G., Liu, P. L-F., and Mei, C. C. 1973. "Mass Transport by Waves and Offshore Sand Bedforms," Journal of the Waterways, Harbors and Coastal Engineering Division, American Society of Civil Engineers, Vol 99, No. WW2, pp 165-184.

Chappell, J., and Eliot, I. G. 1979. "Surf-Beach Dynamics in Time and Space - An Australian Case Study, and Elements of a Predictive Model," Marine Geology, Vol 32, pp 231-250.

Chiu, T. Y. 1977. "Beach and Dune Response to Hurricane Eloise of September 1975," Proceedings of Coastal Sediments '77, American Society of Civil Engineers, pp 116-134.

Dally, W. R. 1980. "A Numerical Model for Beach Profile Evolution," unpublished M.S. Thesis, University of Delaware, Newark, DE.

_____. 1987. "Longshore Bar Formation - Surf Beat or Undertow," Proceedings of Coastal Sediments '87, American Society of Civil Engineers, pp 71-86.

Dally, W. R., and Dean, R. G. 1984. "Suspended Sediment Transport and Beach Profile Evolution," Journal of Waterway, Port, Coastal and Ocean Engineering, Vol 110, No. 1, pp 15-33.

Dally, W. R., Dean, R. G., Dalrymple, R. A. 1985a. "Wave Height Variation Across Beaches of Arbitrary Profile," Journal of Geophysical Research, Vol 90, No. C6, pp 11917-11927.

_____. 1985b. "A Model for Breaker Decay on Beaches," Proceedings of the 19th Coastal Engineering Conference, American Society of Civil Engineers, pp 82-98.

Dalrymple, R. A., and Thompson, W. W. 1977. "Study of Equilibrium Beach Profiles," Proceedings of the 15th Coastal Engineering Conference, American Society of Civil Engineers, pp 1277-1296.

Davidson-Arnott, R. G. D. 1975. "Form, Movement and Sedimentological Characteristics of Wave-Formed Bars - A Study of their Role in Nearshore Equilibrium," unpublished Ph.D. thesis, Department of Geography, University of Toronto, Toronto, Canada.

_____. 1981. "Computer Simulation of Nearshore Bar Formation," Earth Surface Processes and Landforms, Vol 6, pp 23-34.

Davidson-Arnott, R. G. D., and Pember, G. F. 1980. "Morphology and Sedimentology of Multiple Parallel Bar Systems, Southern Georgian Bay, Ontario," In: The Coastline of Canada, ed. S. B. McCann, Geological Survey of Canada, Paper 80-10, pp 417-428.

Davidson-Arnott, R. G. D., and Randall, D. C. 1984. "Spatial and Temporal Variations in Spectra of Storm Waves Across a Barred Nearshore," Marine Geology, Vol 60, pp 15-30.

Davis, R. A., and Fox, W. T. 1972. "Coastal Processes and Nearshore Sand Bars," Journal of Sedimentary Petrology, Vol 42, No. 2, pp 401-412.

Davis, R. A., Fox, W. T., Hayes, M. O., and Boothroyd, J. C. 1972. "Comparison of Ridge and Runnel Systems in Tidal and Non-Tidal Environments," Journal of Sedimentary Petrology, Vol 42, No. 2, pp 413-421.

Dean, R. G. 1973. "Heuristic Models of Sand Transport in the Surf Zone," Proceedings of the Conference on Engineering Dynamics in the Surf Zone, Sydney, Australia, pp 208-214.

_____. 1976. "Beach Erosion: Causes, Processes, and Remedial Measures," CRC Reviews in Environmental Control, CRC Press Inc., Vol 6, Issue 3, pp 259-296.

_____. 1977. "Equilibrium Beach Profiles: U.S. Atlantic and Gulf Coasts," Department of Civil Engineering, Ocean Engineering Report No. 12, University of Delaware, Newark, DE.

_____. 1984. "Applications of Equilibrium Beach Profile Concepts," Coastal Engineering Abstracts, American Society of Civil Engineers, pp 140-141.

_____. 1987. "Coastal Sediment Processes: Toward Engineering Solutions," Proceedings of Coastal Sediments '87, American Society of Civil Engineers, pp 1-24.

De Best, A., and Bijker, E. W. 1971. "Scouring of a Sand Bed in Front of a Vertical Breakwater," Report No. 71-1, Department of Civil Engineering, Delft University of Technology, The Netherlands.

Deguchi, I., and Sawaragi, T. 1985. "Calculation of the Rate of Net On-Offshore Sediment Transport on the Basis of Flux Concept," Proceedings of the 19th Coastal Engineering Conference, American Society of Civil Engineers, pp 1325-1341.

Dette, H. H. 1986. "Untersuchungen über Dünenabbrüche und Stranderosion im Grossen Wellenkanal," Die Küste, Heft 43, pp 247-282.

Dette, H. H., and Uliczka, K. 1987a. "Prototype Investigation on Time-Dependent Dune Recession and Beach Erosion," Proceedings of Coastal Sediments '87, American Society of Civil Engineers, pp 1430-1444.

_____. 1987b. "Velocity and Sediment Concentration Fields Across Surf Zones," Proceedings of the 20th Coastal Engineering Conference, American Society of Civil Engineers, pp 1062-1076.

Dingler, J. R., and Inman, D. L. 1977. "Wave-Formed Ripples in Nearshore Sands," Proceedings of the 15th Coastal Engineering Conference, American Society of Civil Engineers, pp 2109-2126.

Dolan, T. J. 1983. "Wave Mechanics for the Formation of Multiple Longshore Bars with Emphasis on the Chesapeake Bay," unpublished M.S. thesis, University of Delaware, Newark, DE.

Dolan, T. J., and Dean, R. G. 1984. "Multiple Longshore Sand Bars in the Upper Chesapeake Bay," Estuarine Coastal and Shelf Science, Vol 21, No. 5, pp 727-743.

Dyhr-Nielsen, M., and Sørensen, T. 1971 "Some Sand Transport Phenomena on Coasts with Bars," Proceedings of the 12th Coastal Engineering Conference, American Society of Civil Engineers, pp 855-865.

Eagleson, P. S., Glenne, B., and Dracup, J. A. 1963. "Equilibrium Characteristics of Sand Beaches," Journal of the Hydraulics Division, American Society of Civil Engineers, Vol 89, No. 1, pp 35-57.

Ebersole, B. A. 1987. "Measurements and Prediction of Wave Height Decay in the Surf Zone," Proceedings of Coastal Hydrodynamics, American Society of Civil Engineers, pp 1-16.

Edelman, T. 1969. "Dune Erosion During Storm Conditions," Proceedings of the 11th Coastal Engineering Conference, American Society of Civil Engineers, pp 719-722.

_____. 1973. "Dune Erosion During Storm Conditions," Proceedings of the 13th Coastal Engineering Conference, American Society of Civil Engineers, pp 1305-1311.

Evans, O. F. 1940. "The Low and Ball of the Eastern Shore of Lake Michigan," Journal of Geology, Vol 48, No. 5, pp 476-511.

Exon, N. F. 1975. "An Extensive Offshore Sand Bar Field in the Western Baltic Sea," Marine Geology, Vol 18, pp 197-212.

Fairchild, J. C. 1973. "Longshore Transport of Suspended Sand," Proceedings of the 13th Coastal Engineering Conference, American Society of Civil Engineers, pp 1062-1088.

Fenaish, T. A., Overton, M. F., and Fisher, J. S. 1988. "Dune Erosion and Sediment Profile Due to Wave Uprush," Coastal Engineering Abstracts, American Society of Civil Engineers, pp 283-284.

Felder, W. N. 1978. "Simulation Modeling of Offshore Bars," Department of Environmental Sciences, unpublished Ph.D. thesis, University of Virginia, Charlottesville, VA.

Felder, W. N., and Fisher, J. S. 1980. "Simulation Model Analysis of Seasonal Beach Cycles," Coastal Engineering, Vol 3, pp 269-282.

Fox, W. T., and Davis, R. A. 1973. "Simulation Model for Storm Cycles and Beach Erosion on Lake Michigan," Geological Society of America Bulletin, Vol 84, pp 1769-1790.

Galvin, C. J. 1969. "Breaker Travel and Choice of Design Wave Height," Journal of Waterways and Harbors Division, American Society of Civil Engineers, Vol 95, No. 2, pp 175-200.

_____. 1972. "Wave Breaking in Shallow Water," In: Waves on Beaches and Resulting Sediment Transport, ed. R. E. Meyer, Academic Press, pp 413-456.

Gourlay, M. R. 1968. "Beach and Dune Erosion Tests I," Report No. M 935/M 936, Delft Hydraulics Laboratory, Delft, The Netherlands.

_____. 1981. "Beaches: Profiles, Processes and Permeability," Proceedings of the 17th Coastal Engineering Conference, American Society of Civil Engineers, pp 1320-1339.

_____. 1985. "Beaches: States, Sediments and Set-Up," Preprints of the Australasian Conference on Coastal and Ocean Engineering, Vol 1, pp 347-356.

Greenwood, B., and Davidson-Arnott, R. G. D. 1972. "Textural Variation in Sub-Environments of the Shallow-Water Wave Zone, Kouchibouguac Bay, New Brunswick, Canadian Journal of Earth Sciences, Vol 9, No. 6, pp 679-687.

_____. 1975. "Marine Bars and Nearshore Sedimentary Processes, Kouchibouguac Bay, New Brunswick," In: Nearshore Sediment Dynamics and Sedimentation, An Interdisciplinary Review, John Wiley and Sons, New York, pp 123-150.

_____. 1979. "Sedimentation and Equilibrium in Wave-Formed Bars: A Review and Case Study," Canadian Journal of Earth Sciences, Vol 16, No. 2, pp 312-332.

Greenwood, B., and Mittler, P. R. 1979. "Structural Indices of Sediment Transport in a Straight, Wave-Formed, Nearshore Bar," Marine Geology, Vol 32, pp 191-203.

_____. 1984. "Sediment Flux and Equilibrium Slopes in a Barred Nearshore," Marine Geology, Vol 60, pp 79-98.

Guza, R. T., and Bowen, A. J. 1977. "Resonant Interaction for Waves Breaking on a Beach," Proceedings of the 15th Coastal Engineering Conference, American Society of Civil Engineers, pp 560-579.

Guza, R. T., and Thornton, E. B. 1982. "Swash Oscillations on a Natural Beach," Journal of Geophysical Research, Vol 87, No. C1, pp 483-491.

Hallermeier, R. J. 1979. "Uses for a Calculated Limit Depth to Beach Erosion," Proceedings of the 16th Coastal Engineering Conference, American Society of Civil Engineers, pp 1493-1512.

Hallermeier, R. J. 1981. "Terminal Settling Velocity of Commonly Occurring Sand Grains," Sedimentology, Vol 28.

_____. 1982. "Oscillatory Bedload Transport: Data Review and Simple Formulation," Continental Shelf Research, Vol 1, pp 159-190.

_____. 1984. "Wave Cuts in Sand Slopes Applied to Coastal Models," Journal of Waterway, Port, Coastal and Ocean Engineering, Vol 110, No. 1, pp 34-49.

_____. 1987. "Applying Large Replicas of Shore Erosion by Storms," Proceedings of Coastal Sediments '87, American Society of Civil Engineers, pp 1415-1429.

Hands, E. B. 1976. "Observations of Barred Coastal Profiles under the Influence of Rising Water Levels, Eastern Lake Michigan, 1967-71," Technical Report 76-1, Coastal Engineering Research Center, US Army Engineer Waterways Experiment Station, Vicksburg, MS.

Hartnack, W. 1924. "Über Sandriffe," Jahrbuch der Geografischen Gesellschaft zu Greifswald, Band XL/XLII, pp 47-70.

Hashimoto, H., and Uda, T. 1980. "An Application of an Empirical Prediction Model of Beach Profile Change to the Ogawara Coast," Coastal Engineering in Japan, Vol 23, pp 191-204.

Hattori, M. 1982. "Field Study on Onshore-Offshore Sediment Transport," Proceedings of the 18th Coastal Engineering Conference, American Society of Civil Engineers, pp 923-940.

Hattori, M., and Kawamata, R. 1979. "Restoration of Sandy Beaches Fronting Seawalls," Proceedings of Coastal Structures '79, American Society of Civil Engineers, pp 388-404.

_____. 1981. "Onshore-Offshore Transport and Beach Profile Change," Proceedings of the 17th Coastal Engineering Conference, American Society of Civil Engineers, pp 1175-1193.

Hayden, B., Felder, W., Fisher, J., Resio, D., Vincent, L., and Dolan, R. 1975. "Systematic Variations in Inshore Bathymetry," Department of Environmental Sciences, Technical Report No. 10, University of Virginia, Charlottesville, VA.

Hayes, M. O., and Boothroyd, J. C. 1969. "Storms as Modifying Agents in the Coastal Environment," Coastal Environments, Northeast Massachusetts and New Hampshire, Eastern Section, Society of Economic Paleontologists and Mineralogists, Field Guide. Reprinted in Davis, R. A. ed., 1987, Beach and Nearshore Sediments and Processes, SEPM Reprint Series Number 12, SEPM, Tulsa, OK, pp 25-39.

Holman, R. A. 1986. "Extreme Value Statistics for Wave Run-Up on a Natural Beach," Coastal Engineering, Vol 9, pp 527-544.

Holman, R. A., and Bowen, A. J. 1982. "Bars, Bumps, and Holes: Models for the Generation of Complex Beach Topography," Journal of Geophysical Research, Vol 87, pp 457-468.

Holman, R. A., and Sallenger, A. H. 1985. "Set-up and Swash on a Natural Beach," Journal of Geophysical Research, Vol 81, pp 6441-6449.

Horikawa, K., and Kuo, C. 1967. "A Study on Wave Transformation Inside the Surf Zone," Proceedings of the 10th Coastal Engineering Conference, American Society of Civil Engineers, pp 217-233.

Howd, P. A., and Birkemeier, W. A. 1987. "Beach and Nearshore Survey Data: 1981-1984 CERC Field Research Facility," Technical Report CERC-87-9, Coastal Engineering Research Center, US Army Engineer Waterways Experiment Station, Vicksburg, MS.

Hughes, S. A. 1983. "Movable-Bed Modeling Law for Coastal Dune Erosion," Journal of Waterway, Port, Coastal and Ocean Engineering, American Society of Civil Engineers, Vol 109, No. 2, pp 164-179.

_____. 1984. "Movable-Bed Modeling Law for Coastal Dune Erosion," Journal of Waterway, Port, Coastal and Ocean Engineering, Closure, Vol 110, No. 4, pp 504-507.

Hughes, S. A., and Chiu, T. Y. 1981. "Beach and Dune Erosion During Severe Storms," Report UFL/COEL-TR/043, Coastal and Oceanographic Engineering Department, University of Florida, Gainesville, FL.

Hughes, M. G., and Cowell, P. J. 1987. "Adjustment of Reflective Beaches to Waves," Journal of Coastal Research, Vol 3, No. 2, pp 153-167.

Hunt, I. A. 1959. "Design of Seawalls and Breakwaters," Journal of Waterways and Harbors Division, Vol 85, pp 123-152.

Hunter, R. E., Clifton, H. E., and Phillips, R. L. 1979. "Depositional Processes, Sedimentary Structures, and Predicted Vertical Sequences in Barred Nearshore Systems, Southern Oregon Coast," Journal of Sedimentary Petrology, Vol 49, No. 3, pp 711-726.

Inman, D. L. 1957. "Wave Generated Ripples in Nearshore Sand," Technical Memorandum No. 100, Beach Erosion Board, Coastal Engineering Research Center, US Army Engineer Waterways Experiment Station, Vicksburg, MS.

Inman, D. L., and Bagnold, R. A. 1963. "Littoral Processes," In: The Sea, Vol 3, ed. M. N. Hill, Interscience, New York, pp 529-553.

Ippen, A. I., and Eagleson, P. S. 1955. "A Study of Sediment Sorting by Waves Shoaling on a Plane Beach," Technical Memorandum No. 63, Beach Erosion Board, US Army Engineer Waterways Experiment Station, Vicksburg, MS.

Iwagaki, Y., and Noda, H. 1963. "Laboratory Studies of Scale Effects in Two-Dimensional Beach Processes," Proceedings of the 8th Coastal Engineering Conference, American Society of Civil Engineers, pp 194-210.

Jaffe, B. E., Sternberg, R. W., and Sallenger, A. H. 1985. "The Role of Suspended Sediment in Shore-Normal Beach Profile Changes," Proceedings of the 19th Coastal Engineering Conference, American Society of Civil Engineers, pp 1983-1996.

Jansen, P. C. M. 1986. "Laboratory Observations of the Kinematics in the Aerated Region of Breaking Waves," Coastal Engineering, Vol 9, pp 453-477.

Johnson, J. W. 1949. "Scale Effects in Hydraulic Models Involving Wave Motion," Transactions of the American Geophysical Union, Vol 30, No. 4, pp 517-525.

Kajima, R., Shimizu, T., Maruyama, K., and Saito, S. 1983a. "Experiments of Beach Profile Change with a Large Wave Flume," Proceedings of the 18th Coastal Engineering Conference, American Society of Civil Engineers, pp 1385-1404.

Kajima, R., Saito, S., Shimizu, T., Maruyama, K., Hasegawa, H., and Sakakiyama, T. 1983b. "Sand Transport Experiments Performed by Using a Large Water Wave Tank," Data Report No. 4-1, Central Research Institute for Electric Power Industry, Civil Engineering Division. (in Japanese)

Kamphuis, J. W., and Bridgeman, S. G. 1975. "Placing Artificial Beach Nourishment," Proceedings of Coastal Engineering in the Oceans III, American Society of Civil Engineers, pp 197-216.

Kana, T. W. 1977. "Suspended Sediment Transport at Price Inlet, S. C.," Proceedings of Coastal Sediments '77, American Society of Civil Engineers, pp 366-382.

Kemp, P. H. 1961. "The Relationship Between Wave Action and Beach Profile Characteristics," Proceedings of the 7th Conference on Coastal Engineering, American Society of Civil Engineers, pp 262-277.

Keulegan, G. H. 1945. "Depths of Offshore Bars," Engineering Notes No. 8, Beach Erosion Board, Coastal Engineering Research Center, US Army Engineer Waterways Experiment Station, Vicksburg, MS.

_____. 1948. "An Experimental Study of Submarine Sand Bars," Technical Report No. 3, Beach Erosion Board, Coastal Engineering Research Center, US Army Engineer Waterways Experiment Station, Vicksburg, MS.

King, C. A. M., and Williams, W. W. 1949. "The Formation and Movement of Sand Bars by Wave Action," Geological Journal, Vol 113, pp 70-85.

Kobayashi, N. 1987. "Analytical Solutions for Dune Erosion by Storms," Journal of Waterway, Port, Coastal and Ocean Engineering, Vol 113, No. 4, pp 401-418.

Komar, P. D., and Gaughan, M. K. 1973. "Airy Wave Theory and Breaker Height Prediction," Proceedings of the 13th Coastal Engineering Conference, American Society of Civil Engineers, pp 405-418.

Kraus, N. C. 1987. "The Effects of Seawalls on the Beach: A Literature Review," Proceedings of Coastal Sediments '87, American Society of Civil Engineers, pp 945-960.

_____. 1988. "The Effects of Seawalls on the Beach: An Extended Review," In: The Effects of Seawalls on the Beach, eds. N. C. Kraus and O. H. Pilkey, Journal of Coastal Research, pp 1-28.

Kraus, N. C., and Dean, J. L. 1987. "Longshore Sediment Transport Rate Distributions Measured by Trap," Proceedings of Coastal Sediments '87, American Society of Civil Engineers, pp 881-896.

Kraus, N. C., Gingerich, K. J., and Rosati, J. D. 1989. "Toward an Improved Empirical Formula for Longshore Sand Transport," Proceedings of the 21st Coastal Engineering Conference, American Society of Civil Engineers, pp 1182-1196.

Kraus, N. C., and Horikawa, K. in press. "Nearshore Sediment Transport," In: The Sea, Vol 9, eds. B. LeMehaute and D. Hanes, John Wiley and Sons, New York, NY.

Kraus, N. C., and Larson, M. 1988a. "Beach Profile Change Measured in the Tank for Large Waves, 1956-1957 and 1962," Technical Report CERC-88-6, Coastal Engineering Research Center, US Army Engineer Waterways Experiment Station, Vicksburg, MS.

_____. 1988b. "Prediction of Initial Profile Adjustment on Nourished Beaches to Wave Action," Proceedings of Beach Technology '88, Florida Shore and Beach Preservation Association, pp 125-137.

Kraus, N. C., Scheffner, N. W., Hanson, H., Chou, L. W., Cialone, M. A., Smith, J. M., and Hardy, T. A. 1988. "Coastal Processes at Sea Bright to Ocean Township, New Jersey, Volume I: Main Text and Appendix A," Miscellaneous Paper CERC-88-12, Coastal Engineering Research Center, US Army Engineer Waterways Experiment Station, Vicksburg, MS.

Kriebel, D. L. 1982. "Beach and Dune Response to Hurricanes," unpublished M.S. Thesis, University of Delaware, Newark, DE.

_____. 1986. "Verification Study of a Dune Erosion Model," Shore and Beach, Vol 54, No. 3, pp 13-21.

_____. 1987. "Beach Recovery Following Hurricane Elena," Proceedings of Coastal Sediments '87, American Society of Civil Engineers, pp 990-1005.

Kriebel, D. L., and Dean, R. G. 1984. "Beach and Dune Response to Severe Storms," Proceedings of the 19th Coastal Engineering Conference, American Society of Civil Engineers, pp 1584-1599.

_____. 1985a. "Numerical Simulation of Time-Dependent Beach and Dune Erosion," Coastal Engineering, Vol 9, pp 221-245.

_____. 1985b. "Estimates of Erosion and Mitigation Requirements under Various Scenarios of Sea Level Rise and Storm Frequency for Ocean City, Maryland," Preliminary Report, Coastal and Oceanographic Department, University of Florida, Gainesville, FL.

Kriebel, D. L., Dally, W. R., and Dean, R. G. 1986. "Beach Profile Response Following Severe Erosion Events," Report UFL/COEL-86/016, Coastal and Oceanographic Department, University of Florida, Gainesville, FL.

_____. 1987. "Undistorted Froude Model for Surf Zone Sediment Transport," Proceedings of the 20th Coastal Engineering Conference, American Society of Civil Engineers, pp 1296-1310.

Larson, M., and Kraus, N. C. In press. "Prediction of Beach Fill Response to Varying Waves and Water Level," Proceedings of Coastal Zone '89, American Society of Civil Engineers.

Larson, M., Kraus, N. C., and Byrnes, M. R. In prep. "SBEACH: Numerical Model for Simulating Storm-Induced Beach Change," Report 2, Numerical Formulation and Model Test, Technical Report, Coastal Engineering Research Center, US Army Engineer Waterways Experiment Station, Vicksburg, MS.

Lau, J., and Travis, B. 1973. "Slowly Varying Stokes Waves and Submarine Longshore Bars," Journal of Geophysical Research, Vol 78, pp 4489-4497.

Lehmann, F. W. P. 1884. "Das Küstengebiet Hinterpommerns," Zeitschrift das Gesellschaft für Erdkunde zu Berlin, Band XIX.

Longuet-Higgins, M. S. 1952. "On the Statistical Distribution of the Heights of Sea Waves," Journal of Marine Research, Vol 11, pp 245-266.

Longuet-Higgins, M. S., and Stewart, R. W. 1963. "A Note on Wave Set-up," Journal of Marine Research, Vol 21, pp 4-10.

Madsen, O. S., and Grant, W. D. 1977. "Quantitative Description of Sediment Transport by Waves," Proceedings of the 15th Coastal Engineering Conference, American Society of Civil Engineers, pp 1093-1112.

Mason, C., Sallenger, A. H., Holman, R. A., and Birkemeier, W. A. 1985. "DUCK82 - a Coastal Storm Processes Experiment," Proceedings of the 19th Coastal Engineering Conference, American Society of Civil Engineers, pp 1913-1927.

McKee, E. D., and Sterrett, T. S. 1961. "Laboratory Experiments on Form and Structure of Longshore Bars and Beaches," In: Geometry of Sandstone Bodies, eds. Peterson, J. A., and Osmond, J. C., American Association of Petroleum Geologists, pp 13-28.

Mei, C. C. 1985. "Resonant Reflection of Surface Water Waves by Periodic Sandbars," Journal of Fluid Mechanics, Vol 152, pp 315-335.

Meyer, R. D. 1936. "A Model Study of Wave Action on Beaches," unpublished M.S. Thesis, Department of Civil Engineering, University of California, Berkeley, CA.

Miller, R. L. 1976. "Role of Vortices in Surf Zone Prediction: Sedimentation and Wave Forces," In: Beach and Nearshore Sedimentation, eds. R. A. Davis and R. I. Ethington, Society of Economic Paleontologists and Mineralogists, Special Publication No. 24, pp 92-114.

Mimura, N., Otsuka, Y., and Watanabe, A. 1987. "Laboratory Study on Two-Dimensional Beach Transformation Due to Irregular Waves," Proceedings of the 20th Coastal Engineering Conference, American Society of Civil Engineers, pp 1393-1406.

Mizuguchi, M. 1981. "An Heuristic Model of Wave Height Distribution in Surf Zone," Proceedings of the 17th Coastal Engineering Conference, American Society of Civil Engineers, pp 278-289.

Moore, B. D., 1982. "Beach Profile Evolution in Response to Changes in Water Level and Wave Height," unpublished M.S. thesis, University of Delaware, Newark, DE.

Möller, J. P., and Swart D. H. 1988. "Extreme Erosion Event on an Artificially-Nourished Beach," Coastal Engineering Abstracts, American Society of Civil Engineers, pp 244-245.

Mothersill, J. S. 1970. "Relationship of Grain-Size Modes to Nearshore Sedimentary Environments, Lake Superior, Ontario," Canadian Journal of Earth Sciences, Vol 7, pp 522-527.

Nairn, R. B. 1988. "Prediction of Wave Height and Mean Return Flow in Cross Shore Sediment Transport Modelling," Symposium on Mathematical Modelling of Sediment Transport in the Coastal Zone, International Association of Hydraulic Research, Copenhagen, Denmark, pp 193-202.

Nayak, I. V. 1970. "Equilibrium Profiles of Model Beaches," Hydraulic Engineering Laboratory, Technical Report HEL-2-25, University of California, Berkeley, CA.

_____. 1971. "Equilibrium Profiles of Model Beaches," Proceedings of the 12th Coastal Engineering Conference, American Society of Civil Engineers, pp 1321-1340.

Nielsen, P. 1979. "Some Basic Concepts of Wave Sediment Transport," Paper No. 20, Technical University of Denmark, Lyngby, Denmark.

Nilsson, H. D. 1979. "Multiple Longshore Sand Bars: Environments of Deposition and a Model for their Generation and Maintenance," unpublished Ph.D. thesis, University of Massachusetts, Amherst, MA.

Nishimura, H., and Sunamura, T. 1987. "Numerical Simulation of Beach Profile Changes," Proceedings of the 20th Coastal Engineering Conference, American Society of Civil Engineers, pp 1444-1455.

Ostle, B., and Mensing, R. W. 1975. Statistics in Research, The Iowa State University Press, Ames, IA.

Otto, T. 1911 "Der Darss und Zingst," Jahrbuch der Geografischen Gesellschaft zu Greifswald, Band XIII, pp 393-403.

Owens, E. H. 1977. "Temporal Variations in Beach and Nearshore Dynamics," Journal of Sedimentary Petrology, Vol 47, No 1, pp 168-190.

Overton, M. F., and Fisher, J. S. 1988. "Simulation Modeling of Dune Erosion," Coastal Engineering Abstracts, American Society of Civil Engineers, pp 287-288.

Raynor, A. C., and Simmons, G. W. 1964. "Summary of Capabilities," Miscellaneous Paper No. 3-64, Coastal Engineering Research Center, US Army Engineer Waterways Experiment Station, Vicksburg, MS.

Rector, R. L. 1954. "Laboratory Study of Equilibrium Profiles of Beaches," Technical Memorandum No. 41, Beach Erosion Board, Coastal Engineering Research Center, US Army Engineer Waterways Experiment Station, Vicksburg, MS.

Rushu, R., and Liang, W. 1986. "Investigation on Two-Dimensional Transformation of Sandy Beach under Wave Action," Proceedings of the 3rd International Symposium on River Sedimentation, The University of Mississippi, pp 378-387.

Sallenger, A. S., Holman, R. A., and Birkemeier, W. A. 1985. "Storm-Induced Response of a Nearshore-Bar System," Marine Geology, 64, pp 237-257.

Sasaki, T. 1983. "Three-Dimensional Topographic Changes on the Foreshore Zone of Sandy Beaches," Science Report, Institute of Geoscience, University of Tsukuba, Section A, Vol 4, pp 69-95.

Sato, S., and Horikawa, K. 1987. "Laboratory Study on Sand Transport over Ripples Due to Asymmetric Oscillatory Flows," Proceedings of the 17th Coastal Engineering Conference, American Society of Civil Engineers, pp 1481-1495.

Savage, R. P. 1959. "Notes on the Formation of Beach Ridges," Annual Bulletin, Beach Erosion Board, Coastal Engineering Research Center, US Army Engineer Waterways Experiment Station, Vicksburg, MS.

Saville, T. 1957. "Scale Effects in Two Dimensional Beach Studies," Transactions from the 7th General Meeting of the International Association of Hydraulic Research, Vol 1, pp A3-1-A3-10.

Sawaragi, T., and Deguchi, I. 1981. "On-Offshore Sediment Transport Rate in the Surf Zone," Proceedings of the 17th Coastal Engineering Conference, American Society of Civil Engineers, pp 1194-1214.

Sayao, O. S. F. J. 1984. "Movable-Bed Modeling Law for Coastal Dune Erosion," Journal of Waterway, Port, Coastal and Ocean Engineering, Discussion, Vol 110, No. 4, pp 493-495.

Saylor, J. H., and Hands, E. B. 1971. "Properties of Longshore Bars in the Great Lakes," Proceedings of the 12th Coastal Engineering Conference, American Society of Civil Engineers, pp 839-853.

Scott, T. 1954. "Sand Movement by Waves," Technical Memorandum No. 48, Beach Erosion Board, Coastal Engineering Research Center, US Army Engineer Waterways Experiment Station, Vicksburg, MS.

Seelig, W. N. 1983. "Understanding Beach Erosion and Accretion," Journal of Waterway, Port, Coastal and Ocean Engineering, American Society of Civil Engineers, Vol 49, No. 4, pp 490-494.

Seymour, R. J. 1985. "Results of Cross-shore Transport Experiments," Journal of Waterway, Port, Coastal, and Ocean Engineering, Vol 112, No. 1, pp 168-173.

_____. 1986. "Results of Cross-Shore Transport Experiments," Journal of Waterway, Port, Coastal and Ocean Engineering, Vol 112, No. 1, pp 168-173.

_____. 1987. "An Assessment of NSTS," Proceedings of Coastal Sediments '87, American Society of Civil Engineers, pp 642-651.

Seymour, R. J., and Castel D. 1988. "Validation of Cross-Shore Transport Formulations," Coastal Engineering Abstracts, American Society of Civil Engineers, pp 273-274.

Seymour, R. J., and King, D. B. 1982. "Field Comparisons of Cross-shore Transport Models," Journal of Waterway, Port, Coastal, and Ocean Engineering, Vol 108, No. WW2, pp 163-179.

Shepard, F. P. 1950. "Longshore-Bars and Longshore-Troughs," Technical Memorandum No. 15, Beach Erosion Board, Coastal Engineering Research Center, US Army Engineer Waterways Experiment Station, Vicksburg, MS.

Shibayama, T. 1984. "Sediment Transport Mechanism and Two-Dimensional Beach Transformation Due to Waves," unpublished Ph.D. thesis, University of Tokyo, Tokyo, Japan.

Shibayama, T., and Horikawa, K. 1980a. "Bed Load Measurement and Prediction of Two-Dimensional Beach Transformation Due to Waves," Coastal Engineering in Japan, Vol 23, pp 179-190.

_____. 1980b. "Laboratory Study on Sediment Transport Mechanism Due to Wave Action," Proceedings of the Japanese Society of Civil Engineers, No. 296, April, pp 131-141.

Shimizu, T., Saito, S., Maruyama, K., Hasegawa, H., and Kajima, R. 1985. "Modeling of Onshore-Offshore Sand Transport Rate Distribution Based on the Large Wave Flume Experiments," Civil Engineering Laboratory Report No. 384028, Abiko City, Japan. (in Japanese)

Shore Protection Manual. 1984. 4th ed., 2 vols, US Army Engineer Waterways Experiment Station, Coastal Engineering Research Center, US Government Printing Office, Washington, DC.

Short, A. D. 1975a. "Offshore Bars Along the Alaskan Arctic Coast," Journal of Geology, Vol 83, pp 209-221.

_____. 1975b. "Multiple Offshore Bars and Standing Waves," Journal of Geophysical Research, Vol 80, No. 27, pp 3838-3840.

_____. 1979. "Three Dimensional Beach-Stage Model," Journal of Geology, Vol 87, pp 553-571.

Shuto, N. 1974. "Nonlinear Long Waves in a Channel of Variable Section," Coastal Engineering in Japan, Vol 17, pp 1-12.

Singamsetti, S. R., and Wind, H. G. 1980. "Breaking Waves: Characteristics of Shoaling and Breaking Periodic Waves Normally Incident to Plane Beaches of Constant Slope," Delft Hydraulics Laboratory, Report M 1371, Delft, The Netherlands.

Skjelbreia, J. E. 1987. "Observations of Breaking Waves on Sloping Bottoms by Use of Laser Doppler Velocimetry," Report No. KH-R-48, Division of Engineering and Applied Science, California Institute of Technology, Pasadena, CA.

Smith, J., and Kraus, N. C. 1988. "An Analytical Model of Wave-Induced Longshore Current Based on Power Law Wave Height Decay," Miscellaneous Paper CERC-88-3, Coastal Engineering Research Center, US Army Engineer Waterways Experiment Station, Vicksburg, MS.

Sonu, C. J. 1969. "Collective Movement of Sediment in Littoral Environment," Proceedings of the 11th Coastal Engineering Conference, American Society of Civil Engineers, pp 373-400.

_____. 1970. "Beach Changes by Extraordinary Waves Caused by Hurricane Camille," Coastal Studies Institute, Technical Report 77, Louisiana State University, Baton Rouge, LA, pp 33-45.

Stive, M. J. F. 1987. "A Model for Cross-Shore Sediment Transport," Proceedings of the 20th Coastal Engineering Conference, American Society of Civil Engineers, pp 1550-1564.

Stive, M. J. F., and Battjes, J. A. 1985. "A Model for Offshore Sediment Transport," Proceedings of the 19th Coastal Engineering Conference, American Society of Civil Engineers, pp 1420-1436.

Sunamura, T. 1975. "A Study of Beach Ridge Formation in Laboratory," Geographical Review of Japan, 48-11, pp 761-767.

_____. 1980. "Parameters for Delimiting Erosion and Accretion of Natural Beaches," Annual Report of the Institute of Geoscience, University of Tsukuba, No. 6, pp 51-54.

_____. 1981a. "Bedforms Generated in a Laboratory Wave Tank," Science Reports of the Institute of Geoscience, University of Tsukuba, Section A, Vol 2, pp 31-43.

_____. 1981b. "A Laboratory Study of Offshore Transport of Sediment and a Model for Eroding Beaches," Proceedings of the 17th Coastal Engineering Conference, American Society of Civil Engineers, pp 1051-1070.

_____. 1983. "A Predictive Model for Shoreline Changes on Natural Beaches Caused by Storm and Post-Storm Waves," Transactions of the Japanese Geomorphological Union, Vol 4, pp 1-10.

_____. 1984a. "On-Offshore Sediment Transport Rate in the Swash Zone of Laboratory Beaches," Coastal Engineering in Japan, Vol 27, pp 205-212.

_____. 1984b. "Quantitative Predictions of Beach-Face Slopes," Geological Society of America Bulletin, Vol 95, pp 242-245.

_____. In press. "Sandy Beach Geomorphology as Elucidated by Laboratory Modeling," In: Coastal Modeling: Techniques and Application, Elsevier, Amsterdam, The Netherlands.

Sunamura, T., and Horikawa, K. 1975. "Two-Dimensional Beach Transformation Due to Waves," Proceedings of the 14th Coastal Engineering Conference, American Society of Civil Engineers, pp 920-938.

Sunamura, T. and Maruyama, K. 1987. "Wave-Induced Geomorphic Response of Eroding Beaches - with Special Reference to Seaward Migrating Bars," Proceedings of Coastal Sediments '87, American Society of Civil Engineers, pp 884-900.

Sunamura, T., and Takeda, I. 1984. "Landward Migration of Inner Bars," Marine Geology, 60, pp 63-78.

Svendsen, I. A. 1984. "Wave Heights and Set-Up in a Surf Zone," Coastal Engineering, Vol 8, pp 303-329.

_____. 1987. "Analysis of Surf Zone Turbulence," Journal of Geophysical Research, Vol 92, No. C5, pp 5115-5124.

Svendsen, I. A., Madsen, P. A., and Buhr Hansen, J. 1979. "Wave Characteristics in the Surf Zone," Proceedings of the 14th Coastal Engineering Conference, American Society of Civil Engineers, pp 520-539.

Swart, D. H. 1975. "A Schematization of Onshore-Offshore Transport," Proceedings of the 14th Coastal Engineering Conference, American Society of Civil Engineers, pp 884-900.

_____. 1977. "Predictive Equations Regarding Coastal Transport," Proceedings of the 15th Coastal Engineering Conference, American Society of Civil Engineers, pp 1113-1132.

Takeda, I. 1984. "Beach Changes by Waves," Science Report, Institute of Geoscience, University of Tsukuba, Japan, Sect A, Vol 5, pp 29-63.

Takeda, I., and Sunamura, T. 1987. "Beach Changes by Storm waves," Proceedings of the 20th Coastal Engineering Conference, American Society of Civil Engineers, pp 1612-1622.

Thomas, K. V., and Baba, M. 1986. "Berm Development on a Monsoon-Influenced Microtidal Beach," Sedimentology, Vol 33, pp 537-546.

Uliczka, K., and Dette, H. H. 1987. "About the Effect of Monochromatic and Irregular Waves on Beach and Dune Profiles," Proceedings of Seminar on Hydrologie und Küsteningenieurwesen, Hannover, Germany.

University of California. 1982. "Surface Water Temperatures at Shore Stations, United States West Coast," Scripps Institution of Oceanography, La Jolla, CA.

van de Graaff, J. 1983. "Probabilistic Design of Dunes," Proceedings of Coastal Structures '83, American Society of Civil Engineers, pp 820-831.

van Hijum, E. 1975. "Equilibrium Profiles of Coarse Material Under Wave Attack," Proceedings of the 14th Coastal Engineering Conference, American Society of Civil Engineers, pp 939-957.

_____. 1977. "Equilibrium Profiles and Longshore Transport of Coarse Material Under Oblique Wave Attack," Proceedings of the 15th Coastal Engineering Conference, American Society of Civil Engineers, pp 1258-1276.

van Hijum, E., and Pilarczyk, K. W. 1982. "Gravel Beaches - Equilibrium Profile and Longshore Transport of Coarse Material under Regular and Irregular Wave Attack," Delft Hydraulics Laboratory, Publication No. 274, Delft, The Netherlands.

Vellinga, P. 1982. "Beach and Dune Erosion During Storm Surges," Publication No. 276, Delft Hydraulics Laboratory, Delft, The Netherlands.

_____. 1983. "Predictive Computational Model for Beach and Dune Erosion During Storm Surges," Proceedings of Coastal Structures '83, American Society of Civil Engineers, pp 806-819.

_____. 1984. "Movable-Bed Modeling Law for Coastal Dune Erosion," Journal of Waterway, Port, Coastal and Ocean Engineering, Discussion, Vol 110, No. 4, pp 495-504.

_____. 1986. "Beach and Dune Erosion During Storm Surges," Delft Hydraulics Communication No. 372, Delft Hydraulics Laboratory, Delft, The Netherlands.

Verhagen, H. J. 1985. "Guideline for the Judgement of Safety of Dunes as Coastal Defense," Ministerie van Verkeer en Waterstaat, Amsterdam, The Netherlands.

Visser, C. 1983. "Design of Dunes as Coastal Protection in the Delta Area of the Netherlands," Proceedings of Coastal Structures '83, American Society of Civil Engineers, pp 792-805.

Wang, H., Dalrymple, R. A., and Shiau, J. C. 1975. "Computer Simulation of Beach Erosion and Profile Modification Due to Waves," Proceedings of the Symposium on Modeling Techniques, American Society of Civil Engineers, pp 1369-1384.

Watanabe, A. 1982. "Numerical Models of Nearshore Currents and Beach Deformation," Coastal Engineering in Japan, Vol 25, pp 147-161.

_____. 1985. "Three-Dimensional Predictive Model of Beach Evolution Around a Structure," Proceedings of International Symposium on Water Wave Research, University of Hannover, Germany, pp 121-142.

Watanabe, A., Riho, Y., and Horikawa, K. 1981. "Beach Profiles and On-Offshore Sediment Transport," Proceedings of the 17th Coastal Engineering Conference, American Society of Civil Engineers, pp 1106-1121.

Waters, C. H. 1939. "Equilibrium Slopes of Sea Beaches," unpublished M.S. thesis, University of California, Berkeley, CA.

Watts, G. M. 1953. "A Study of Sand Movement at South Lake Worth Inlet, Florida," Technical Memorandum No. 42, Beach Erosion Board, Coastal Engineering Research Center, US Army Engineer Waterways Experiment Station, Vicksburg, MS.

_____. 1954. "Laboratory Study of Effect of Varying Wave Periods on Beach Profiles," Technical Memorandum No. 53, Beach Erosion Board, Coastal Engineering Research Center, US Army Engineer Waterways Experiment Station, Vicksburg, MS.

Watts, G. M., and Dearduff, R. F. 1954. "Laboratory Studies of Effect of Tidal Action on Wave-Formed Beach Profiles," Technical Memorandum No. 52, Beach Erosion Board, Coastal Engineering Research Center, US Army Engineer Waterways Experiment Station, Vicksburg, MS.

Weggel, R. J. 1972. "Maximum Breaker Height," Journal of the Waterways, Harbors and Coastal Engineering Division, American Society of Civil Engineers, Vol 98, No. 1, pp 529-547.

Wells, D. R. 1967. "Beach Equilibrium and Second-Order Wave Theory," Journal of Geophysical Research, Vol 72, No. 2, pp 497-504.

Winant, C. D., Inman, D. L., and Nordstrom, C. E. 1975. "Description of Seasonal Beach Changes Using Empirical Eigenfunctions," Journal of Geophysical Research, Vol 80, No. 15, pp 1979-1986.

Wood, W. L., and Weishar, L. L., 1985. "Beach Response to Long Period Lake-Level Variation," Proceedings of the 19th Coastal Engineering Conference, American Society of Civil Engineers, pp 1571-1583.

Wright, L. D., Chappel, J., Thom, B. G., Bradshaw, M. P., and Cowell, P. 1979. "Morphodynamics of Reflective and Dissipative Beach and Inshore Systems: Southeastern Australia," Marine Geology, Vol 32, pp 105-140.

Wright, L. D., Nielsen, P., Shi, N. C., and List, J. H. 1986. "Morphodynamics of a Bar-Trough Surf Zone," Marine Geology, Vol 70, pp 251-285.

Wright, L. D., and Short, A. D. 1984. "Morphodynamic Variability of Surf Zones and Beaches: a Synthesis," Marine Geology, Vol 56, pp 93-118.

Wright, L. D., Short, A. D., and Green, M. O. 1985. "Short-Term Change in the Morphodynamic State of Beaches and Surf Zones: An Empirical Predictive Model," Marine Geology, Vol 62, pp 339-364.

Wright, L. D., Short, A. D., Boon, J. D., Hayden, B., Kimball, S., and List, J. H. 1987. "Morphodynamic Responses of an Energetic Beach to Temporal Variations in Wave Steepness, Tide Range, and Incident Wave Groupiness," Marine Geology, Vol 74, pp 1-20.

Zenkovich, V. P. 1967. "Submarine Sand Bars and Related Formations," In: Processes of Coastal Development, ed. J. A. Steers, Oliver and Boyd Ltd, New York, NY, pp 219-236.

## APPENDIX A: CORRELATION AND REGRESSION ANALYSIS

1. Correlation and regression analysis deals with the investigation and inference of dependencies between variables as derived solely from statistical techniques. Even if a high degree of association between variables is found by this method, the resultant relation does not necessarily have, and usually will not have, a clear physical basis. However, these statistical methods can provide an indication of possible relationships to be accepted or rejected after physical considerations. Information in this appendix may be obtained from any textbook on regression analysis, e.g., Ostle and Mensing (1975)*, and is included here to facilitate understanding of the statistical techniques and terminology extensively employed in the data analyses presented in the main text of this report.

### Correlation Coefficient

2. The correlation coefficient $r$ expresses the degree of linearity between variables. For a set of discrete data, $r$ is defined as:

$$r = \frac{s_{xy}}{s_x s_y} \tag{A1}$$

where

$$s_{xy} = \frac{1}{n-1} \sum_{i=1}^{n} (x_i - \bar{x})(y_i - \bar{y}) \tag{A2}$$

$$s_x^2 = \frac{1}{n-1} \sum_{i=1}^{n} (x_i - \bar{x})^2 \tag{A3}$$

---

* References cited in the Appendix can be found in the Reference list at the end of the main text.

$$s_y^2 = \frac{1}{n-1} \sum_{i=1}^{n} (y_i - \bar{y})^2 \qquad \text{(A4)}$$

in which

$s_{xy}$ = covariance between x and y

$n$ = number of values in the data set

$x_i$, $y_i$ = corresponding values from the data sets to be correlated

$\bar{x}$, $\bar{y}$ = mean values for the respective data sets

$s_x^2$ = variance of x

$s_y^2$ = variance of y

3. Values of the correlation coefficient are in the domain $-1 \leq r \leq 1$. A value of $r = 1$ implies a perfect linear relationship between the studied variables, $r = -1$ indicates an inverse linear dependence, and $r = 0$ means no linear dependence.

## Coefficient of Determination

4. In regression analysis, the parameters of a chosen functional relationship are estimated in an optimal way to provide the best fit with the measured data according to a predetermined criterion. The criterion typically used to optimize the parameter values is a minimization of the sum of the squares of the difference between predicted and measured values of the dependent variable. For example, if $y$ is considered a function of the $m$ variables $x_1, x_2, \ldots, x_m$, the parameters in the function $y(x_1, x_2, \ldots, x_m)$ should be estimated to minimize the function $R$, defined as:

$$R = \sum_{i=1}^{n} (y_i^p - y_i^m)^2 \qquad \text{(A5)}$$

where

$y_i^p$ = value predicted with a regression equation

$y_i^m$ = measured value

5. To find the optimal estimate, the partial derivative of R is taken with respect to each parameter contained in the regression equation. The equations thus obtained are set equal to zero to obtain an extremum (minimum) for R. For the case of a linear regression equation involving m independent variables, a linear set of m equations is obtained and may be solved directly by matrix theory. If the system of equations has a nonlinear form, the solution can be obtained numerically, usually by iteration.

6. A nonlinear regression equation can sometimes be reduced to linear form by an appropriate transformation of variables. For example, exponential or power equations can be transformed to linear form by taking the logarithm. However, this manipulation involves a modification of the original problem since the minimization is carried out with respect to the logarithmic values and not the original untransformed values. The difference is usually small but can be significant if the measured values vary over a large range.

7. A quantity expressing the ratio between the explained variation by the regression model and the total variation in the data, denoted as the coefficient of determination $r^2$, is defined as

$$r^2 = \frac{\sum_{i=1}^{n} (y_i^p - \bar{y})^2}{\sum_{i=1}^{n} (y_i^m - \bar{y})^2} \qquad \text{(A6)}$$

The equation for the coefficient of determination may be rewritten in a slightly different form to more easily allow interpretation:

$$r^2 = \frac{\sum_{i=1}^{n} (y_i^m - \bar{y})^2 - \sum_{i=1}^{n} (y_i^p - y_i^m)^2}{\sum_{i=1}^{n} (y_i^m - \bar{y})^2} = 1 - \frac{\sum_{i=1}^{n} (y_i^p - y_i^m)^2}{\sum_{i=1}^{n} (y_i^m - \bar{y})^2} \qquad \text{(A7)}$$

8. The last term on the right side of this equation can be interpreted as expressing the variation in the data not explained by the regression model (Equation A5 normalized with the total variation in the data). Thus, if the regression model fits the data perfectly, the second term will be zero, and $r^2 = 1$. It is also recognized that the coefficient of determination varies between 0 and 1 since the sum of squares of the difference between measured and predicted values is normalized by the total variation.

## Use in Present Study

9. In the data analysis conducted in this study, correlation and regression techniques were extensively used to investigate dependencies and establish empirical relationships between variables. A correlation analysis was first carried out irrespective of physical dimensions to identify variables which had marked influence on the quantity being studied. From this information on dependencies, supplemented by physical considerations, regression equations involving pertinent variables were derived, in most cases consisting of dimensionless groups formed by the studied variables.

10. In some cases, nonlinear equations were used to develop functional relationships between variables when it was not possible to transform the equations to a linear form. A special computer solution procedure was developed to obtain the optimal parameter values for these cases. Even if it was possible to transform some regression equations to linear form, results from the original nonlinear equation were used if an appreciable difference in the optimal parameter estimates occurred. Also, to evaluate the performance of the numerical model, coefficients of determination based on the difference between calculated values and measured values were frequently used.

## APPENDIX B: NOTATION

| | |
|---|---|
| $A$ | Shape parameter for equilibrium beach profile, $m^{1/3}$ |
| $D$ | Median grain size of beach sand, m |
| $D$ | Wave energy dissipation per unit water volume, $Nm/m^3/sec$ |
| $D_{eq}$ | Equilibrium energy dissipation per unit water volume, $Nm/m^3/sec$ |
| $E$ | Wave energy density, $Nm/m^2$ |
| $F$ | Wave energy flux, Nm/m/sec |
| $F_s$ | Stable wave energy flux, Nm/m/sec |
| $g$ | Acceleration due to gravity, $m/sec^2$ |
| $h$ | Water depth, m |
| $h_c$ | Depth-to-bar crest, m |
| $h_i^c$ | Calculated profile depth at grid point i, m |
| $h_i^m$ | Measured profile depth at grid point i, m |
| $h_t$ | Depth-to-bar trough, m |
| $H$ | Wave height, m |
| $\bar{H}$ | Mean wave height, m |
| $H_{mo}$ | Energy-based wave height, m |
| $H_{rms}$ | Root mean square wave height, m |
| $H_{so}$ | Significant wave height, m |
| $i$ | Integer number |
| $k$ | Integer number |
| $K$ | Transport rate coefficient, $m^4/N$ |
| $\ell_b$ | Berm length, m |
| $\ell_B$ | Bar length, m |
| $\ell_p$ | Plunge distance, m |
| $\ell_R$ | Runup length, m |
| $\ell_t$ | Trough length, m |
| $\ell_{tc}$ | Distance between break point and bar trough, m |
| $L$ | Wavelength, m |
| $n$ | Exponent determining spatial decay of transport rate in wave reformation zones |
| $N$ | Number of cells where avalanching occurs |
| $q$ | Cross-shore sand transport rate, $m^3/m/sec$ |

| | |
|---|---|
| $q_b$ | Transport rate at break point, $m^3/m/sec$ |
| $q_m$ | Peak transport rate, $m^3/m/sec$ |
| $q_{mo}$ | Peak transport rate at time t=0, $m^3/m/sec$ |
| $q_r$ | Transport rate at wave reformation point, $m^3/m/sec$ |
| $Q_A$ | Average absolute transport rate, $m^3/m/sec$ |
| r | Correlation coefficient |
| $r^2$ | Coefficient of determination |
| R | Sum of squares of difference between measured and calculated beach profile, $m^2$ |
| S | Specific gravity of sand |
| $S_{xx}$ | Radiation stress component directed onshore, N/m |
| t | Time, sec |
| T | Wave period, sec |
| U | Ursell number |
| V | Bar or berm volume, $m^3/m$ |
| w | Sand fall velocity, m/sec |
| x | Cross-shore coordinate, m |
| $x_1$ | Seaward location of no profile change, m |
| $x_m$ | Location of minimum transport rate in wave reformation zone, m |
| $x_o$ | Shoreward location of no profile change, m |
| $x_r$ | Location of wave reformation point, m |
| $x_{CM}$ | Location of bar mass center, m |
| z | Depth coordinate |
| $Z_b$ | Maximum berm height, m |
| $Z_B$ | Maximum bar height, m |
| $Z_R$ | Height of active subaerial profile, m |
| $\alpha$ | Temporal rate coefficient, $sec^{-1}$ |
| $\beta$ | Beach slope |
| $\beta_1$ | First seaward bar slope |
| $\beta_2$ | Second seaward bar slope |
| $\beta_3$ | Shoreward bar slope |
| $\beta_4$ | Terrace slope |
| $\beta_5$ | Step slope |
| $\gamma$ | Ratio between wave height and water depth at breaking |

| | |
|---|---|
| $\Gamma$ | Stable wave height coefficient |
| $\Delta$ | Change in quantity |
| $\epsilon$ | Slope-related transport rate coefficient, $m^2/sec$ |
| $\eta$ | Wave setup or setdown, m |
| $\kappa$ | Wave decay coefficient |
| $\lambda$ | Spatial decay coefficient, $m^{-1}$ |
| $\nu$ | Spatial decay coefficient, $m^{-1}$ |
| $\rho$ | Density of water, $kg/m^3$ |
| $\phi_1$ | Shoreward berm slope |
| $\phi_2$ | Seaward berm slope |

Subscripts and Superscripts:

| | |
|---|---|
| b | Breaking condition |
| eq | Equilibrium condition |
| i | Specific value of a variable |
| m | Measured quantity |
| o | Deepwater condition |
| p | Predicted quantity |
| 1,2 | Specific value of a variable |
| k | Specific value of a variable |

**DEPARTMENT OF THE ARMY**
WATERWAYS EXPERIMENT STATION, CORPS OF ENGINEERS
P.O. BOX 631
VICKSBURG, MISSISSIPPI 39180-0631

Official Business
Penalty for Private Use, $300
CEWES-IM-TS-T

SPECIAL FOURTH CLASS RATE
POSTAGE & FEES PAID
Department of the Army
Permit No. G-5

DOCUMENTS LIBRARY/SMITH 206 37907/12/01
WOODS HOLE OCEANOGRAPHIC INSTITUTION
WOODS HOLE MA 02543-1098